ERDC/CHL TR-12-7

Coastal and Hydraulics Laboratory

US Army Corps
of Engineers®
Engineer Research and
Development Center

Monitoring Completed Navigation Projects Program

Kaumalapau Harbor, Hawaii, Breakwater Repair

Jessica H. Podoski and Thomas D. Smith

May 2012

ERDC/CHL TR-12-7
May 2012

Kaumalapau Harbor, Hawaii, Breakwater Repair

Jessica H. Podoski and Thomas D. Smith

U.S. Army Corps of Engineers, Honolulu District
Bldg. T223, CEPOH-EC-T
Fort Shafter, Hawaii 96858-5440

Final report

Prepared for U.S. Army Corps of Engineers
441 G. Street, NW
Washington, DC 20314-1000

Under MCNP Work Unit Kaumalapau Harbor, Hawaii, Breakwater Repair

Abstract: Cumulative damage to the Kaumalapau Harbor breakwater over the years resulted in nearly total failure of the breakwater armor layer both above and below the waterline. Breakwater repair incorporated use of the largest CORE-LOC® concrete armor units (35 ton) ever placed on a U.S. Army Corps of Engineers structure. Actual construction took about 18 months, and was completed in June 2007.

Four different pertinent aspects of this rehabilitation were monitored. Lessons learned from monitoring these four aspects include:

1. **CORE-LOC® armor unit material strength and breakage due to movement:** (a) Standard methods of specifying concrete strength are not necessarily applicable to coastal structures composed of concrete armor units – more research and development is needed; (b) Construction methods are an integral part of concrete armor unit stability, and variability of methods may contribute to armor layer vulnerability; (c) Small-scale post-construction armor unit movement will not necessarily lead to armor unit breakage.
2. **Breakwater structure and armor layer settlement:** (a) T-LiDAR is an accurate and comprehensive method for monitoring changes in complex coastal structures such as those with concrete armor units; (b) Maintaining packing density around bends in structure and structure head as much as possible may limit the amount of unit movement and/or damage following construction; (c) Minor settlement and movement of armor units following construction does not affect the integrity of the structure.
3. **Concrete breakwater cap:** (a) Small-scale post-construction armor unit movement will not necessarily lead to concrete cap settlement or damage; (b) Stability of concrete cap can likely only be field-verified if a wave event causing overtopping of the structure is experienced.
4. **Armor layer toe stability:** (a) "Cannon" and "straddled" orientation of the first and second rows of CORE-LOC® toe units appears to be a successful placement scheme in this case; (b) Combination of traditional high-density survey methods augmented by visual observation techniques provided a thorough evaluation of underwater structure conditions.

Contents

Figures and Tables

Figures

Tables

Preface

The studies reported herein were conducted as part of the Monitoring Completed Navigation Projects (MCNP) program under MCNP Work Unit, "Kaumalapau Harbor, Hawaii, Breakwater Repair". Overall program management of the MCNP is provided by Headquarters, U.S. Army Corps of Engineers (HQUSACE), Washington DC. The U.S. Army Engineer Research and Development Center (ERDC), Coastal and Hydraulics Laboratory (CHL), Vicksburg, MS, is responsible for technical and data management, and support for HQUSACE review and technology transfer. The HQUSACE program monitor for the MCNP program at the time of this study was James E. Walker, Chief, Navigation Branch, HQUSACE. W. Jeff Lillycrop, CHL, was the ERDC Technical Director for Navigation. MCNP program Manager during the conduct of this study was Dr. Lyndell Z. Hales, Technical Programs Office, CHL. Dr. Jacqueline S. Pettway, was Chief of the Harbors, Entrances, and Structures Branch, CHL.

This research was conducted during the time period October 2005 – November 2010 under the general supervision of Thomas W. Richardson, former Director, CHL; and Dr. William D. Martin, present Director, CHL. MCNP Principal Investigators were Dr. Steven A. Hughes, CHL; and Jessica H. Podoski, U.S. Army Engineer District, Honolulu (POH). Research Team Members included Dr. Steven A. Hughes; Jessica H. Podoski; Thomas D. Smith, POH; and Dr. Jeffrey A. Melby, CHL, who developed the CORE-LOC™ armor unit at CHL. The monitoring plan for the study was developed by this team. This final report was prepared by Jessica H. Podoski and Thomas D. Smith.

Appreciation is extended to the following entities and persons for technical assistance in executing this study: (a) Sea Engineering, Inc., Waimanalo, HI; Scott Sullivan (breakwater repair design and construction summary), Jim Barry and Tony Ramirez (multibeam surveys and analyses), Monte Hansen (wave modeling and wave data collection), and Chris Goody (KPWAVE development); (b) U.S. Geological Survey, Remote Sensing and Visualization Center, Sacramento, CA; Gerald Bawden, Sandra Bond, Mike Shulters, James Howle, and Justin Brandt (Tripod LiDAR (T-LiDAR) data acquisition and analyses); (c) Optech, Inc., Kiln, MS; Jimmy Green (T-LiDAR instrumentation support); (d) University of Hawaii, Pacific

Geospatial Positioning System (GPS) Facility, Manoa, HI; James Foster and Benjamin Brooks (GPS support); (e) University of Hawaii, Oceanography Department, Manoa, HI; Mark Merrifield and Jerome Aucan (Coastal Data Information Program (CDIP) wave buoy installation and maintenance); (f) University of California San Diego, Scripps Institution of Oceanography, LaJolla, CA; Julie Thomas (CDIP wave buoy installation, maintenance, and data processing); (g) Control Point Surveying, Inc., Honolulu, HI; (survey benchmark updates); (h) Bevilacqua Research Corporation, Vicksburg, MS, Edward O'Neil, and ERDC Information Technology Laboratory, Vicksburg, MS, Richard Haskins (CORE-LOC™ concrete testing and analyses); and (i) Ultimate Whale Watch, Inc., Lahaina, HI; Lee James (boat support during multiple research activities around Kaumalapau Harbor during this study).

At the time of publication of this report, COL Kevin J. Wilson was Commander and Executive Director of ERDC. Dr. Jeffery P. Holland was Director.

Unit Conversion Factors

Multiply	By	To Obtain
acres	4,046.873	square meters
cubic feet	0.02831685	cubic meters
cubic yards	0.7645549	cubic meters
degrees (angle)	0.01745329	radians
degrees Fahrenheit	(F-32)/1.8	degrees Celsius
feet	0.3048	meters
inches	0.0254	meters
miles (U.S. statute)	1,609.347	meters
pounds (force)	0.45359237	kilograms
pounds (force) per square inch	6.894757	kilopascals
pounds (force) per second	0.45359237	kilograms
pounds (mass)	0.45359237	kilograms
pounds (mass) per cubic foot	16.01846	kilograms per cubic meter
square miles	2.58999	square kilometers
tons (2,000 pounds, mass)	907.1847	kilograms

1 Introduction

1.1 Monitoring Completed Navigation Projects (MCNP) program

The goal of the Monitoring Completed Navigation Projects (MCNP) program (formerly the Monitoring Completed Coastal Projects (MCCP) program) is the advancement of coastal and hydraulic engineering technology. The program is designed to determine how well projects are accomplishing their purposes and how well they are resisting attacks by their physical environment. These determinations, combined with concepts and understanding already available, will lead to the creation of more accurate and economical engineering solutions to coastal and hydraulic problems, thus strengthening and improving design criteria and methodology, improving construction practices and cost-effectiveness, and improving operation and maintenance techniques. Additionally, the monitoring program will identify where current technology is inadequate or where additional research is required.

To develop direction for the program, the U.S. Army Corps of Engineers (USACE) established an ad hoc committee of engineers and scientists. The committee formulated the objectives of the program, developed its operation philosophy, its recommended funding levels, and established criteria and procedures for project selection. A significant result of their efforts was a prioritized listing of problem areas to be addressed. This is essentially a listing of the areas of interest of the program.

USACE offices are invited to nominate projects for inclusion in the monitoring program as funds become available. The MCNP program is governed by Engineer Regulation 1110-2-8151 (Headquarters, USACE (HQUSACE) 1997). A selection committee reviews and prioritizes the nominated projects based on criteria established in the regulation. The prioritized list is reviewed by the program monitors at HQUSACE. Final selection is based on this prioritized list, national priorities, and the availability of funding.

The overall monitoring program is under the management of the Coastal and Hydraulics Laboratory (CHL), U.S. Army Engineer Research and Development Center (ERDC), with guidance from HQUSACE. An individual monitoring project is a cooperative effort between the submitting District and/or Division office and CHL. Development of monitoring plans and

conduct of data collection and analyses are dependent upon the combined resources of CHL and the District and/or Division.

1.2 Project location and background[1]

Kaumalapau Harbor is a small barge harbor located on the southwest coast of the Island of Lanai (Figure 1.1). Lanai is the sixth largest island in the state of Hawaii, covering about 140 square miles with about two percent of the state's land area. The island has about 2,500 full time residents, most living in or around the island's only town, Lanai City. Almost the entire island is privately owned by Castle and Cooke, Inc., the third largest private landowner in the state.

Kaumalapau Harbor was constructed in 1925 by the Hawaiian Pineapple Company (Dole Company) for the export of pineapple, the island's primary product and business up until the early 1990s. The harbor is located in a small embayment providing a 10-acre berthing area with water depths of 20 to 60 feet (ft) (Figure 1.2). A breakwater was constructed in the 1920s extending toward the south from the northwest headland of the embayment. The original length of the breakwater was about 350 ft, with a crest elevation of +10 ft above Mean Lower Low Water (MLLW) or less. The breakwater was constructed of quarried stone and field stone from the island. Shore side facilities on the north side of the embayment in the lee of the breakwater include a 400-ft-long pier, sheds, and barge loading and unloading equipment.

In the early 1990s the growing of pineapple was terminated, two luxury resort hotels were built, and the island changed from an agricultural economy to an economy based on tourism. Primary use of the harbor changed from the export of pineapple to the import of fuel and goods to support the new economic base industry.

The original harbor was constructed and maintained by private interests, and current ownership of the surrounding land area resides with Castle and Cooke, Inc. and its subsidiary, Lanai Company, Inc. Ownership of 2.3 acres, including the existing pier and harbor backup area and the landward terminus of the breakwater, was transferred to the State of Hawaii in July 2000. The State Department of Transportation, Harbors Division, now operates the harbor as part of the statewide harbor system.

[1] This section is extracted essentially verbatim from Sea Engineering, Inc. and Group 70 International (2008).

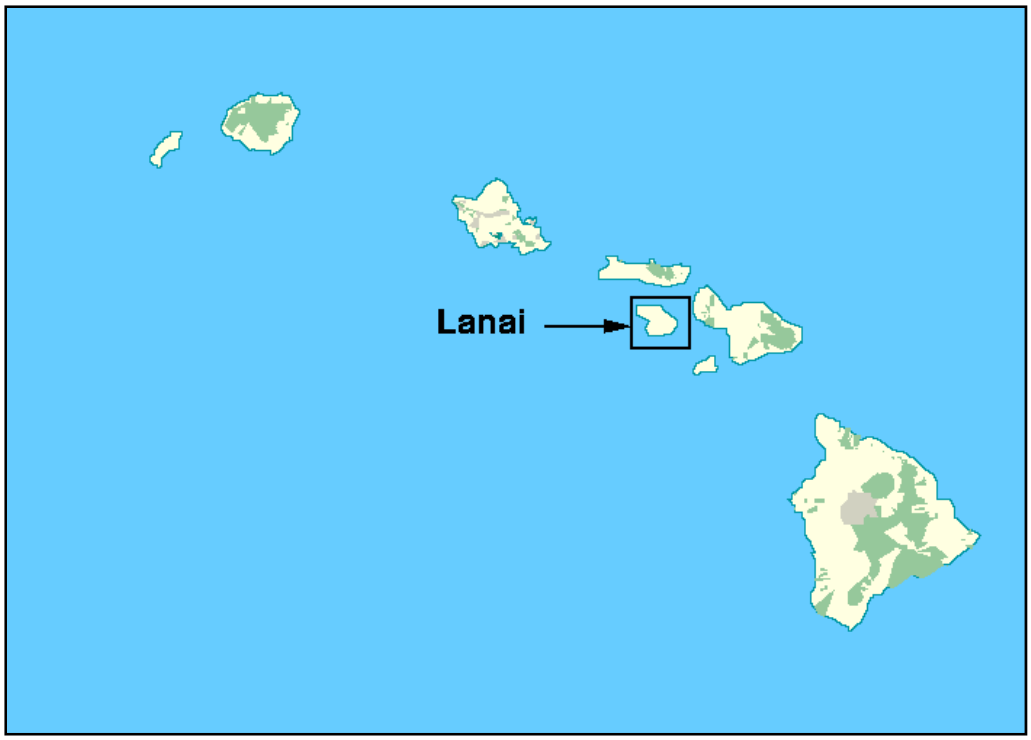

Figure 1.1(a). Hawaiian Islands, with Island of Lanai highlighted.

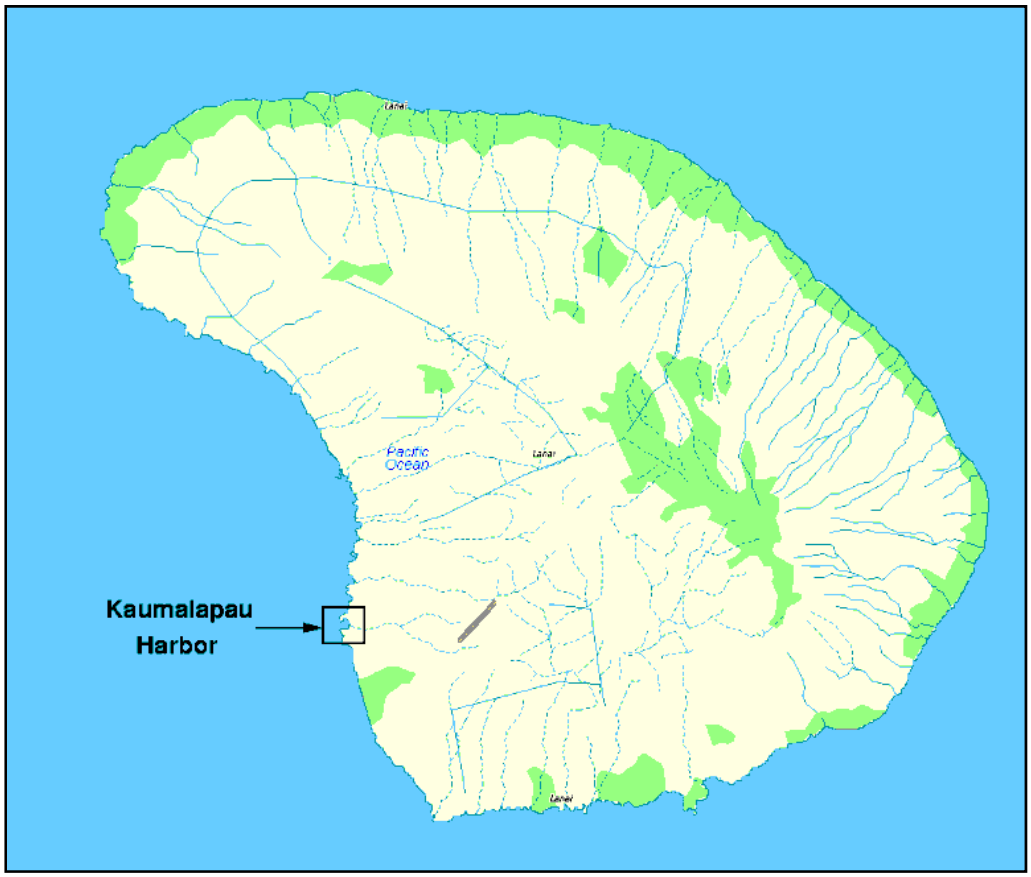

Figure 1.1(b). Island of Lanai, with Kaumalapau Harbor project area highlighted.

Figure 1.2. Kaumalapau Harbor barge landing and breakwater prior to 2007 repair.

The original breakwater structure may have been an "engineered" design, or it may have simply been a rubble mound constructed of a random mix of available stone. Even if it was an engineered structure, it would not have met the criteria required by modern breakwater design practice, nor would sufficient information regarding oceanographic design conditions have been available to the designer. The breakwater suffered extensive damage over the years, and has been repaired numerous times. A severe "Kona" storm resulting from a low-pressure front southwest of Hawaii damaged the breakwater significantly in January 1980, and Hurricane Iwa caused further damage in 1982.

1.3 Problem statement

Kaumalapau Harbor is Lanai's only commercial harbor and provides the only deep-water access point to the island. Maintenance of the breakwater appears to have been done using rock, concrete rubble, cut-off pile butts, concrete filled pineapple wagons, etc. Repairs were made using dolos concrete armor units; however, the armor unit size using existing forms available in Hawaii was apparently too small for the design conditions as the units were quickly broken and turned into concrete rubble. In 1992, Hurricane Iniki damaged the breakwater badly, and only a portion of the structure remained above water level. Seventy-five years of existence, storm

events, and repairs, resulted in a large, broad rubble mound, with a side slope of about 1 vertical on 1.5 horizontal. By the 1990s, the deteriorated condition of the breakwater permitted significant wave energy to reach the pier, resulting in berthed vessel motion that rendered cargo handling and fuel offloading difficult, and at times hazardous or impossible (Figure 1.3).

Figure 1.3. Deterioration of Kaumalapau Harbor breakwater prior to 2007 repair.

With exposure to storms arriving from the south through northwest, Kaumalapau Harbor was closing several times during each winter storm season. These storms had steadily damaged the breakwater structure with a loss of about half of its original 400-ft length. Waves had removed armor stone over the outer 200 ft of the structure to the point where the structure crest elevation was below the MLLW elevation.

As a direct consequence of the breakwater deterioration, more wave energy was entering the harbor, thus making loading and unloading operations problematic during some conditions. Local barge operators were using multi-ton ballast weights on the barges fore and aft to counter the harbor surge during loading operations. The situation worsened with continued deterioration of the breakwater, and during the winter of 1995 the fuel barge refused to dock in the harbor because of dangerous

conditions at the fuel pier. This caused serious concern about fuel availability on Lanai. The fuel shipper at that time decided to stop fuel delivery at the end of 1996 due to unsafe conditions in the harbor.

Cumulative damage to the Kaumalapau Harbor breakwater over the years resulted in nearly total failure of the breakwater armor layer both above and below the waterline. Project authorization and construction appropriation were provided by Congress, and non-Federal matching funds were received for repair of the structure. Because of the non-existence of stone on the Island of Lanai large enough to be stable under expected wave conditions at the site, it was necessary to manufacture concrete armor units to use in the rehabilitation of the breakwater.

1.4 Breakwater rehabilitation

The purpose of the Kaumalapau Harbor breakwater rehabilitation was to repair the existing breakwater to reduce wave action in the harbor, and increase harbor safety and usability. The breakwater was rebuilt on the footprint of the old rubble mound structure, and utilized the existing structure for the core of the new breakwater. The repair design was based on present day coastal engineering criteria, and oceanographic design parameters considered appropriate for the site and purpose of the structure.

Project design incorporated use of the largest CORE-LOC® (hereafter referred to as Core-Loc) concrete armor units (35 ton) ever placed on a Corps of Engineers structure. This was the first time that Core-Loc concrete armor units had ever been used to armor an entire breakwater. A 1-layer design would be used in deep water (up to 70-ft deep near the structure) under high wave conditions (up to 35 ft), on a steep slope (1 vertical to 1.5 horizontal).

A construction contract for repair of the breakwater was awarded on 9 July 2004, but a delay in the project forced a change in the construction schedule into a two-phase plan so that work could continue. Phase I was the casting of 817 Core-Loc armor units at the Barbers Point Harbor casting yard on the Island of Oahu. Phase II was reshaping of the existing structure base and placing the Core-Loc armor layer.

During 2005, the contractor fabricated Core-Loc forms and shipped them to the casting yard at Barbers Point Harbor on Oahu. The contractor initially had difficulty with the concrete mix design not meeting contract

specifications during the required testing of sample concrete specimens. These problems were resolved during the summer of 2005, but the delay meant that completion of Core-Loc fabrication extended into 2006, and the breakwater was not completed until June 2007.

1.5 Project aspects to be monitored by the MCNP program

The monitoring program for Kaumalapau Harbor breakwater was designed around the following hypotheses:

1. Settlement of the breakwater is expected as waves shift the armor units into a more compact matrix, but this settlement should not affect either structural integrity or project functionality.
2. A distinct correlation exists between concrete strength, Core-Loc movement, and armor unit breakage. If adequate strength is not achieved or excessive movement occurs, then breakage could be expected for very large Core-Locs.
3. Armor layer stability and long-term breakwater integrity depends critically on placement and stability of the toe units.
4. The breakwater concrete cap will remain intact and functioning correctly despite expected breakwater settlement.
5. The breakwater will reduce wave heights at the loading dock to acceptable levels for routine loading operations.

The four following aspects of the Kaumalapau Harbor breakwater rehabilitation project were proposed for monitoring under the MCNP program. The objectives of monitoring these aspects were to obtain sufficient data to address the above specific hypotheses related to project performance.

1.5.1 Core-Loc armor unit material strength and potential armor breakage

Little knowledge exists on Core-Loc material strength distribution over the unit, material strength increases with aging, and the relationship between Core-Loc strength, movement, and breakage. There are numerous examples in the literature of various concrete armor shapes breaking as a result of movement and/or inadequate material strength (Davidson and Magoon 1989). Examining individual armor unit strength, detailed structural response, and movement to correlate evidence of cracking or breakage of units is useful for developing improved concrete mixture designs and detailed guidance on armor construction.

1.5.2 Breakwater structure and armor layer settlement

Quantifying structure and armor layer settlement as a function of time and spatial location on the structure has never been done for a Core-Loc structure. Monitoring data would give insight into the relationship between packing density and settlement. The number of armor units monitored and their locations, and the timing and frequency of monitoring, are important parameters related to monitoring costs.

1.5.3 Concrete breakwater cap

The concrete breakwater cap was cast in place before initial settlement of the rubble mound, and it is important to judge how the cap and breakwater integrity is affected by armor layer settlement. The main purpose of the breakwater cap is to hold the structure crest together during severe wave overtopping events. Differential settlement of the rubble mound may fracture or dislodge portions of the cap that could then be carried away by strong storm waves.

1.5.4 Armor layer toe stability

Toe placement is expected to be critical to the success of the Kaumalapau breakwater rehabilitation, and USACE Honolulu District will be monitoring and documenting the underwater placement of the toe units. By augmenting the District's monitoring, sufficient data will be gathered to judge the success of the toe design and placement scheme. This information will be important for future application of Core-Loc armor layers, and it will allow assessment of the relationship between breakwater toe stability and armor layer settlement.

1.6 Kaumalapau Harbor breakwater monitoring plan

The monitoring plan for the Kaumalapau Harbor breakwater rehabilitation includes the following seven specific elements. Each element of the monitoring plan supports one or more of the four aspects presented above. The implementation of the plan as described below will be detailed in this report.

1.6.1 Core-Loc concrete strength measurements

A variety of structural stress measurements will be made during Core-Loc casting and after the units have been placed on the breakwater. During

casting, one Core-Loc unit will be provided by POH for destructive testing. Cores will be taken from this unit at selected times during the curing process, and on the 28th day of curing the unit will be loaded until fracture in tension occurs.

The data from the destructive test will provide calibration for ultra-sonic nondestructive testing methods that map the strength distribution throughout the armor unit. Poured cylinders from the same concrete mixture will be tested, and a sampling of cylinders will be placed in the water at Kaumalapau Harbor for subsequent testing at prescribed time intervals. After breakwater construction, selected in-situ armor units will be field tested using the nondestructive techniques to judge strength increase with age. These data will be correlated with fracture strength results obtained from breaking test cylinders being aged at the site.

The project aspect supported by this element is Core-Loc armor material strength and breakage.

1.6.2 In-Situ wave measurements

Breakwater settlement and Core-Loc armor movements are likely to be correlated to wave height and period. It is expected that the breakwater will experience the most settlement during the first year after construction, and it is imperative that local wave measurements are acquired during this first year. One uni-directional bottom-mounted wave sensor will be placed directly seaward of the breakwater to measure the local incident wave climate. These data will be correlated to armor layer settlement, and they will also be used to verify transformation of deepwater wave hindcasts to shallow water using a numerical wave model.

At least one bottom-mounted gauge will be located inside the harbor basin to measure the breakwater's effectiveness in damping waves that interfere with loading operations. These wave data will be compared to earlier numerical harbor wave simulations conducted in support of breakwater design.

Project aspects supported by this element include:

1. breakwater structure and armor settlement,
2. concrete breakwater cap,
3. armor layer toe stability, and
4. Core-Loc armor material strength and potential armor breakage.

1.6.3 Wave hindcasts and transformation

A lookup table for relating offshore wave hindcasts to near-structure wave conditions will be developed. Commercial deepwater wave hindcasts for the period coinciding with field wave gauging will be transformed into shallow water using a numerical wave transformation model. Transformed results will be compared to measurements obtained near the breakwater during the first year of monitoring. Verification of the methodology will permit a better correlation between settlement, possible breakage, and wave conditions in subsequent years when nearshore wave data are not being collected. This task will also serve as a case example for similar monitoring efforts by quantifying differences between transformed hindcasts and measured data. The hindcast data and the wave transformation lookup table will be placed into the eCoastal Geographic Information System (GIS) database.

Project aspects supported by this element include:

1. breakwater structure and armor settlement,
2. concrete breakwater cap,
3. armor layer toe stability, and
4. Core-Loc armor material strength and breakage due to movement.

1.6.4 Breakwater settlement measurements

Numerous methods are available for documenting breakwater settlement, including airborne laser digital terrain mapping, photogrammetry, Global Positioning System (GPS), and conventional surveying. The benefits, costs, and drawbacks of the various systems will be compared, and a methodology will be selected before the first survey. This information will provide much needed insight into how concrete armor layers nest in the first few years after construction, and how settlement affects armor layer stability, and armor unit breakage.

Project aspects supported by this element include:

1. breakwater structure and armor settlement, and
2. Core-Loc armor material strength and potential armor.

1.6.5 Armor unit movement measurements

The measurement system used to document breakwater settlement will be precise enough to map movement of individual armor units. Movements may be the result of settlement, wave loading, impacts from adjacent units, or some combination of these factors. Examination of movement data in the context of known settlement and knowledge of wave exposure will reveal vital information that will lead to better breakwater construction. Relating observed breakage, should breakage occur, to movement distance will provide design guidance on allowable movement.

Project aspects supported by this element include:

1. concrete breakwater cap, and
2. Core-Loc armor material strength and potential armor breakage.

1.6.6 Toe stability monitoring

During construction, the Honolulu District plans to monitor placement for all the critical toe Core-Loc units using an underwater remotely-operated vehicle (ROV) fitted with video cameras. Each unit must be positioned accurately and oriented as per plans. The MCNP monitoring will support the Honolulu District to conduct follow-on underwater surveys using the ROV to determine if the toe units have remained undisturbed. If any units have become dislodged, the settlement and breakage data will be examined to see if failure of the toe unit has led directly to problems upslope.

Project aspects supported by this element include:

1. breakwater structure and armor settlement, and
2. armor layer toe stability.

1.6.7 Breakwater inspections

At prescribed intervals after construction (or immediately after major storm events), visual inspections of the breakwater will be conducted to locate and document any broken Core-Loc units, identify displaced units, and assess the overall structural condition of the breakwater. These inspections will be concurrent with other monitoring activities, and spot measurements will be taken for ground-truthing the technique used to measure breakwater settlement and armor unit movement. Inspections

will be made of the concrete cap to determine if breakwater settlement has affected the functionality of the cap.

Project aspects supported by this element include:

1. breakwater structure and armor settlement,
2. concrete breakwater cap,
3. armor layer toe stability, and
4. Core-Loc armor material strength and potential armor breakage.

1.7 2006 through 2010 monitoring activities

The following chapters describe the detailed monitoring activities that were conducted at Kaumalapau Harbor between fiscal years 2006 and 2010 as part of the MCNP program. In addition, a discussion is provided that includes the conclusions drawn from analysis of the data collected, as well as the implications of the monitoring results in terms of the original project elements designated for monitoring, and the associated lessons that may be learned and applied to future comparable navigation projects.

2 Breakwater Design Elements[1]

Based on results of numerical modeling and three-dimensional (3-D) breakwater stability and harbor response small-scale physical model tests conducted at ERDC/CHL in 1994-1995 (M&E Pacific, Inc. et al. 2002, Smith 1998), the breakwater alignment was designed for a best-fit position on the existing rubble mound, with the head of the breakwater in the approximate location of the dogleg configuration tested in the physical model studies. The crest extends from shore 100 ft toward the south-southwest (azimuth 210 deg from north), then makes a 44 deg turn landward and extends 220 ft to the south-southeast (azimuth 166 deg). The total crest length is 320 ft, and the toe of the new breakwater terminates at the previous location of the "Green" channel navigation buoy. Note that there are two configurations of the Core-Loc unit, Core-Loc I with chamfers in the central section and Core-Loc II with fillets in the central section. All of the pre-2002 investigations for this project were done with Core-Loc I.

The existing rubble mound was excavated and shaped to form the core of the new breakwater. Excavated material was used as core material for the breakwater head, and as stone for a harbor side toe berm. Underlayer stone weighing 2.5 to 4.5 tons was salvaged from the existing structure to the maximum extent possible, and necessary supplemental stone was barged to the project site from the Island of Molokai (Figure 2.1).

2.1 Crest elevation, crest width, and side slope

The crest cap elevation is +14.5 ft MLLW, and provides for no overtopping during all prevailing wave conditions when the harbor can reasonably be expected to be operating, and only minor overtopping during typically occurring storm wave conditions. Portions of the Core-Loc units randomly extend about 5 to 6 ft above the crest cap. The crest width is 40 ft at the top of the underlayer stone (+9.5 ft MLLW elevation) as shown in Figure 2.1, which permitted use of a ringer crane for construction.

[1] This section is extracted essentially verbatim from Sea Engineering, Inc. and Group 70 International (2008).

Figure 2.1. Breakwater underlayer prior to placement of Core-Loc armor layer.

A horizontal row of Core-Loc units was placed on the ocean side of the crest to improve armor stability and energy dissipation during wave overtopping conditions. It was not considered practical to construct a non-overtopping structure for the very infrequent extreme storm wave conditions to which the breakwater could possibly be subjected. The sheer size of such a structure would not fit the physical confines of the project site, and the cost would have been prohibitive. In addition, there are limited harbor facilities that would be damaged by wave overtopping. The breakwater has been designed to be stable under probable significant wave overtopping conditions.

The ocean side and harbor side breakwater slope is 1 vertical to 1.5 horizontal.

2.2 Toe depth and configuration

On the ocean side, the landward end of the breakwater toe was placed in a 4-ft-deep toe trench excavated into hard rock, and then secured by filling the trench with tremie concrete. This extends for approximately 100 ft, at which point the toe transitions down the existing bottom slope to a toe

trench excavated into the existing rubble mound at the -44 ft MLLW depth. The Core-Loc was placed over underlayer stone in the toe trench, and buttressed by a 15-ft-wide stone berm, with a depth of 41.5 ft below MLLW. The 15-ft-width of the toe berm also aids in stabilizing the structure during possible seismic (earthquake) loading conditions.

On the harbor side, the toe extends into a toe trench excavated into the existing rubble mound at a depth of 20 ft MLLW, and is buttressed by a 30-ft-wide stone berm at a depth of 15 ft MLLW.

2.3 Armor layer

The two dimensional (2-D) breakwater stability model study conducted at ERDC/CHL in 2001 (Smith 2001) recommended that one size of armor unit, the 34.6-ton Core-Loc unit, be used to construct the Kaumalapau Harbor breakwater repair. The model results indicated that this size Core-Loc appeared to be stable with no damage for waves up to 35 ft and periods of 12 and 16 sec, when ocean side toe units were placed at a depth of 45 ft MLLW. The model results did show significant rocking in place during waves 25 ft and higher.

The final design of the armor layer consists of 35-ton Core-Loc concrete armor units, placed in a random matrix and oriented to achieve maximum interlocking. A detailed Core-Loc placement grid pattern was developed and specified to ensure that the desired packing density was maintained. A packing density coefficient of $\phi = 0.58$ was considered to be the tightest placement that could realistically be achieved with such large units. This was revised to $\phi = 0.62$ during construction after a change was made to use Core-Loc II rather than Core-Loc I and additional placement testing was accomplished. Here, the packing density is defined as $N/A = \phi V^{-2/3}$, where N/A is the number of units per unit slope area, ϕ is the packing density coefficient, and V is an armor unit volume.

The placement grid specified a precise x, y, z coordinate (position) for each Core-Loc unit. The placement pattern also considered the physical reality of placing 35-ton, 13-ft-long armor units, and makes minor adjustments to the toe elevation and toe trench widths to permit proper unit placement. The placement grid was based both on the hydraulic considerations of stable toe depth (as determined in the 2-D model tests), and on achieving a uniform top surface with Core-Loc termination at the crest to maximize stability during design wave overtopping conditions.

2.4 Concrete crest cap

The initial breakwater design utilized a concrete “rib” cap to buttress the top row of Core-Loc units. The rib cap concept has been developed and utilized on several breakwater projects in Hawaii involving large concrete armor units. The rib cap was cast in place, and fastened in place by dowelling the cap into the large cap stones underneath, with the ribs formed around the armor units. The primary purpose for utilizing a rib cap design is its porosity, and thus its ability to vent and relieve uplift forces during storm wave attack. The rib cap design also reduces the volume of concrete required.

The rib cap design, however, was not modeled accurately in either the 2-D or 3-D model tests such that its performance could be evaluated. In the 2-D stability tests, the model rib cap was actually fastened to the sides of the flume to hold it in place. It was noted in the 2-D tests that the settlement and consolidation of armor units on the breakwater slope would result in exposure and loss of underlayer stone and core material from beneath the rib cap. In addition, the breakwater repair design did not utilize large capstones on the crest on which the rib cap could be constructed and fastened. In fact, the underlayer stone was approximately the same size as the rib spacing. Given that there would be significant overtopping during design storm wave conditions, there was concern about loss of stone from around and under the rib cap, and possible movement of the cap itself. Should the Core-Loc units shift away from the crest rib cap, exposing underlayer stone that could be removed by wave action, the stability of the rib cap and crest Core-Loc units could be in jeopardy.

To improve the durability of the crest, the final design utilized a solid mass non-reinforced concrete crest cap to better contact and buttress the Core-Loc units, and to contain the underlayer stone on the crest. On the ocean side, the crest was positioned such that the front edge has minimal exposure to wave uprush and pressure within the stone underlayer, and a horizontal row of Core-Loc units was placed on the underlayer stone crest fronting the concrete crest cap to help further dissipate overtopping wave energy. The crest cap was then formed completely around the Core-Loc crest units.

The 5-ft-thick, nominal 25-ft-wide crest cap was cast in 15-ft sections, with shear keys between each section and a continuous key into the breakwater crest along the axis of the breakwater. The cap weighs about 9 tons per lin ft, and 135 tons per 15-ft section.

A summary of final design parameters and dimensions is shown in Table 2.1. Figures 2.2 and 2.3 show the final breakwater repair plan and typical sections.

Table 2.1. Breakwater design parameters and dimensions. (Sea Engineering, Inc. and Group 70 International 2008)

Crest	Elevation:	+14.5 ft MLLW (top of concrete cap)	
	Width:	Approx. 25-ft clear width across concrete cap between ocean and harbor side Core-Locs. 40 ft wide across top of underlayer and core stone at +9.5-ft elevation.	
	Type:	Solid mass concrete cap, 5-ft thick, unreinforced, formed around top row of Core-Loc units.	
Side Slope	1V:1.5H		
Armor Layer Toe	Ocean Side: Sta. 0+00 to (-)1+00:	Elevation	4 ft below existing hard bottom
		Buttress	Toe Trench with Tremie Concrete
	Sta. 0+00 to 2+20:	Elevation	-45 ft (trunk and head)
		Buttress	15-ft wide stone berm
	Harbor Side:	Elevation	-20 ft
		Buttress	30-ft wide stone berm
Armor Layer	Type	Concrete Core-Loc	
	Weight	35 tons	
	Placement	Single layer, random orientation, individual unit position specified by a x, y, z coordinate placement grid to achieve ϕ= 0.57 (revised to 0.62).	
Underlayer	Material	Stone (Quarried and Salvaged)	
	Weight	2.5 to 4.5 tons	
	Placement	Layer thickness of 7 ft	
Core	Material	Salvaged stone and concrete rubble	

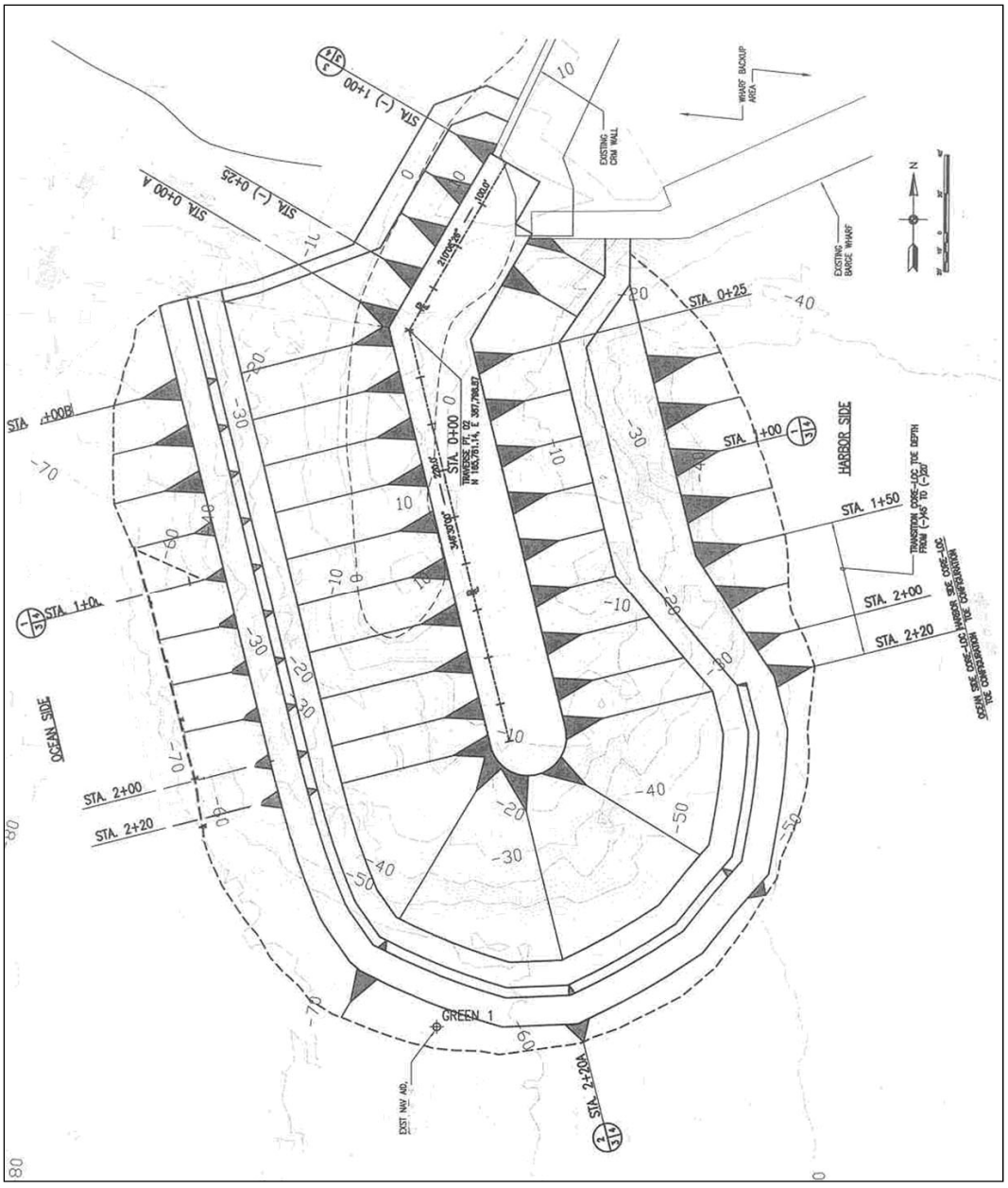

Figure 2.2. Kaumalapau Harbor breakwater rehabilitation plan (U.S. Army Engineer District, Honolulu 2003).

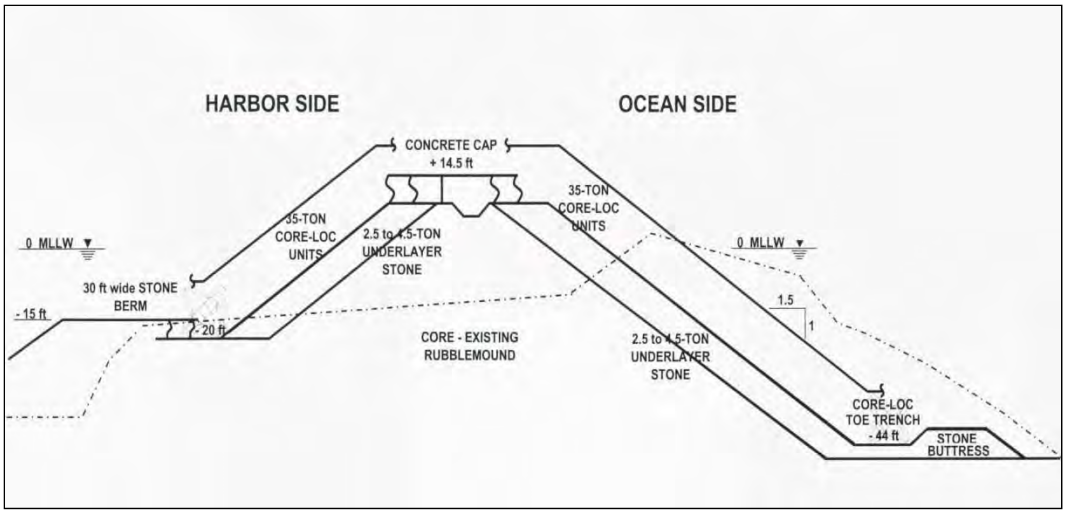

Figure 2.3. Typical Kaumalapau Harbor breakwater cross-section, Sta. 0+00 to Sta. 2+20 (Sullivan and Werren 2003).

3 Core-Loc Design Considerations[1]

3.1 Core-Loc shape

A structural strength study of the 35-ton Core-Loc I was conducted in 2002 for the Kaumalapau project (Melby 2002). The study included finite element analyses and small scale physical model structural measurements. The study concluded that the factor of safety for structural strength was insufficient, and recommended increasing the strength and changing the central shape from chamfers to fillets to avoid stress concentrations. Honolulu District decided to only increase the concrete strength but not use the modified shape at that time.

As design of the Kaumalapau Harbor project was proceeding, another project to rehabilitate a breakwater protecting a U.S. Navy pier in the Azores Archipelago was initiated with nearly the same size Core-Loc I units. The project was to be implemented in phases, with an initial emergency repair that was to be later removed and replaced with a final engineered armor layer. The emergency repair was initiated with non-buttressed Core-Locs that were subsequently displaced by a large storm. A number of these units were broken. An investigation of these units by ERDC engineers from CHL and Geotechnical and Structures Laboratory (GSL) (Mlakar 2005) suggested that the material strength and the distribution of material strength throughout each individual unit was inadequate and perhaps was not to specification. The study suggested that the large Core-Loc I units require an additional factor of safety with respect to strength to allow for material strength variabilities. Unfortunately, there was not adequate time to investigate these issues thoroughly because the Kaumalapau project was underway.

This led the Honolulu District to decide to improve the structural factor of safety through the use of the filleted unit from Melby (2002). The unit shape was refined for this project and called Core-Loc II. The shape changes were principally made to add larger radius fillets in the chamfer regions at the intersection of the Core-Loc legs, and to thicken the center section to accommodate the fillet. This reduced stress concentrations at the interior of the flukes on the units. A filleted edge replaced a chamfered edge. The new

[1] This section is based primarily on Sea Engineering, Inc. and Group 70 International (2008).

Core-Loc shape is more "compact"; i.e. for Core-Loc I and II units with the same mass, the characteristic length, "C" (leg length), is shorter on the Core-Loc II.

No hydraulic model tests were done to determine the performance of the Core-Loc II, and the assumption was made that hydraulic stability performance would be similar to the Core-Loc I. Thus, the hydraulic stability would be similar at the same total weight (35 tons); and therefore, the "C" dimension was adjusted to obtain the 35 ton weight with the new unit. The "C" dimension changed from 12.9 ft for the Core-Loc I to 12.6 ft for the Core-Loc II. This increased the packing density coefficient from $\phi = 0.57$ to 0.62. The final design Core-Loc II and dimensions are shown in Figure 3.1.

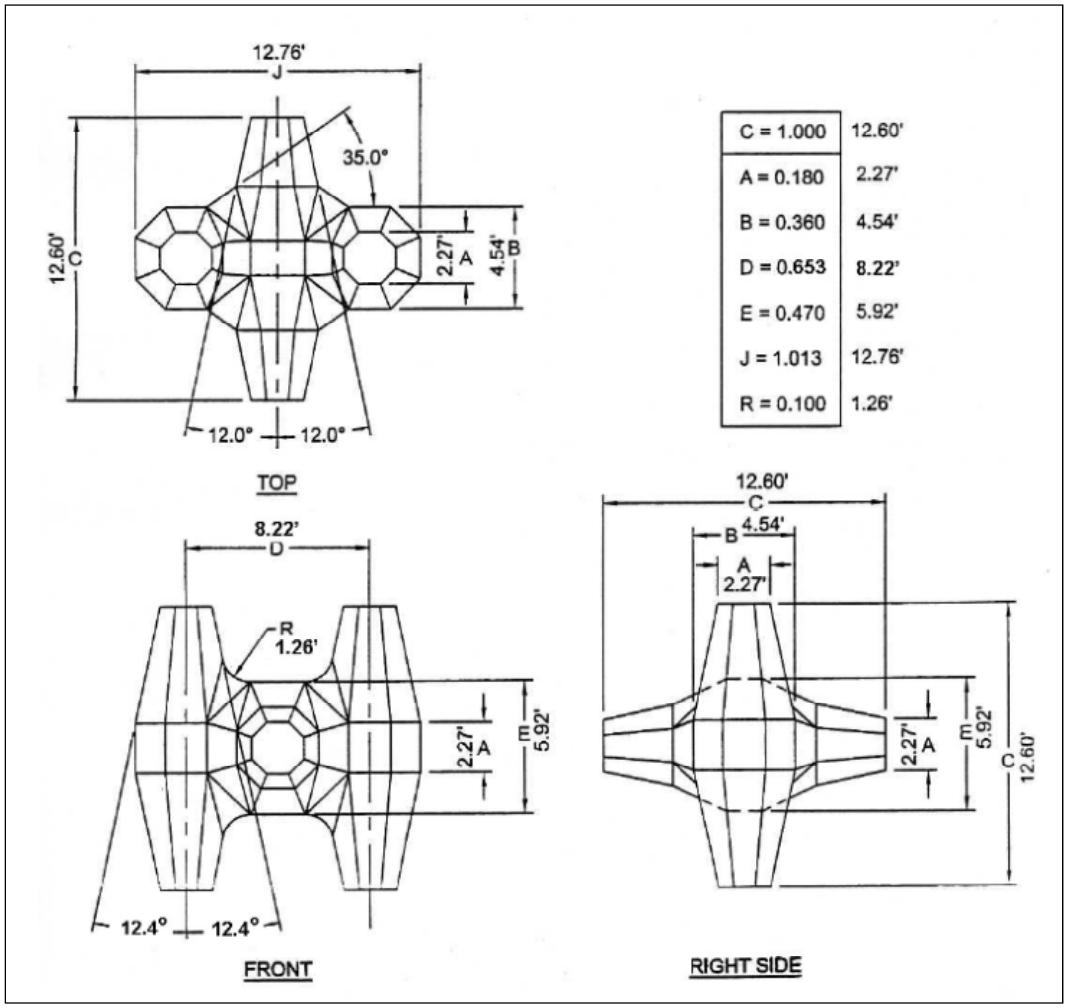

Figure 3.1. Core-Loc II unit shape and dimensions used on Kaumalapau Harbor breakwater rehabilitation.

3.2 Core-Loc packing density and placement

A sufficient packing density must be achieved to provide adequate and uniform coverage on the breakwater slope, and to maintain unit-to-unit interlocking and contact. This is particularly critical for concrete armor units in a single layer configuration.

As noted previously, packing density is defined as N/A, the number of individual units required to cover a given area of slope, and is related to the volume of the unit. In general, the larger the unit becomes, the lower the practicable achievable packing density. Larger units become more difficult to handle, which limits the ability to pack them together, and the concrete crushes where they contact, increasing friction and making them "sticky" so they do not slip together as easily as lighter units.

Initial testing of the Core-Loc by ERDC/CHL (Smith 1998) showed stable structures built with ϕ ranging from 0.54 up to 0.64, with 0.60 generally recommended. Hydraulic model studies conducted for the Kaumalapau Harbor breakwater project used a $\phi = 0.62$. Subsequent flume tests of breakwater stability used a $\phi = 0.58 - 0.59$ (Smith 2001). In the initial Kaumalapau breakwater design, $\phi = 0.58$ was used to prepare the placement plan.

Following the Core-Loc shape change, and additional packing density experiments conducted by ERDC/CHL, Honolulu District, and Baird & Associates, the packing density coefficient was revised to $\phi = 0.62$ for preparation of the prototype placement plan. This packing density was estimated based on limited model scale test placement in a dry test box with various test grids and a string and quick release system used to simulate placement by crane. This is a high coefficient for units weighing 35 tons; however, the contractor was able to achieve it during construction of the Kaumalapau Harbor breakwater project.

Core-Loc was designed to be placed in a single layer thickness in a random placement. The specified packing density must be strictly maintained during construction to assure proper interlocking between units to achieve the desired hydraulic stability. For the Kaumalapau project a Core-Loc placement plan was specified, with each unit being assigned a specific x, y, z coordinate for its location on the structure. To ensure that each unit would be placed in its specific x, y, z location, the contractor was required to build a table-size physical model of the structure and place scaled-size Core-Loc

units on the scaled breakwater structure (Figure 3.2). As placement of the units proceeded from the lower elevations to higher elevations on the structure, fewer and fewer units would be needed in a row. Hence, around the head of the structure, adjusted placement was necessary to get the correct number of units on the structure at the prescribed packing density. A total of 817 scale-size Core-Loc units were required for the model, the same number as ultimately placed on the breakwater.

Figure 3.2. Contractor scale-model of Kaumalapau Harbor breakwater and Core-Loc armor units.

3.3 Core-Loc orientation and interlocking

Although Core-Loc units can be placed randomly along the toe, a uniform pattern placement has been shown to be more stable if it can be achieved in the field. The Kaumalapau construction plans specified that the Core-Loc toe units be placed in the toe trench in a “cannon style” pattern placement. The first course was set with the central fluke pointing seaward at a 45-degree (deg) angle like a cannon barrel, and were placed side-by-side with a minimal space between adjacent units. The second course was placed such that they straddled the first course toe units. Subsequent armor units moving up the slope to the crest were placed in a random matrix and oriented to achieve maximum interlocking. The typically very

clear water at the project site facilitated greatly the placement of the toe units in a uniform pattern, and permitted camera and diver placement verification prior to the placement of subsequent units.

The specifications for Core-Loc placement also included requirements for building a test section of the Core-Loc placement on land. Constructing with 35-ton armor units is not easy, and errors in prototype construction can be costly and time consuming. Thus, a test section of the Core-Loc placement on land was required prior to starting work on the actual breakwater (Figure 3.3). This gave the contractor a chance to practice slinging units and an understanding of unit attitude variation to facilitate interlocking, and practice adhering to a precise placement plan prior to placing units underwater.

Figure 3.3. Test section constructed on land showing approximation of actual toe trench, and non-random "cannon" orientation (lower row) and "straddled" orientation (upper row) of structure toe Core-Loc armor units.

The combination of random unit orientation and precise positioning proved a challenging task during construction. However, by first placing test sections on land and then devoting a significant amount of time and effort into positioning the several dozen initial units placed along the ocean side

root of the structure, the contractor was able to become proficient at following the placement plan. The contractor again encountered difficulty in achieving both satisfactory random placement of units and precise positioning when placing Core-Locs along the rounded head of the breakwater, and some adjustments to the placement plan in this area were required. However, adherence to the original plan was regained when the contractor continued placement along the straighter interior side slope of the structure.

Placement of Core-Loc units on the slope was based on the following parameters.

- Maintain the specified packing density by insuring that each unit is placed at its specified location according to the placement plan, with the centroid of each unit being within 15 in. of the specified location. Care must be taken to avoid small error "creep" in the placement of individual units which may be additive, eventually resulting in being unable to place the units at their specified location.
- Moving up the slope, successively higher units should be "keyed" into and between two units below (i.e., fit the higher Core-Loc into the "pocket" between two adjacent lower units). Keying into the lower units should result in contact between at least one, and usually both, of the lower units. The keying into and between the lower units also results in units on the same horizontal row not being in contact.
- Every Core-Loc unit must rest on and contact the underlayer stone.
- The units shall be placed randomly, with different attitudes so as to interlock with and contact adjacent units to the maximum extent practicable. Every reasonable effort should be made to rotate and adjust the individual unit orientation so as to achieve the best interlocking and contact possible. However, it is recognized that interlocking and contact will vary, and that every unit may not have direct contact between all adjacent units.
- Effort should be made to not place units with an H-member parallel to the slope, and less than one-third of the units shall be oriented this way, and they should be scattered throughout the structure and not placed in groups.

3.4 Core-Loc formwork and concrete

The formwork specification was essentially a generic pre-cast concrete armor unit steel form specification, written to insure the adequacy and

suitability of the forms for their intended purpose of casting 35-ton Core-Loc units (Figure 3.4). The specification stated that forms shall not be removed from the Core-Loc within 24 and 72 hr after casting for non-supporting and supporting forms, respectively. A provision was made to permit earlier removal of the forms provided that a structural analysis of concrete strength was made to show that the concrete in the forms had compressive and flexural strength sufficiently higher than the minimum required for form removal. The Kaumalapau contractor did not elect to remove any forms early.

Figure 3.4. Insulated formwork for casting 35-ton Core-Loc armor units.

The specified flexural strength of the Core-Loc concrete was 700 psi at 28 days. The maximum allowable water/cement ratio was 0.40 by weight, and the total air content could not exceed 5 percent. Particular attention was given to the concrete temperature during curing. At no time could the temperature of the concrete exceed 165 degrees Fahrenheit (°F), and the maximum temperature differential between the interior and exterior concrete could not exceed 36°F. Portland Type II low alkali cement was specified. Pozzolan, if used, had to be fly ash conforming to the requirements of ASTM C 618, Class F. (Pozzolan is not used commonly in Hawaii, and was not used for this project.) Fiber reinforced concrete was specified,

in accordance with ASTM C 1116, Type III, synthetic reinforced concrete, with 7.5 pounds (lb) of structural fibers per cubic yard (cu yd) of concrete (forta fiber or equal). The concrete-placing temperature was not permitted to exceed 85°F, which basically necessitated that the contractor cast the Core-Loc at night (Figure 3.5).

Figure 3.5. Casting concrete Core-Loc armor units at night for better temperature control.

In addition, to meet the concrete curing temperature requirements, the contractor used a significant amount of water in the form of ice in the mix. The concrete mix resulted in a concrete unit weight of 150 lb per cubic foot (cu ft). These stringent temperature requirements necessitated that the Core-Loc concrete forms be encased in insulated plywood curing boxes to ensure that the actual temperatures during curing did not deviate beyond the contract specification limits (Figure 3.6).

Figure 3-7 shows a portion of the Core-Loc armor units after removal from the forms at the Island of Oahu casting yard, and prior to transport by barge to Kaumalapau Harbor breakwater construction site on the Island of Lanai.

Figure 3.6. Insulated plywood curing boxes encasing the Core-Loc concrete forms to maintain contract temperature specifications limits.

Figure 3.7. Core-Loc armor units awaiting transport to Island of Lanai.

4 Core-Loc and Cap Placement on the Breakwater

The Core-Loc concrete armor units were cast on the Island of Oahu, and then transported by barge to Kaumalapau Harbor on the Island of Lanai. There was no available room for storage of the units at the breakwater construction site as they arrived by barge, so they were carried to a storage yard approximately one-quarter mile from the construction site (Figure 4.1). The units then had to be re-transported by truck from the storage yard to the construction site as required for placement on the breakwater (Figure 4.2).

4.1 Contractor's general methodology[1]

On-site construction was accomplished primarily by one piece of heavy equipment, a Manitowoc 2250 crane that was used to shape the existing rubble mound to form the core, place all the stone, and place the Core-Loc units (Figure 4.3). Ancillary equipment included a smaller Manitowoc 999 crane for handling of the Core-Loc units on the barge, and lowboy trailers used for moving Core-Loc units to and from the inland stockpile area. Any necessary supplemental underlayer stone for forming the core of the breakwater was obtained from a quarry site on the Island of Molokai and barged to Lanai. Suitable stone salvaged from on-site, as approved by the

Figure 4.1. Core-Loc units at the storage yard on Island of Lanai, awaiting transport to Kamalapau Harbor breakwater construction site.

[1] This section is extracted essentially verbatim from Sea Engineering, Inc. and Group 70 International (2008).

Figure 4.2. Core-Loc unit rigged for offloading at the breakwater construction site after being transported from the storage yard (Sea Engineering, Inc. and Group 70 International 2008).

Figure 4.3. Manitowoc 2250 crane, primary equipment used to rehabilitate the breakwater.

Honolulu District, was also utilized in the construction. Positioning for survey of the lines and grades of the core and underlayer, and precise positioning of the Core-Loc units, was accomplished by using a Novatel Propak L1L2 Real Time Kinematic (RTK) Differential GPS (DGPS) Base Station OEM4, and a Rover OEM4 Receiver with an antenna mounted on the crane boom head, outputting to Winops Positioning Software.

4.2 Toe trench construction[1]

The Core-Loc toe trench at a depth of -44 ft MLLW on the ocean side was constructed of 2.5- to 4.5-ton underlayer stone. The required cannon style Core-Loc toe unit placement necessitated careful and uniform placement of the units so that they provide a solid foundation for the armor layer. Gaps between the large underlayer stone could be as big as a Core-Loc fluke, and it was noted during construction of the test section on land that unit placement could be affected by gaps between stones. There was also concern that, even if breakwater toe units were placed solidly on stone but with a fluke near a gap between stones, the unit could shift slightly during loading as subsequent units were placed up the slope. This could result in a fluke slipping into a gap, with a greater movement and possible loss of contact occurring that was undesirable.

To eliminate this problem, the contractor recommended chinking (using graded stone to fill voids) the bottom of the trench between the large stones with 100- to 1,000-lb stone. This would provide a more secure and stable platform for the Core-Loc toe unit to rest on, and help ensure that a fluke was not inadvertently placed near a large void between trench stones. This was approved provided that:

1. The stone was well graded between the upper and lower size range so as to form a tight matrix.
2. No chinking stone was placed above the level of the trench stone elevation neat line so that the Core-Loc units rested primarily on the large trench stone.
3. No chinking stone would be placed seaward of the Core-Loc units so as to not effect interlocking of the second layer of 2.5- to 4.5-ton stone placed seaward of the Core-Loc units to form the seaward side of the trench and the toe buttress.

[1] This section is extracted essentially verbatim from Sea Engineering, Inc. and Group 70 International (2008).

It should also be noted that the construction plans called for the toe trench to be backfilled with 500- to 5,000-lb stone following Core-Loc placement. Thus, the chinking stone would be covered with larger stone. The purpose of the stone backfill was to further help prevent movement of the Core-Loc toe units.

4.3 GPS positioning of armor units[1]

The packing density specified for the armor units' size and shape required that a placement plan be developed, giving each unit a unique location (Figure 4.4). These locations were based on a horizontal coordinate system that is tied to benchmarks at the project site. The benchmarks are precisely set using a GPS, which incorporates satellites, ground base stations, and hand-held GPS receiving units. To place each Core-Loc in its specified location, a method was developed that included the use of a real-time kinematic GPS mounted at the top of the crane boom used to place the armor units. The substantial weight of the units caused them to hang directly below the GPS unit. This, in combination with position targeting

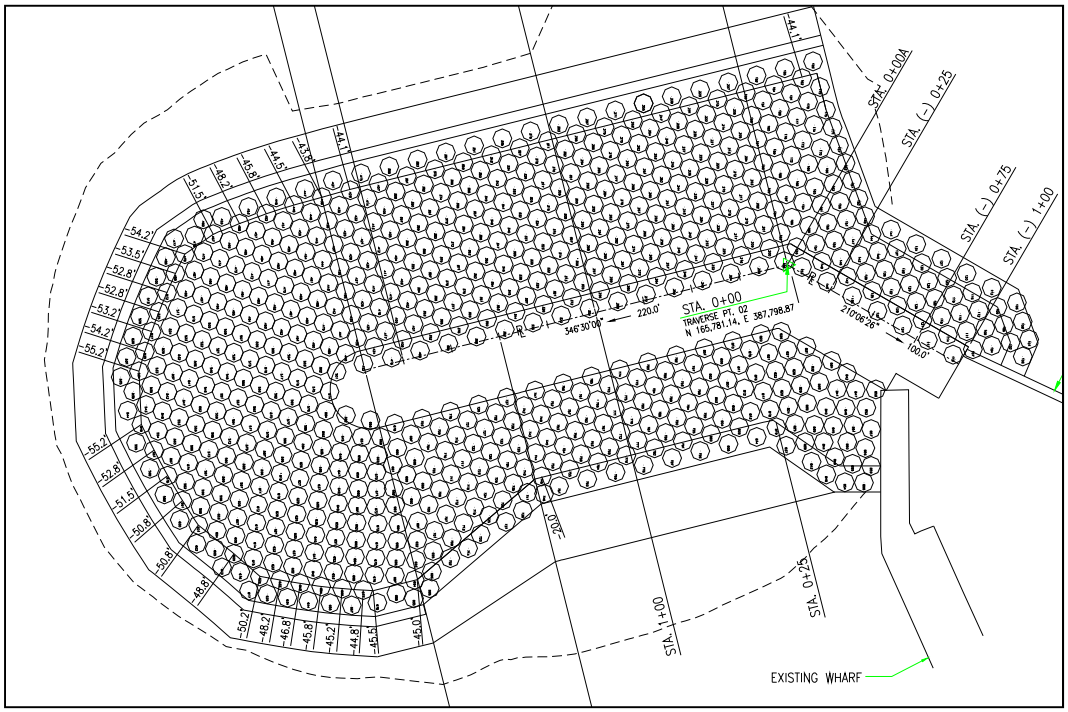

Figure 4.4. GPS horizontal coordinates of each Core-Loc unit placed on the breakwater, based on packing density coefficient of $\phi = 0.62$.

[1] This section is extracted essentially verbatim from Hays, Smith, and Sullivan (2006).

software, allowed the crane operator to place the center of each armor unit in its predetermined location. Although external factors such as wind and waves affect the precision with which the units can be located underwater, the accuracy achieved during the initial placement of armor units was within ± 15 cm of the target location. Placement of the armor units on the structure is shown in Figure 4.5.

Figure 4.5. GPS placement of Core-Loc armor units on Kaumalapau Harbor breakwater during rehabilitation.

4.4 Innovative Core-Loc placement techniques[1]

The importance of the orientation and interlocking of the armor units when placed required that the handling of the units be highly maneuverable. The use of a double-sling arrangement (Figure 4.6), as well as quick-release hooks on the slings, allowed the crane operator to have more control over each unit's stability during placement, and ensured that once a unit was in the correct position, the slings could be removed easily. The sling had three ways of wrapping around the unit. Thus, six different Core-Loc orientations could be achieved during the lifting operation.

[1] This section is extracted from Hays, Smith, and Sullivan (2006), Hays, Smith, and Hughes (2007), and Sea Engineering, Inc. and Group 70 International (2008).

Figure 4.6. Double-sling with quick-release hooks for placing Core-Locs on the breakwater.

The contractor developed a lifting frame from I-beams for the Core-Loc units to which the sling was attached (Figure 4.7), and for which the rotation could be controlled with tugger winches from the crane. The combination of different unit sling orientations and the ability to rotate the unit permitted a wide range of Core-Loc orientations to be achieved and maintained underwater. For the cannon style toe unit placement, two slings were used to maintain the proper uniform Core-Loc orientation.

It is extremely important that the Core-Loc units are placed at the correct grid locations. The use of a pre-determined placement plan with each unit assigned an x, y, z coordinate location assures that the units are placed at the right packing density on the slope, and that there are no unexpected voids or gaps between units. The placement grid is tied to the project coordinate system so that each unit can be presented to the slope at the correct x, y location. Correct underlayer stone lines and grades insure that the z (elevation) coordinate will be met at the respective x, y (horizontal) locations. The control is provided by the GPS positioning system that reports the precise location of the head-works of the crane. The GPS x, y location is fed into a computer at the crane controls, and with positioning software is overlain onto the placement plan. Using a targeting feature in

Figure 4.7. Lifting frame with tugger cables attached to double-sling for precise placement of Core-Loc units on the breakwater (Hays, Smith, and Sullivan 2006).

the software, the crane operator can position the head-works of the crane and, thus, the center of mass of the Core-Loc unit hanging directly below it, to the correct x, y location. Wind, waves (particularly long period swell), and currents caused the Core-Loc to move slightly around the position reported by the GPS antenna. The operator was able to compensate for these slight movements by use of overhead video cameras and on-site divers aiding with positioning and orientation.

The fact that the majority of this structure is underwater added an increased level of difficulty to armor unit placement. To provide the crane operator with a visual aid to orientation of the units, four cameras were placed around the edges of the lifting frame. The real-time video from the cameras was displayed on a 4-way split screen monitor inside the crane, showing the armor unit from four angles. This additional information improved the operator's ability to achieve the required orientation and interlocking of armor units. The lifting frame with the four camera mounts is shown in Figure 4.8, and a view of the split screen monitor in the operator cab is shown in Figure 4.9.

Figure 4.8. Lifting frame with four camera mounts.

Figure 4.9. 4-way split screen for operator control of orientation and interlocking of armor units.

An ROV camera similar to that shown in Figure 4.10 provided USACE construction officers with a way to inspect completed stages of underwater breakwater construction, and to verify adherence to specified tolerances. The ROV system can record video for a more detailed examination at a later date (Figure 4.11). However, divers greatly facilitated the underwater Core-Loc placement. It was a challenge to determine compliance with points of contact between adjacent units and the back-slope. Cameras mounted on

Figure 4.10. Underwater remotely operated vehicle (ROV) similar to that used to inspect stone and armor unit placement during construction.

Figure 4.11. Use of ROV for underwater structure inspection of stone underlayer.

lifting frame allowed the crane operator to have real-time information on unit orientation. But divers were still required to get unit orientation, especially canon units at the toe. Divers were used to:

1. Verify contact between Core-Loc units and the underlayer stone, and between adjacent Core-Loc units.
2. Release the lifting sling once the correct placement was verified.
3. Re-sling the Core-Locs if they had to be repositioned.

A diver with a helmet-mounted camera was used for final verification of correct Core- Loc placement before it was released from the sling (Figure 4.12). The diver was important particularly for placement of the cannon style toe units and the second row above them. The contractor used diver placement and verification assistance for almost all of the below water Core-Loc placement. The remote cameras worked well, and reduced the reliance on divers as well as providing visual observation as the units were being moved into position when it would have been too dangerous for a diver to be up close. However, the mobility of a diver and the ability to see close up was very important to be sure the unit interlocking was optimized and that the required contact between adjacent units and the underlayer stone was maintained for every unit placed.

Figure 4.12. Operator view of underwater placement of Core-Loc unit from a diver camera.

Six armor units were broken during placement operations and had to be removed from the armor layer. However, all six broken units were later placed on the harbor side of the breakwater at the tie-in to the barge pier due to the fact that full-size units would not fit in this area, and wave energy expected in this location is significantly less than on the rest of the structure.

4.5 Concrete crest cap construction[1]

The concrete crest cap was constructed in segments, beginning from the breakwater head and proceeding landward. The segments were to be 10 ft long initially; however, the contractor requested approval to pour them in 15-ft lengths to optimize the use of the batch plant production capability. Figure 4.13 shows a crest cap segment being prepared. Note the shear key female halves cast in the end of the previous segment, and the 3-ft-deep key trench excavated into the crest core material. Heavy wire mesh fencing material lined with geotextile filter fabric was used as the flexible formwork around the Core-Loc crest units, and between the crest units and the cap.

Figure 4.13. Breakwater crest cap segment being prepared, showing 3-ft-deep key trench into core material (Sea Engineering, Inc. and Group 70 International 2008).

[1] This section is extracted essentially verbatim from Sea Engineering, Inc. and Group 70 International (2008).

This worked very well as it could be made to conform easily to the varying contours of the Core-Loc units, and it could be made to project into gaps between units. The mesh was held in place by a steel cable system until the concrete cured, and then any mesh and cables projecting above the concrete were cut off. The completed cap is shown in Figure 4.14.

Figure 4.14. Completed breakwater crest cap.

A view of the harbor side of the completed breakwater Core-Loc placement is shown in Figure 4.15. The head of the completed breakwater is shown in Figure 4.16. The construction contract was awarded in July 2004. Following delays due to construction funding issues and a revision to the design of the Core-Loc armor unit, construction was completed in June 2007. The actual on-site construction work took about 18 months.

Figure 4.15. Harbor side of completed Kaumalapau Harbor breakwater rehabilitation with Core-Loc armor units (photo taken by Traylor Bros, Inc.).

Figure 4.16. Completed Kaumalapau Harbor breakwater from above, with container barge moored at pier (photo taken by Traylor Bros, Inc).

5 Testing and Analysis of a Core-Loc Unit[1]

Non-destructive and destructive testing of one 35-ton Core-Loc concrete armor unit purchased from the normal production run of armor units being cast for the Kaumalapau Harbor breakwater was performed during September 2006 by representatives from the ERDC Geotechnical and Structures Laboratory and Bevilacqua Research Corporation. The tests were conducted at the Grace Pacific Corp. casting yard on the Island of Oahu.

The objective of the testing was to gather non-destructive material property data on the armor unit, and to determine the tensile load needed to break one of the legs of the unit from the rest of the body. These data were meant to further knowledge of the structural and materials properties of Core-Loc armor units in general, and specifically those units being used for the Kaumalapau breakwater repair. A design change was made to the shape of the saddle area of the Core-Loc in early 2006, and these tests were conducted to evaluate the new Core-Loc II armor unit shape, as well as to gather further information on the concrete mix design used for these armor units. It was also hoped that the testing would provide further information on the relationship between the compressive and tensile flexural strength of the concrete (as determined by standardized testing practices and dictated in the contract specifications) and the tensile flexural load required to break a leg of the armor unit. The Core-Loc terminology is defined in Figure 5.1.

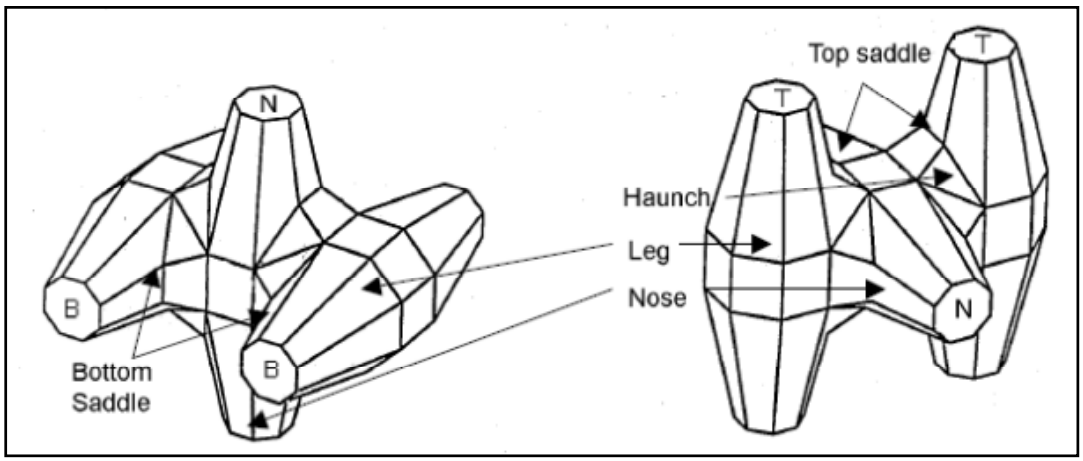

Figure 5.1. Core-Loc terminology (O'Neil and Haskins 2008).

[1] This chapter is extracted from O'Neil and Haskins (2008), with some additions and modifications for clarity.

5.1 Non-destructive testing using pulse-velocity measurements

The purpose of the pulse-velocity measurements was to obtain a record of the length of time it took for a sound wave to travel through the concrete at various chosen locations. Typically, these arrival times are converted to velocities. These speeds are an indicator of the quality and material properties of the concrete, and can be correlated to concrete strength through accompanying compressive strength tests on cores taken from the same armor unit. Pulse-velocity data can also be used to show material variations within a given unit.

The pulse-velocity measurement apparatus consists of a transmitter and receiver connected to electronic circuitry that generates a pulse sent by the transmitter, and calculates the elapsed time for that pulse to reach the receiver. The transmitter is placed on one face of the concrete section to be measured and emits an acoustical pulse that is transmitted through the concrete. The receiver is placed on an opposite face of the armor unit, or on any face of the concrete for which an accurate thru-distance can be measured or calculated. The receiver detects the pulses and calculates the time of travel of the pulse from transmitter to receiver. This generates a value for the time of travel in micro-seconds that, coupled with the known distance, allows a velocity to be calculated. This velocity is then evaluated for its relationship to concrete strength.

In previous pulse-velocity data collected from Core-Loc units located at a project on the Island of Tercia in the Azores, Portugal, significant vertical variation in the concrete material properties was observed. It was concluded in that case that vibration levels and mix properties resulted in some material segregation. More large aggregate was found in the bottom of the placement, resulting in higher velocities toward the bottom of the units. In light of these previous observations, it was deemed important to check for a similar occurrence in the Kaumalapau Core-Loc units. Pulse-velocity measurements were taken from the intact Core-Loc unit at the locations identified in Figure 5.2. Since velocity is calculated by dividing the measured time of arrival by the transmitter and receiver separation distance, the longitudinal distance must be known. Due to the Core-Loc unit's complex geometry, efforts to estimate these distances proved unsatisfactory. As an alternative method, pulse-velocities from core samples taken after failure of the unit (described later in this report) were used, as well as relative comparisons in time of arrivals collected from the in-situ concrete measurements, to verify condition and statistical variation.

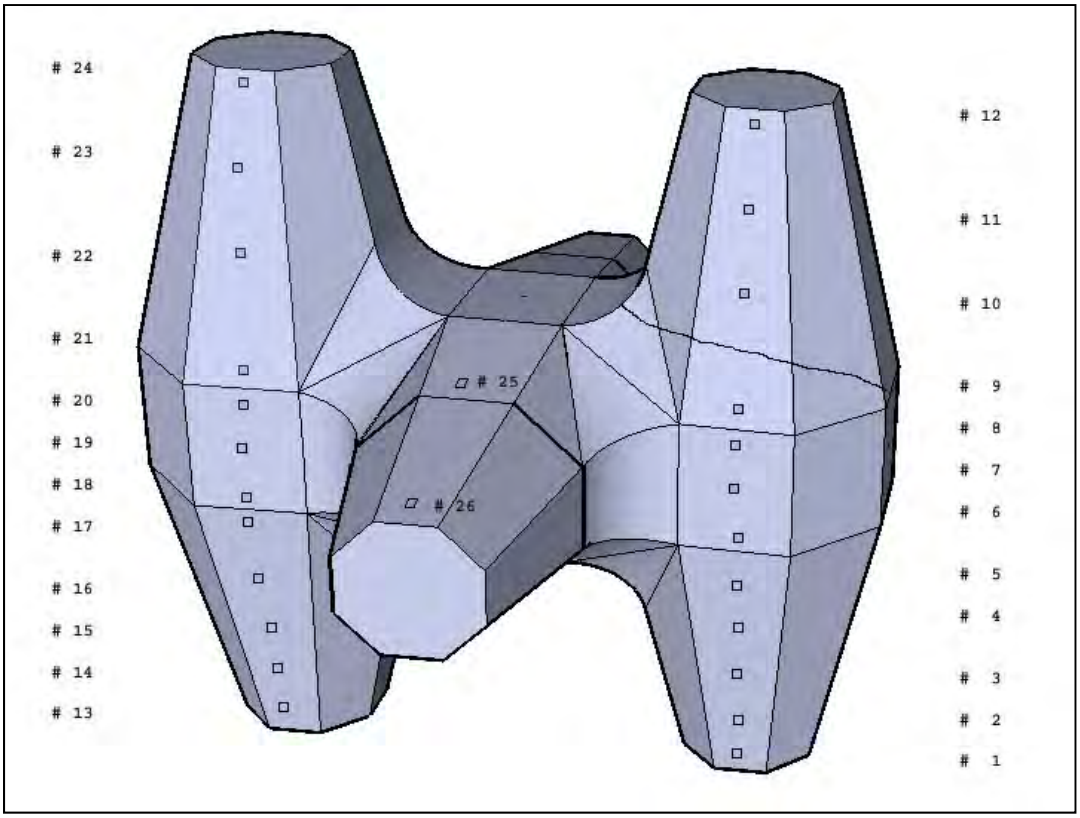

Figure 5.2. Location of pulse velocity readings (O'Neil and Haskins 2008).

The pulse-velocity measurements collected from core samples were within acceptable ranges according to uncorrelated estimation guidelines. Due to the complex geometry of the Core-Loc units, times-of-arrival could not be converted to velocities; however, a relative comparison of percent differences of arrival times (using structural symmetry) indicated that the material properties were consistent throughout the structure.

No concrete segregation, as observed in the Tercia (Azores, Portugal) Core-Loc units, appeared to occur within this specimen according to the in-situ collected data as well as the core specimen data. Visual observation of cut cross-sections from the 4-inch-diameter (in.-diam) collected cores also confirmed consistency from the top to bottom in terms of aggregate distribution (Figure 5.3).

5.2 Destructive testing of a Core-Loc armor unit

A surface evaluation of the armor unit was made to document the as-received condition. The overall appearance of the surface of the unit was good. There were no bugholes (surface voids that result from the migration of entrapped air or water to the fresh concrete-form interface) or

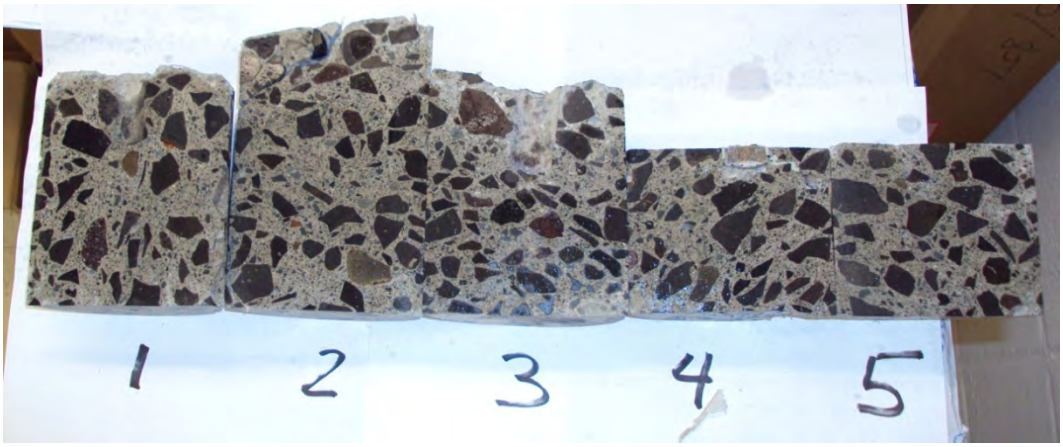

Figure 5.3. Photograph of saw-cut sections of Kaumalapau Core-Loc 4-in.-diam core samples (O'Neil and Haskins 2008).

honeycombing defects (voids left in concrete due to failure of the mortar to effectively fill the spaces among course aggregate particles) in the surface, and the unit otherwise appeared smooth and well consolidated. Several small surface cracks were found which were attributed to drying shrinkage and were assumed to be structurally insignificant. Similar surface cracks were present in a number of other units that were stored nearby.

Theoretical structural calculations were used to size a hydraulic loading system with a loading capacity of 300,000 pounds force (lbf) and a stroke of 6 in. to fit between the two legs of the Core-Loc unit such that a pushing force would break one of the two legs of the armor unit. The loading mechanism consisted of a ganged matrix of six 50-kip hydraulic rams, each with a 100-kip load cell attached to its piston arm for monitoring the load of each ram and the overall load of the system. A graphic of the hydraulic arrangement is shown in Figure 5.4.

Since it was not known which leg of the Core-Loc would fail, both legs were fitted with strain gages on both the inside and outside to collect both tension and compression data of the failure, regardless of the failure site. A total of eight strain rosettes were bonded to the Core-Loc, each with three gages for a total of 24 channels of strain data. Additionally, six pressure cells attached to each hydraulic ram were used to estimate the applied load. All instrumentation, including two linearly variable differential transformers, was digitized with a Pacific Instruments System. Figure 5.5 shows one of the rosettes bonded to the Core-Loc. The locations of all eight rosettes on the armor unit are shown in Figure 5.6.

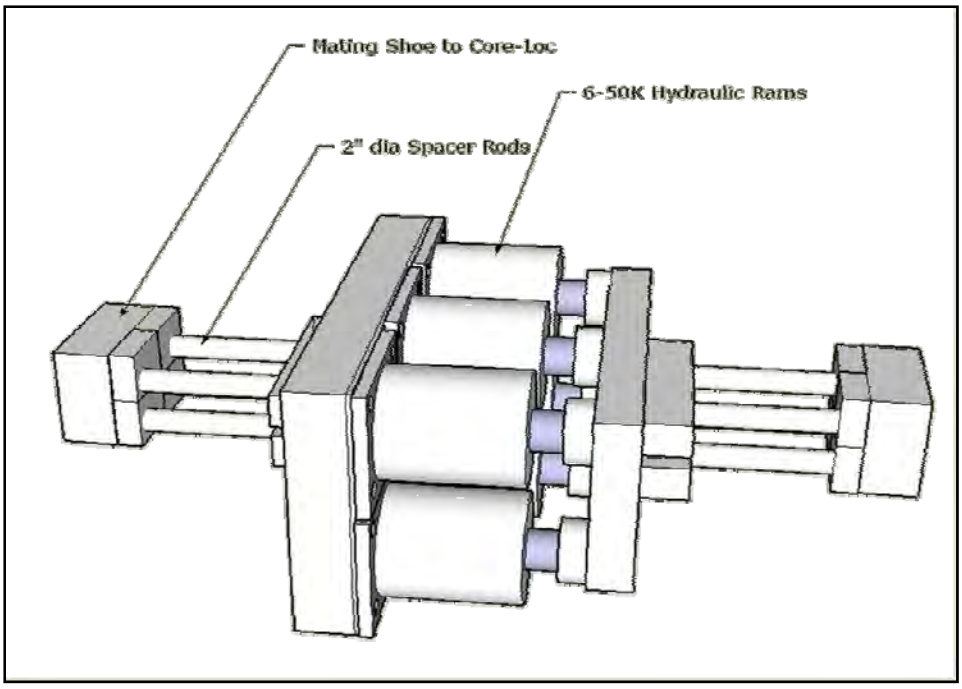

Figure 5.4. Hydraulic ram loading system (O'Neil and Haskins 2008).

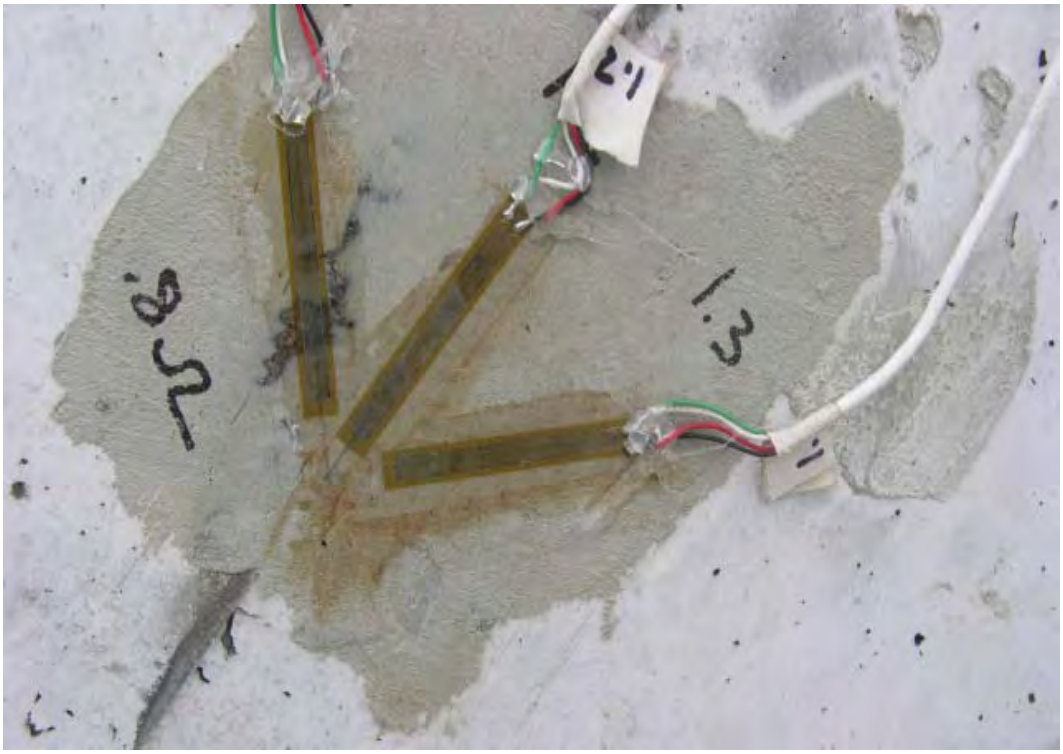

Figure 5.5. A strain rosette bonded to Core-Loc prior to testing (O'Neil and Haskins 2008).

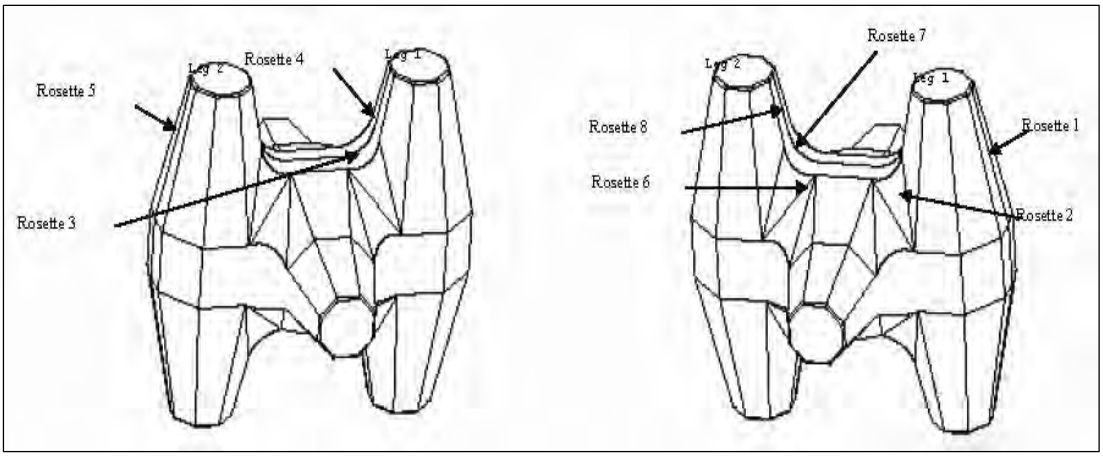

Figure 5.6. Location of strain rosettes on the test armor unit (O'Neil and Haskins 2008).

The primary purpose of the destructive test was to establish a load that would fail one leg of a Core-Loc. The hydraulic ram was arranged to push from between the two legs and break one of the legs with tension on the inside of the leg and compression on the outside. Figure 5.7 shows the loading assembly being placed between the Core-Loc legs.

Figure 5.7. Hydraulic ram placed between the Core-Loc legs (O'Neil and Haskins 2008).

When the assembly was in place, a small pre-load was placed on the Core-Loc so that the loading assembly would support itself between the legs, and the straps supporting the assembly could be relaxed. Throughout the test, the straps remained around the assembly so that when the leg broke the straps would catch the loading assembly and prevent it from falling to the ground.

All of the load cells and strain gages were adjusted to zero condition and a small load (trial run) was applied to the legs and then removed. This was done to check the integrity of the strain gage bond to the concrete. When it was shown that the strain gages were well bonded, the load was returned to zero, and the data from the strain gages was checked to ensure that they had also returned to zero. When this was confirmed, the test (failure run) was started.

The Core-Loc failed just above the saddle in the upper half of the leg (Figure 5.8). The extreme outer fiber tensile strain on the failure plane occurred at the location of strain rosette 3. The failure plane started at the mid-height of the rosette and traveled in a plane that was at an angle of approximately 35 deg downward from the horizontal until it emerged from the Core-Loc leg on the compression face approximately 14 in. below strain rosette 1.

Figure 5.8. Core-Loc armor unit after testing to failure (O'Neil and Haskins 2008).

After failure of the armor unit, 4-in.-diam core samples were taken from the locations shown in Figure 5.9. The sample cores were returned to the ERDC laboratory and were tested for density, and subjected to ultrasonic pulse-velocity measurements to calculate the Modulus of Elasticity and Poisson's ratio. The cores also were prepared for determining the structural properties of compressive and splitting tensile strength.

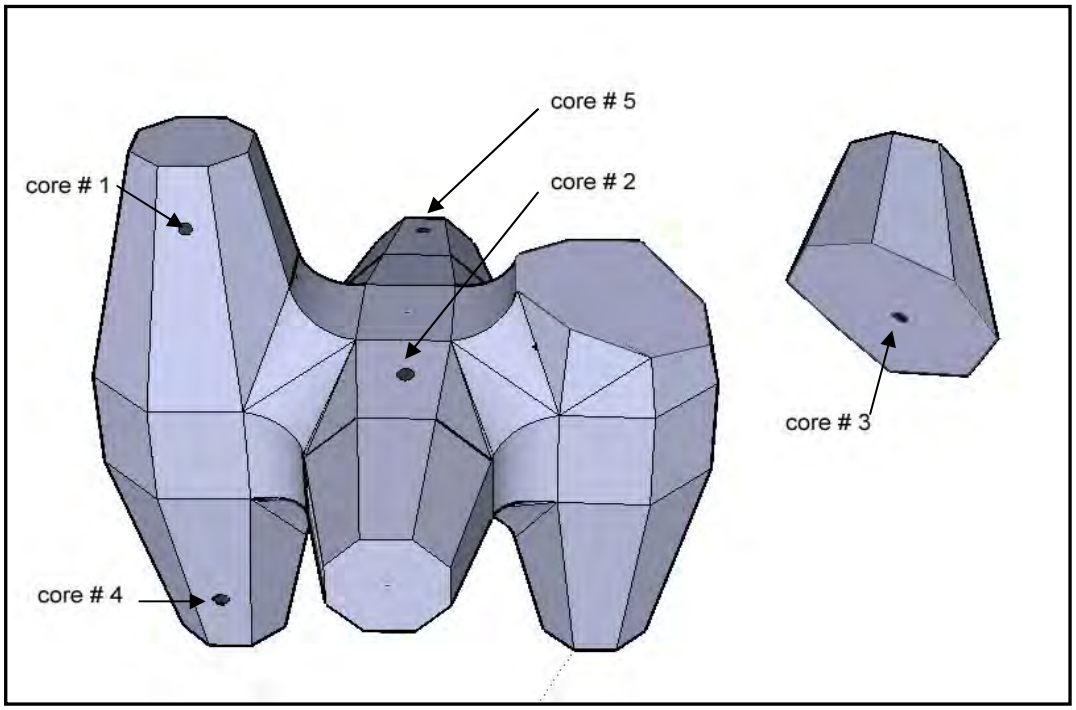

Figure 5.9. Location of core samples transported to ERDC (O'Neil and Haskins 2008).

The load vs. time results of the trial run and the failure run are presented in Figure 5.10. The stair-step loading methodology that is evident in the figure was the result of limited hydraulic control of the loading mechanism that was available. An average loading rate of 500 lbf per second (lbf/s) was achieved for both the trial and failure runs. The load during the trial run was increased to approximately 67,000 lbf before it was removed. The failure run load was applied until the load cells indicated a major drop in load denoting failure of the leg. The highest recorded load in the failure run was 94,000 lbf.

The 94,000 lbf actual failure load was approximately 42 percent of the 223,600 lbf theoretical failure load. In the theoretical calculations, the tensile stress capacity of the concrete was chosen as the highest test result achieved from an entire month of material flexural tests (925 lbf per square inch (psi)), while the contract required tensile stress was only 700 psi at 28

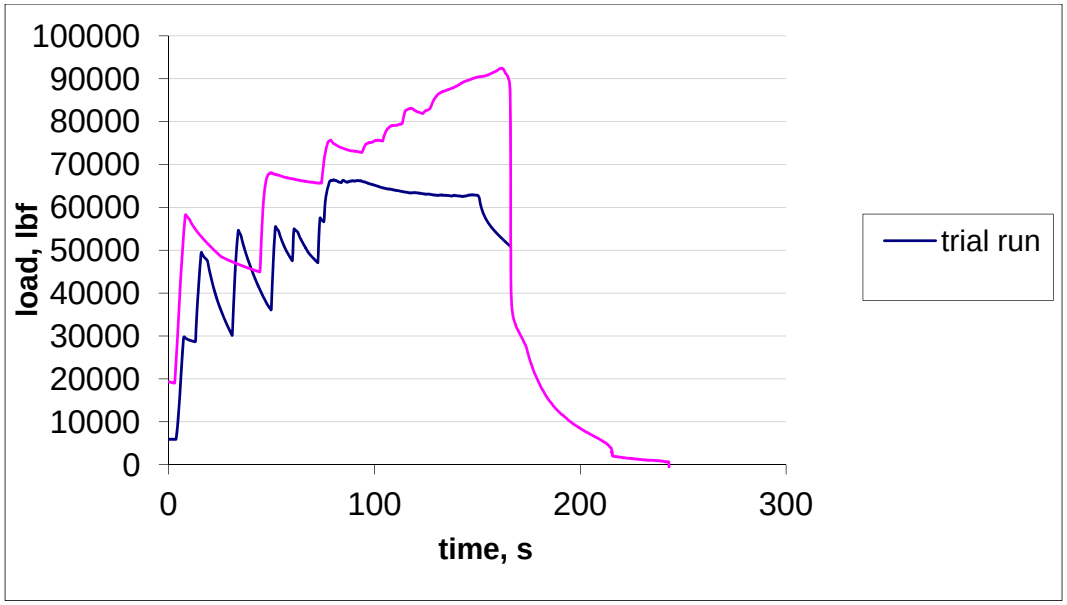

Figure 5.10. Load vs. time plots for the trial and failure runs of the test Core-Loc (O'Neil and Haskins 2008).

days. Additionally, in the theoretical calculations, the failure plane was assumed to be an octagonal plane perpendicular to the longitudinal axis of the Core-Loc leg. When the armor unit failed, the orientation of the actual failure plane was at an angle rotated about 35 deg below the plane perpendicular to the longitudinal axis of the leg, thus producing a stretched octagon with a larger moment of inertia (I_{xx} = 246,372 in.^{4}), a larger distance to the extreme fiber (24.23 in.), and a larger moment arm.

These differences in geometry and material properties do not fully account for the large difference between the theoretical and actual failure loads. Using the actual failure load, the adjusted moment of inertia, and the distance to the extreme fiber to calculate the tensile capacity of the concrete yields only 436.2 psi (see Appendix A), well below the contract required tensile flexural strength of 700 psi (as determined by ASTM C78). This computation leads to the apparent conclusion that some additional factor was responsible for the lower than anticipated failure load.

5.3 Laboratory results from field cores

Preliminary data from laboratory pulse velocity testing of the five cores taken in the field are presented here in Table 5.1. The Modulus of Elasticity (E) and Poisson's ratio (p) were calculated using the equations below. For these equations E is the Modulus, p is Poisson's ratio, d is the specific gravity, C_p is the compressional velocity, and C_s is the shear wave velocity (all in SI units).

$$E \cong 4d \frac{\left(.75 \cdot C_p{}^2 - C_s{}^2\right)}{\left(\frac{C_p}{C_s}\right)^2 - 1} \qquad p \cong \frac{\left(.5 \cdot C_p{}^2 - C_s{}^2\right)}{\left(C_p{}^2 - C_s{}^2\right)}$$

Table 5.1. Pulse velocity testing of Kaumalapau Core-Loc samples, from laboratory data.

Core samp	Wt (air), g	Wt (water)g	Density, lb/ft³	Specific gravity	Length, in.	ToA – P, sec E-05	ToA – S, sec E-05
1	659.9	314.3	119.03	1.91	4.263	26.8	49.6
2	738.2	367.8	124.23	1.99	3.982	23.2	46.0
3	559.1	282.5	126.00	2.02	3.593	20.3	39.6
4	513.1	234.6	114.85	1.84	2.929	16.6	34.0
5	526.9	249.9	118.57	1.90	3.166	17.9	37.2
Core samp	P-Vel., ft/s	S-Vel., ft/s	Impedance, MegaRayls	Modulus, N/m² E10	Modulus, psi E06	Poisson's Ratio	
1	13256	7162	7.71	2.3527	3.41141	0.29	
2	14303	7214	8.68	2.5596	3.71148	0.33	
3	14750	7561	9.08	2.8356	4.11158	0.32	
4	14704	7179	8.25	2.3682	3.43392	0.34	
5	14739	7092	8.54	2.3968	3.47537	0.35	

In addition to non-destructive estimation of these material properties from cores, the destructive data were collected and used to extract the maximum compressive strength and splitting tensile strength. These results are presented in Table 5.2.

Table 5.2. Compressive and split-tensile strengths from Kaumalapau Core-Loc tests.

Core	Compressive strength, psi	Tensile-split strength, psi
1	6373	717
2	6416	806
3	7057	702
4	7537	721
5	6488	691

The numbers reported for the densities of the cores brought back from the field work and their specific gravities appear low. The densities that range

between 115 and 126 lb/ft^3 and are expected to be close to 148 lb/ft^3 for normal weight concrete, and the specific gravities that range between 1.9 and 2.02 should be close to 2.37 for normal weight concrete. The reported values would be acceptable for lightweight concrete but there was no provision for any lightweight concrete being used to fabricate Kaumalapau armor units. In addition, the values of Modulus of Elasticity should be closer to 3.0E+06 psi.

The data in Table 5.2 show that the tensile strength of four of the five cores extracted from the Core-Loc unit tested at the Grace Pacific casting yard were indeed stronger in tensile strength than the required 700 psi strength specified in the construction contract.

5.4 Rosette strain data analyses

Duplicate rosettes for strain measurements were attached to the Core-Loc to ensure adequate field data would be acquired, regardless of which leg of the unit failed. These back-up rosettes were attached in mirror image locations on the armor unit. Rosettes 1 and 5 were in mirror image locations, as were rosettes 2 and 6, rosettes 3 and 7, and rosettes 4 and 8 (Figure 5.6). Rosettes 1 and 5 were in areas of compression. Rosettes 2, 3, 4, 6, 7, and 8 were in areas of tension. Rosettes 2, 3, and 4 failed during testing and yielded no useable data. The remaining five rosettes functioned correctly and produced strain readings throughout the failure loading. Therefore, usable data were acquired from rosettes 1 and 5 in compression, and rosettes 6, 7, and 8 in tension. These five rosettes provided information to calculate the major and minor principle strains, and the angle from the reference grid to the referenced principle strain.

The major and minor principle stresses (σ_p and σ_q) can be calculated from strain measurements with knowledge of the material's Modulus of Elasticity and Poisson's ratio. These properties were calculated using pulse-velocity measurements of the cores returned to the ERDC, as part of the standard materials property data needed to characterize the Core-Loc concrete and as shown above. The average Modulus of Elasticity and Poisson's ratio determined from the five cores studied in those data were 3,628,768 psi and 0.33, respectively (see Appendix A for calculations). The major and minor principle stresses determined from strain data from the five functioning rosettes are presented in Table 5.3, with negative values indicating compressive stress and positive values indicating tensile stress.

Table 5.3. Kaumalapau Core-Loc principal stresses from field data (psi).

rosette	σ_p	σ_q
1	-716	-336
5	-549	72
6	277	158
7	71	21
8	144	-129

The major principal stress determined from rosette 1 (716 psi) is the highest stress determined from observed strain, and the only reportable stress near the actual failure location. Rosette 1 was in a compressive region of the armor unit. Rosette 5, also in a compressive stress region, recorded the second largest stress (549 psi) and was the mirror image rosette to rosette 1. Both of these rosettes were located on the centerline of the outside of the leg approximately 40 in. below the point of application of the load. An analysis of the elongated octagonal failure plane indicates a compressive stress of 306 psi on the outside of leg 1 at a distance of approximately 61 in. below the point of application of the load (when calculated using the measured failure load of 94,000 lbf).

The higher compressive stresses determined from rosette 1 and 5 strain gage data are not in agreement with this geometrical approach. The values of Modulus of Elasticity taken from the pulse velocity-data (3,628,768 psi) is about 21 percent higher than what is considered a Modulus of Elasticity of a normal strength concrete (3×10^6 psi). Using the more typical value of 3×10^6 psi with the measured strain data reduces the rosette 1 principal stresses by about 100 psi down to a value of about 615 psi. However, this is still higher than the stresses calculated from the failure plane geometry and the 94,000 lbf failure load (306 psi).

It is unfortunate that the strain gage rosettes beneath the tensile failure area of the saddle (rosettes 3 and 4) failed before giving good strain data. They would have provided the best data for the tensile stress in the armor unit at failure. None of the strain gage data that were taken from tensile strain areas produced tensile stresses near 700 psi, the criterion for satisfactory concrete specified in construction contract documents. The rosettes on leg 2 that were counterparts to rosettes 3 and 4 were rosettes 7 and 8. These principal tensile stresses were 71 and 144 psi, respectively. However, these

rosettes would not have experienced stresses as high as would have been found in the area of initial failure (under rosette 3).

The discrepancy between measured stresses and calculated stresses being on the order of a few hundred psi, and the fact that they are both (measured and calculated) less than the required minimum flexural tensile stress of 700 psi, is perplexing. Clearly, the test sample beams made for flexural tensile testing of the concrete for contract acceptance purposes met the requirement of 700 psi; otherwise, the concrete would not have been accepted for use. It should also be recognized that the tensile stress capacity of a complex geometry armor unit such as a Core-Loc would be different from that of a small rectangular prism tested to failure in pure bending. The low failure load of 94,000 lbf, and the odd failure plane the leg breakage of the Core-Loc took, implies that there are other factors involved in the unexpectedly low performance of this particular Core-Loc unit.

5.5 Cement paste and aggregate bond

Observation of the failure surface of the Core-Loc revealed that a large percentage of the aggregate was pulled out of the concrete rather than fracturing, indicating a poor bond between the aggregate and cement paste. To roughly quantify this observation, Figures 5.11a and 5.11b show an identical 1-sq ft image of the Core-Loc failure surface. Figure 5.11a is unedited. Figure 5.11b has been enhanced with different colors to indicate whether the aggregate beneath the color was fractured (red), aggregate had pulled out of the cement paste and was showing on the interface (green), or was a cement paste pocket indicating the aggregate had pulled out of the cement paste and was in the other face of the fracture plane (yellow).

This analysis is subjective to a degree, but indicates that in the 1-sq ft area, there are 89 fractured aggregates, 83 aggregates pulled out on this face of the fracture plane, and 19 cement paste pockets indicating aggregates that pulled out on the opposite face. Of the total 191 visible areas of aggregate to paste bond, approximately 53 percent pulled out of the cement paste. This is undesirable because, if the cement paste does not bond well to the aggregate, the aggregate does not contribute to the strength of the concrete. This can have a tremendous effect on the overall strength of the composite because the strong tensile properties of the aggregate are not part of the composite strength. Poor quality concrete paste or dirty aggregate could be responsible for this condition, and are discussed in further detail below.

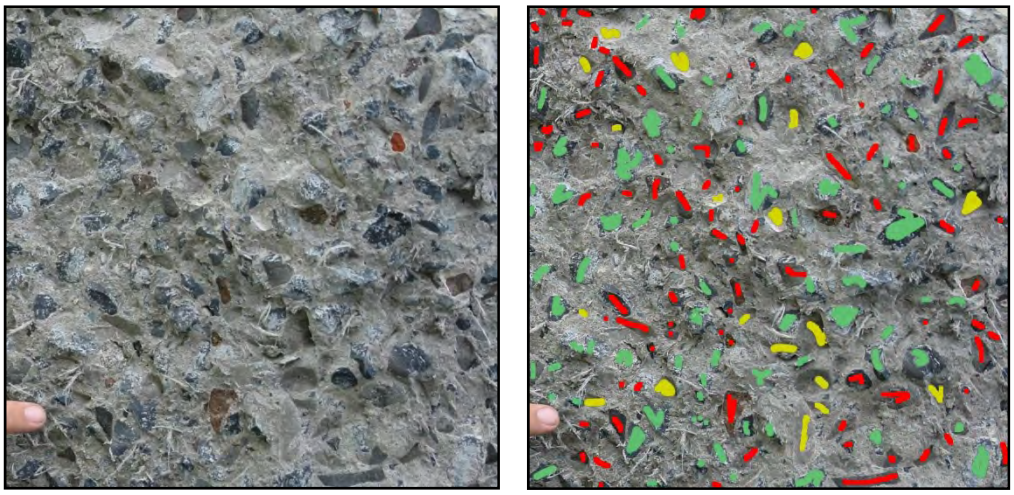

a. Unedited details of fracture face. b. Color-coded detail of fracture face.

Figure 5.11. Core-Loc failure fracture face showing details of broken aggregate and locations where aggregate pulled out of the cement paste (O'Neil and Haskins 2008).

Concrete is a composite material consisting of cement, sand, coarse aggregate, and water. Each material in the composite has its own material properties and contributes to the overall strength of the concrete in its own way. Since the aggregate makes up close to 75 percent of the volume of the concrete, its properties and how it interacts with the cement paste is very important to the strength of the concrete. When aggregate is added to cement and water, the cement paste covers the aggregate and attempts to bond to the surface of the aggregate, producing a strong bond with the aggregate.

With clean aggregate, the bonding process is simple and straight forward, and the hardened cement paste clings tightly to the surface of the aggregate. However, if the aggregate is dirty and contaminated with dust or silt, the cement paste will cover the aggregate, but instead of bonding to the aggregate it will bond to the dirt. This leaves a poor quality interface between the cement paste and aggregate that is weak and easily fractured. When the concrete is put under stress, the strength will be lower because the bond to the aggregate is poor and the aggregate particles will separate from the cement paste more easily.

Another potential cause of a weak interface between cement paste and aggregate is a high water-to-cement (w/c) ratio. If the w/c ratio used in the mixture is greater than approximately 0.42, then there is more water in the mixture than can be combined with the cement to form cement paste. This excess water has a tendency to collect around aggregate particles and dilute

the cement paste in the vicinity of the aggregates surface. This makes the local w/c ratio of the cement paste near the aggregate higher than the bulk of the cement paste. This, in turn, makes the cement paste around the aggregate weaker and more easily susceptible to failure by the aggregate pulling out of the cement paste. The w/c ratio required by contract specifications was 0.4.

5.6 Conclusions from material tests of Kaumalapau Core-Loc unit

Conclusions from breakage tests of this specific Core-Loc armor unit were based on:

1. visual observations of the as-received and post-test conditions of the provided Core-Loc concrete armor unit,
2. analysis of the load and strain data collected during the failure test of the armor unit,
3. measured field data and calculations derived from that collected data, and
4. data from laboratory testing of cores for pulse-velocity, and compressive and split-tensile load data.

These conclusions apply only to this particular specific armor unit, and not to the condition of any other Core-Loc units used in the Kaumalapau Harbor breakwater rehabilitation or elsewhere.

5.6.1 As-received condition of the armor unit

From observations made during receiving and set-up of the Core-Loc armor unit provided for non-destructive and destructive testing, it was concluded that the armor unit appeared normal in all aspects pertaining to dimensions of the unit and appearance, including surface cracking and blemishes. No readily apparent abnormalities were observed.

5.6.2 Concrete quality

In the visual analysis of the failure surface of the broken Core-Loc armor unit, it was observed that there were a high percentage of aggregate particles that had debonded from the cement paste and pulled out of one or the other face. This high percentage of debonded aggregate (>53 percent) leads to the possibility that the low tensile stress in the concrete that propagated a failure under a load of 94,000 lbf was partially due to low strength created by aggregate particles not participating in the strength

development of the composite. The cause of this condition is related to the development of a micro-thin layer of poor quality concrete forming at the paste/aggregate interface either from an accumulation of dirt and silt material on the aggregate or the accumulation of excess water on the surface of the aggregate that accompanies high water-to-cement pastes. These conditions cause weak bond strength, frequent pullout of aggregate particles, and ultimately lower strength concrete because the strength of the aggregate cannot contribute to the strength of the composite.

5.6.3 Loss of strain gage data during testing

Failure of three of the eight strain rosettes during actual field testing to failure caused a loss of pertinent data necessary for full analysis of the principal strains and stresses experienced during the failure testing. The full complement of strain data necessary to conduct a complete investigation of the principal strains and stresses were lacking; however, sufficient data were collected to draw valid, although limited, conclusions about strain and stress in the unit.

5.6.4 Measurement of strain, stress, and ultimate load

Collection of strain data during this investigation was entirely through physical application of strain gages to the armor unit; thus, all strain data are measured and none are derived. This is also true for load data. Stress data, on the other hand, are purely derived data and were deduced from three sources:

1. application of the Modulus of Elasticity and Poisson's ratio (derived from pulse velocity measurements) to primary strain data collected during the field and laboratory testing,
2. calculation of tensile and compressive stresses at outer fiber locations on the geometry of the structure using the failure load of 94,000 lbf as load input, and
3. calculation of maximum split-tensile strength from laboratory testing of cores obtained from the specimen Core-Loc.

The ultimate load of 94,000 lbf was a valid failure load of the upper leg of the armor unit, although this magnitude was significantly lower than theoretically predicted. The cause of the low failure load cannot be fully explained by the primary and derived stress and strain data collected during the investigation. The strain data from the five intact rosettes provided the

only physical field data that are based on primary measurement and, thus, are the best quality field data available. The stresses calculated from these strains rely on derived properties that may be only approximate measures of the true properties and, thus, should also be considered as secondary in quality.

The laboratory data of compression and split-tension load obtained by destructive testing of portions of the cores extracted from the armor unit provide a primary source of stress information for the analysis. These data are considered to be the best quality laboratory data.

All stress and strain data, whether primary or derived, and whether best or secondary quality, imply that the tensile stresses at and near critical failure locations in this particular specific Core-Loc armor unit were at or slightly above the minimum flexural tensile stress required by Core-Loc concrete contract acceptance criteria. No conclusions about the structural capacity of other armor units used in the Kaumalapau Harbor breakwater rehabilitation can be made, except that all units placed on the structure exceeded the contract minimum stress.

However, observations about their health can be addressed. The largest tensile stresses calculated from the incomplete strain gage field data were in the range of 549 to 716 psi. The laboratory split-tensile stresses ranged from approximately 691 to 806 psi (727 psi when averaged, and 713 psi average when the highest and lowest results are removed). Although less than desired, the field data could be low as a result of the less than ideal conditions of the testing, and it is possible the actual stresses are all closer to the required 700 psi.

It is safe to assume that the samples taken from the batch casting of the concrete met minimum contract criteria of 700 psi tensile stress; otherwise, the Core-Locs would have been rejected. Thus, the health of the Core-Loc armor units placed on the structure are in compliance with contract specifications, but could be near the minimum criteria for acceptance.

5.6.5 Observations from laboratory specimens

The pulse-velocity readings collected from core samples are within the acceptable ranges according to uncorrelated estimation guidelines. Due to the geometry issues associated with the Core-Loc units, times-of-arrival could not be converted to velocities; however, a relative comparison of

percent differences of arrival times (using structural symmetry) indicate that the material properties were consistent throughout the structure.

No concrete segregation as observed in Tercia (Azores) placed units appeared to occur within this specimen according to the in-situ collected data as well as the core specimen data. Visual observation of cut cross-sections from the collected cores also confirmed consistency from the top to bottom in terms of aggregate distribution.

6 Wave Climate and Wave Measurements

The Hawaiian Island chain is subject to a wide variety of incident wave conditions. Consistent tradewinds generate local wind waves while distant storms in the North and South Pacific Ocean generate significant swell energy that travels thousands of miles before reaching Hawaii's coastline. Nearshore exposure to these wave conditions is highly dependent on location as well as shoreline orientation, due to the significant wave sheltering by adjacent islands and land features such as peninsulas and headlands. Refraction due to wave propagation over rapid changes in bathymetry also greatly affects Hawaii's wave climate.

Assessing the wave climate at a project site is imperative to both design and post-construction monitoring of navigation projects, particularly when coastal structures are employed to reduce wave impacts on vessels using the harbor. At Kaumalapau Harbor, wave data was collected pre-construction to aid in design, as well as post-construction to aid in assessment of wave impacts on the completed structure and wave conditions at the barge pier.

6.1 Regional wave climate[1]

Four general wave types typically characterize the wave climate in Hawaii. These include easterly trade wind waves, South Pacific (southern) swell, North Pacific swell, and Kona wind waves. Wave types are most readily distinguished by the direction from which they approach (Figure 6.1).

Trade wind waves are the most persistent feature of the wave climate in Hawaii, and occur throughout the year. The direction of approach of trade wind waves normally varies between NNE clockwise to ESE in accord with the winds that generate them. Deepwater wave heights usually vary from 3 to 8 ft with periods of 5 to 10 sec. Very little, if any, trade wind wave energy reaches Kaumalapau Harbor due to its location on the west central coast of Lanai.

[1] This section is extracted essentially verbatim from Sea Engineering, Inc. and Group 70 International (2009).

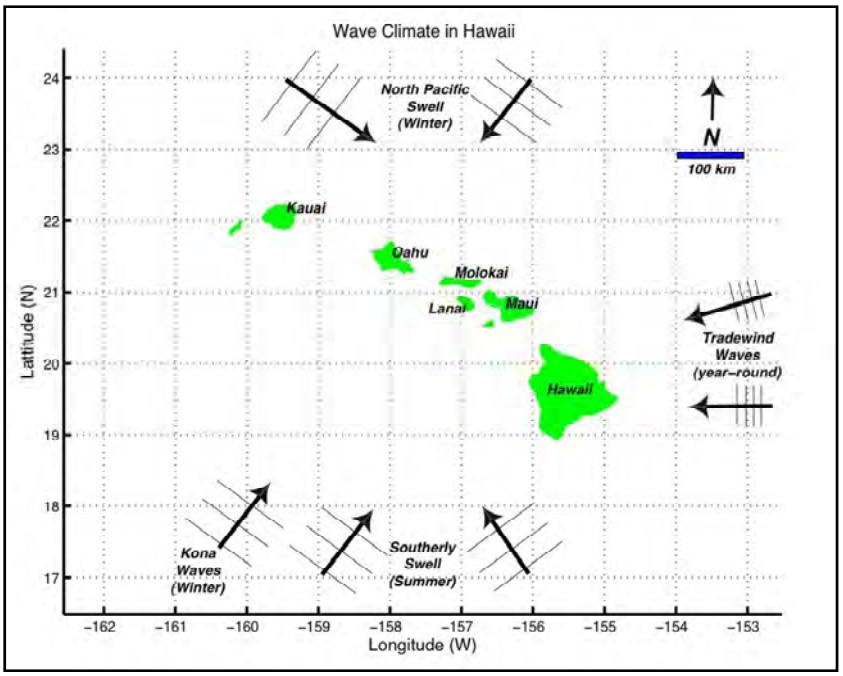

Figure 6.1. Hawaii wave climate (Sea Engineering, Inc. and Group 70 International 2009).

Strong storms in the southern hemisphere generate waves that propagate into the central Pacific, regularly reaching exposed Hawaiian Island shores during summer months in the northern hemisphere. Traveling distances of up to 5,000 miles, these waves arrive with relatively small deepwater wave heights of 1 to 4 ft and peak periods of 14 to 20 sec. On rare occasions, deepwater wave heights from southern hemisphere storms reach 6 ft with peak periods of 25 sec. Depending on the position and track of southern hemisphere storms, south swells approach the Hawaiian Islands from the southeast (SE) through the southwest (SW). Kaumalapau Harbor is directly exposed to wave energy from these directions.

During the winter months, strong storms frequent the North Pacific at mid latitudes and near the Aleutian Islands. These storms generate large swells that propagate to the northern Hawaiian shores with minimal attenuation of wave energy. Direction of approach of North Pacific swell can vary from west-northwest (W-NW) clockwise to north-northeast (N-NE). Deepwater wave heights often reach 15 ft, and in extreme cases can reach 30 ft. Periods vary between 12 and 20 sec, depending upon the storm track.

The project site is partially sheltered from North Pacific swell primarily by the Island of Molokai and to some extent by Maui, Oahu, Kauai, and Lanai itself. The degree of sheltering is heavily dependent upon the direction of

approach. For example, during a due-North swell, Kaumalapau Harbor is almost completely shadowed by Molokai, while during a W-NW swell, a significant amount of energy can refract around Oahu and Kauai resulting in an almost direct approach at Kaumalapau Harbor.

Waves that approach from the southeasterly to southwesterly direction associated with Kona winds and Kona lows are known as Kona storm waves. These events are infrequent; however, they can result in very large waves with deepwater heights up to 15 ft. Wave periods generated from Kona Storms range from 6 to 10 sec. The project site is directly exposed to Kona storm waves.

Waves from tropical storms and hurricanes are less frequent but potentially more threatening to operations and infrastructure at Kaumalapau Harbor. Although hurricane occurrence in Hawaiian waters is infrequent, the occurrence of two such storms in a 10-year period (Hurricane Iwa in 1982 and Hurricane Iniki in 1992) shows hurricane conditions should be considered as part of the extreme wave climate. Hurricane wave conditions including hindcast wave heights for these storms (Hs = 22 ft for Hurricane Iwa, and Hs = 20 ft for Hurricane Iniki) and modeled scenario hurricane waves (Hs = 25 to 52 ft and Tp = 11.1 to 15.8 sec) were used for selection of design waves and to evaluate breakwater stability in physical model testing (Sea Engineering, Inc. 2008). Hs is the significant wave height.

6.2 Offshore wave data collection

A Datawell Waverider buoy, located approximately 1 mile west of the harbor in 650-ft depth was deployed in May 2007 as part of this monitoring program by the largely USACE-funded Scripps Institution of Oceanography (2007), Coastal Data Information Program (CDIP). The University of Hawaii Oceanography Department (UH) was responsible for the actual installation of the buoy and its subsequent maintenance (see Figure 6.2 for buoy location). Buoy data, including both spectral and parameterized wave height, period, and direction, are available on the web in near real-time, at 30-min intervals. The wave data recorded since deployment of the buoy includes waves from the northwest (315 deg True North (TN)) counter-clockwise through south-southeast (158 deg TN), with the majority of waves arriving from south-southwest (32 percent) and south (30 percent). Typical wave periods range from 8 to 20 sec, with the majority of long period swell energy coming from the southwest, and some to some extent from the northwest.

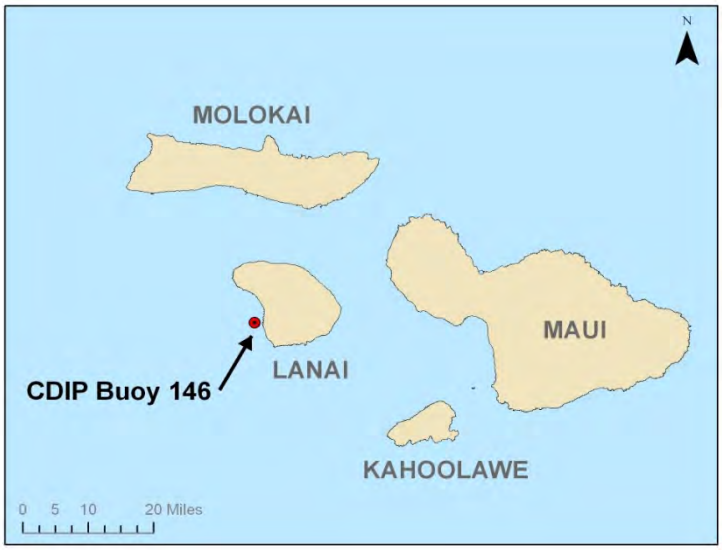

Figure 6.2. Location of CDIP Buoy 146.

The buoy is completely sheltered from the trade wind waves that approach the islands from the northeast, due to its sheltered location in the lee of Lanai. Figures 6.3a and 6.3b show wave rose plots of wave height and period at the buoy for the 4.25-year period of record from May 2007 through August 2011. Figure 6.4 is a time-series plot of significant wave height (reported as H_{m0}, the spectral estimate of significant wave height) over the entire period of record, with some data gaps due to periodic instrumentation failure. Several of the larger wave events during this period were selected to examine their characteristics (red circles in Figure 6.4). These events were also chosen based on their concurrence with nearshore wave data collection at the harbor, which is further detailed in the next section of this chapter.

The largest wave event recorded at the buoy occurred in December 2007 with a maximum significant wave height of 14 ft, a typical wave period of 8.3 sec, and wave directions from southwest. This event was a Kona storm, an upper level subtropical cyclone that forms near the islands and causes high winds and waves to approach from the southeast through southwest. In this case, waves approached from the south through west-northwest, which allowed for direct propagation to the harbor located on the southwest coast of the island. The event's duration was approximately 3 days, with a rapid peak in wave height, a steady increase in wave period due to locally-generated wind-wave growth (unlike distant storms which are characterized by gradually decreasing wave period), and dramatic shifts in wave direction beginning from the south and moving clockwise to the west-northwest by the third day as the storm moved from east to west.

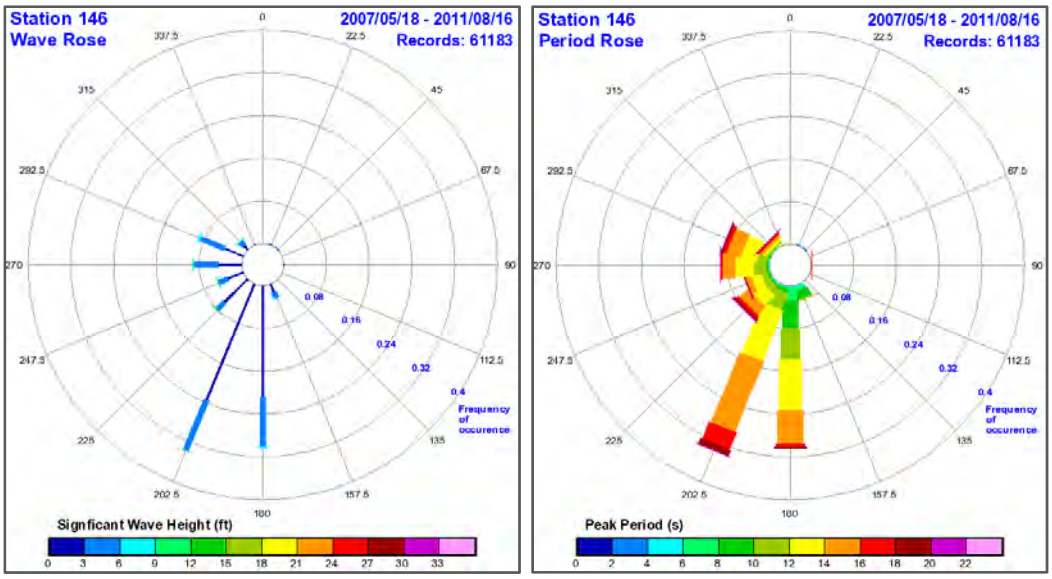

Figure 6.3(a). Wave height rose, and (b) Wave period rose for CDIP 146 (CDIP Website).

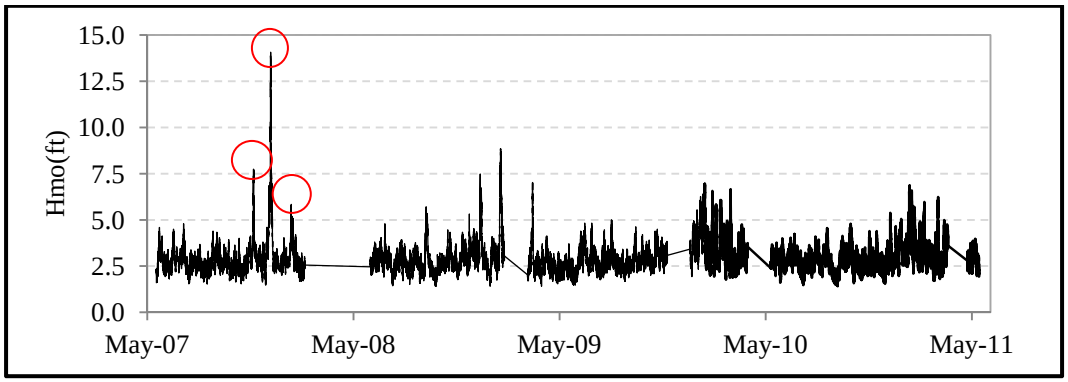

Figure 6.4. Time-series plot of significant wave height (H_{m0}) for CDIP 146 from May 2007 – May 2011, and wave events selected for further analysis.

Figure 6.5 shows a time series plot of significant wave height, peak wave period, and wave direction recorded during this event, indicated by the red box in the figure.

In November 2007, a late-season south swell generated by a storm off New Zealand resulted in a significant wave height of 7.5 ft at the buoy, with wave periods between 14 to 20 sec, and wave directions from south-southwest. The duration of the event was approximately 3.5 days, with the peak of significant wave heights occurring on the 2nd day of the swell. The time-series of significant wave height, peak wave period, and wave direction at the buoy during this event, indicated by the red box, is shown in Figure 6.6.

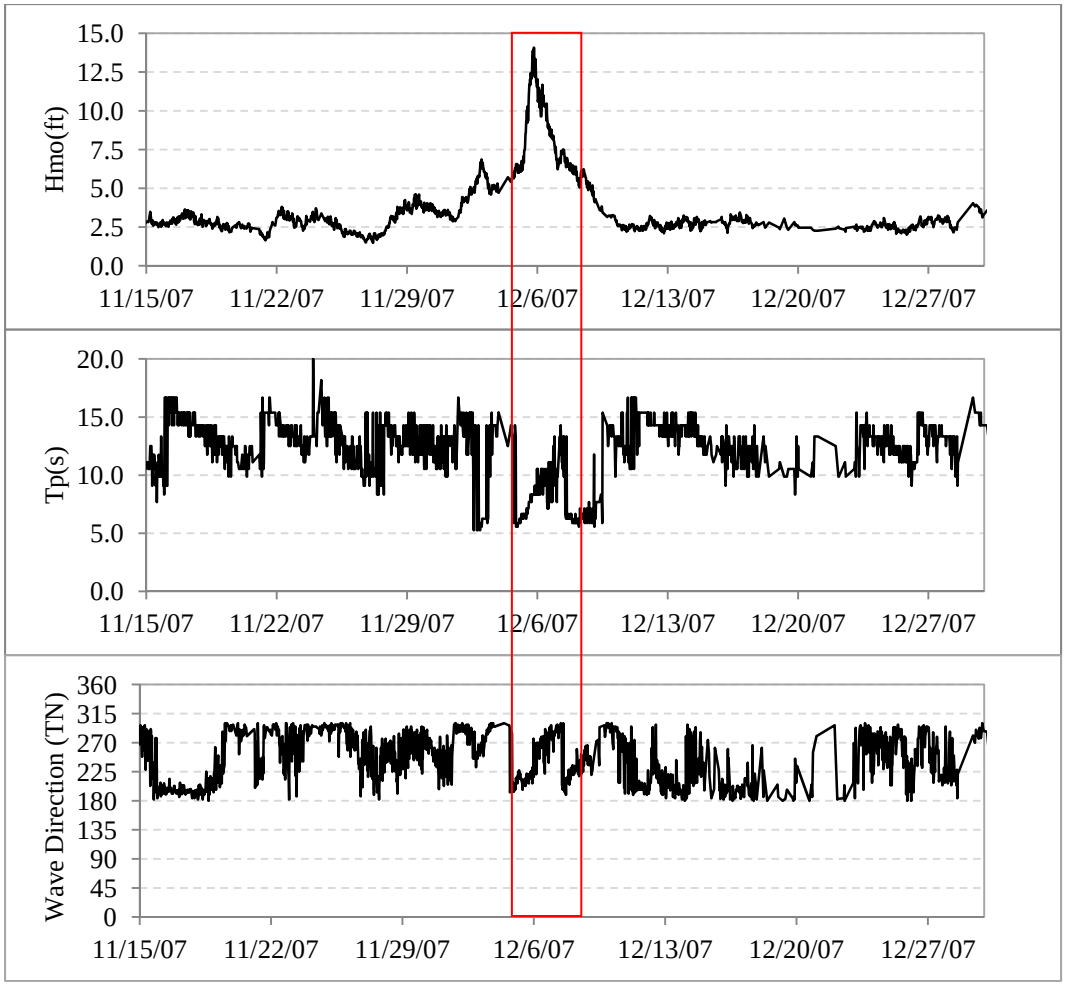

Figure 6.5. Time series of H_{m0}(ft), T_p(s) and wave direction (deg TN) at CDIP 146 for the December 2007 Kona storm.

In January 2008, a west-northwest swell generated a significant wave height of 5.5 ft at the buoy, with wave periods between 12 to 20 sec, and wave directions from west-northwest (290 to 300 deg TN). The duration of this event was approximately 3 days, with the peak of significant wave heights occurring about 24 hr after the arrival of the swell. The time-series plot of this event is shown in Figure 6.7. It is also interesting to note that another slightly smaller (peak H_{m0}= 5.0 ft) and more westerly event (260 to 300 deg TN) occurred immediately following this swell; however, wave periods for this event are shorter in the 12 to 18 sec range. These seemingly minor variations in swell characteristics can have a significant effect on the resulting conditions at the harbor, and will be discussed further in the following section.

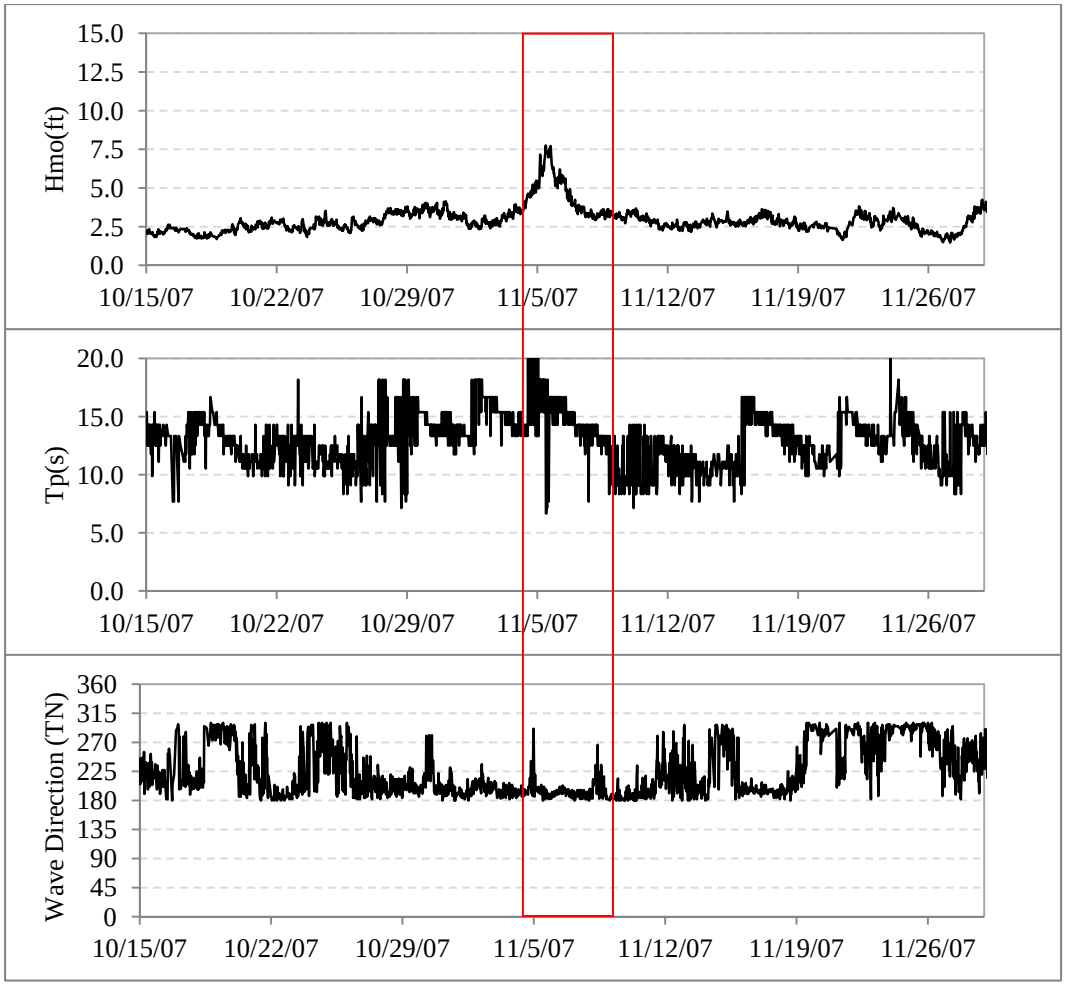

Figure 6.6. Time series of H_{m0}(ft), T_p(s) and wave direction (deg TN) at CDIP 146 for the November 2007 south swell.

This long-term source of offshore data has proven to be an extremely valuable resource for both this monitoring program, as well as to users of Kaumalapau Harbor. The directional capability of the buoy (in contrast with other non-directional southerly exposed deepwater buoys in the Hawaiian Islands) as well as its trade wind wave-sheltered location just offshore of the harbor have ensured that the wave data collected at the buoy are an accurate representation of the wave climate at the harbor itself. As an added benefit of the buoy installation, harbor users have noted that the availability of real-time wave data from the offshore CDIP buoy has aided significantly in the determination of whether vessels (particularly the fuel barge owned by Lanai Oil Company, Inc. which travels bi-monthly from Maui to Kaumalapau Harbor for delivery) will be able to safely enter and tie up within the harbor. This has reduced costly delays in inter-island transits that would previously have been terminated either in progress or upon arrival to Lanai due to unsafe conditions within the harbor basin.

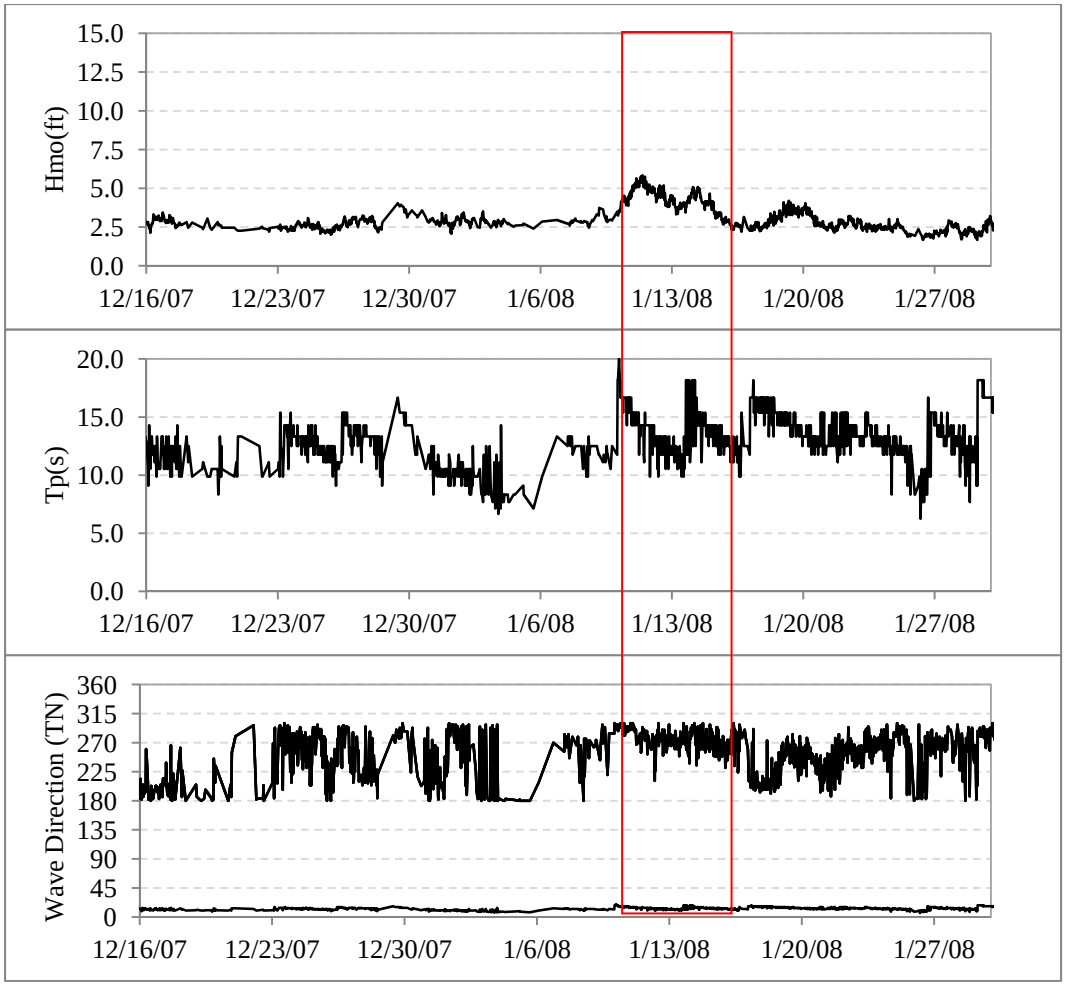

Figure 6.7. Time series of H_{m0}(ft), T_p(s) and wave direction (deg TN) at CDIP 146 for the January 2008 west-northwest swell.

6.3 Temporary wave gage data collection

6.3.1 Wave gage data collection and analysis

Also in support of the MCNP program, the University of Hawaii's Department of Oceanography deployed two bottom-mounted, non-directional pressure sensor wave gages in and near the harbor in the month immediately following construction completion. The interior wave gage (Ko1) was located in the lee of the breakwater adjacent to the barge pier (in a water depth of approximately 27 ft), to determine typical mooring conditions and obtain a "lower bound" of incident wave energy since this is the most sheltered location within the harbor. This gage was active between July 2007 and September 2008, with a 6 week data gap in September – October 2007. The exterior wave gage was located near the entrance to the harbor at a depth of roughly 49 ft (Figure 6.8).

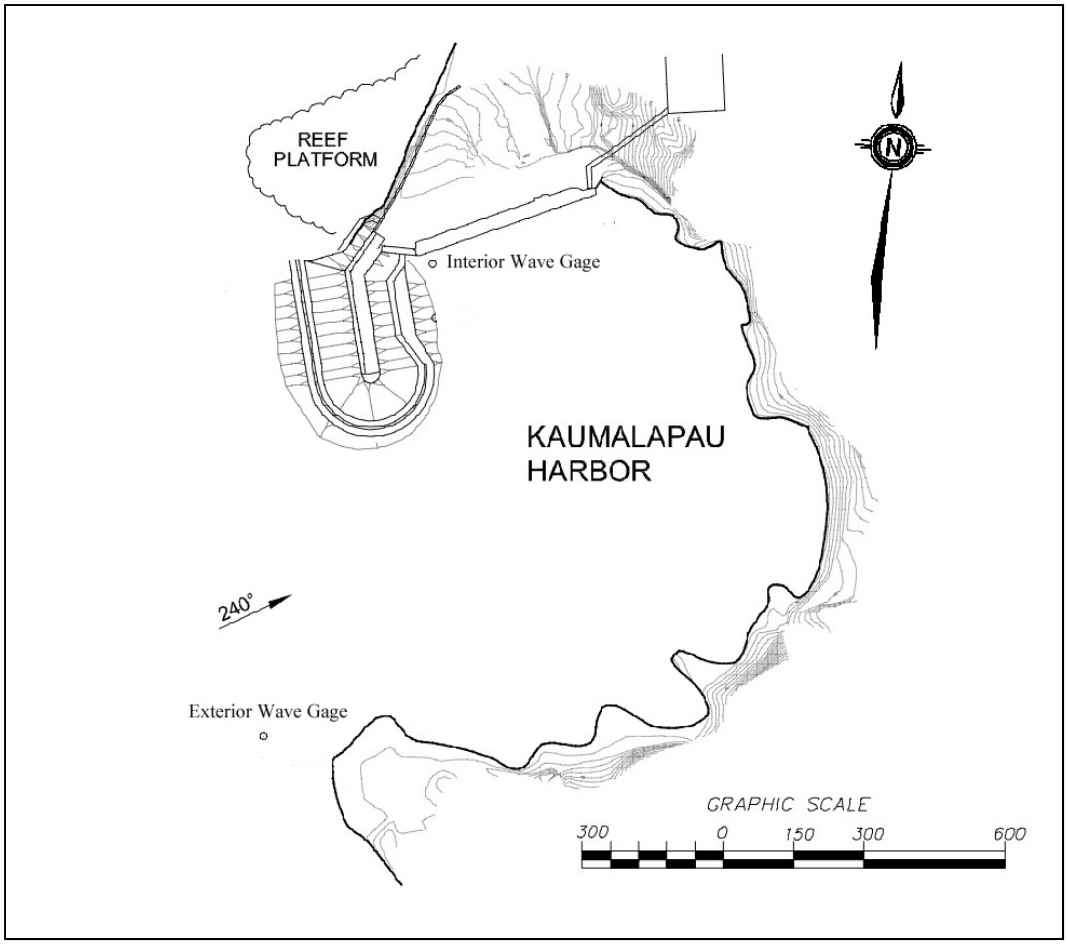

Figure 6.8. Temporary wave gages at Kaumalapau Harbor between June 2007 – September 2008 (modified from Sea Engineering, Inc. and Group 70 International 2009).

Although the original intent was to place the exterior gage just seaward of the breakwater, to obtain data on the waves impacting the structure directly, the logistics of gage deployment and retrieval at such depths (70 to 80 ft) made this impractical. Placement of the gage on a slightly shallower shelf adjacent to the headland opposite the breakwater was completed with the assumption that wave exposure would be similar in this location. The exterior gage was active from October 2007 through early November 2008. All wave gage data were contained within memory cards onboard each instrument, and became available after recovery of the instruments and data processing, in early 2009.

Comparison of this nearshore wave gage data with the offshore wave buoy data during the same time periods shows the correlation between the amount of wave energy that is observed at the buoy versus that which reaches the entrance of the harbor and that which diffracts around the breakwater toward the barge pier. The amplification factor (A') is defined

as ratio of the local wave height to the incident wave height measured at the offshore wave buoy. Data collected during the selected wave cases that were shown in the previous section (Kona storm, south swell, and west-northwest swell) are examined further in terms of significant wave height (H_{m0}) only, since the peak wave period (T_p) does not vary significantly with wave transformation and the interior and exterior wave gages were non-directional (Figures 6.9 through 6.11). In addition, it is assumed for these typical (non-hurricane) conditions that, based on water depths and visual observation of the site, no wave breaking occurs between the buoy and the nearshore wave gage locations, so any wave dissipation observed is due to refraction and/or diffraction and/or bottom friction.

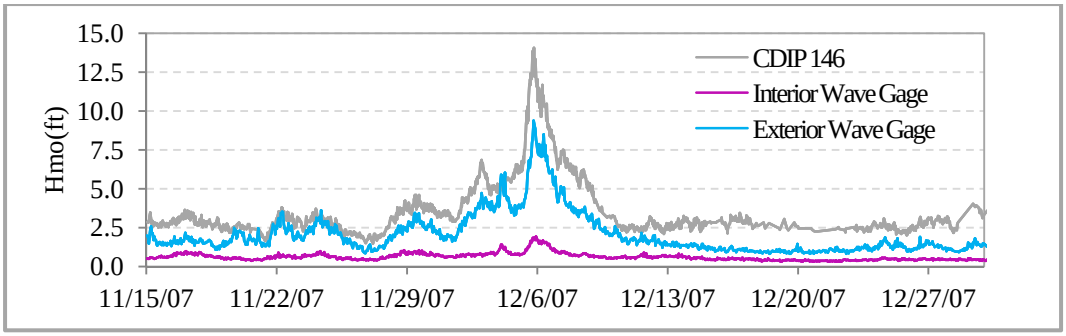

Figure 6.9. Time series of H_{m0}(ft) at CDIP 146 and wave gages for Dec. 2007 Kona storm.

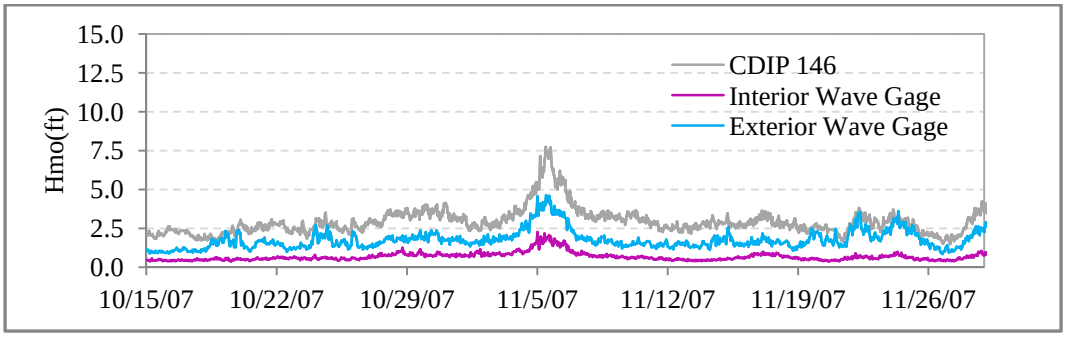

Figure 6.10. Time series of H_{m0}(ft) at CDIP 146 and wave gages for Nov. 2007 south swell.

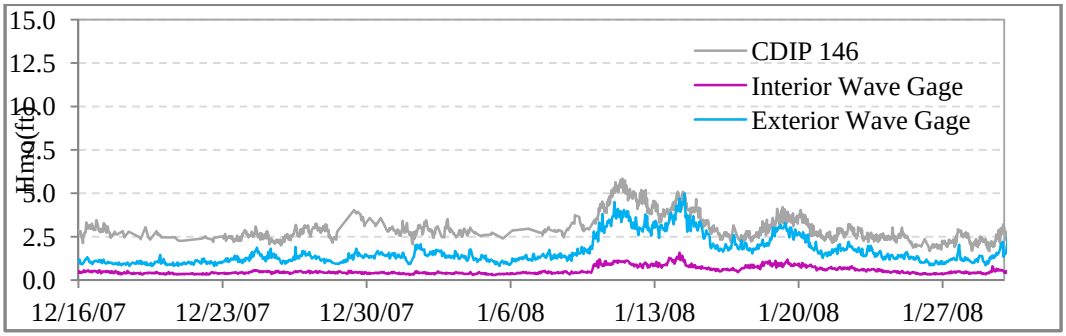

Figure 6.11. Time series of H_{m0}(ft) at CDIP 146 and wave gages for Jan. 2008 west-northwest swell.

Figure 6.9 shows that a considerable amount of offshore wave energy during the Kona storm event reached the entrance of the harbor. The amplification factor determined by the ratio of local wave height at the exterior wave gage (blue line in figure) to incident wave height at the offshore buoy (gray line) at the peak of the storm is 0.67 (A' = 9.4 ft/14.1 ft). However, the wave height recorded at the interior gage (pink line) was significantly less at 1.8 ft during this event peak, making the amplification factor at this location 0.13 (A' = 1.8 ft/14.1 ft).

This calculation of wave height amplification factor between both the interior and exterior gages and the offshore buoy was completed for the peak of all three selected wave events. Though this value of A' represents only the amplification factor at the peak of the storms, a calculation of A' at various times over the duration of each event showed that these values are representative of the average amplification factor during the storm. Therefore, these values will be considered a good indication of the overall A' for each event for the remainder of this analysis. These results, along with typical offshore wave parameters for each event are summarized in Table 6.1 below. The secondary west-northwest swell in January 2008 mentioned previously is also included as a fourth wave event to further extend the comparative analysis.

Table 6.1. Comparison of peak wave height amplification factor (*A'*) at wave gages.

Storm Event	Buoy H_{m0} (ft)	Buoy T_p (s)	Buoy Dir	Ext. H_{m0} (ft)	Ext. *A'*	Int. H_{m0} (ft)	Int. *A'*
Kona Storm (12/07)	14.1	8.3	224 (SW)	9.4	0.67	1.8	0.13
South Swell (11/07)	7.7	16.7	190 (S)	4.3	0.56	2.0	0.26
W-NW Swell 1 (01/08)	5.6	15.4	298 (W-NW)	3.7	0.66	1.1	0.20
W-NW Swell 2 (01/08)	5.0	15.4	281 (W-NW)	5.0	1.00	1.1	0.23

Comparison of the amplification factors illustrates both the dependence of wave conditions at the harbor on deepwater wave period and direction, as well as the difference between the type of wave energy observed at the harbor entrance versus what is observed in the lee of the breakwater near the barge pier. At the exterior wave gage, the amplification factor for the Kona storm and the west-northwest "Swell 1" are virtually the same (0.67 and 0.66, respectively), despite the fact that the offshore buoy wave height during the Kona storm was more than double that of the

west-northwest swell, and that the Kona storm waves approach the harbor more directly (from southwest). This indicates that the difference in wave period has some effect on how wave energy propagates from the offshore buoy to the harbor entrance. The longer-period swell waves are experiencing a greater amount of shoaling and refraction over the intermediate depths between the buoy and the harbor, allowing an equal ratio of wave height as compared to the shorter-period but larger and more directly approaching waves of the Kona storm. In addition, bottom friction will be greater for longer waves, larger waves, and shallower depths.

Wave direction is clearly a factor as well, evidenced by comparison of the exterior gage amplification factor during both west-northwest swells. The "secondary" slightly smaller (in terms of offshore wave height) swell with maximum offshore wave height of 5.0 ft has a higher amplification factor (A' = 1.0) than the initial swell (A' = 0.66), though both events have the same wave period. This is due to the fact that the wave direction had shifted to a more westerly direction by this secondary swell, causing less shadowing by the other islands in the chain. This shadowing effect is also evident when examining the lowest amplification factor of 0.56 during the south swell. This event had a larger offshore wave height than either of the west-northwest swells, as well as a slightly longer wave period, but due to its more oblique approach from the south, the waves were somewhat shadowed by the southern portion of Lanai, and refraction between the buoy and the harbor entrance causes the wave energy to spread and therefore the amplification factor to be lower in comparison.

Analysis of amplification factors at the interior wave gage indicates a slightly different dependence on wave direction and wave period during the wave transformation between the harbor entrance and the harbor basin. It appears that deepwater wave period plays the dominant role in determining how much of the wave energy reaches the sheltered area in the lee of the breakwater. As mentioned previously, the relatively short-period Kona storm waves experience a significant reduction in wave height between the gage at the harbor entrance and the interior wave gage (A' = 0.67 and 0.13, respectively). These short-period waves do not diffract around the breakwater as efficiently as long-period waves due to their shorter wavelength in comparison to the distance from the point of diffraction (head of the breakwater) to the location of the wave gage. This dependence on wave period applies to the other wave cases, most notably to the south swell condition which has the longest wave period at 16.7 sec, and maintains the

highest amplification factor at the interior gage (0.26). This condition also caused the largest overall significant wave height (H_{m0} = 2.0 ft) at the interior wave gage for the four selected wave cases.

The amplification factors of long-period (T_p = 15.4 sec) west-northwest swell are comparable to the south swell at 0.20 and 0.23 for "Swell 1" and "Swell 2", respectively; however, the actual wave heights at the interior gage are approximately half that of the south swell event, due to the smaller magnitude of the offshore significant wave heights of these events. The west-northwest events again show some correlation with wave direction, in that the more westerly event allows a slightly higher percentage of wave energy to diffract in toward the interior wave gage. However, the resulting wave heights of the Kona storm condition show that wave period, not direction, is the primary factor that determines the proportion of wave energy that propagates around the breakwater and into the sheltered areas near the barge pier.

Finally, the recently collected wave data at the interior wave gage can be used to make a general although somewhat limited evaluation of operational conditions at the most sheltered area of the barge pier following breakwater construction. The Special Design Report completed by the U.S. Army Engineer Division, Pacific Ocean (POD) (1996) stated that, "*The operational condition established by POD, after discussion with the end-users, was that for a 4.6 m [15.1 ft] wave outside the harbor, waves along the pier face would be 1.5 m [4.9 ft] or smaller. No specific wave parameters (i.e., wave period or direction) were defined as the operational conditions; therefore, a range of wave parameters were chosen.*" Only one event during the data collection period (the December 2007 Kona storm) approached the specified offshore wave height of 15.1 ft. Though the interior wave gage height peaked at 1.9 ft during this event (well below the specified wave height of 4.9 ft along the pier face), this is not likely to be a condition in which vessels would be transiting or mooring in the harbor. However, if the maximum allowable wave amplification factor A' is calculated for the design criteria as 0.32 (A' = 4.9 ft/15.1 ft), it is evident from Table 6.1 that the criteria was satisfied (at location K01) for all wave events during the data collection period.

6.3.2 Comparison of 2007-2008 wave gage data to previous wave data collection efforts

Historical wave gage data is also available from a field data collection effort completed by the USACE's ERDC, CHL, Prototype Measurement and Analysis Branch in support of numerical modeling done as part of the original design effort for breakwater rehabilitation (U.S. Army Corps of Engineers 1994, Smith 1998). Two bottom-mounted pressure sensors were in place from January through December of 1994 at the head of the breakwater (HI001 at approximately 70-ft depth) and near the center of the barge pier (HI002 at approximately 21-ft depth), as shown in Figure 6.12. An attempt to examine and use this data to compare the wave conditions at the barge pier prior to and following the breakwater repair is discussed in the following.

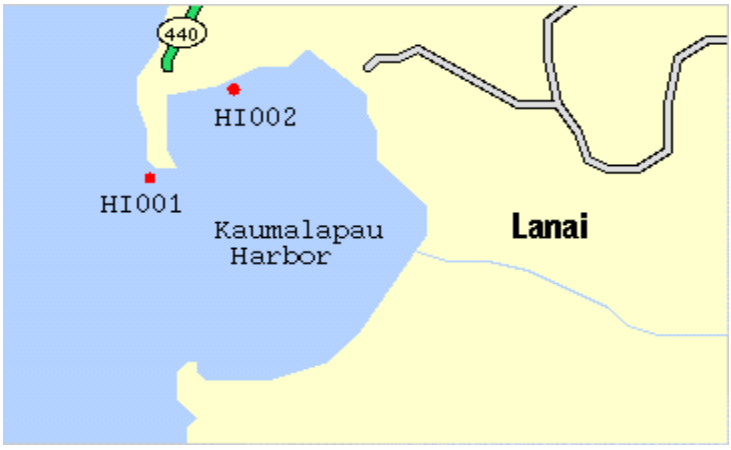

Figure 6.12. Location of wave gages during 1994 field data collection effort (figure from http://sandbar.wes.army.mil/public_html/pmab2web/htdocs/hawaii/hawaii.html).

As noted in the 1996 Special Design Report, "*Wave conditions were not very energetic over the course of the study. The mean incident wave height was 0.5 m [1.65 ft]. The largest wave occurred in January, with a height of 1.5 m [4.9 ft] and a peak period of 15.1 sec [at gage HI001].*" Based on the time of year and the wave period, this was likely a swell event from the northwest or west-northwest. The largest recorded wave at gage HI002 occurred in August 1994, with a wave height of 3.7 ft and wave period of 14.2 sec. Again based on the time of year and wave period of this observation, this was likely a south swell event. Unfortunately, no deep water wave information was available in the vicinity at this time, so it is difficult to discern the exact swell characteristics that were occurring during these nearshore observations.

In addition, the location of the wave gage inside the harbor (HI002) is significantly different than the location of the more recent data's interior wave gage shown in Figure 6.8. Though both wave conditions are located adjacent to the barge pier, the sheltering effect of the breakwater (even in its pre-project condition) varies significantly along the length of the pier, with less diffraction and, therefore, more wave energy able to reach the center of the barge pier where the 1994 gage was located, as compared to the location of the 2007 - 2008 wave gage. Therefore, it is difficult to make a pre- to post- project comparison of wave energy at the barge pier using this data without completing either an analytical or a numerical analysis of the diffraction patterns in the lee of the breakwater for both conditions. That is beyond the scope of this investigation, and would also have some inherent assumptions that would render it only qualitatively useful in any case.

Finally, though a full year of wave data was collected during both field wave gaging efforts, this period of record only characterizes the seasonal variability of the wave climate. Without a much longer dataset (on the order of a decade or more), the year-to-year variability of wave conditions cannot be accounted for accurately. This makes any direct comparison of wave data from two different years inherently biased if one year had a significantly greater wave climate than the other.

6.3.3 Roving buoy wave data collection

In support of the wave transformation modeling completed as part of the monitoring program, a portable, directional wave buoy was deployed at various locations around the harbor entrance and barge pier on 5 December 2008 by Sea Engineering, Inc. (Sea Engineering, Inc. and Group 70 International 2009). The free-floating buoy (a Datawell DWR-G4, see photo in Figure 6.13) is designed for short-term data collection and it is required that the buoy be observed during deployment by a trailing watercraft since there is no mooring. Raw data processing occurs on-board the buoy at 30-min intervals. To ensure that a minimum of one complete processing cycle was obtained at each deployment location, the buoy remained in each location for one hour. This instrument was chosen for the additional wave measurements because of its ability to measure multiple incident wave directions and frequencies as well as reflected wave energy, making it ideal for measurements of complicated wave conditions in the nearshore and within a harbor.

Figure 6.13. Datawell DWR-G4 roving buoy (typical).

The complete analysis of data collected by the roving buoy and its use in improving predictive capabilities at the harbor are presented in Chapter 7 in Tables 7.5 and 7.6, as excerpted from the 2009 Sea Engineering, Inc. and Group 70 International report. The wave conditions in the islands during the deployment were dominated by a relatively mild northwest swell, with wave conditions at CDIP 146 ranging from 3.7 to 4.3 ft with periods of 13 to 15 sec and direction between 270 and 290 deg. It is of note that this event was similar in size and direction to W-NW "Swell 2" presented in Table 6.1 above. The swell had a significant westerly component in wave direction and as shown in Table 7.5, the amplification factors of wave height (referred to as A' in Table 7.5) at both the entrance (shown as location W5 in Table 7.5 and collocated with the exterior wave gage) and the barge pier (shown as location K01 in Table 7.5 and collocated with the interior wave gage) are comparable to the amplification factors for W-NW "Swell 2" presented above. Specifically, the two amplification factors shown in Table 7.5 at the entrance channel (W5) during the roving buoy deployment are 0.89 and 0.85 (rounded), as compared to the exterior amplification factor of 1.00 shown in Table 6.1. Similarly, the amplification factors shown at the barge pier (K01) in Table 7.5 are 0.31 (rounded) and 0.25 (rounded), as compared to the interior amplification factor of 0.23 shown in Table 6.1. This general comparison demonstrates that there is some consistency in the amount of wave energy at both the harbor entrance and the barge pier for similar wave events.

The detailed analysis of the roving buoy data presented in the next chapter also reinforces the findings from the 2007 - 2008 wave gage data analysis above that the wave response at all locations within the harbor is highly dependent on offshore wave period and direction. In addition, the roving

buoy data analysis includes a discussion of wave reflection at the various deployment locations and the likely sources of this reflected energy. This information provides another level of insight into conditions at the harbor that was not available from the wave gage deployment, due to the non-directional nature of those measurements. Overall, despite the very short deployment period of the roving buoy, the flexibility in deployment location provided by the buoy's portability and its directional spectral data capability enabled the collection of a very useful data set. This data augmented the offshore permanent buoy and the temporary wave gage data in defining the wave climate at the harbor entrance and mooring areas and in verification of predictive algorithms presented in the next chapter.

6.4 Summary

The dependence of wave climate in the Hawaiian Islands on location and exposure necessitated the collection of multiple types of wave data to accurately characterize the wave transformation process from deepwater to nearshore. The use of different instrument types including buoys and wave gages enabled the collection of data in a range of temporal and spatial scales and wave conditions. The varying lengths of wave records collected in the measurements described in this chapter have captured the short and mid-term wave climate, offshore and nearshore conditions during typical seasonal events, as well as a detailed snapshot of nearshore conditions during individual events at Kaumalapau Harbor. In addition, the multiple locations of the instruments have enabled a better understanding of wave processes in the region including shadowing, refraction, diffraction, reflection, as well as the difference between wave conditions experienced inside and outside of the harbor.

Analysis of the selected wave events that occurred over the one-year period in which both offshore buoy data and nearshore gage data were being collected indicates three findings. First, the amount of wave energy that reaches the areas just offshore of Kaumalapau Harbor (and would therefore be affecting both navigation into the harbor, as well as breakwater stability) is highly dependent on refraction and bottom friction of waves over intermediate depths and island shadowing, and therefore depends greatly on both the wave direction and wave period of a storm or swell. Secondly, the waves that propagate from the harbor entrance toward the barge pier (areas where mooring operations would be affected) experience a significant amount of diffraction, and therefore proportional wave height at these locations is strongly correlated with wave period. From this, it can be

concluded that high-intensity local events such as Kona storms or hurricanes would have the greatest effect on breakwater stability, while distant events generating long-period waves approaching the islands from south or west-northwest would be most likely to impact mooring operations at the barge pier. Third, it is evident from these short-term wave measurements that the operational criteria established during the design phase of the project was satisfied under the conditions measured, at the most sheltered harbor location.

While pre-project wave data within the harbor does exist, it is difficult to make a direct pre- versus post-project comparison between this and the more recent wave data inside the harbor to determine whether the repaired breakwater is reducing wave energy significantly at the barge pier. Due to the lack of offshore buoy data during the pre-project data collection, the different locations of the wave gages, the relatively short duration of each dataset, and year-to-year variability of the wave climate, an attempt to draw meaningful conclusions from even a seasonally adjusted comparison of wave height data and/or period would be conjecture at best.

Although the existing data record does not include a hurricane event similar to that which was used for breakwater stability design, the full range of more typical events has been documented. It is intended that the deepwater buoy shall remain in its current location with maintenance by the CDIP and UH for as long as practical, so that if an extreme event such as a hurricane occurs, the conditions offshore will be recorded. Given the continued operation of the wave buoy offshore of Kaumalapau Harbor and the predictive capability described in the next chapter, hindcasting of wave conditions incident to the breakwater and within the basin during future events will be possible.

7 Wave Transformation Modeling[1]

This element of the monitoring study quantifies both typical and extreme wave energy incident to Kaumalapau Harbor using available wave datasets and transformation models. This work includes transformation of deepwater waves from an offshore buoy to various locations near the harbor entrance and quantification of extreme wave events with respect to potential breakwater damage. Modeled wave conditions at the harbor entrance were then used to estimate wave conditions at points near and within the harbor. The points were located in such a manner as to be useful both for estimation of wave conditions affecting operations in the harbor as well as inference of potential breakwater impacts. Correlation of these modeled wave parameters with offshore buoy conditions will allow for future estimation of harbor sea state.

7.1 WIS dataset analysis

USACE maintains a wave database generated from a 24-year Pacific Basin hindcasting effort associated with the Wave Information Studies (WIS) initiated in 1976 (USACE, http://frf.usace.army.mil/wis2010/wis.shtml). Parametric wave information such as significant wave height (H_{m0}), peak period (T_p), and peak direction (D_p) are provided for predetermined save points beginning January 1981 and ending December 2004. Wave spectra are also available upon request. WIS hindcast save points near Kaumalapau (WIS113, WIS114, WIS115, and WIS116) are shown in Figure 7.1, along with the National Oceanographic and Atmospheric Administration (NOAA) National Data Buoy Center (NDBC) buoy 51027.

7.1.2 Prevailing wave climate affecting Kaumalapau based on WIS stations

To provide an objective and quantifiable analysis of wave climate relevant to the project site, WIS stations WIS113, WIS114, WIS115, and WIS116 were selected due to their close proximity to Kaumalapau Harbor. The entire 24-year hindcast record for each WIS location was downloaded from the WIS website for further analysis. The 24-year WIS dataset consists of 210,383 hourly records of wave and wind parameters, including significant

[1] This section is extracted essentially verbatim from Sea Engineering, Inc. and Group 70 International (2009).

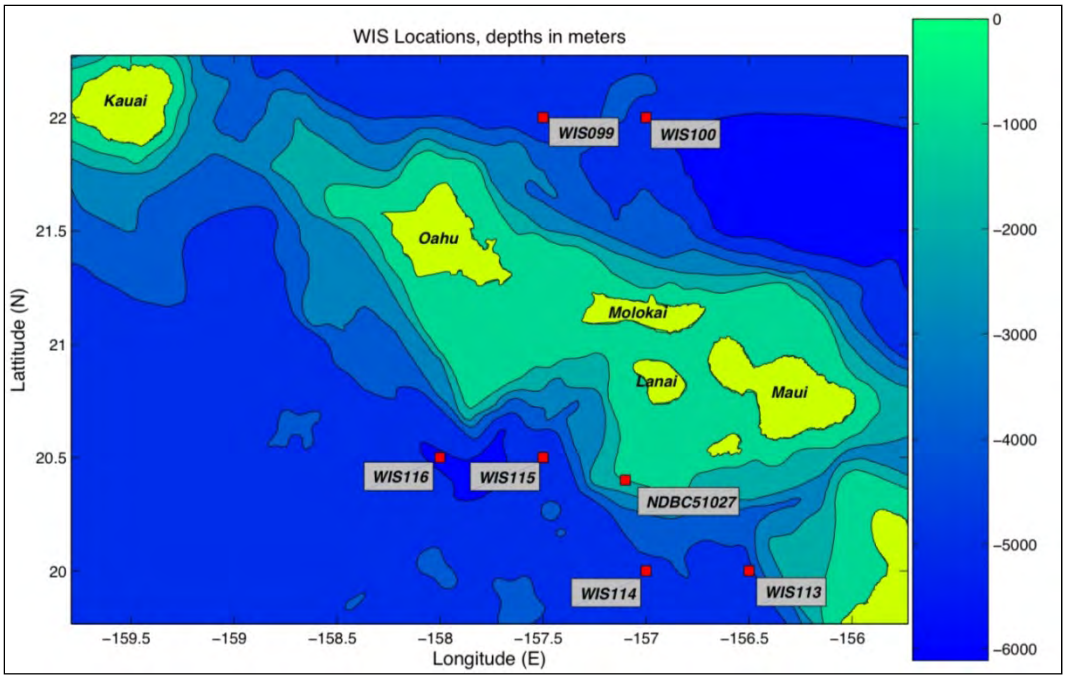

Figure 7.1. USACE WIS station locations, and NOAA NDBC buoy NDBC51027 location, near Kaumalapau Harbor breakwater (Sea Engineering, Inc. and Group 70 International 2009).

wave height (H_{m0}), peak period (T_p), average period (Av_p), peak direction (D_p), mean direction (Av_d), wind speed (W_{sp}), and wind direction(W_{dir}) for each WIS station. The hourly wave data was first sorted into directional histogram bins of 30 deg with bin centers from 15 deg clockwise to 345 deg.

The primary components of the wave climate are readily detected in the histograms. Inspection of the directional bins reveals groupings centered roughly at ENE, SSW, and WNW corresponding to trade wind waves, southerly swell, and North Pacific swell, respectively. These groupings are referred to here as Scene 1, Scene 2, and Scene 3, respectively. Additionally, Kona wind and hurricane generated waves were appended to Scene 2, and were specified rather than obtained from analysis due to their relatively low frequency of occurrence. The Scene directional range azimuths (in nautical degrees) are (a) Scene 1 direction range = 30 to 120 deg, (b) Scene 2 direction range = 150 to 240 deg, and (c) Scene 3 direction range = 270 to 360 deg.

7.1.2 WIS dataset validation

Duration and accuracy are two primary factors in determining the suitability of a model dataset for establishing the wave climate at a given location. The availability of 24 years of data from the WIS station satisfies

the first requirement. Validation of the WIS dataset in the immediate vicinity of Kaumalapau was necessary.

NOAA buoy NDBC 51027 is located approximately 24 miles to the south-west of Kaumalapau Harbor (Figure 7.2). NDBC 51027 was deployed during the period between 7 December 1994 and 26 November 1995, providing about a year of directional wave data. NDBC 51027 shared a similar exposure as Kaumalapau Harbor since it was partially sheltered from west northwest clockwise to southeast swells by the Hawaiian Island chain. To determine the accuracy of the WIS data as well as its suitability for use of deepwater wave climate development, the NDBC51027 dataset was compared to WIS data located WIS113, WIS114, WIS115, and WIS116 during the same time period.

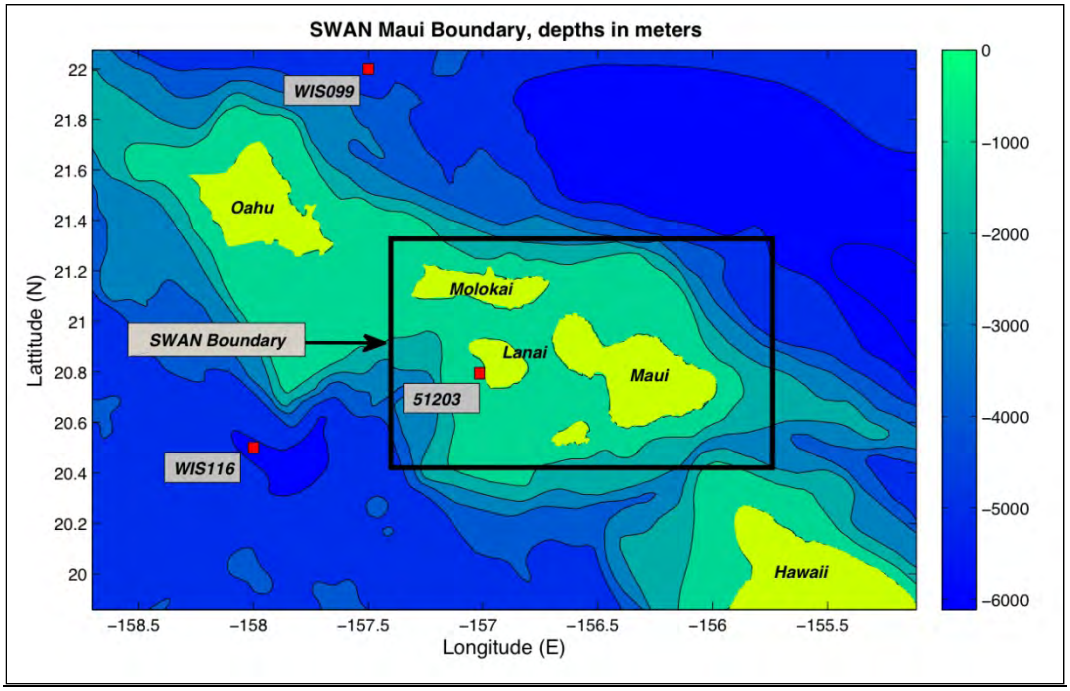

Figure 7.2. SWAN Maui domain (Sea Engineering, Inc. and Group 70 International 2009).

The ability of a wave model to predict conditions at a given location can be quantified by a number of statistical parameters, including Mean Error (ME), Root Mean Squared Error (RMSE), and Scatter Index (SI). These parameters provide valuable insight to the magnitude and nature of differences between observed and predicted values. ME, also known as bias, is the calculated average difference between the predicted WIS values and the observed NDBC 51027 values. RMSE, also known as rms_{error}, can be thought of as the amount by which the predicted WIS value is expected

to differ from the observed NDBC 51027 value. It supplies a single measure of predictive power. SI is the expected difference between the predicted and observed value (rms_{error}) normalized by the average observed value. This affords an estimate of the amount by which a prediction differs from an observation in terms of the average magnitude of the observation. For example, an SI value of 1.0 would indicate that on average, the predicted value differs by 100 percent of the observed value, while a value of 0.1 would be indicative of a 10 percent difference on average. Wave datasets from the four WIS locations were compared to the NDBC 51027 dataset in terms of these parameters. Each WIS location performed differently in terms of ME, RMSE, and SI. For example, WIS 115 exhibited almost no bias (ME = 0.13 ft) but had an average error of 1.64 ft (RMSE = 0.51). SI for all locations was greater than 30 percent. Since none of the WIS locations are exactly collocated with NDBC51027, they can be expected to experience different wave exposure conditions due to shadowing from the nearby islands. For this reason, the source of errors in prediction cannot be attributed to model shortcomings alone, since wave conditions can vary significantly depending on position relative to wave shadowing.

It is logical to assume that one WIS station may perform better than another depending primarily upon the predominant wave direction at the time of prediction. During an easterly trade wind swell, WIS113 and WIS114 are relatively sheltered by the Big Island, while WIS115 and WIS116 could be expected to share similar exposure conditions as NDBC51027. Likewise, during a swell with a direction close to due north, WIS115 and WIS116 are relatively exposed, while NDBC51027, WIS113 and WIS114 are shadowed by the Islands of Maui, Molokai, and Lanai. For this reason, error analysis was extended to distinguish differences in model performance, taking into consideration differences in performance based upon primary swell direction. The goal of this undertaking was to establish a more realistic evaluation of performance based upon incident wave conditions and model output location. RMSE and bias were calculated for the four nearby WIS stations for each of the Scenes. Results are presented in Table 7.1.

7.1.3 Incident wave conditions from WIS analysis

The WIS dataset was primarily utilized to limit the number of incident wave conditions for modeling to those that can reasonably be expected to occur and the WIS dataset compared favorably to the NDBC 51027

Table 7.1. Scene-based performance analysis.

	Hs		Tp		Dp	
	bias	rmse	bias	rmse	bias	rmse
Scene 1						
wis113	-0.68	0.75	-1.18	4.06	-8.18	21.16
wis114	-0.46	0.58	-1.46	4.08	-4.60	18.59
wis115	-0.33	0.46	-0.15	3.99	-0.30	22.46
wis116	-0.29	0.47	-0.33	3.81	-1.86	20.75
Scene 2						
wis113	-0.20	0.30	1.76	3.38	9.39	28.31
wis114	-0.02	0.18	1.42	3.34	10.44	30.01
wis115	0.04	0.18	1.58	3.49	11.03	28.91
wis116	0.03	0.15	1.42	3.25	11.52	29.70
Scene 3						
wis113	-0.12	0.41	1.70	3.50	-20.58	36.34
wis114	0.27	0.54	1.54	3.35	-18.92	35.79
wis115	0.51	0.69	1.57	3.41	-9.87	32.59
wis116	0.59	0.81	1.46	3.35	-14.41	32.10

(Note – green indicates best performance)

measurements. It was concluded that the WIS dataset was sufficiently accurate to establish the wave climate. Further analysis of this dataset was necessary to provide incident wave conditions for higher resolution wave modeling. This included reduction of directional bin size to 15 deg, and further sorting records into H_{m0} bins of 1.0 ft and T_p bins of 2.0 sec. Additionally, selection of a single WIS location dataset for use was necessary to accurately quantify frequency of occurrence of a particular wave condition. A threshold frequency of occurrence could then be established as criteria for selection of a particular wave condition for higher resolution modeling. WIS116 was selected since it compared more favorably for Scene 2 conditions, and performed reasonably well for Scenes 1 and 3.

A threshold value for frequency of occurrence of 0.2 percent was then applied to the sorted data. Any wave condition within a defined Scene with a frequency of occurrence exceeding this value became an incident condition or ”case” to be evaluated in higher resolution modeling, and anything below this was filtered out. The resulting cases selected for modeling are shown in Table 7.2.

Table 7.2. Model cases: Scenes 1, 2, and 3.

Scene 1	WIS 116				
Case ID	direction	height (ft)	peak period	occurrences	% of total
1	30	3.5	9	543	0.3%
2	30	4.5	9	764	0.4%
3	45	3.5	9	565	0.3%
4	45	4.5	9	648	0.3%
5	60	3.5	9	555	0.3%
6	60	4.5	9	689	0.3%
7	75	3.5	9	1079	0.5%
8	75	4.5	5	635	0.3%
9	75	4.5	9	1093	0.5%
10	90	3.5	9	1173	0.6%
11	90	4.5	9	1180	0.6%
12	90	5.5	5	510	0.2%
13	90	5.5	9	731	0.3%
14	105	3.5	9	715	0.3%
15	105	4.5	9	525	0.2%
				11405	5.4%

Scene 2	WIS 116				
Case ID	direction	height (ft)	peak period	occurrences	% of total
1	150	3.5	11	529	0.3%
2	150	4.5	11	559	0.3%
3	165	3.5	11	1244	0.6%
4	165	4.5	11	937	0.4%
5	165	4.5	13	431	0.2%
6	180	3.5	11	1618	0.8%
7	180	3.5	13	1387	0.7%
8	180	3.5	15	491	0.2%
9	180	4.5	11	1583	0.8%
10	180	4.5	13	1884	0.9%
11	180	4.5	15	1087	0.5%
12	180	4.5	17	562	0.3%
13	180	5.5	13	801	0.4%
14	180	5.5	15	445	0.2%
15	195	3.5	11	1618	0.8%
16	195	3.5	13	3289	1.6%
17	195	3.5	15	1397	0.7%
18	195	3.5	17	706	0.3%
19	195	4.5	11	1512	0.7%
20	195	4.5	13	5361	2.5%
21	195	4.5	15	3169	1.5%
22	195	4.5	17	1523	0.7%
23	195	5.5	13	2217	1.1%
24	195	5.5	15	1831	0.9%
25	195	5.5	17	1142	0.5%
26	195	6.5	13	453	0.2%
27	195	6.5	15	882	0.4%
28	195	6.5	17	521	0.2%
29	210	3.5	11	718	0.3%
30	210	3.5	13	2199	1.0%
31	210	3.5	15	1106	0.5%
32	210	3.5	17	607	0.3%
33	210	4.5	11	495	0.2%
34	210	4.5	13	2126	1.0%
35	210	4.5	15	1667	0.8%
36	210	4.5	17	662	0.3%
37	210	5.5	13	649	0.3%
38	210	5.5	15	672	0.3%
39	225	3.5	11	467	0.2%
40	225	4.5	13	563	0.3%
41	240	4.5	13	425	0.2%
				51535	24.5%

Table 7.2 (continued)

Scene 3	WIS 116				
Case ID	direction	height (ft)	peak period	occurrences	% of total
1	270	3.5	11	457	0.2%
2	270	4.5	11	602	0.3%
3	270	4.5	13	558	0.3%
4	270	5.5	13	426	0.2%
5	285	3.5	11	617	0.3%
6	285	4.5	11	973	0.5%
7	285	4.5	13	777	0.4%
8	285	5.5	11	482	0.2%
9	285	5.5	13	912	0.4%
10	285	6.5	13	562	0.3%
11	300	3.5	11	970	0.5%
12	300	4.5	11	2188	1.0%
13	300	4.5	13	1741	0.8%
14	300	5.5	11	1875	0.9%
15	300	5.5	13	3554	1.7%
16	300	5.5	15	649	0.3%
17	300	6.5	11	748	0.4%
18	300	6.5	13	4071	1.9%
19	300	6.5	15	1011	0.5%
20	300	7.5	13	2642	1.3%
21	300	7.5	15	1069	0.5%
22	300	8.5	13	1353	0.6%
23	300	8.5	15	1263	0.6%
24	300	9.5	13	601	0.3%
25	300	9.5	15	794	0.4%
26	300	10.5	15	678	0.3%
27	315	3.5	11	979	0.5%
28	315	4.5	11	3026	1.4%
29	315	4.5	13	1897	0.9%
30	315	4.5	15	515	0.2%
31	315	5.5	11	2507	1.2%
32	315	5.5	13	4116	2.0%
33	315	5.5	15	849	0.4%
34	315	6.5	11	1212	0.6%
35	315	6.5	13	4322	2.1%
36	315	6.5	15	1509	0.7%
37	315	6.5	17	472	0.2%
38	315	7.5	13	2659	1.3%
39	315	7.5	15	1298	0.6%
40	315	7.5	17	489	0.2%
41	315	8.5	13	1501	0.7%
42	315	8.5	15	1360	0.6%
43	315	9.5	13	601	0.3%
44	315	9.5	15	961	0.5%
45	315	9.5	17	459	0.2%
46	315	10.5	15	539	0.3%
47	330	3.5	11	723	0.3%
48	330	4.5	11	2105	1.0%
49	330	4.5	13	1107	0.5%
50	330	5.5	11	1910	0.9%
51	330	5.5	13	1825	0.9%
52	330	5.5	15	552	0.3%
53	330	6.5	11	783	0.4%
54	330	6.5	13	1820	0.9%
55	330	6.5	15	687	0.3%
56	330	7.5	13	965	0.5%
57	330	7.5	15	703	0.3%
58	330	8.5	13	593	0.3%
59	330	8.5	15	619	0.3%
60	345	4.5	11	1118	0.5%
61	345	5.5	11	791	0.4%
62	345	5.5	13	568	0.3%
63	345	6.5	11	497	0.2%
64	345	6.5	13	463	0.2%
				80673	38.3%

7.2 Wave transformation modeling

7.2.1 Simulating WAves Nearshore (SWAN) modeling

SWAN is a third generation wind wave model developed at the Delft University of Technology. SWAN is capable of computing the generation, propagation, and transformation of waves in coastal regions as well as in deep water. It accounts for refractive propagation over arbitrary bathymetry and can be driven by boundary conditions and wind, either independently or in concert. SWAN was employed to transform incident wave cases at the deepwater model boundaries to intermediate/shallow water near Kaumalapau Harbor.

The model was set up to run in stationary mode, meaning that the incident wave conditions are not time dependent. Computational resolution was set at 18 sec, or approximately 500 m. Bathymetric resolution is higher (1 sec) to ensure that the interpolated depth at the computational grid point is as accurate as possible. Bathymetry for the domain was compiled from the 1-min General Bathymetric Charts of the Oceans, Scanning Hydrographic Operational Airborne Lidar Survey (SHOALS), USGS 5-sec, EROS Data Center, and the National Elevation 10-m topographic grid datasets.

Validation of the SWAN model results was performed using forecast wave data during the period from 18 August 2007 to 28 October 2007. This model in its current state includes a global wave model, Hawaii wave model, and separate nearshore domains for Kauai, Oahu, Maui, and the Big Island (The Maui domain including Kaumalapau Harbor is shown in Figure 7.2). The global wave model is a duplicate of NOAA's Wavewatch3 (NWW3) operational forecast model. The Hawaii model is a nested regional implementation of NWW3. The individual nearshore domains utilize SWAN, and are nested within the Hawaii Domain.

For this period, output data from the forecast model point VBL01 was compared to the existing Kaumalapau buoy data to obtain performance indices. VBL01 is collocated with the existing Kaumalapau buoy to facilitate performance analysis and lookup table development. The Maui SWAN model was determined to perform sufficiently well for use as a transformation model for the incident wave cases. In comparison, the validation of the WIS dataset yielded ME for H_{m0} ranging from ~0.33 ft to ~1.31 ft, RMSE for H_{m0} on the order of 1.64 ft and SI for H_{m0} on the order 0f 0.33. The VBL01 H_{m0} performance indices include a ME of -0.43 ft, RMSE of 0.66 ft and SI

of 0.24. In other words, the Maui SWAN model will perform as good as, or better than, the model used to develop the incident wave conditions.

Parametric output wave data from the model was obtained at three locations, VBL01, VBL02, and VBL03 (Figure 7.3). VBL02 is located directly in the entrance of the harbor, and VBL03 is located approximately 0.1 nm west of the harbor entrance, and was used to provide boundary conditions to subsequent Refraction/Diffraction (REF/DIF) modeling. VBL02 is located within the subsequent REF/DIF modeling domain, therefore conditions at VBL02 are most appropriately obtained from the higher-resolution domain.

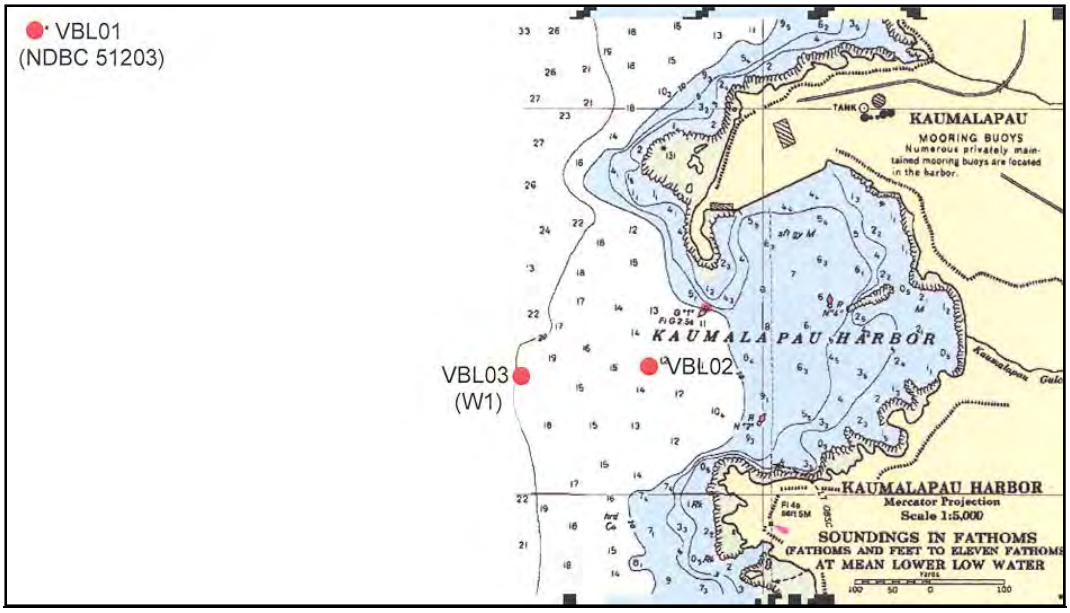

Figure 7.3. SWAN output points for Kaumalapau Harbor; VBL01 is coincident with CDIP 146 (Sea Engineering, Inc. and Group 70 International 2009).

Incident wave conditions from each case derived from the WIS116 analysis were applied uniformly across each boundary of the SWAN model. For Scene 2 (southern swell), the WIS116 condition was applied at all boundaries (North, East, South, and West) since there is no shadowing from the other Hawaiian Islands at Kaumalapau from the directions considered in that Scene. In Scene 3 (North Pacific Swell), the application of WIS116 boundary conditions to the northern boundary of the model was determined to be problematic since WIS116 experiences significant shadowing from Oahu and Kauai during swells originating from the Northwest-to-North directions. For this reason, WIS099 was selected as the source of boundary conditions for the northern SWAN boundary. This

was accomplished by searching the WIS116 dataset to identify time steps corresponding to the case condition. The corresponding WIS099 conditions at the same time steps were obtained and applied to the northern boundary.

Additional Scene 2 cases were included in the model runs to augment those determined during WIS116 analysis with cases of particular interest and those known to occur frequently (Table 7.3). These cases included smaller long-period south swell, hurricane conditions, and Kona wind waves. This was done to ensure a more complete set of incident wave conditions.

Table 7.3. Additional Scene 2 cases.

Scene 2			
Case ID	Height (ft)	Peak period (s)	Direction
42	1.5	15	180
43	1.5	17	180
44	2.5	15	180
45	2.5	17	180
46	1.5	15	195
47	1.5	17	195
48	2.5	15	195
49	2.5	17	195
50	40	16	225
51	40	12	225
52	35	12	225
53	30	12	225
54	13	10	215
55	10	10	215
56	17	9	225

Due to its very limited exposure to easterly tradewind swell, Scene 1 cases were replaced with more extreme tradewind swell cases. This was done to limit model cases to those which would result in a detectable wave condition at the Kaumalapau Buoy (NDBC 51203). Based on the results of the Scene 1 extreme tradewind swell cases, it was determined that it is highly unlikely that tradewinds can produce swell that will impact the harbor. Very small wave heights occur at VBL01 from ~310 deg. The combination of small wave height, short wave period, and oblique approach direction limits incident wave energy at harbor.

7.2.2 REF/DIF modeling

To transform wave conditions resultant from SWAN modeling to points in and near the harbor, the REF/ model was employed utilizing a smaller, higher resolution domain focused on the harbor area. The model used, REF/DIF1, version 2.5, was developed by Kirby and Dalrymple (1991).

This nonlinear model includes processes of wave refraction, diffraction, shoaling, and energy dissipation. Wave refraction involves changes in wave height and direction as waves pass over changing bottom contours. Wave diffraction is the process by which wave energy spreads laterally along the wave crest in the lee of an obstruction such as a breakwater. Wave shoaling is the increase in wave height as the waves move into increasingly shallower water. Energy dissipation is primarily due to bottom friction and wave breaking. The breaker height in shallow water is a function of the water depth, the bottom slope, and the incident wave height and period.

The initial wave conditions for the model were obtained from VBL03 at a water depth of 107 ft MLLW, located approximately 0.1 nm offshore of the harbor entrance. Two grid systems were used; one was 2,250 ft x 2,650 ft for southerly incident waves, and the other was 2,210 ft x 3,190 ft for northerly incident waves. A grid size of 10 ft was used for both grid systems.

The model results were used to develop lookup tables for preliminary wave heights at seven additional wave stations (Figure 7.4); one at the harbor entrance (W2 = VBL02), one each at front and back of the breakwater (W3 and W4, respectively), three along the barge pier (K01 collocated with exterior wave gage from Chapter 6, K02, and K03), and one at the location where the exterior wave gauge was deployed in May 2007 (W5). Station W1 was collocated at the driver gage VBL03. These lookup tables were refined using additional techniques mentioned later in this chapter. A mean sea level tide (0.9 ft MLLW) was used for model analyses. Results of the REF/DIF modeling indicated good agreement with previous physical model results at output stations K01, K02, and K03, as presented in the following section.

7.2.3 Comparison of modeling results with previous physical model study

In 1998, the USACE performed undistorted, 3-D physical model testing of Kaumalapau Harbor to evaluate two harbor improvement alternatives (Smith 1998). The improvements as constructed most closely resemble

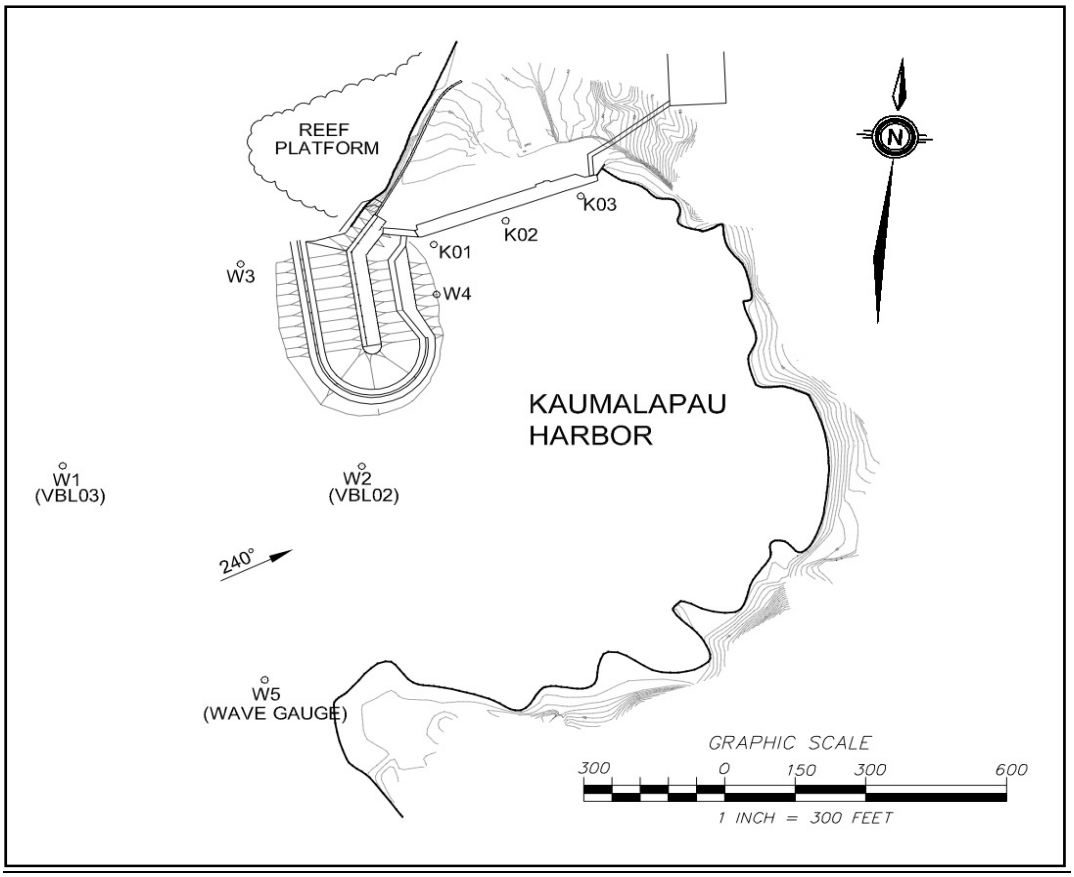

Figure 7.4. Refraction/diffraction numerical model REF/DIF output locations (Sea Engineering, Inc. and Group 70 International 2009).

the "dogleg breakwater" alternative of that study. To evaluate the effectiveness of the alternatives, wave heights at points (H_i) along the pier were normalized by the incident deepwater wave height (H_o). The resultant amplification factor, A':

$$A' = \frac{H_i}{H_o}$$

was calculated for various directions and periods at each "gauge" location (1-4) depicted in Figure 7.5 below. Results for the 220 deg deepwater conditions are presented in Figure 7.6.

In a similar manner, amplification factors were developed from the REF/DIF results with Ho at VBL03 = W1, and Hi as REF/DIF output points K01, K02, and K03 which are analogous to gauge points 3, 1, and 4 respectively. This allows for direct comparison of the physical model amplification factors with the numerical model coefficients presented in Figure 7.7 below.

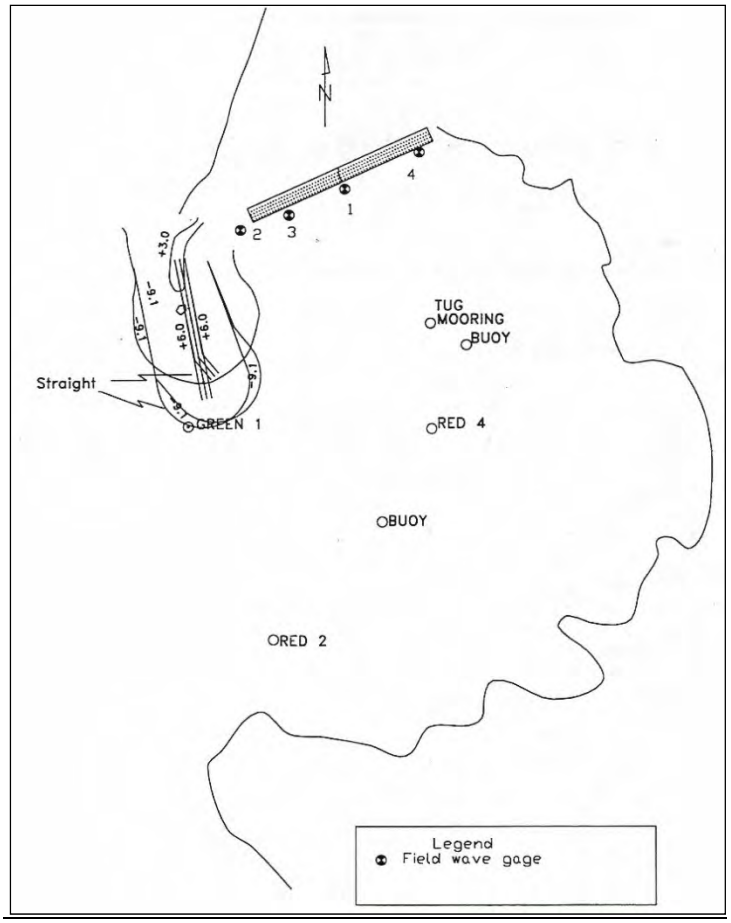

Figure 7.5. Physical model testing output points (Smith 1998).

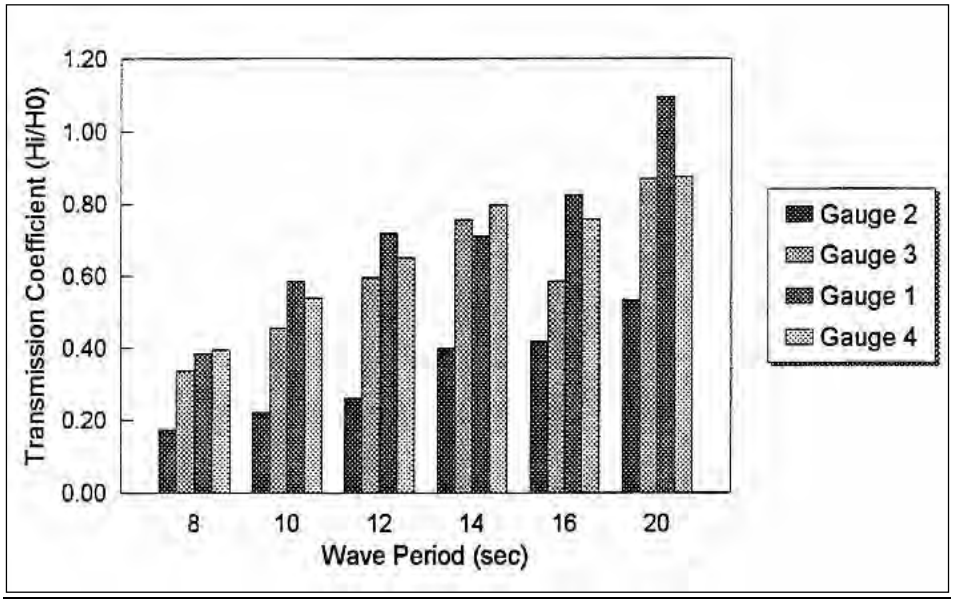

Figure 7.6. Calculated amplification factor (shown as Transmission Coefficient) from physical model for 220-deg case (Smith 1998).

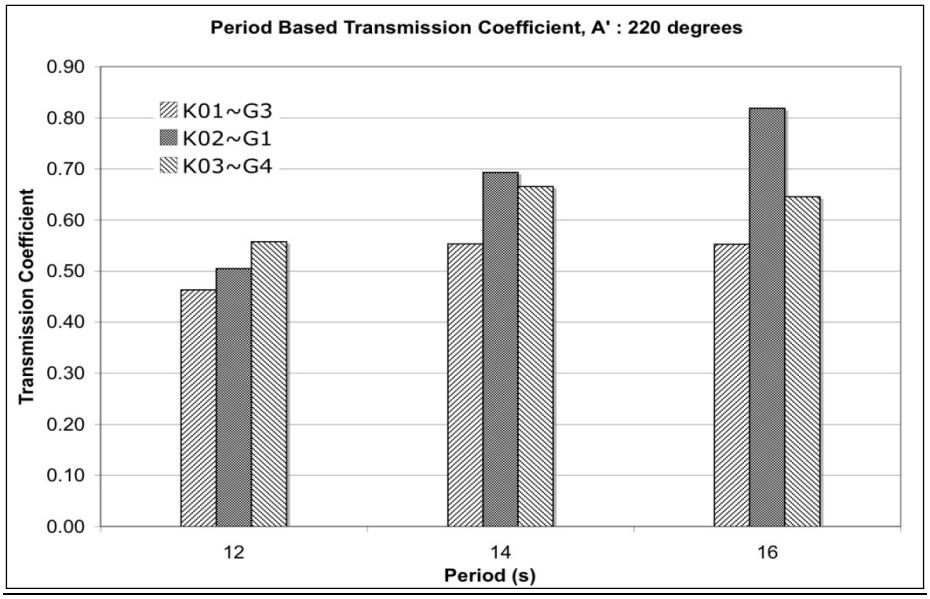

Figure 7.7. Calculated amplification factor (shown as Transmission Coefficient) from numerical modeling using REF/DIF.

For periods of 12 sec, REF/DIF *A′* varies from 0.45 to 0.55 along the pier length, while physical model A' varies from 0.60 to 0.75. For periods of 14 sec, REF/DIF *A′* varies from 0.55 to 0.70 along the pier length, while physical model A' varies from 0.65 to 0.80. For periods of 16 sec, REF/DIF *A′* varies from 0.55 to 0.82 along the pier length, while physical model *A′* varies from 0.60 to 0.82. While REF/DIF seems to predict amplification factors (roughly within 25 percent of measurements) corresponding to higher levels of wave reduction, this comparison is indicative of general agreement between the two modeling methods.

7.3 Direction based amplification factor

The ratio of surge and wave heights at a specific location inside the harbor to incident waves (at station CDIP 146) is defined as the amplification factor, *A′*. An *A′* value of 1.0 would indicate that the wave height inside the harbor was equal to the incident wave height, while a value of 0.5 would be indicative of a 50 percent reduction in wave height.

The orientation of the harbor as well as the sheltering afforded by the breakwater gives rise to a dependency of amplification factor, *A′*, with direction. For this reason, direction-based *A′s* were developed for the points within the REF/DIF modeling shown in Figure 7.4. To arrive at a single amplification factor, all *A′s* within a 10-deg directional bin were averaged without regard to wave period. The results of this analysis are presented in Table 7.4 below.

Table 7.4. Direction based amplification factor (shown as Transmission Coefficient) from REF/DIF results.

	Direction-Based Transmission Coefficient, A'							
Direction	W1	W2	W3	W4	W5	K01	K02	K03
180	0.86	1.05	0.81	0.53	0.49	0.28	0.42	0.55
190	0.86	0.74	0.62	0.58	0.69	0.33	0.34	0.47
200	0.85	0.81	0.76	0.50	0.73	0.57	0.47	0.40
210	0.87	0.83	0.74	0.46	0.80	0.61	0.55	0.42
220	0.88	0.84	0.77	0.54	0.73	0.49	0.58	0.52
230	0.89	1.09	0.77	0.79	0.95	0.50	0.54	0.44
240	0.90	1.12	1.00	0.93	1.07	0.62	0.62	0.43
260	0.91	0.79	0.85	0.33	0.92	0.27	0.44	0.32
270	0.93	0.75	0.82	0.25	0.98	0.24	0.40	0.31
280	0.93	0.86	0.84	0.30	1.01	0.33	0.37	0.40
290	0.93	0.87	0.77	0.34	0.97	0.35	0.33	0.47
300	0.92	0.87	0.64	0.19	0.78	0.26	0.27	0.42

A directional dependency of the amplification factor can be detected in this table. For example, K02 amplification factors are at a minimum for the southerly and west-northwesterly directions. This result agrees with the observable physical condition of the harbor since the rocky point to the south of harbor affords natural protection from the southerly direction, while the breakwater should be most effective when waves approach from the west-northwest. As expected, the maximum amplification factor occurs with an incident wave at VBL01 of 240 deg which corresponds to the direction of maximum exposure of the harbor entrance and points K01, K02, and K03 along the pier as shown in Figure 7-4.

7.3.1 Correlation and prediction using amplification factor

Due to the complexities involved in natural physical systems, and the limitations of state-of-the-art numerical wave models, it is recommended practice to augment and validate the results of modeling with measurements at a given location. A comparison of model results and available measured data was made for location K01.

It is common practice in breakwater diffraction/refraction analysis to assume that A' at a specific location is a function of two variables, namely peak wave period, T_p, and peak wave direction, D_p. The preliminary model results for each output location were compiled into a dataset for each scene that consisted of A' values as a function of T_p and D_p. A three-dimensional surface was then fitted through this dataset (T_p versus D_p versus A'). A typical three-dimensional surface plot is shown in Figure 7.8 for location K01 (surface plots for other lookup table output locations are presented in

Appendix B), with D_p on the x-axis, T_p on the y-axis, and the color bar representing values of A'. To obtain an estimate of wave height at a particular output location, multiply the measured wave height at the buoy by the A' value for the corresponding measured T_p and D_p. The advantage to this strategy is that this "predictive surface" allows for interpolative, and to some extent, extrapolative estimates of A'. This surface can be binned and sampled, and readily incorporated into algorithms that can ascertain A' and estimate wave heights in an automated fashion. Similarly, predictive surfaces were developed for other points in and near the harbor (K02, K03, W2, W3, W4, and W5). These surfaces were used to update previously mentioned lookup tables (originally derived from non-interpolated numerical modeling results only) to provide more accurate wave height estimates. These resulting "improved" lookup tables are presented in Appendix B in Table B.1 and B.2.

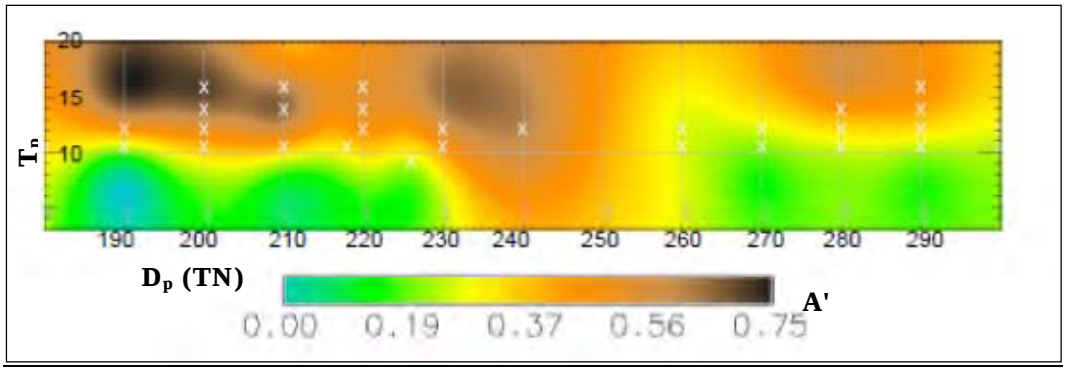

Figure 7.8. Three-dimensional surface plot showing predicted values of A' at Location K01.

7.3.2 Validation and improvement of amplification factors using field data[1]

The University of Hawaii (on behalf of the MCNP program) deployed a pressure sensor at station K01 from July 2007 through June 2008, as presented in Chapter 6 (the "interior" wave gage). A portion of the measured data from this pressure sensor was utilized to develop an additional surface of A' values (as a function of T_p and D_p). The magnitude of the difference between the station K01 measurements and predictions from the numerical modeling can be readily discerned by subtraction of the measured A' value surface from the modeled A' value surface (Figure 7.9). The difference between predicted and measured A' values varied between

[1] This section is extracted from Sea Engineering, Inc. and Group 70 International (2009), but has been modified substantially.

+0.49 (over predicted) for wave periods between 15 to 20 sec coming from the south through south-southwest direction (180 – 215 deg TN) to -0.21 (under predicted) for shorter wave periods (~5 to 10 sec) coming from the south (190 deg TN). The observed difference surface is also indicative of a general over prediction of *A'* values by the numerical modeling at this location, as most of the Figure 7.10 plot is in the green to red range. The two datasets for station K01 (predicted and measured *A'* values) were combined, and a new surface was developed using the combined dataset (Figure 7.10). The resultant combined surface represents the best estimate of *A'* values at this location, and is reflected in the K01 column of the Appendix B tables.

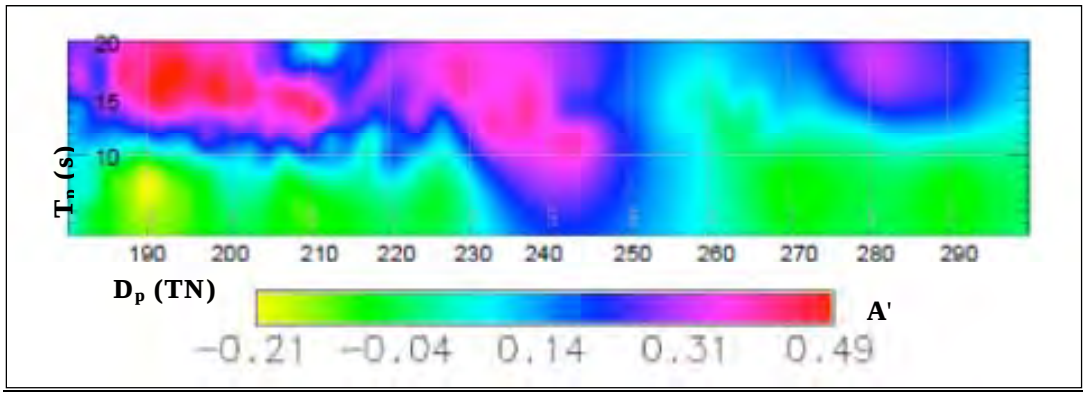

Figure 7.9. Three-dimensional surface plot showing difference between measured and predicted values of *A'* at Location K01.

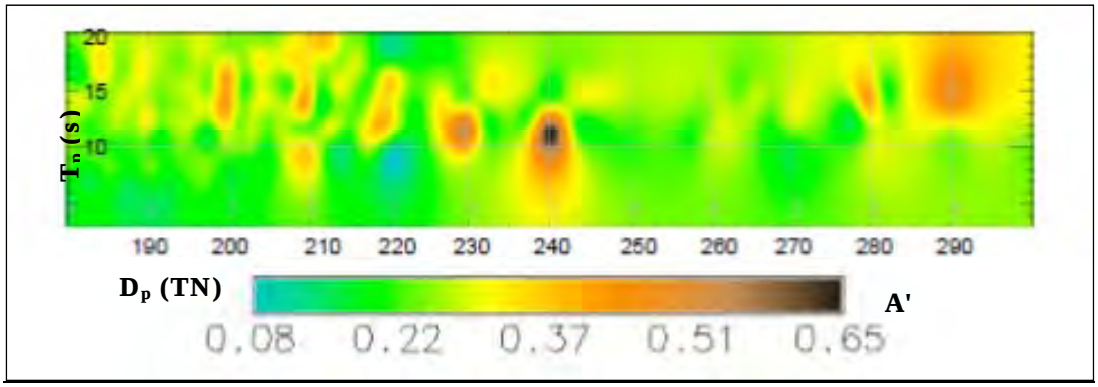

Figure 7.10. Three-dimensional surface plot showing predicted values of *A'* at Location K01, combined with partial measured data from 2007-2008 wave gage deployment.

To further ascertain the accuracy of the modeling effort, a portable directional GPS-based wave buoy was deployed on 5 December 2008, as previously mentioned in Chapter 6. Deployment locations included model output stations W1, W5 (collocated with exterior wave gage from Chapter 6), K01 (collocated with interior wave gage from Chapter 6), K02, and K03. Winds at the project site were light and variable resulting in a nearly

complete lack of wind waves which provided ideal conditions for the measurement of long-period wave energy that can penetrate the harbor. Wave conditions were relatively mild during the measurement period. The dominant event was a large northwesterly swell. Measured wave conditions at NDBC 51203 (CDIP 146) ranged from 3.7 to 4.3 ft with periods of 13 to 15 sec and direction between 270 and 290 deg.

Table 7.5 provides a summary of concurrent parametric wave measurements at the buoy and each of the Kaumalapau Harbor observation locations. Measured amplification factors (A') are also presented in this table. Figure 7.11 depicts the primary directions of incident and reflected wave energy in Kaumalapau Harbor. Wave spectral plots resulting from the measurements are provided in Appendix B.

Station K01 exhibits the lowest wave height and amplification factor in the harbor due to its protected position relative to the breakwater. Examination of wave spectral information (Appendix B) collected indicates the primary direction of refracted wave approach was approximately 190 deg with wave periods between 10 and 20 sec. Average wave height attenuation at this location was 73 percent, most likely a result of refraction, diffraction, and bottom dissipation. Signals of reflected wave energy are visible in the spectral energy data at ~300 deg, ~350 deg, ~150 deg, and ~10 deg. The ~300 deg signal most likely originates from the breakwater itself, while the ~350 deg and ~10 deg signals originate from the pier. The ~150-deg signal can be explained as reflection from the steep natural shoreline on the southeastern part of the harbor.

Table 7.5. Measured offshore and harbor wave parameters during field data collection, and calculated amplification factors.

Measurement	Date.Time	CDIP 146 Conditions			Measured Conditions			A'
Location	(HST)	Hs(ft)	Tp(s)	Dp(°)	Hs(ft)	Tp(s)	Dp(°)	Coeff.
K01	20081205.0940	3.9	15.4	283	1.2	15.3	190	0.308
K01	20081205.1008	4.3	14.3	281	1.0	15.3	190	0.246
K02	20081205.1108	3.7	14.3	267	1.5	14.3	200	0.402
K02	20081205.1138	4.3	14.3	283	1.4	17.1	200	0.321
K03	20081205.1218	4.0	15.4	286	2.0	15.4	235	0.512
K03	20081205.1246	4.2	15.4	286	1.6	15.4	235	0.391
W5	20081205.1346	4.2	14.8	280	3.7	15.4	280	0.890
W5	20081205.1416	4.1	13.8	275	3.4	15.4	280	0.847
W1	20081205.1446	3.8	14.4	276	3.5	14.8	280	0.915
W1	20081205.1516	3.9	14.4	276	3.4	15.4	270	0.875

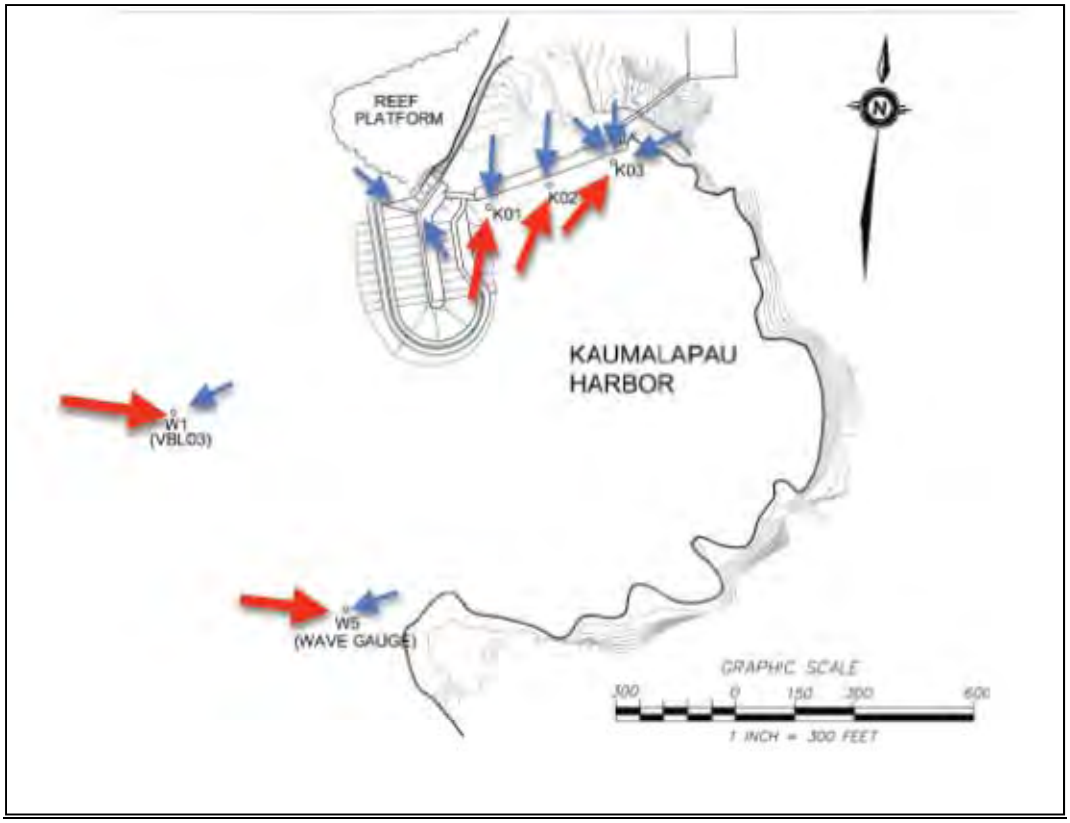

Figure 7.11. Primary (red) and reflected (blue) wave energy at measurement locations.

Station K02 exhibits slightly higher wave energy than K01. The primary direction of refracted wave approach was approximately 200 deg with wave periods between 10 and 20 sec. Average wave height attenuation at this location was 65 percent, again most likely a result of refraction, diffraction, and bottom dissipation. Signals of reflected wave energy are visible at ~0 and ~20 deg, both of which represent pier reflection.

Station K03 represents the least protected location along the pier. The primary direction of refracted wave approach is from 235 deg with periods between 13 and 20 sec. Average wave height attenuation at this location was 55 percent most likely a result of refraction, diffraction, and bottom dissipation. The close proximity of K03 with multiple reflective surfaces makes for a complicated directional wave spectrum. It appears that there are reflective signals at ~300 deg, ~250 deg, ~0 deg, and ~40 deg. The ~300-deg and ~0-deg signals can readily be attributed to pier reflection. It is likely that the ~250-deg signal originates from the breakwater. The ~40-deg signal is probably due to the adjacent steep natural shoreline. The resultant spectrum is consistent with field observations during the measurement period that this location was convergent for many directions.

Wave energy was observed as more of a "heaving" of the water surface rather than detectable separate wave trains, indicating a likely antinode in the incident-reflected wave field.

W5 is located outside the protection of the harbor. As anticipated, significantly more wave energy was measured here than at the inner harbor positions. The 280 deg incident wave direction was nearly the same as that measured at the buoy. Periods ranged from 20 sec to 8 sec. Average wave height attenuation at this location was 15 percent, most likely due to bottom dissipation only. The incident wave energy was significantly larger than reflected energy and only a small reflective signal was detected from approximately 50 deg. This reflection most likely originated from the steep natural shoreline of the inner harbor.

W1 is representative of the Kaumalapau Harbor incident wave condition. Wave measurements here are nearly identical to the concurrent buoy measurements for direction and period, with a ~10 percent attenuation of wave height most likely due to bottom friction since very little refraction occurs between the two locations. A reflective signal can be detected from ~50 deg which can readily be attributed to the breakwater to the northeast.

A comparison was made between predicted wave heights based on numerical modeling results and measured wave heights obtained with the portable wave buoy. Results of this comparison are shown in Table 7.6.

Table 7.6. Comparison of measured vs. predicted wave heights and amplification factors for 5 Dec 2008 at specified locations.

Measurement	Date.Time	CDIP 146 Conditions			Predicted		Measured		Difference	
Location	(HST)	Hs(ft)	Tp(s)	Dp(°)	Hs(ft)	A'	Hs(ft)	A'	Hs(ft)	A'
K01	20081205.0940	3.9	15.4	283	1.6	0.399	1.2	0.308	0.4	0.091
K01	20081205.1008	4.3	14.3	281	1.3	0.316	1.0	0.246	0.3	0.070
K02	20081205.1108	3.7	14.3	267	1.6	0.43	1.5	0.402	0.1	0.023
K02	20081205.1138	4.3	14.3	283	1.4	0.32	1.4	0.321	0.0	0.001
K03	20081205.1218	4.0	15.4	286	2.6	0.66	2.0	0.512	0.6	0.150
K03	20081205.1246	4.2	15.4	286	2.8	0.66	1.6	0.391	1.1	0.271
W5	20081205.1346	4.2	14.8	280	4.3	1.02	3.7	0.890	0.5	0.131
W5	20081205.1416	4.1	13.8	275	4.2	1.04	3.4	0.847	0.8	0.188

The results of this comparison show that the predictive algorithm is capable of providing satisfactory estimates of H_{m0} in and near the harbor, though there is a consistent positive bias (over prediction of measured data) in the resulting wave heights. In most cases, the prediction was within 0.5 ft of the measured H_{m0}. Inclusive of the outlier difference of 1.1 ft at K03, errors in predicted wave heights ranged from 0 to 69 percent, with a mean value of 25 percent.

This comparison also demonstrates that the predictions exhibit similar sensitivity to changing input peak period (T_p) conditions. For example, at K01, the CDIP 146 T_p condition for the second measurement (20081205.1008 HST) was about 1 sec less than the previous measurement, while the direction remained relatively unchanged. The corresponding measured amplification factor (A') dropped from 0.308 to 0.246. This is also exhibited in the predicted amplification factor which drops from 0.399 to 0.316.

Additionally the predictions exhibit similar sensitivity to changing peak direction (D_p) input. For example, the CDIP 146 D_p condition for the second K02 measurement (20081205.1138 HST) was 16 deg more northerly than the previous measurement while the T_p remained unchanged. This is reflected in the measured amplification factor dropping from 0.402 to 0.321. Similarly, the predicted amplification factor dropped from 0.425 to 0.322. The physical explanation for the reduction in amplification factor lies in the orientation of the harbor entrance, which faces almost due west. As the deepwater wave direction turns more northerly, the pier locations are less exposed to wave energy for the same T_p conditions.

7.4 Analysis of post-construction harbor wave conditions

7.4.1 Development of a program to automate lookup tables: KPWAVE[1]

The previously presented wave data from both measured and modeled sources and the resulting lookup tables in Appendix B were used to develop a FORTRAN-based program (KPWAVE) which calculates predicted wave height values at the seven designated locations in and around the harbor (W2, W3, W4, W5, K01, K02 and K03) when given the offshore wave conditions at Kaumalapau Buoy (CDIP 146/NDBC 51203). The program also has the capability to read a time series input file of wave parameters produced directly from the CDIP buoy data server website, and create an output file of the corresponding time series at the output locations. The maximum input file size for KPWAVE is one year at 30 min intervals or 17,520 records.

The predictive surfaces that were developed (example shown in Figure 7.10) were binned into 680 bins for wave periods ranging from 3 to 20 sec and 480 bins for direction ranging from 180 to 300 deg. A gridded text file was

[1] This section extracted essentially verbatim from Sea Engineering, Inc. (2009)

then generated for each of these predictive surfaces and used as input to the predictive algorithm described in the separate report "KPWAVE: Program Modification and User Manual" (Sea Engineering, Inc. 2009).

The basic algorithm developed for this program is essentially a lookup table operation based on either user-entered or file-read wave conditions for the Kaumalapau Buoy offshore location (CDIP 146 / NDBC 51203). All wave height stations in KPWAVE are referenced to this offshore location. Inside the program, the user is prompted to input desired wave height, period, and direction for the offshore location and is shepherded to keep values within certain realistic ranges. If an input file is chosen for processing, the program will filter out any input records that contain a parameter which exceeds the stated limits, as follows:

$$H \text{ (in feet)} > 0,\ 3s \leq T \leq 20s,\ 180° \leq \theta \leq 300°$$

The input is then transformed into corresponding matrix indices, which consequently identify the linked A' values for the seven reporting stations listed above. If a returned value is flagged, it will still be printed but it will also be qualified by the text, "EXTRAPOLATED" to indicate to the user that the value may be less accurate. If input parameters in a file exceed range limits, then the flag column will report the string, "OUTOFBOUNDS" and the wave height reporting stations will all be set to '0' for that time step.

KPWAVE was compiled for both DOS and UNIX operating systems as FORTRAN 77/90 compatible source code. Following compilation, the program was debugged and checked against REF/DIF results and recorded wave data from Sea Engineering's field effort of 5 December 2008 for locations K01, K02, K03, and W1 and W5. Agreement between the various checks was considered satisfactory for all updated locations.

7.4.2 Comparison of KPWAVE output with wave gage data

As an additional validation, a direct comparison of the wave height time-series between the measured 2007 - 2008 wave gage data at K01 and the predicted wave height (developed using the CDIP buoy data as input to the KPWAVE program) is shown in Figure 7.12. This time-series comparison includes the events selected for further analysis in Chapter 6 as points of reference, namely the Kona storm, the south swell, and W-NW "Swell 1" and "Swell 2" as indicated in the figure.

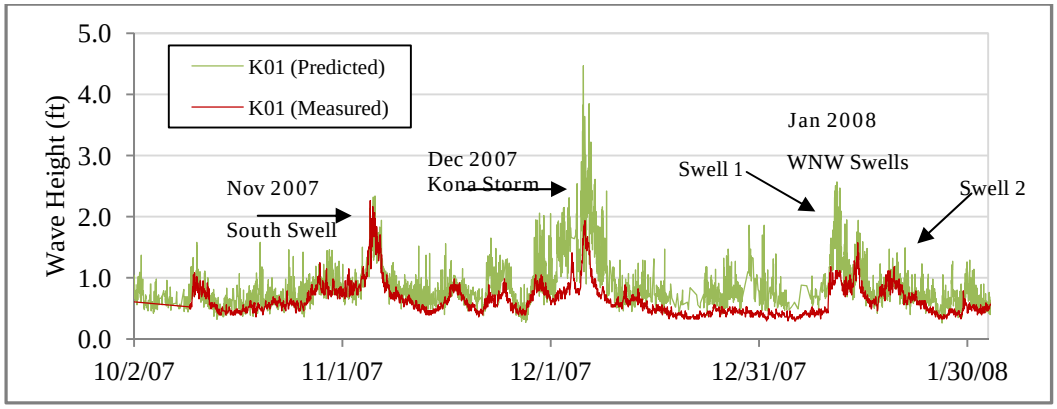

Figure 7.12. Time-series comparison of wave height for measured gage data at K01 (red) and predicted data derived with KPWAVE (green) at the same location.

Figure 7.12 shows that the KPWAVE-predicted wave height is in good agreement with measured data for the south swell and W-NW Swell 2; however, it is significantly over predicting wave height for the Kona storm condition and W-NW Swell 1. Possible explanations for this over prediction during certain wave conditions are:

- These specific offshore wave conditions were not adequately represented in the model runs completed to create the lookup table (requiring extrapolation by KPWAVE).
- The wave transformation model (REF/DIF) does not accurately represent the diffraction occurring in the lee of the breakwater under these conditions.
- And/or, the wave gage measurements from K01 that were incorporated into this predictive surface for improvement did not include these conditions.

A combination of two or more of these elements is also likely.

Further improvement of the KPWAVE program could be completed with additional measurements and model runs, but for the purposes of this monitoring study, the program is considered an adequate estimation of wave height at the barge pier (K01, K02, and K03) for the south swell condition and the W-NW swell condition with wave directions from approximately 290 deg or less. These conditions represent the most extreme cases at which the harbor would still be considered operational (i.e., barges would not be attempting to enter or tie up to the pier during Kona storms or hurricanes). The program is also considered a reasonable estimation of wave height at the location seaward of the breakwater (W3)

during all conditions. Though no validation data has been collected at this location, it is assumed that because there are virtually no effects due to diffraction and waves propagate directly from the buoy to this location experiencing only refraction and bottom friction, that the numerical model should be able to predict the wave height at this location reasonably well.

7.4.3 Transformation of buoy time-series using KPWAVE

Prediction of the full time-series of wave heights at all seven KPWAVE output locations (W2, W3, W4, W5, K01, K02, and K03 – located as shown in Figure 7.4) was completed using the 3.75-year CDIP buoy data from May 2007 through December 2010. Examination of the results in the following will focus on the locations adjacent to the barge pier (K01, K02, and K03) to evaluate post-construction mooring conditions, as well as the location seaward of the breakwater (W3), to evaluate incident wave conditions affecting the repaired breakwater.

Comparison of the time-series of wave heights at K01, K02, and K03 (shown in Figure 7.13) was completed in terms of the peak wave height for an event exceeding a pre-determined threshold of 3.0 ft for all three locations (indicated by dashed line in the figures).

This is a lower threshold than the 4.9 ft barge pier wave height condition specified by the 1996 Special Design Report during a 15.1 ft offshore wave condition (as described in the previous chapter). The lower threshold was chosen to include a wider range of wave responses in the analysis and to represent the various types of events recorded during the period of record.

Beginning with Station K01 (top panel of figure), the most sheltered of the output locations along the barge pier, it is evident from the plot that there were two events during the 3.75-year time-series that were predicted to have exceeded the threshold at this location. The first event was the December 2007 Kona Storm which, as shown previously in Figure 7.12, is a condition in which the KPWAVE program has significantly over predicted the actual wave height at this location. The actual measured peak wave height during this event at K01 was approximately 2.0 ft. In addition, as mentioned above, this is not considered a condition in which barges would be attempting to transit to or moor inside the harbor, so this event will be discounted in this and the following discussion of predicted data at the barge pier.

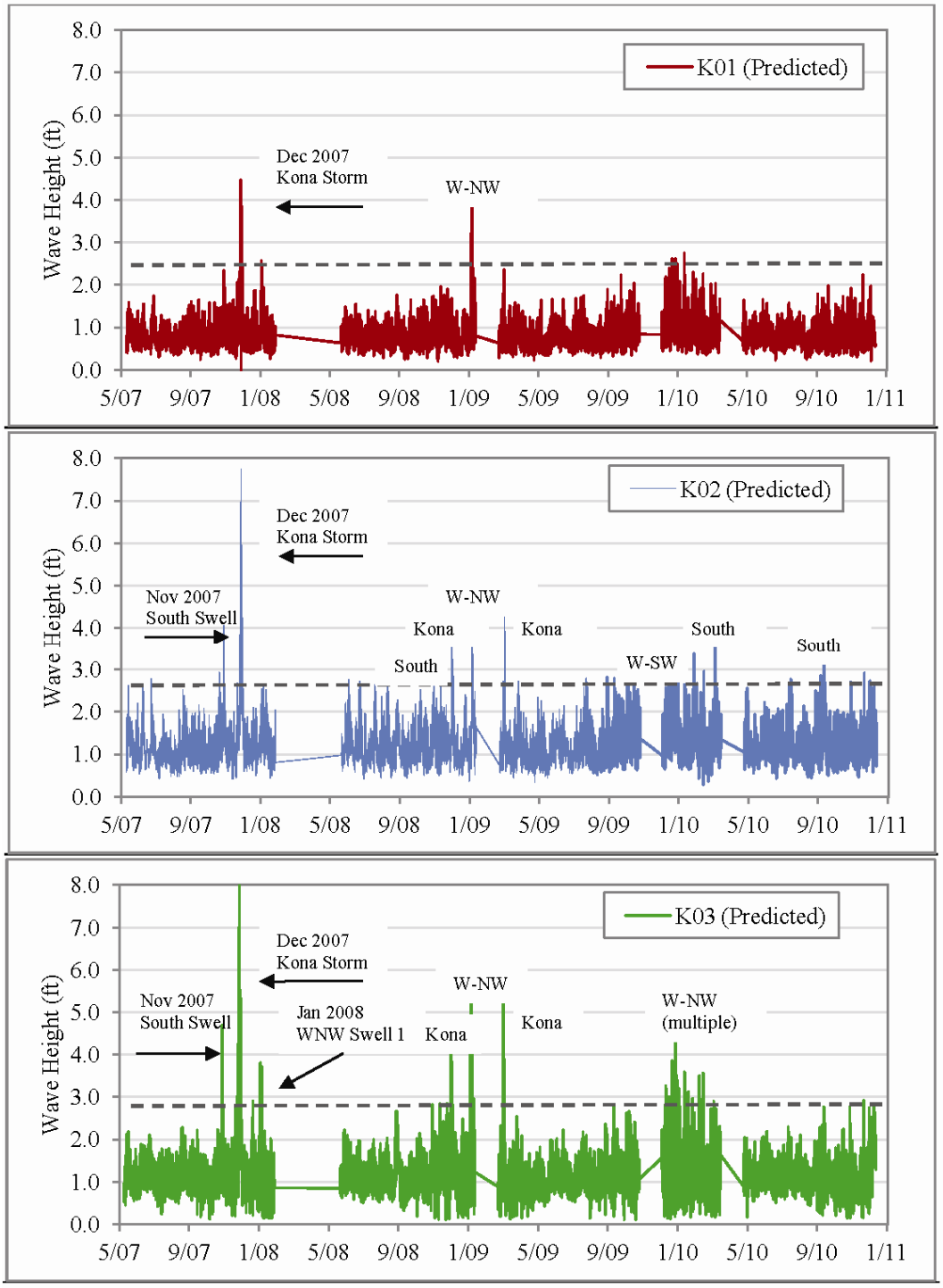

Figure 7.13. Time-series of KPWAVE-predicted wave height at K01, K02, and K03 stations.

The second event that was predicted to have exceeded the 3.0-ft threshold at K01 was a W-NW swell occurring in January 2009 with offshore conditions of 7- to 9-ft significant wave height, 12- to 16-sec wave period, and wave directions in the range of 275 to 300 deg TN. The largest wave

heights at K01 during this event (3.75 to 4.0 ft) were predicted to occur when offshore wave heights had wave period of 14.3 sec and wave direction of 290 deg TN. Though in light of the previous analysis these specific occurrences may also be exhibiting some level of over prediction by KPWAVE (290 deg cutoff in confidence mentioned previously), it is likely that this was a significant wave event at K01 due to the response at other times during the event when wave directions and periods offshore were in ranges where KPWAVE predictions agreed well with measured data. Smaller wave height responses between 2 and 3 ft are also evident at this location during wave events with westerly components of direction (Kona and W-NW swell conditions), and this may be partially due to wave reflection originating from the barge pier, breakwater, and southeast shoreline of the harbor (as described in the previously presented energy spectrum data) or it may be the result of an over prediction during Kona and certain W-NW conditions. No south swell events within the period of record caused a response at K01 above the 3-ft threshold.

At the K02 location, roughly at the center of the barge pier, there are several more wave conditions that exceed the 3-ft threshold during the period of record, resulting in a total of nine events fitting this criterion (middle panel of Figure 7.13). This greater number of events is as expected since this is a less sheltered location within the harbor. Again, the most evident is the December 2007 Kona storm (with a predicted peak wave height of 7.75 ft), but this event is considered a likely over prediction and is outside the normal operating conditions of the harbor. Of the remaining eight events, one was the January 2009 W-NW swell that showed a response above 3 ft at the K01 location (described above), two were Kona storms, and five were south or southwest swells. While the wave response during the Kona conditions may be exaggerated as mentioned above, the predicted response at K02 during south swells is considered reasonable. The peak wave heights predicted at this location during the south swell conditions vary between 3.2 and 4.1 ft.

Finally, at the K03 station located at the northeast end of the barge pier, there were approximately 11 wave events that caused a predicted response in excess of 3 ft during the period of record (bottom panel of Figure 7.13). Of the three barge pier observation stations, this location is the least sheltered by the breakwater. Again, the largest predicted response occurs during the December 2007 Kona Storm. The January 2009 W-NW swell that exceeded the 3-ft threshold at stations K01 and K02 was also a

significant event at K03 with a peak significant wave height predicted at 5.3 ft. The November 2007 South swell shown to be accurately predicted at K01 in Figure 7.12 also exceeds the threshold at K03, the only south swell to meet this criterion at this location during the period of record examined. Of the remaining events, two were Kona storms (same events exceeding threshold at K02), and six were W-NW swell events (in addition to the January 2009 W-NW). The majority of the W-NW swells (five of seven) affecting location K03 occurred during the 3-month period between December 2009 and February 2010. These five events were considered separate since there was a minimum 6-day window between wave heights that exceeded the threshold. All of the events during this short window consisted of offshore wave heights in the 4- to 6-ft range, wave periods primarily in the 12- to 16-sec range, and wave directions from 270 to 300 deg TN. Peak predicted wave heights at station K03 during the W-NW swells (not including January 2009 event) varied from 3.3 to 4.3 ft.

Comparison of the wave height time-series derived by the KPWAVE program at the three barge pier locations K01, K02, and K03 shows interesting results. First, it appears that a sizeable wave event (offshore wave height of approximately 6.0 ft or greater) of any type or direction is likely to cause a noticeable response at all locations along the pier. This is evident in the predicted wave heights during the November 2007 South swell, the December 2007 Kona storm (even considering positive bias), and the January 2009 W-NW swell, all of which show a marked increase in wave heights at the barge pier locations. However, during non-swell conditions (approximately 95 percent of this data sample), the wave heights along the barge pier were less than 3 ft. Second, the K02 output station shows a greater response to south swell events, while the K03 output station exhibits greater energy during W-NW swell events. This result is likely due to both the sheltering of the breakwater and the overall geometry of the harbor. This finding is also somewhat analogous to the previously presented spectral data collected by the roving buoy on 5 Dec 2008, which indicated that the greatest wave energy at K02 was from 200 deg TN, while the greatest energy density at K03 was in the direction band of approximately 235 deg TN, which is roughly a direct approach through the harbor entrance. Since moored barges typically occupy the locations adjacent to both K02 and K03, they can anticipate experiencing waves as high the 3- to 5+-ft range at the pier during long-period W-NW and south swell conditions. Without pre-construction wave data at either of these locations, it is not possible to make a definitive determination on the possible post-project

reduction in wave heights; however, based on discussions with harbor users and field observations it is reasonable to conclude that conditions along the barge pier have improved significantly during typical operational conditions (where short-period wave energy was transmitted through the pre-construction breakwater) and moderately during longer period swell events.

Figure 7.14 shows the time-series of wave height predicted by KPWAVE at the location W3, representing the incident conditions at the breakwater structure. This plot indicates that typical waves are in the 1.0- to 5.0-ft range (zero measurements occur outside the valid range of the KPWAVE algorithm), with several occurrences of 6 ft and over each year (indicated by dashed line in Figure 7.14). The median wave height value is 2.2 ft. The three most extreme predicted wave heights occur in November 2007 (previously identified south swell), December 2007 (previously identified Kona storm), and January 2009 (a W-NW swell) with peak significant wave heights of 9.6 ft, 10.0 ft, and 8.2 ft, respectively.

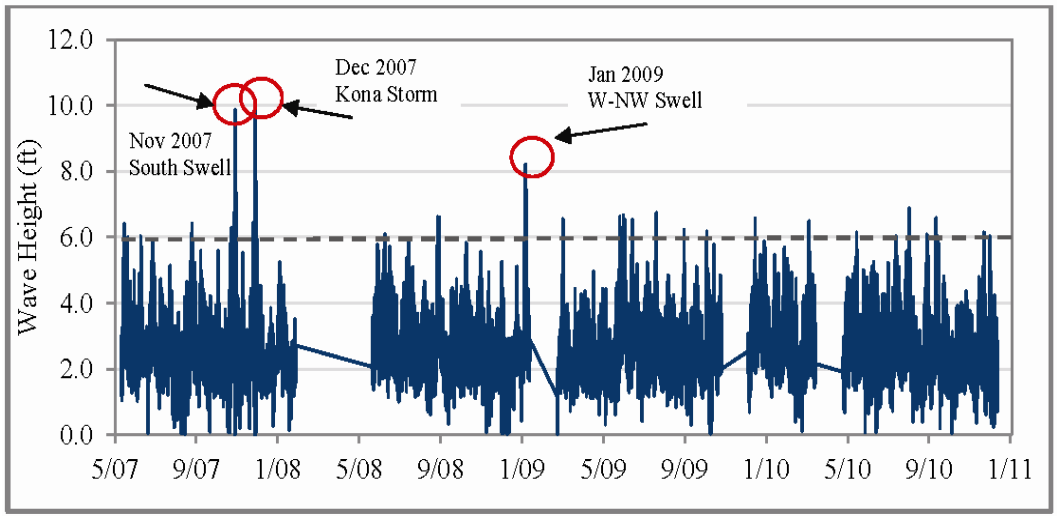

Figure 7.14. Time-series of predicted wave height incident to breakwater (Location W3).

As previously noted, these extremes are much lower than the breakwater design wave height of approximately 35 ft, due to the fact that the design is based on a hurricane wave which is not part of the data collected in the May 2007 to December 2010 timeframe. Running KPWAVE with test wave parameters indicates that a deep water wave of 35 ft must occur at the buoy location (with T_p = 12 or 16 sec and θ = 240 deg TN) to generate a 35 ft incident wave height at location W3. This is in agreement with the A' value of 1.00 shown in Table 7.4 for location W3 and θ = 240 deg TN.

Waves from more oblique directions would need to be in excess of 35 ft to generate the incident 35-ft wave at W3.

It is also of note that the wave climate appears to be comparatively mild in magnitude (though not in total number of events) during 2009 and 2010, with several events exceeding 6 ft, but no predicted wave heights exceeding 7 ft. These observations will be discussed further in later chapters of this report, in terms of the effect of the wave climate has had on the overall stability of the breakwater as well as its components.

7.5 Summary

The availability of 25 years of wave hindcast data and the presence of long-term NDBC buoys in the islands, in addition to the medium- and short-term wave data sets collected as part of this monitoring program, has enabled an evaluation of the accuracy of WIS hindcast data, the implementation of three validated wave transformation models (WW3 forecast model, SWAN, and REF/DIF), and development of a wave lookup table to correlate offshore buoy data to nearshore wave conditions at Kaumalapau Harbor. The lookup table output has been compared to physical model results conducted during the design phase of the breakwater project as well as compared and calibrated to short-term wave gage and buoy data in the areas of interest in and around the harbor. Finally, an easy to use computer program has been created which includes a predictive algorithm for relating real-time buoy data to wave heights at various harbor locations, based on these lookup table results. This program has enabled the calculation of several multi-year time series of estimated incident wave height at the breakwater as well as estimated wave conditions at locations along the barge pier within the harbor.

The analysis of calculated wave height time series indicates that the wave response along the barge pier varies in magnitude with location, the type of offshore conditions (swell direction, wave period) as well as the magnitude of particular wave events in terms of wave height. The sheltered location adjacent to the western end of the pier (location K01) remains relatively calm, except in the largest wave events where wave heights approach 2.0 to 2.5 ft (according to measured data). This area may be experiencing a significant amount of reflected wave energy from the breakwater, pier and nearby steep and rocky shoreline. The areas adjacent to the middle and eastern ends of the barge pier experience larger wave heights because they are less sheltered by the breakwater. The location at the middle of the barge

pier (K02) appears to respond more often to wave events with a southerly direction, with wave heights in the 3.0- to 4.0-ft range (according to modeled data and excluding events such as the December 2007 Kona storm). In contrast, the location at the eastern end of the barge pier (K03) appears to respond most often to wave events with a west-northwest direction, and is likely also experiencing reflected wave energy during these events. The maximum wave heights at this location are in the 3.5- to 5.5-ft range (according to modeled data and excluding events such as the December 2007 Kona storm). These results at the locations along the barge pier, now protected by the repaired breakwater, indicate that safe mooring and offloading should be possible during all but the most extreme events such as hurricanes, large Kona storms and extreme W-NW or south swells.

The time series of calculated wave heights at the location incident to the breakwater (W3) shows that waves impacting the structure are in the 1.0- to 5.0-ft range typically, with some wind-wave and swell events generating incident waves of almost 10 ft in height. This dataset (developed from available wave observations) indicates that only the most extreme events (hurricanes passing south of the island chain or approaching the islands directly) are likely to generate incident waves approaching the design wave height of 35 ft and thereby threaten armor stability. Correlation between offshore buoy data and nearshore wave heights (enabled through application of KPWAVE) has already proven to be valuable to both breakwater monitoring efforts and harbor users. This resource will continue to serve various agencies and private sector requirements as long as the wave buoy remains operational in its current location. A correlation of this time-series data to armor layer settlement is discussed later in this report.

8 Ground-Based Tripod-LiDAR Surveys[1]

One of the primary goals of the monitoring program at this project is to examine and measure the above water armor layer movement and cap settlement in the first years following construction. To accomplish this goal, it was desired that a method that could quantify the overall structure and armor layer movement as a function of both time and spatial location be used. It was intended that this monitoring method would provide information on the process of how Core-Loc concrete armor units nest following construction, would help determine whether there is a relationship between design packing density and structure settlement, and would aid in determining how the overall settlement of the structure affected both the stability of the armor layer as a whole, as well as the concrete cap. Finally, the method used to monitor the above water structure needed to be able to identify any breakage of concrete armor units and potentially the cause, should breakage occur.

Tripod (or Terrestrial) Light Detection and Ranging remote sensing technology, known as T-LiDAR, was used to collect settlement and movement data at the repaired breakwater at Kaumalapau Harbor. Ground-based T-LiDAR data were collected and post-processed by the U.S. Geological Survey (USGS) as part of the monitoring program shortly before the breakwater construction was completed in June 2007, one year later in July 2008, and again in August 2010. The results of this application of T-LiDAR, including the challenges encountered and the conclusions drawn regarding initial concrete armor unit movement are presented in the following.

The instrumentation and software employed for this technology require measurement and analysis in the International System of units (SI), and therefore the discussion, figures, and results of this portion of the monitoring will be presented in meters (m), centimeters (cm) and millimeters (mm), with English units in parenthesis as applicable.

[1] This chapter is based substantially on Podoski et al. (2009), Bawden et al. (2011), and Podoski et al. (2011).

8.1 T-LiDAR technology

Quantifying structure and armor layer spatial changes on both rubble mound and concrete armor structures has been a challenging part of post-construction structure monitoring, and has typically been attempted using GPS or traditional observation of widely-spaced survey marks along the structure, or remote sensing techniques such as photogrammetry or airborne LiDAR. Survey marks, while often inexpensive and potentially very accurate, only capture changes in specific locations on the structure. This is particularly inefficient for monitoring of a concrete armor unit structure, where the surface of the structure has tremendous variation and movement of a particular unit may be closely related to movement of those surrounding it. Photogrammetry and/or airborne LiDAR can document the entire structure, but these methods can be expensive, require specialized equipment (airplane or helicopter), weather dependent acquisition and significant lead time, and currently do not have the accuracy to monitor motion associated with settling that is less than approximately 0.5 m (1.6 feet) (Crane et al. 2004).

T-LiDAR is a portable remote sensing instrument that uses an infrared laser to scan the landscape and generate very detailed (centimeter to sub-centimeter point spacing with ±4 mm 3-D point positional errors) and accurate (±3 mm) digital models of the scanned target at distances from 3 to 800+ m (10 to 2,600 ft) from the instrument. A 3-D image of a scanned target is obtained by measuring the two-way travel time of each laser pulse, calculating distance (distance = [speed of light * travel time]/2) and measuring the exact horizontal- and vertical-look angle to obtain angular positioning with respect to the center of the instrument. The point positions are combined to generate a comprehensive 3-D (x, y, z, i; where i is the intensity or infrared reflectivity of the target) image map of the target, referred to as a “point cloud”.

At 2,000 laser shots per sec, over 7 million point position measurements can be collected in an hour (scan rates, data densities, and point positional errors vary among the different T-LiDAR systems). T-LiDAR is an active source technology that collects measurements in many weather conditions and does not require an unobstructed view of the sky, but is limited to line-of-sight measurements. A full 3-D image is obtained by scanning a target from multiple directions to characterize all sides of the target and to minimize shadowing from targets on nearby features. T-LiDAR scans, which are imaged from different vantage points, are aligned and combined

through an algorithm that generates a best-fit surface through the individual points in each scan and then minimizes the misfit between common surfaces in each scan. There are typically several hundred thousand to millions of data points in common between each scan, which routinely achieves sub-millimeter standard deviation in the data misfit between scans.

T-LiDAR as a monitoring technique offers two primary advantages over other above-water measurement techniques: data density and accuracy. More than 280 million data points were collected by the three surveys of the breakwater, with most of the outermost armor units imaged with tens of thousands of 3-D point positioning measurements and tens of millions of point measurements on the concrete cap. Additionally, when analyzed in a local reference frame, accuracies on the order of 2 to 3 cm (0.8 to 1.2 in.) can be obtained to image small changes in the armor layer of a structure over time. Since the laser scanner is ground-based system, it can image and detect positional changes along the underside of armor units - areas that are not visible from an air-based platform (although shadow zones do limit effective monitoring of portions of the structure not in the instrument's line of sight). In addition, the relatively small crew (two people in this application) and minimal equipment needs for this data collection method make it an attractive possibility for post-event damage assessment on short notice. The increased coverage area of the structure, data density, accuracy, and relatively easy set up and collection of a very dense spatial dataset make T-LiDAR a potentially very useful tool in short and long-term monitoring of coastal structures, and provided an ample amount of data for achieving the monitoring goals at Kaumalapau Harbor.

The T-LiDAR technology also has some disadvantages as compared to conventional techniques such as traditional surveying and photogrammetry. Sensitivity of the instrument and measurements to environmental conditions, shadowing, the low altitude vantage point which requires measurement from many positions, extensive data analysis and the required high level of user and data analyst expertise are discussed below.

8.2 T-LiDAR data collection and processing

8.2.1 Instrument setup and coverage

T-LiDAR scans were collected from a number of vantage points on the Kaumalapau Harbor breakwater and from the surrounding harbor

infrastructure to ensure that the breakwater was imaged from as many different angles as possible. Table 8.1 shows the number of tripod setup locations, the total number of T-LiDAR scans, and the total number of data points collected during each survey. The variation in the quantity and locations of data collected during each survey was based primarily on the time available for scanning after incorporating equipment setup and adjustment time, weather and tide windows, and the initial learning curve. Though each survey has a variable number of total data points, all data sets were considered more than adequate in quantity and reasonable in the amount of spatial coverage achieved. Some redundant and erroneous data was discarded; however, it was not necessary to reduce the data sets to a common number of data points for comparison purposes.

Table 8.1. T-LiDAR survey information.

Survey Date	# of setup locations	# of scans	Data points
June 2007	7	115	66 million
July 2008	17	312	128 million
August 2010	26	151	86 million

Optech, Inc. ILRIS 3-D laser scanners were used for the data collection efforts. In addition, a high-resolution digital camera was mounted atop the scanners so that multiple color images could be collected at each setup location corresponding to the scan area where T-LiDAR data was collected. A typical Optech, Inc. laser scanner and the mounted camera are shown in Figure 8.1a, and the tripod-mounted instrument scanning the harbor side of the breakwater is shown in Figure 8.1b.

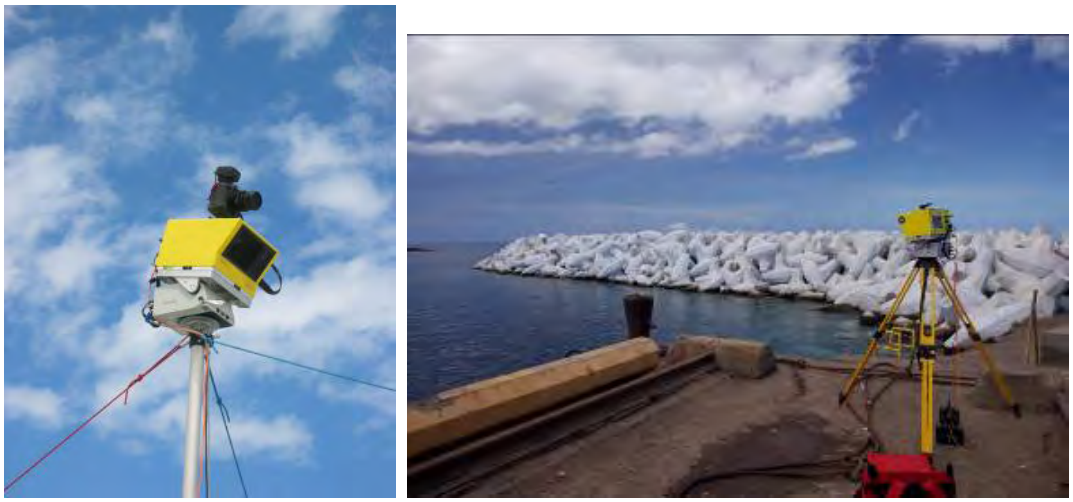

Figure 8.1. Images of T-LiDAR instrumentation in use. (a) Laser scanner and mounted digital camera (left), and (b) tripod-mounted scanner setup at breakwater (right).

One of the main logistical challenges of data collection was to ensure that there was sufficient data coverage on the ocean side of the breakwater such that 3-D movement along the entire breakwater could be fully documented. Ideally, the breakwater would be scanned from a stable platform, free of wave induced motions, and anchored about 50 m (164 ft) offshore from the breakwater, but this was not a viable option given an average water depth of approximately 21 m (70 ft). A combined approach was utilized to solve this problem.

The T-LiDAR system was lifted upward 4.25 m (14 ft) above the breakwater cap with a specially designed elevated tripod to obtain an aerial view of the structure, and the instrument was set up at low tide on rock outcrops on the side of the harbor opposite from the breakwater (Figures 8.2a and 8.2b). Multiple elevated tripod setup locations on the ocean side of the breakwater cap were timed to coincide with low tide to allow the laser scanner to look down on armor units close to the waterline. This technique provided data for approximately 70 percent of the visible armor units on the ocean side of the breakwater. Data collected from the small rock outcrops (reached by boat) on the southern side of the harbor and from the dock provided close to 100 percent coverage of the breakwater head and harbor side of the breakwater. This combined approach imaged a majority of the above water Core-Loc armor units at an approximate density of 10,000 points per sq m (~ 930 points per sq ft). Since the armor units are touching each other, settlement in one unit often results in the positional adjustments of many of the neighboring armor units. This condition often allows for an indirect measurement of any interrelated movements in areas where T-LiDAR coverage is less than complete.

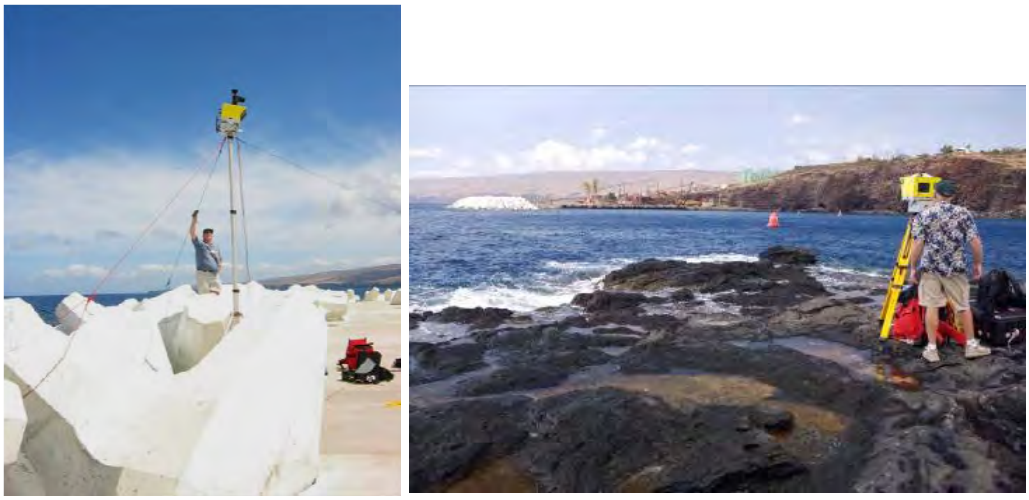

Figure 8.2. Photos of T-LiDAR setup locations. (a) Elevated tripod setup on breakwater (left), and (b) laser scanner recording data from rock outcrop opposite breakwater (right).

8.2.2 Data processing and change detection methods

The laser scans from data collection were individually aligned using the InnovMetric Software, Inc. Polyworks® align module and georeferenced with GPS data collected from existing and newly installed benchmarks by the University of Hawaii Pacific GPS Facility (Figure 8.3). In total, six benchmarks were surveyed: four new GPS benchmarks located on the breakwater cap, one new site installed in bedrock above the harbor, and a local historic tidemark. The data was processed and tied to the University of Hawaii Pacific GPS Facility's island-wide GPS network to ensure highly accurate geospatial positioning. Ultra-high density laser scanner imagery (typically laser spot spacing of a few mm) of the GPS antenna and aligning sphere (placed on fixed-height survey poles on the benchmarks) was collected (Figure 8.3, inset). Since each aligning target had tens of thousands of individual point measurements, the center of the antenna was identified by fitting mathematically determined spheres to the GPS antennas. The center of each sphere is at a known distance above the benchmark. Therefore, it was possible to take the GPS-determined benchmark position and assign its geospatial location to the T-LiDAR point cloud dataset. By repeating this process for all of the benchmarks, the T-LiDAR datasets were fully georeferenced.

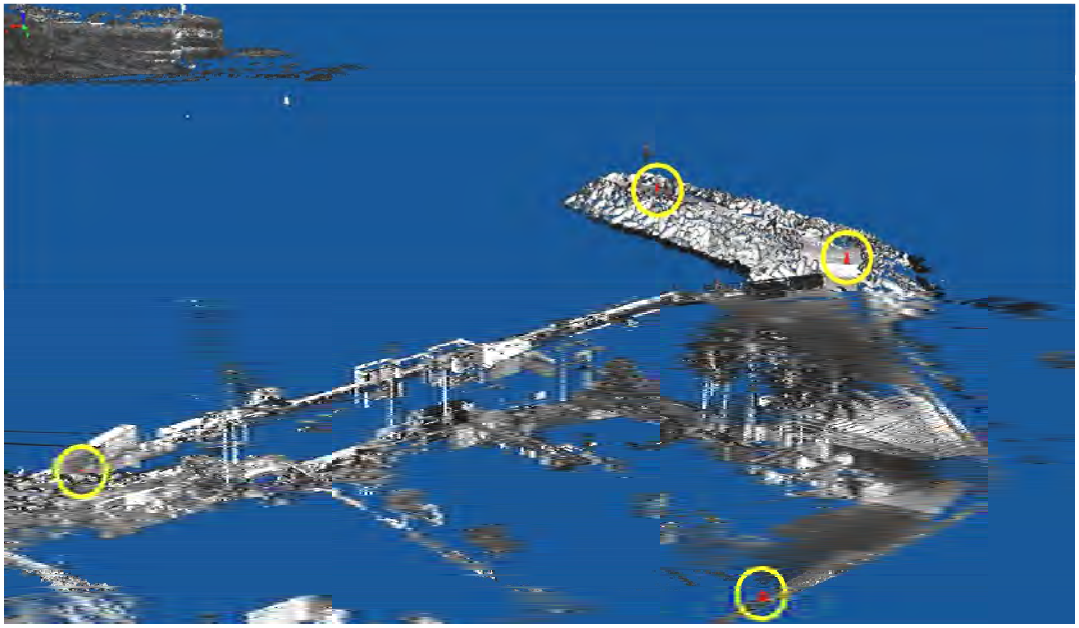

Figure 8.3. Four of six total GPS data collection stations overlaid on T-LiDAR point cloud data of Kaumalapau Harbor and GPS antenna (inset).

Data noise from a variety of sources (environmental, laser physics, reflected light from the concrete cap and hardware) produced additional uncertainties in the datasets. During the 2007 survey, there was a strong midday to late afternoon trade wind that shook the instrument. Subtle shaking of the instrument produced large angular changes in the far-field, thereby adding decimeter-level positional uncertainties in some scans. Given that most of the Core-Loc armor units were imaged from multiple angles, many of the scans that had obvious wind artifacts were able to be removed from the dataset. Many of the scans collected from locations on the breakwater also had a type of noise that is referred to as data echoes; these are point cloud artifacts created when a high power laser pulse hits two close objects with one laser pulse. The laser sees both objects and returns a point position somewhere between both objects. This type of noise occurs for very close objects outward to about 30 m (98 ft) from the instrument. The data echoes were removed manually and the alignment process was completed with no increase in the positional uncertainties.

Additionally, recently placed concrete along the breakwater crest located within about 7 m (23 ft) of the laser scanner produced a range bias with the position determined to be closer than the true position. This is likely due to the fact that concrete is a very reflective surface in the instrument's infrared wavelength; therefore, more signal was recorded at the instrument with a close range bias. Any data collected within 7 m (23 ft) of the instrument in areas where the range bias was observed was omitted. During the 2008 survey, one of the instruments used developed an irregular timing board anomaly where positional warping occurred as the instrument warmed up. The point positions had an artificial range bias of upwards of 0.5 m (1.64 ft) at the beginning of the scan. Once the laser had reached a stable operating temperature, the apparent warping disappeared. The scans that were impacted by the timing anomaly were identified and used only as essential non-redundant scans for the analysis.

Once the different noise sources were isolated and either corrected or omitted, a reliable high-resolution dataset of the breakwater was generated for each survey. A typical point cloud of the survey coverage (from a single scan) is shown in Figure 8.4. The georeferenced dataset of the breakwater was used to create a Digital Elevation Model (DEM), a 3-D surface that may be stored in a GIS database and used for visual and quantitative purposes (i.e., to generate cross-sections of the structure),

Figure 8.4. Point cloud image of breakwater and adjacent harbor facilities (single scan).

without extensive computer resources needed to visualize and analyze the entire point cloud dataset. However, DEM generation was not suitable for armor unit change detection for several reasons:

1. A DEM does not allow for the ability to measure positional changes of overlapping armor units by reducing the complex 3-D structure to only one measurement in the vertical direction.
2. DEM creation reduces data density levels from sub-centimeter data to decimeter grids where only large scale vertical motions could be detected.
3. DEM generation results in unrealistic artifacts from averaged positions among adjacent units and the breakwater cap.

The positional uncertainties that resulted from the noise and artifacts of the georeferenced DEM were greater than some of the small-scale motion visually observed on some of the armor units along the breakwater cap. Therefore, the DEM did not contribute to the change detection process.

The T-LiDAR technology should be able to image centimeter scale motion; however, the noise sources described above masked some of the motion. Since the breakwater was imaged from so many different positions (see Table 8.1), there were often individual armor units that were imaged from three to five different positions, with some of the far-field scans only imaging small portions of a particular Core-Loc. During the aligning process, it was determined that small angular misalignments from lower

density data scans (> 5 cm [~2 in.] spot spacing) produced significant noise in the dataset. To address this issue, the breakwater was subdivided into smaller sections for change detection analysis. Each section was prescribed a local reference frame based on stable objects and benchmarks in that section, any far-field inconsistent data was removed, data that had wind induced noise sources was isolated, and then the datasets were realigned.

The displacement of each armor unit was measured using the 3-D virtual reality software package Virtual Reality User Interface (VRUI) (Kreylos et al. 2008) which allowed direct measurements of the data in 3-D with specialized goggles. The virtual reality software enabled measurement of 3-D positional changes of unique points (such as corners and edges) on each armor unit and a subsequent determination of the maximum displacement of each armor unit, based on the visible area of coverage captured in multiple surveys. This measurement process would have been very difficult, if not impossible, using conventional two-dimensional software. This approach resulted in much higher resolution change detection (accuracy of +/- 2 to 3 cm [0.8 to 1.2 in.]) than simply differencing the georeferenced DEMs or making 3-D measurements from a 2-D computer monitor (Kreylos et al. 2008).

8.3 T-LiDAR data analysis results and breakwater assessment

Comparison of these ultra-dense georeferenced positional data (in point cloud form) has enabled the detection of armor unit movement (measured as maximum displacement at any point on an individual unit) as small as 5 cm, and in excess of one meter, as shown by the comparison of 2007 and 2008 point cloud images in Figure 8.5. This figure is an overlay of two point cloud datasets (2007 data in blue, and 2008 data in white), viewed on the ocean side of the breakwater head. The measured maximum displacement of several units, including one armor unit with a maximum landward rotation of 114 cm (44.9 in.), is represented by arrow-arcs in orange for rotational displacement and straight line arrows in yellow for translational displacement.

The comprehensive coverage area and high positional accuracy of these surveys resulted in the ability to visualize and compare movement of almost every armor unit visible above the waterline as well as the concrete cap, allowing for an overall analysis of the above water stability of the structure in the three years following construction. Armor unit movement was

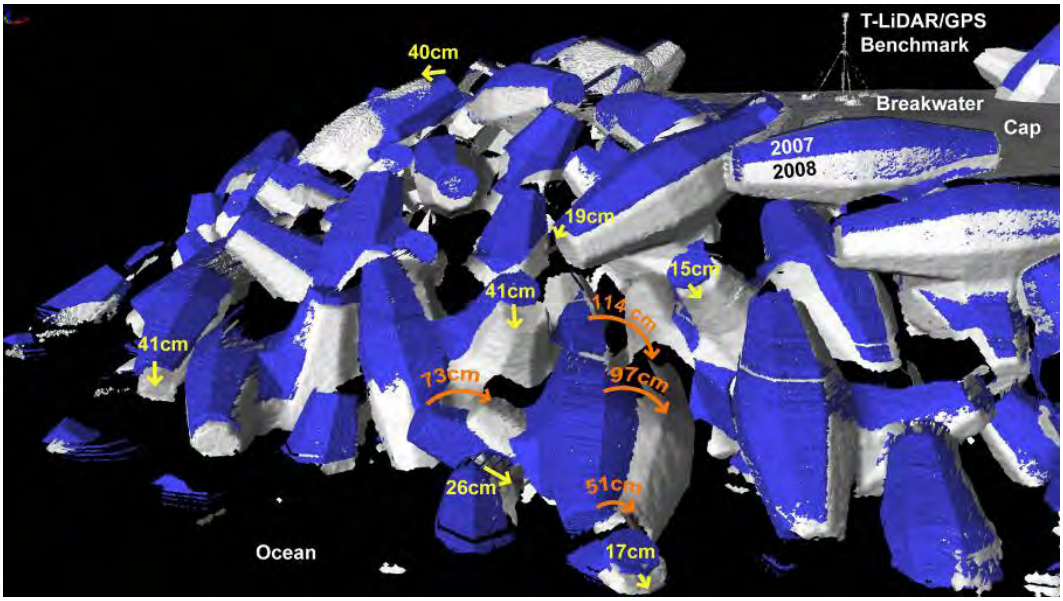

Figure 8.5. Point cloud data showing measured armor unit displacement from 2007 to 2008.

analyzed through both visual inspection of point cloud overlays such as that in Figure 8.5 and the use of color-coded change detection "maps" generated by USGS. These maps are point cloud images of a single survey in which each armor unit has been graphically colored based on a graduated scale corresponding to the measured maximum armor unit displacement described above. Change detection maps were developed for three comparative time periods: 2007 – 2008, 2008 – 2010, and 2007 – 2010.

The change detection map for 2007 - 2008, including a plan view of the entire breakwater, oblique angle views of specific areas of interest, and plan view of the breakwater head, is shown in Figures 8.6, 8.7, and 8.8. Cool colors (blue/purple/green) in the figures indicate displacement <20 cm (7.9 in.), while warmer colors (yellow/orange/ red) show measured displacement from 20 to 50 cm (7.9 to 19.7 in.). Armor units colored magenta indicate that the measured displacement was 50 cm (19.7 in.) or greater. Armor units colored blue (0 to 5 cm displacement) are considered stationary, as change detection accuracy is estimated to be +/- 2 to 3 cm (0.8 to 1.2 in.). Armor units that are shown in gray (primarily on the ocean side of the breakwater) were not able to be compared to determine displacement, due to insufficient data coverage in one or both of the surveys.

The analysis of the point cloud overlays and change detection maps has revealed several interesting characteristics of the movement that has occurred during this time. Firstly, the visible movement of individual armor

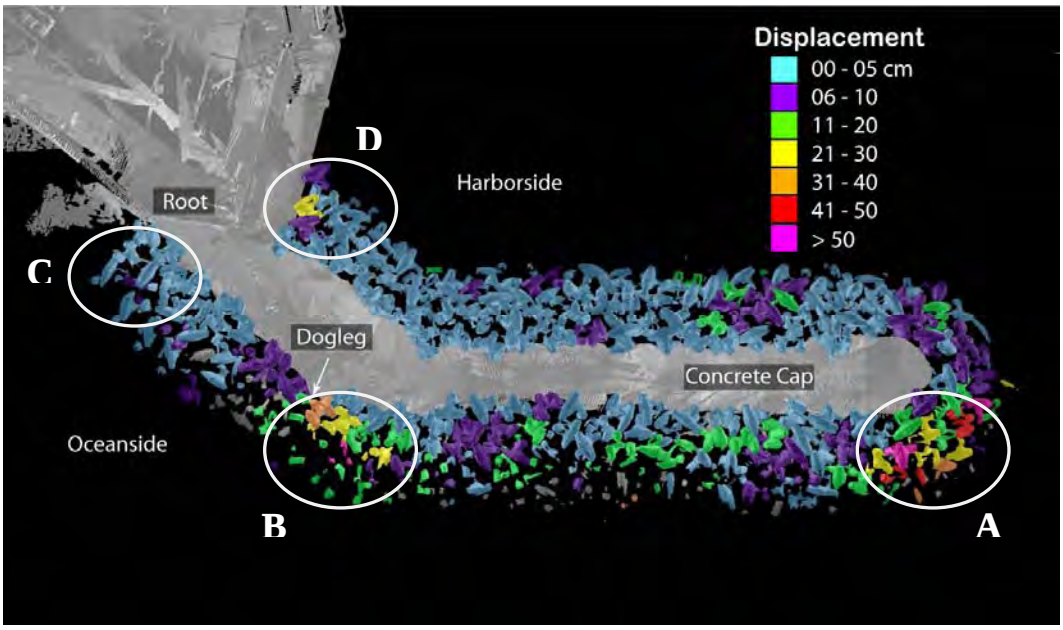

Figure 8.6. Plan view of 2007-2008 T-LiDAR change detection map: A. Ocean side head, B. Ocean side dogleg, C. Ocean side root, D. Harbor side root.

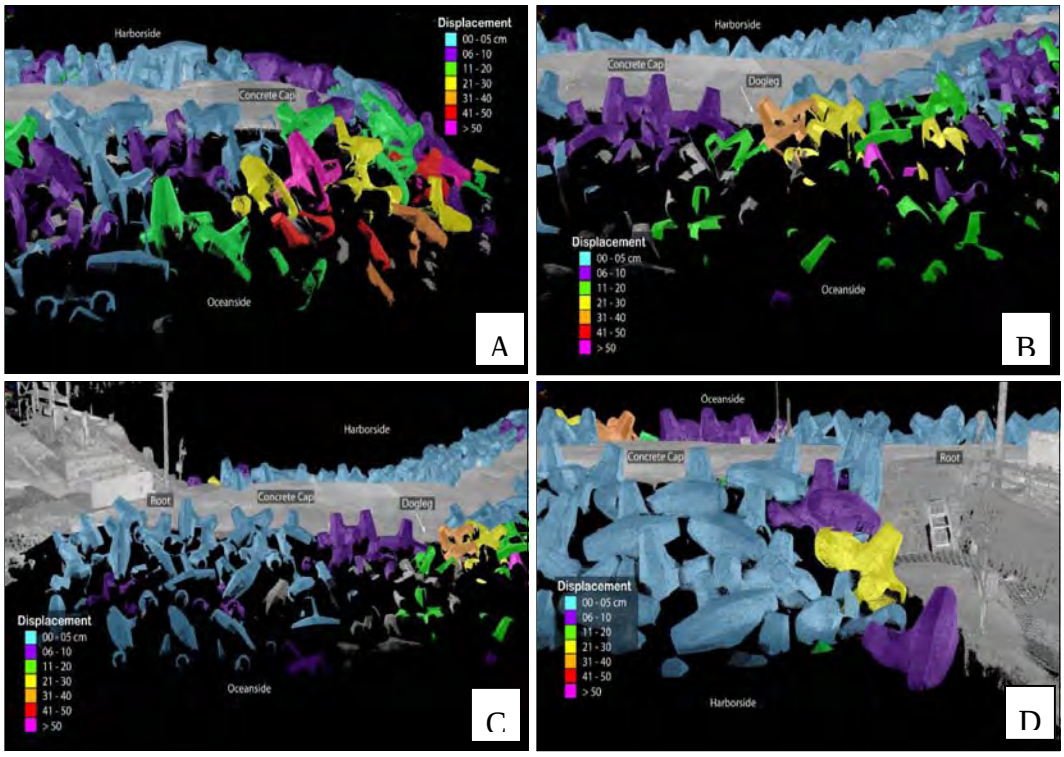

Figure 8.7. Oblique angle views of 2007-2008 T-LiDAR change detection map: A. Ocean side head, B. Ocean side dogleg, C. Ocean side Root, D. Harbor side root.

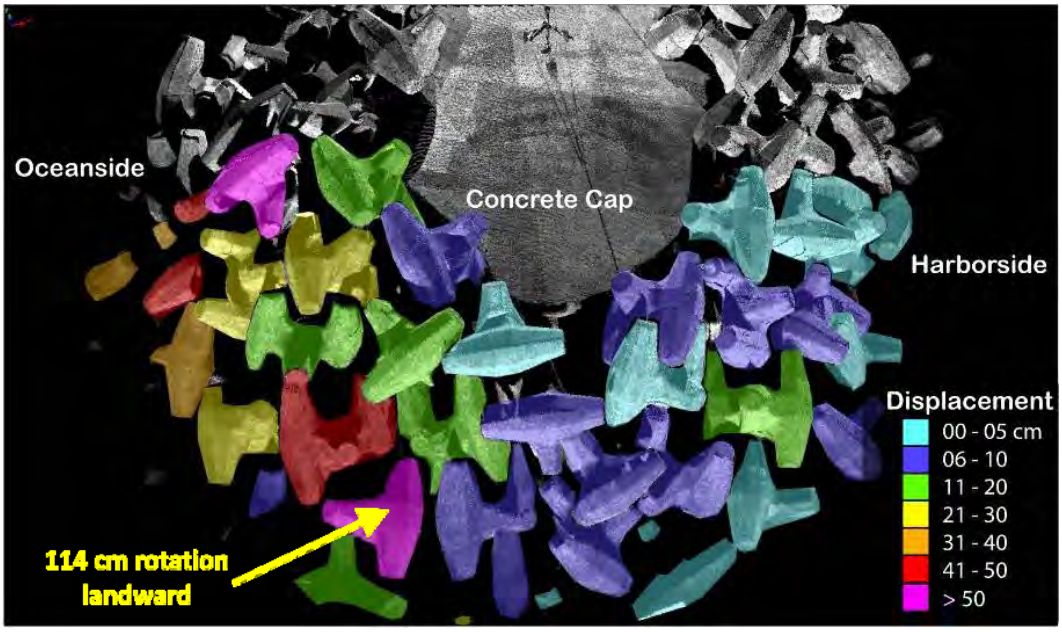

Figure 8.8. Plan view of 2007-2008 T-LiDAR change detection map at breakwater head.

units has been both rotational and translational, but has been primarily toward the structure (rather than being pulled away or "off" the breakwater) and/or lower in elevation (indicated by displacement arrows shown in Figure 8.5). This appears to indicate that the units are indeed settling and "nesting" into a tighter matrix, rather than being loosened or pulled apart. Secondly, the movement has typically been observed to occur in groups of several adjacent armor units, as shown in locations A (ocean side head), B (ocean side dogleg), and D (harbor side root) of the 2007-2008 change detection map in Figures 8.6 and 8.7. This illustrates the interdependence of each armor unit on those surrounding it and in direct contact with it, whether above, below, or alongside.

In addition, the change measurements over the 2007 - 2008 time period indicate that the largest movements of individual armor units, on the order of 20 cm to over 1 m (0.7 to 3.3 ft), occur at one of two locations: the ocean side head or ocean side dogleg of the structure (Figure 8.6 and 8.7 at locations A and B). This is also illustrated by the plan view of the change detection map at the breakwater head in Figure 8.8, which shows a dramatic difference in the magnitude of displacement between the harbor side and ocean side of the structure head. This distinction is evidenced by the range of colorization on the left side of the figure in comparison with that on the right side of the figure. The armor unit identified previously in Figure 8.5 that rotated landward a distance of 114 cm (44.9 in.) is called out in this figure. Photos taken at the completion of construction show

that the armor units in this area were placed such that a void existed between this rotated unit and the unit just landward of it. Movement of 11 to 50 cm (4.3 to 19.7 in.) in the nearby armor units is also evident in Figure 8.8. Since the T-LiDAR laser does not penetrate the water, it is not possible to quantitatively determine whether the motion observed at this location is regionally independent, or was caused by movement below the waterline. However, again referring back to Figure 8.5, portions of two Core-Loc units protruding above the waterline directly below these units moved about 17 cm (6.7 in.) and 26 cm (10.2 in.), respectively. Therefore, it is likely that the larger scale motion observed at the head of the breakwater may relate to nesting of armor units below the water surface.

This concentration of armor unit displacement at the ocean side head and dogleg is also evident, though less dramatically so, in change detection maps for the 2008 - 2010 time period (Figure 8.9, locations A and B) as well as in the combined measurements over the entire three-year survey period (shown in Figure 8.10, locations A and B). This phenomenon may be explained by one or more of the following factors:

1. The constructed packing density of armor units is likely lower in these areas in comparison to other areas on the breakwater, due to the change in structure orientation and thereby armor layer shape in these areas (i.e. – armor units become more spread out during construction when being placed around a bend or curve).
2. Interlocking and contact of adjacent armor units at these locations is potentially less optimal than that in other locations, due to the above mentioned increases in the breakwater curvature and possibly lower packing density.
3. Wave impact and wave surge forces are greatest along the ocean side of the breakwater due to its increased exposure to incoming waves, which in combination with either or both of the above factors, could initiate movement of armor units.
4. The lack of significant armor unit displacement seen on the harbor side may be a result of the fact that the structure has not been overtopped by any major wave events.

Next, and likely one of the most significant results from this data collection, is the variation in both the quantity and magnitude of armor unit movement evident when comparing the change detection map from the first year following construction (Figure 8.7) to the map for the two following years

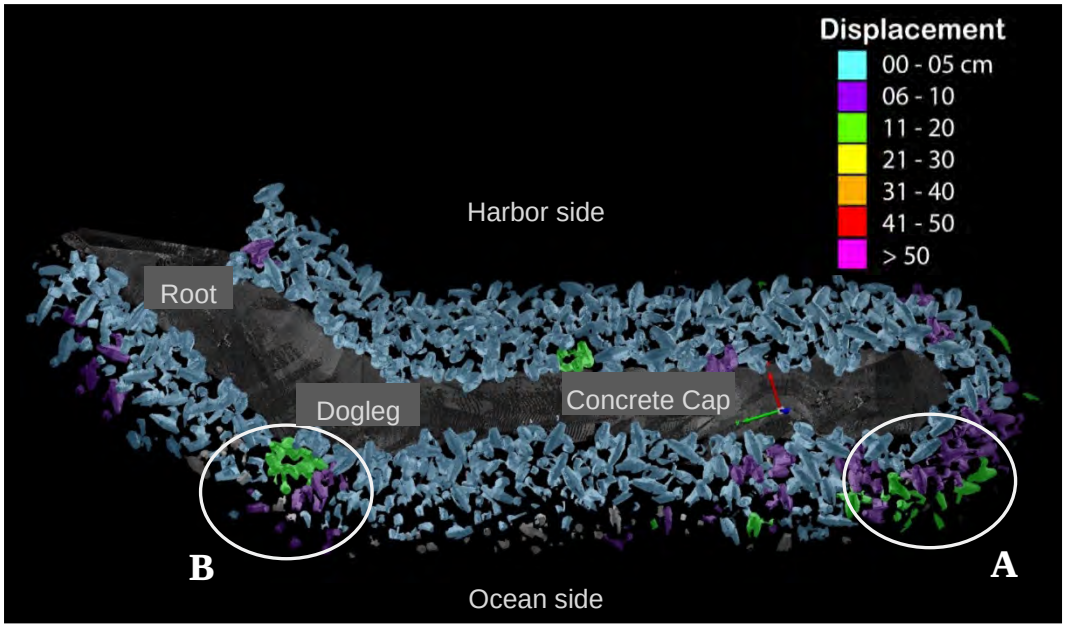

Figure 8.9. Plan view of 2008-2010 T-LiDAR change detection map: A. Ocean side head, B. Ocean side dogleg.

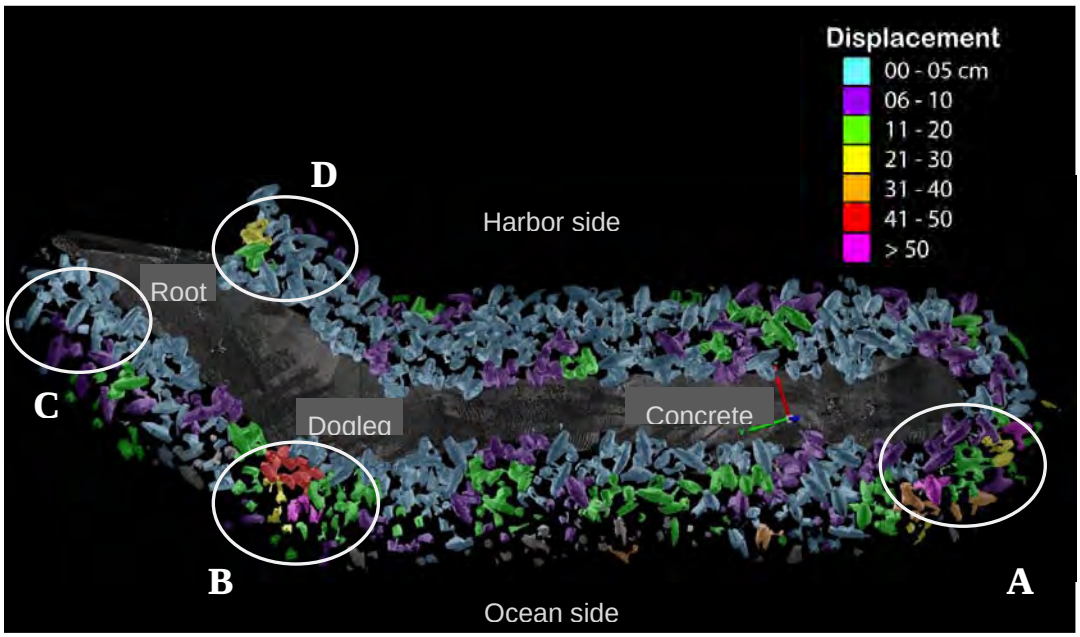

Figure 8.10. Plan view of 2007-2010 T-LiDAR change detection map: A. Ocean side Head, B. Ocean side Dogleg, C. Ocean side Root, D. Harbor side Root

(Figure 8.9). Side-by-side evaluation of colorized change detection maps for these two time periods clearly shows that the majority of notable armor unit movement (defined here as movement greater than 10 cm (3.9 in.) for an individual unit) occurred within the first year post-construction, with comparatively much less discernable change in armor unit positions occurring between the second and third T-LiDAR surveys in 2008 and

2010. This may be due in part to a less energetic incident wave climate during 2008 - 2010, as alluded to in Chapter 8 of this report. However, it is difficult to make a direct correlation between the magnitude of armor unit displacement and wave climate with only two relatively short-term periods of armor unit change analysis. It is more likely that the majority of armor layer settling and nesting occurred within approximately the first year after placement due to a combination of gradual gravitational settling and persistent dynamic wave forces over this time.

Other observations that have been made through analysis and comparison of the T-LiDAR data sets have provided information on specific areas that were of concern during the design phase and also the construction phase. There has been minimal (less than 10 cm (3.9 in.)) displacement of armor units at the ocean side root of the structure (Figure 8.10, Location C). This was an area of concern during the design phase of the project due to a large submerged rock platform that exists adjacent to this part of the structure. Physical model tests showed that there could be armor unit stability issues due to the surge action caused by this feature, so the design of the structure incorporated the use of tremie-placed concrete to secure toe armor units along the structure root.

The harbor side of the structure at the root, adjacent to the barge pier (Figure 8.10, Location D), became an area of concern during construction when a modification was made by using a partial armor unit (breakage occurred during placement at the head, so the unit was removed) to abut the existing bulkhead wall, due to the fact that a complete armor unit would not fit into this area. The displacement measured in this unit between the 2007 and 2008 surveys (Figure 8.6) was in the range of 21 to 30 cm (8.3 to 11.8 in.), and in two adjacent armor units, displacement was measured in the range of 6 to 10 cm (2.4 to 3.9 in.). However, the displacement measured between the 2008 and 2010 surveys (Figure 8.9) shows that the partial armor unit has not experienced additional movement, and only one of the adjacent units experienced detectible movement, less than 10 cm (3.9 in.).

Finally, the analysis of the T-LiDAR survey data (and verification by visual inspection) has shown that there has been no breakage of any above water armor unit to date, which indicates that the scale of armor layer settlement and movement has not been significant enough to cause considerable stress on the individual armor units above the water line. This leads to the conclusion that the overall stability of the armor layer in the three years

since construction has been satisfactory and although expected settling has occurred, the constructed packing density and interlocking of the armor units has been sufficient to limit or preclude the amount of wave-induced dynamic movement that could result in unit-to-unit impacts and possible armor unit breakage. The data analysis also shows that there has not been a detectable settling of the concrete structure cap since its construction. This suggests that the concrete cap has remained intact and is functioning as designed despite the armor layer settlement and movement that have been observed.

The data showed that, while there was considerable movement of a number of units, no units were dislodged from their original positions within the armor layer. The movement can be described as in-place rotation and settlement into generally more stable positions. It does not appear that the settlement is excessive, indicated by relatively minor settlements over the bulk of the armor layer. As such, it appears that the packing density coefficient of $\phi = 0.62$ for the new Core-Loc-II is reasonable. This is a significant finding and should be reviewed in follow-on surveys. The Core-Loc Technical Guidelines (Turk and Melby 1997) suggest that the Core-Locs should be packed as tightly as possible. So if the units settle considerably more and gaps form between units near the crest of the structure as the structure is exposed to more severe storms, then the packing density coefficient may require adjustment. For now, it appears as though $\phi = 0.62$ for the Core-Loc II is adequate.

All of these observations, which begin to answer key questions that were posed at the outset of the monitoring plan, would have been very difficult or impossible to obtain by solely visible inspection or even traditional survey techniques. The comprehensive and precise T-LiDAR data has enabled the thorough quantitative evaluation of the settling and movement of the above water components of the breakwater both spatially and temporally. The analysis of this data has helped to better the understanding of how the Core-Loc concrete armor units at this project have nested following construction and has indicated that there is likely a relationship between both design and constructed packing density and armor unit movement. In addition, the data assessment has demonstrated that the settling of the armor layer that has been observed has not had a noticeable effect on the integrity of the breakwater cap or the functioning of the structure as a whole, and that no breakage of armor units has occured. Finally, it is reasonable to conclude that the T-LiDAR surveys conducted following the Kaumalapau Harbor

breakwater repair have demonstrated that the structure has performed as designed in the years immediately following construction.

8.4 Future applications of T-LiDAR

This analysis method and its results brought to light several new possible methods and uses for T-LiDAR data collected on coastal structures. As mentioned, this analysis determined displacement through measurement of several unique points on the surface of each armor unit, but it did not determine the 3-D positional change of the Core-Loc centroid. Fitting of a mathematical primitive Core-Loc shape to point cloud data from all three surveys would allow the georeferenced position of the centroid of each visible armor unit to be determined. Centroid positions of each armor unit could be used in tandem with surface movement measurements to determine the magnitude and direction of rotation and/or translation that is contributing to overall displacements. In addition, comparison of the original centroid position of each armor unit to that which was specified in the design Core-Loc placement plan would assist in confirming the accuracy with which the armor units were originally placed during construction, as well as aiding in assessing the breakwater design criterion for future breakwater projects.

If collected on a consistent basis, T-LiDAR data could be used to compare the changes observed in the armor layer of a concrete armor unit structure to parameters of coincident wave data being collected at the project site. Ideally, multiple change detection datasets collected over several time periods could be used to correlate observed armor layer movement and armor unit damage to incident wave conditions over those same periods. This site-specific analysis at Kaumalapau Harbor or other locations could potentially provide information on which wave parameters (wave height, period, storm duration, direction, etc.) are most damaging to a particular structure. This information would be highly useful for adaptive management and/or repair of the structure. Additionally, this relationship between armor unit movement and wave conditions may help to indicate some distinction between wave-induced movement of armor units and movement which is due purely to gravitational settlement over time.

This technology could also be implemented at this or other locations as an event-based structure damage assessment tool. Provided a baseline T-LiDAR survey of a structure was conducted prior to a storm season or impending event such as a hurricane, it could be compared to a survey

conducted immediately after the storm season or event, similar to the analysis currently done along large areas of coastline by airborne LiDAR data collection techniques. The minimal ramp-up time needed for a T-LiDAR survey, as well as the data density and accuracy of the technology, would lend itself well to a more targeted analysis of a particular structure (or structures) for pre- and post-storm damage analysis.

The final component of this technology that is needed for its comprehensive use in monitoring of coastal structures is the ability to deploy the T-LiDAR instrument from a boat or other watercraft, so that more complete coverage of a structure can be mapped. Until recently, this method of T-LiDAR was not possible due to the multiple degrees of freedom related to ship motion (surge, sway, heave, roll, pitch, and yaw), and the associated position corrections needed by an inertial measurement unit (IMU) which would not be precise enough to maintain the high degree of accuracy obtained from a land-based instrument. However, recent advancements in this technology using a combination of differential GPS and an IMU instrument are in development. One such system is being tested and implemented by the Condition Indexing Work Unit of the USACE Navigation Systems Program at present, and has been deployed at several locations including Kaumalapau Harbor.

The application of T-LiDAR was well-suited to this structure because of its relative ease of access and short length. However, using this technology on much longer structures could prove more difficult and time consuming due to the greater number of setups that would be needed to capture the entire structure surface. In addition, T-LiDAR currently has the same disadvantage of traditionally used structure monitoring methods in that it is not able to monitor below-water changes to the structure. Use of high-resolution multibeam surveying techniques is required when sub-aqueous data is needed. The challenges in data processing due to data noise (especially due to laser physics and instrumentation) are limitations in the technology that are being addressed and improved as the instrumentation is developed and refined, but for now must be screened through a diligent quality control process. Even with these limitations to the technology, the advantages of this data collection method over traditional monitoring methods in terms of the ability to precisely track movement of armor units along the entire structure and relate these changes to one another, make it a practical and comprehensive means of gaining insight into the response of concrete armor unit structures to consolidation over time as well as the effects of wave forces.

9 Underwater Geophysical Survey of the Breakwater[1]

Sea Engineering, Inc. (SEI) conducted a marine geophysical survey in July 2008 to image the post-construction underwater portion of the Kaumalapau Harbor breakwater rehabilitation. The survey consisted of high resolution and high precision multi-beam instrumentation for accurate mapping of the breakwater structure. The primary objective was to provide a baseline for measurement and monitoring of any future changes to the structure due to settling or other movement of the Core-Loc concrete armor units. Multi-beam backscatter intensity was also analyzed and used in conjunction with several grab samples for identifying bottom sediment types in the project area. SEI was assisted with this survey by Solmar Hydrographics, who provided expertise with the Reson 8125 multi-beam system; and Control Point Surveying, Inc. (Control Point), who provided RTK GPS equipment.

The areas surveyed include the Core-Loc armor units, the structural connections to the existing rock on the ocean side and to the pier on the harbor side, and the seafloor immediately surrounding the breakwater. In addition to the depth information provided by the sonar system, high resolution backscatter intensity data were extracted from the sonar data for seafloor characterization. The goal of the backscatter classification is to identify bottom types in the study area as well as distinguishing between the new Core-Loc units and the underlying berm from the previous breakwater structure. 3-D point cloud imagery of the bathymetric data was also developed.

All data collected were referenced to the High Accuracy Reference Network (HARN) North American Datum of 1983 (NAD83) using the 1980 Geodetic Reference System (GRS80) spheroid. The survey was conducted in Hawaii State Plane Zone 2 Transverse Mercator projection in US Survey Feet according to the Federal Information Processing Standards (FIPS). All elevation data are referenced to the Mean Lower Low Water (MLLW) as determined by the University of Hawaii (UH), School of Ocean and Earth Science and Technology (SOEST), Sea Level Center.

[1] This section is extracted essentially verbatim from Sea Engineering, Inc. (2009).

9.1 Underwater survey design

The underwater survey was designed to maximize upslope coverage of the breakwater. There were two techniques employed to accomplish this. First, the survey was conducted approximately at high tide. This enabled the vessel to get closer to the higher Core-Loc units along the breakwater and, thus, increase the area of interest that was surveyed. In addition to timing the survey for high tide, the multi-beam sonar head was rotated 15 deg away from the vessel (to starboard) to maximize the upslope extent of the survey coverage.

To image the breakwater completely, two lines were surveyed around the structure. The first was in as close as possible, while the second was out a bit further to complete the coverage of the lower portion of the structure. Several additional lines were run parallel to the breakwater to complete the survey requirements. Survey track-lines are shown in Figure 9.2.

9.2 Equipment

9.2.1 Multi-beam sonar

Due to the shallow depths of the harbor and the need for the highest resolution bathymetry and backscatter data possible, the Reson SeaBat 8125 sonar system was selected for this project. The system operates at 455 kHz and utilizes 240 dynamically focused beams with a swath width up to 120 deg. The instrument was designed specifically for shallow water surveys. The sonar head was mounted on a rigid pole on the starboard side of the survey vessel just below the keel of the vessel. Coastal Oceanographics Hypack/Hysweep 2008 navigation and data collection software was used for the collection of the sonar data and for integration of the data with vessel position, heave, pitch and roll motions.

9.2.2 Navigation

A Trimble 5700 GPS was used to generate Real-Time Kinematic (RTK) corrections for on-board GPS units. The RTK system was leased from and operated by Control Point Survey, Inc. The control point “KHTB” was used as a base for RTK corrections. This point was later renamed “BM5” when re-surveyed by Control Point. A rover unit on the boat was secured to the sonar head mounting pole and used to generate vertical tide corrections. RTK corrections were also fed to GPS units of the Coda F180 Motion Reference Unit (MRU) for horizontal positions.

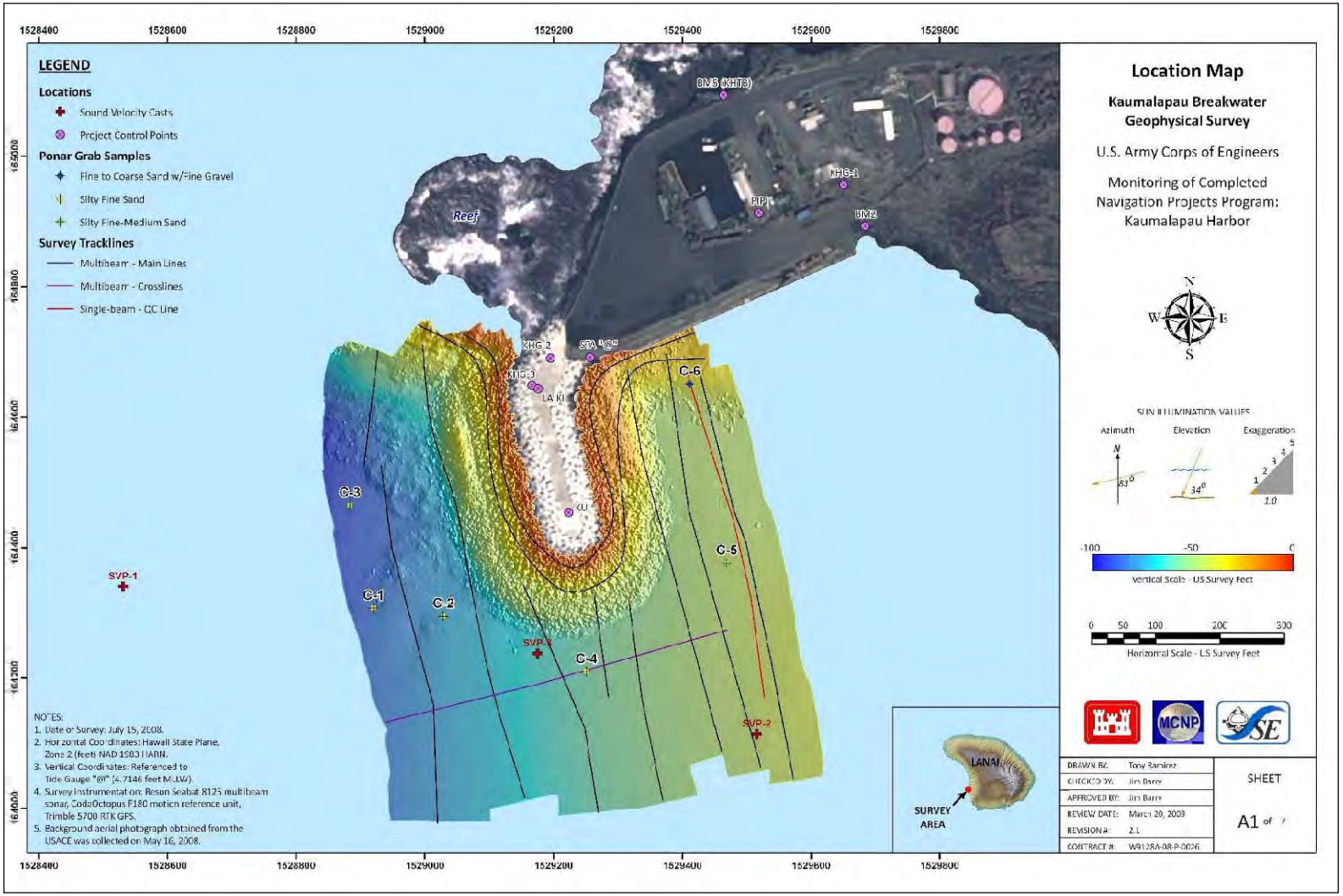

Figure 9.1. Locations of sound velocity casts and project control points, Ponar grab samples, and survey track-lines (multi-beam main lines, multi-beam cross-lines, and single-beam quality control line) (Sea Engineering, Inc. 2009).

9.2.3 Motion reference unit

The Coda-Octopus F-180 MRU was used for measuring vessel motions such as heave, pitch and roll as well as vessel heading. The F-180 utilizes two GPS antennas mounted approximately 2 m apart to calculate vessel heading information. The GPS antennas integrate with a deck-mounted processor and inertial unit that measures vessel motion for heave, pitch and roll corrections.

9.2.4 Sound velocity profiles

Conductivity, temperature, and depth (CTD) measurements were made using a SeaCat Profiler SBE-19 to calculate the sound velocity of the water column in the survey area. Three casts were made with the SBE-19 throughout the day for determining the sound velocity at the sea surface for multi-beam acquisition, and to generate sound velocity profiles (SVPs) for use in post-processing.

The first cast was located west of the survey area to ensure it covered the maximum depth to be surveyed. The second cast was made just prior to starting the multi-beam survey, and was located inside the harbor in a representative location of the survey. The profile from this cast was compared to the previous profile and found to be very similar with a slightly increased surface velocity. The surface value from this cast was used in the acquisition system for the entire survey (5,047.5 ft per sec). The third CTD cast was performed after the survey was completed at the mouth of the harbor just off the nose of the breakwater structure. This cast was performed to constrain the range of sound velocity fluctuations in the sea water for the survey. The third cast showed a slight change in the overall profile, but the surface sound velocity remained the same.

During post-processing, all three SVPs were used to correct the ping return time and subsequent calculated depths. The decision for which profile to use for each line was based on the distance in time and space from the cast and the depth of the profile compared to the maximum depth along the survey line.

9.2.5 Bottom sediment samples

Six bottom samples were collected from the survey area using a Ponar grab sampler. The samples were collected to assist with the classification of

bottom types using the backscatter results. The six sampling locations shown in Figure 9.1 were selected from a preliminary output of the backscatter data.

9.3 Data accuracy and quality control

9.3.1 Patch test

A patch test was performed to quantify residual biases from the alignment between the motion reference unit and the multi-beam sonar (yaw, pitch, and roll). The patch test also calculated the latency of the GPS system which is the difference in time between the when positioning data were received and when the computed position was logged by the acquisition system. The patch test was conducted using parallel control lines near the project site. Patch test corrections were calculated with the CARIS calibration program and applied during post-processing.

9.3.2 Cross-lines

A cross-line was run perpendicular to the primary survey lines to check for any roll offsets, timing delays or offsets due to tidal fluctuations. The cross-line data were compared with the primary survey data using CARIS processing software. No offsets were identified.

9.3.3 Single-beam calibration line

A single beam instrument was used for quality control (QC) to verify that data collected from the two independent sonar systems yields the same approximate depths along a chosen track-line. For this test, a track-line was selected inside the harbor where there is some vertical relief seen in the multi-beam data. Although this QC check only compares the vertical results from the two systems, in uneven terrain horizontal offsets also show up as vertical differences.

The selected track-line was run using an Odom Hydrotrac single beam echo-sounder for comparison with the collected multi-beam data. Depth values were extracted every two ft along the track-line from both the single-beam data and from the multi-beam data to look for vertical offsets. Although this QC check alone does not indicate if any vertical offsets seen are due to an incorrect sound velocity or from horizontal position errors, it will show if there is a problem in the acquisition system that needs to be corrected.

Comparing the single-beam and multi-beam data sets show the variation between the two instruments ranges from -0.406 to +0.147 ft, with an average offset of -0.019 ft. These differences are within the range expected due to the different input data resolutions.

9.3.4 Bar check

The bar check is a standard hydrographic system calibration technique that uses an acoustically reflective plate hung below the transducer at pre-measured intervals. The bar check verifies transducer draft and sound velocity accuracies by looking in the sonar data and verifying that the bar (reflective plate) shows up at the correct depth. A bar check was performed for both the multi-beam and single-beam sonar systems at a 5-ft depth to calibrate draft, and a 20-ft depth to check sound velocity. The 5-ft depth check is for verifying the accuracy of the vessel draft that was measured and entered into the acquisition system. Both the single-beam and multi-beam systems indicated that the correct draft was being used and no adjustments to the draft values were necessary. The 20-ft depth interval check is for verifying the accuracy of the sound velocity that was measured and entered into the acquisition system. With the sound velocity at 5,047.5 ft per sec, the multi-beam and single-beam systems showed the correct depth for the reflective plate, thus indicating that no adjustments were necessary to the measured sound velocity.

9.3.5 Sound velocity

Detailed measurements of the sound velocity profile throughout the water column are crucial in multi-beam surveys. Changes in the velocity profile will not only affect acoustic distance measurements but also can cause refraction or bending of the sonar path as it passes through layers in the water column with different velocities.

Three casts were performed during the day to look for velocity changes at the sea surface and throughout the water column. After each cast, the data were downloaded for use in the acquisition system. The calculated SVPs were compared to verify that the correct values were used for both acquisition and post-processing.

While there was some difference between the inside and the outside of the harbor, the two profiles used from before and just after the survey are consistent in the upper water column with a slight increase in sound

velocity at the end of the survey (SVP-3) with depth. Errors in sound velocity will also show as vertical offsets in overlapping track-lines. The overlapping data from each survey line were reviewed closely using CARIS processing software, and no vertical offsets were identified between lines.

9.3.6 Position controls

Survey controls used for this field program were originally surveyed by the UHSOEST Sea Level Center prior to this study in July 2008. The control locations were provided by the USACE for use during data acquisition. The benchmark elevations provided were referenced to MLLW as determined from data collected at an on-site UH tide gauge from July 2007 through April 2008.

Following the hydrographic survey program, the USACE retained Control Point Survey, Inc. to re-survey the benchmarks in the Kaumalapau Harbor area on 18 November 2008. Following the receipt of the new benchmark locations, the horizontal positions of the acquisition data obtained during the field program were corrected to the new NAD83 State Plane locations and then projected to NAD83-HARN using *Corpscon*, a USACE datum conversion software package. The vector translation between NAD83 and NAD83-HARN is approximately 5.6 ft to the northwest. Upon review of the new control point locations, the elevation for the RTK station "BM5 (KHTB)" showed an offset of +0.075 ft from the UH vertical value. The re-surveyed benchmark locations are shown in Figure 9.1.

9.3.7 Tide corrections

Tide data used for this survey were obtained directly from the RTK corrected GPS system. In addition to the RTK tide data collected, there are two existing tide gauges deployed in the project area and managed by UHSOEST that were used for quality control verification. The two instruments are a VegaPulse microwave radar located on the mast above the tide ruler, and a pressure gauge deployed in the water beneath it. Both of these sensors are located at benchmark "@" (Figure 9.1) in a sheltered corner of the harbor near the intersection of the Kaumalapau breakwater structure and the pier. An additional pressure gauge was installed by SEI for quality control purposes during the survey, although it was not adjusted to the project datum due to on-site difficulties.

Upon comparison of the RTK tide data to the two existing tide gauges, the radar gauge and the RTK data align well vertically. The pressure gauge data contained an offset due to instrument drift and were not used. Long period oscillations in the water level observed in the RTK data also show in the SEI pressure gauge data, and are thought to be a real phenomenon although not well understood. The UHSOEST gauge data are smoothed by a running average process that removes much of the amplitude from the oscillations. The RTK tide measurements determine the elevation of the survey vessel that is some distance removed from the tide gauge.

Since the RTK motions represent the actual vertical motions on the survey vessel due to the changing tides and localized swell and surge, it was selected for use in post-processing. The lack of vertical offsets seen between survey lines during post-processing validates the use of the RTK for tidal fluctuations.

9.3.8 Estimated vertical accuracy

The potential error in the depth measurements collected with swath sonar systems is a function of the inaccuracies due to residual systematic and system specific instrument measurement accuracies, such as the velocity of sound in water, tide measurements, and vessel motions. Combining these individual potential depth errors yields the total estimated uncertainty in vertical accuracy.

There are two basic types of errors. Bias errors are constant errors such as draft offsets or errors in tidal benchmarks. Random errors are errors present in the measurement system, such as GPS accuracies, motion sensor accuracies, and accuracy of the multi-beam system. An estimate of the total survey accuracy is a RMS summation of both bias errors and random errors. Bias errors included here are:

Benchmark: The difference between UH measurement of KHTB/BM5 and the Control Point measurement is 0.075 ft. This value was used to give an estimate of 0.1 ft for maximum error in the offset of the RTK control point from the tidal benchmark “@”.

Draft: Maximum error in draft measurement is estimated to be 0.1 ft

Velocity of Sound: Maximum error in velocity of sound, based on multiple CTD casts is an estimated 2 ft per sec. At 100-ft range and

two-way travel time, the maximum difference in depth measurement is estimated at 0.08 ft. An error estimate of 0.1 ft is used.

Random errors include total system errors (i.e., combined multi-beam "black box" and GPS positioning) and tide measurements. The total system error was estimated using Hysweep data statistics in relatively flat portions of the survey area. The standard deviation for 3-ft by 3-ft bin areas examined (with approximately 100 data points per bin) was consistently found to be 0.1 ft, giving a 95 percent confidence level at 0.196 ft. Tide offsets were estimated by smoothing the RTK and UH tide curves, and estimating a maximum offset of the two resulting data sets of 0.1 ft. A conservative estimate of total system RMS vertical accuracy is therefore:

$$RMS = (0.1^2 + 0.1^2 + 0.1^2 + 0.196^2 + 0.1^2)^{1/2} = 0.28 \text{ ft.}$$

9.4 Data processing and analysis

9.4.1 Bathymetric data

Post-processing of depth information from the multi-beam data was conducted utilizing CARIS HIPS multi-beam analysis and presentation software. Patch test data were analyzed and alignment corrections were applied to the sonar data. RTK water-level data were verified and applied to correct all depth measurements to the MLLW datum. Velocity profiles were applied to correct slant range measurements and compensate for any ray path bending. In addition, each survey line was reviewed and processed using the CARIS swath editor. The vessel's position and attitude data were reviewed, filtered, and accepted. Filters were applied to reject the outer swath limits of the multi-beam data. Sounding data were reviewed and edited for data outliers. Sounding data, including sonar beams reflecting from noise or aeration in the water column, were reviewed carefully before being flagged and rejected in the editing process.

After swath editing, all data were reviewed through the CARIS HIPS subset-editing program to ensure that no outliers remained in the data set and to analyze swath-to-swath comparisons. The survey lines were "tiled" to ensure that all sounding data were edited systematically and reviewed for completeness. The subset editing procedure also provided confidence in vessel positioning and sonar calibration by observing features mapped at the same location. All the accepted data were used to create sun-illuminated digital terrain models (DTM). This process creates a 0.82-ft grid over the

survey coverage area, and then assigns values to each grid node with an inverse-distance-weighted algorithm. These models were used to identify residual biases, and assisted in 3-D visualization during the subset-editing procedure. Areas of interest were identified through the DTMs, and investigated further with the subset-editing program.

The DTM generated by CARIS was exported as xyz data and brought into ArcGIS for conversion into a surface grid. The bathymetry grid is draped over a sun-illuminated hill-shade generated in ArcGIS that best illustrates the seafloor features and is presented in Figure 9.2. Bathymetric contours were generated at two-ft intervals to help illustrate seafloor structures and are presented in Figure 9.3. Examination of this figure clearly shows the delineation between the Core-Loc side slope of the structure and the ocean side toe buttress, at the 40-ft depth contour. Also visible is the dramatic change in side slope between the toe of the rock foundation of the breakwater, and the existing sandy bottom at the 70-ft contour along the ocean side and the 50- to 60-ft contour around the structure head. In addition, the approximately 30-ft-wide toe berm on the harbor side of the structure is clearly visible in the contours, and is at a depth of between 10 to 20 ft below MLLW, as specified in the breakwater design (nominal depth of toe berm = 15 ft MLLW). A 3-D perspective view of the bathymetric data is presented in Figure 9.4, which shows an exaggerated vertical scale of the previously mentioned slope variations along the ocean side and head of the structure.

9.4.2 Backscatter intensity data

Two backscatter intensity formats are presented, known as “snippet” and “side scan”. While essentially using the same return signal, the snippet data is more accurate spatially and uses the beam focusing capabilities of the sonar system to position the seafloor features accurately. The side scan image is generally sharper and is better at identifying seafloor features. Both data sets were processed using Hypack/Hysweep software. The snippet data were exported as *xyb* files, with ‘*b*’ representing intensity values measured in decibels. The side scan data were exported from Hypack/Hysweep as a geo-referenced .tiff and brought into ArcGIS. Both the snippet and side scan data are draped over the sun-illuminated hill-shade generated from the bathymetry data, and are presented in Figures 9.5 and 9.6, respectively.

Analysis of the backscatter data, in combination with the select bottom samples collected, produced an estimation of bottom types within the

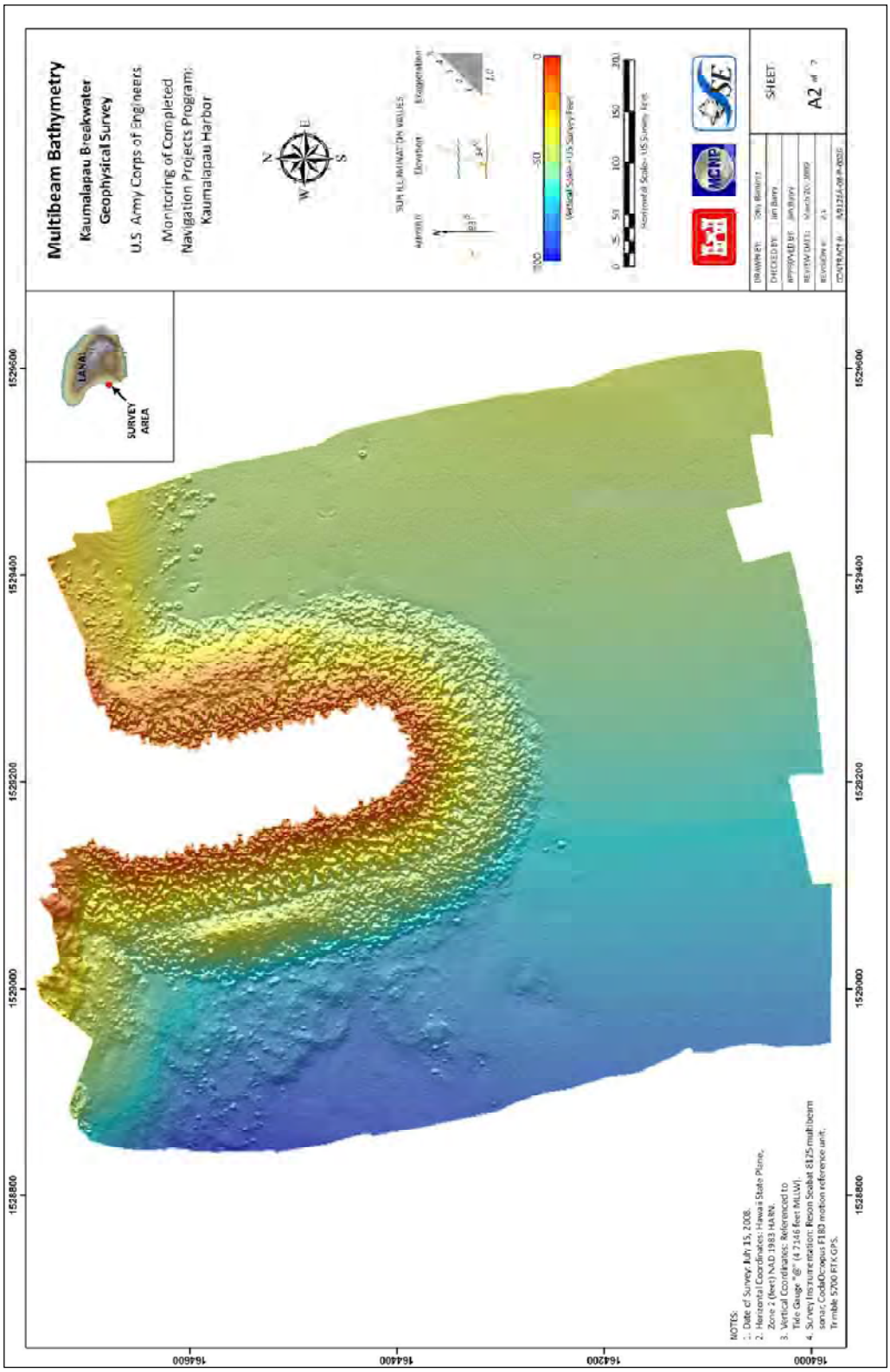

Figure 9.2. Multi-beam bathymetry of the Kaumalapau Harbor breakwater, and near vicinity, 15 July 2009 (Sea Engineering, Inc. 2009).

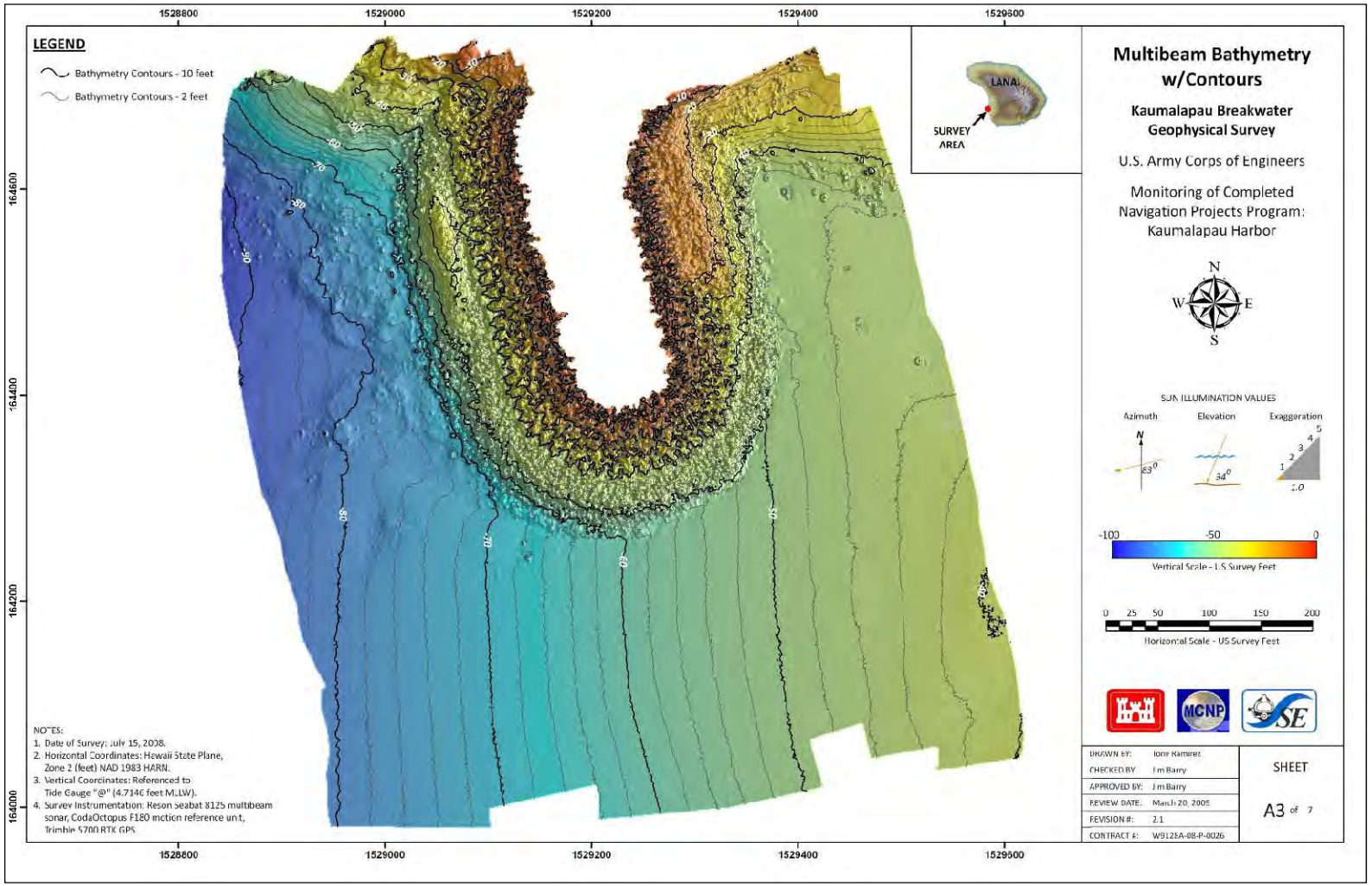

Figure 9.3. Multi-beam bathymetric contours of the Kaumalapau Harbor breakwater, and near vicinity, 15 July 2009 (Sea Engineering, Inc. 2009).

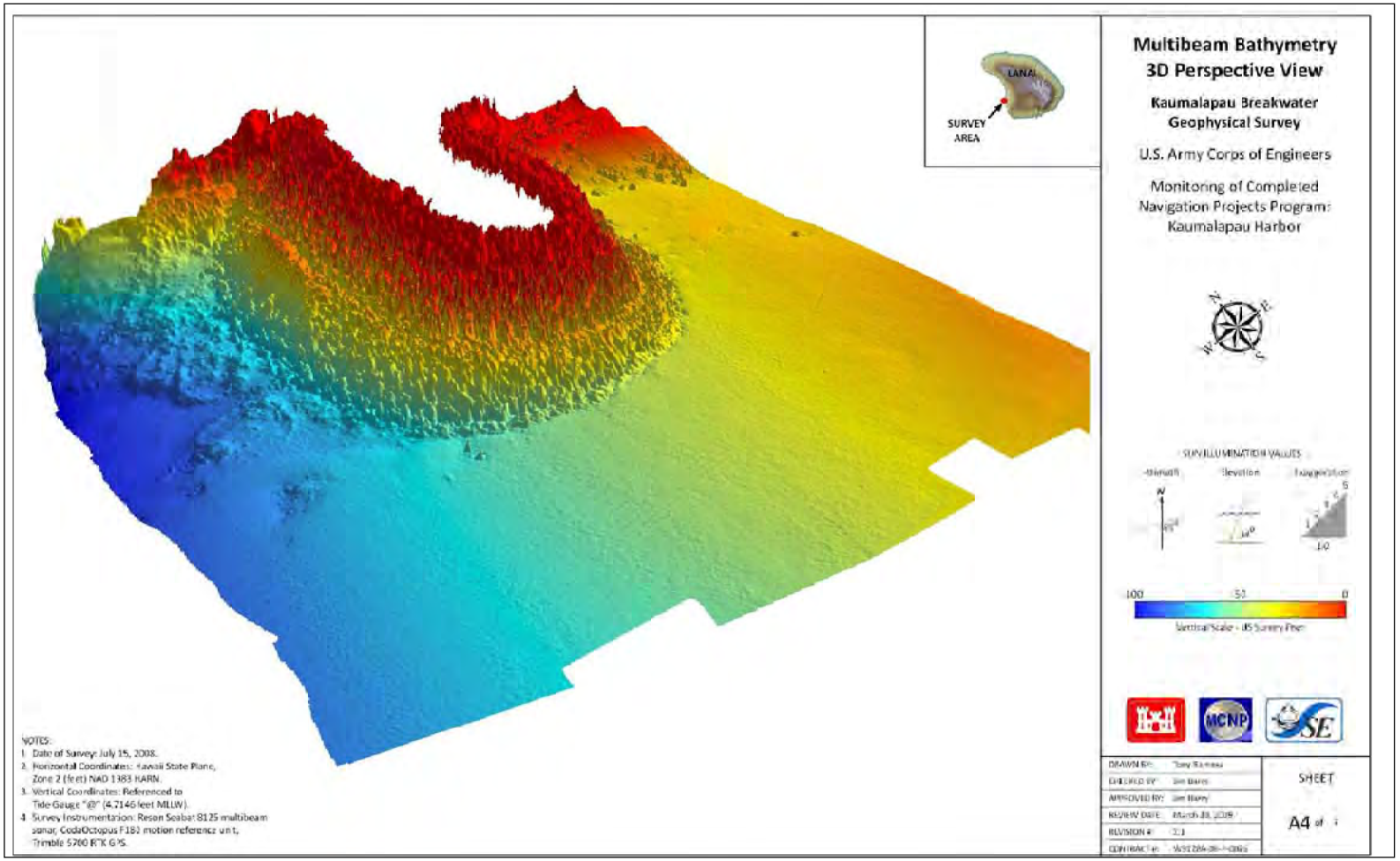

Figure 9.4. Multi-beam bathymetric 3-D perspective view of the Kaumalapau Harbor breakwater, and near vicinity, 15 July 2009 (Sea Engineering, Inc. 2009).

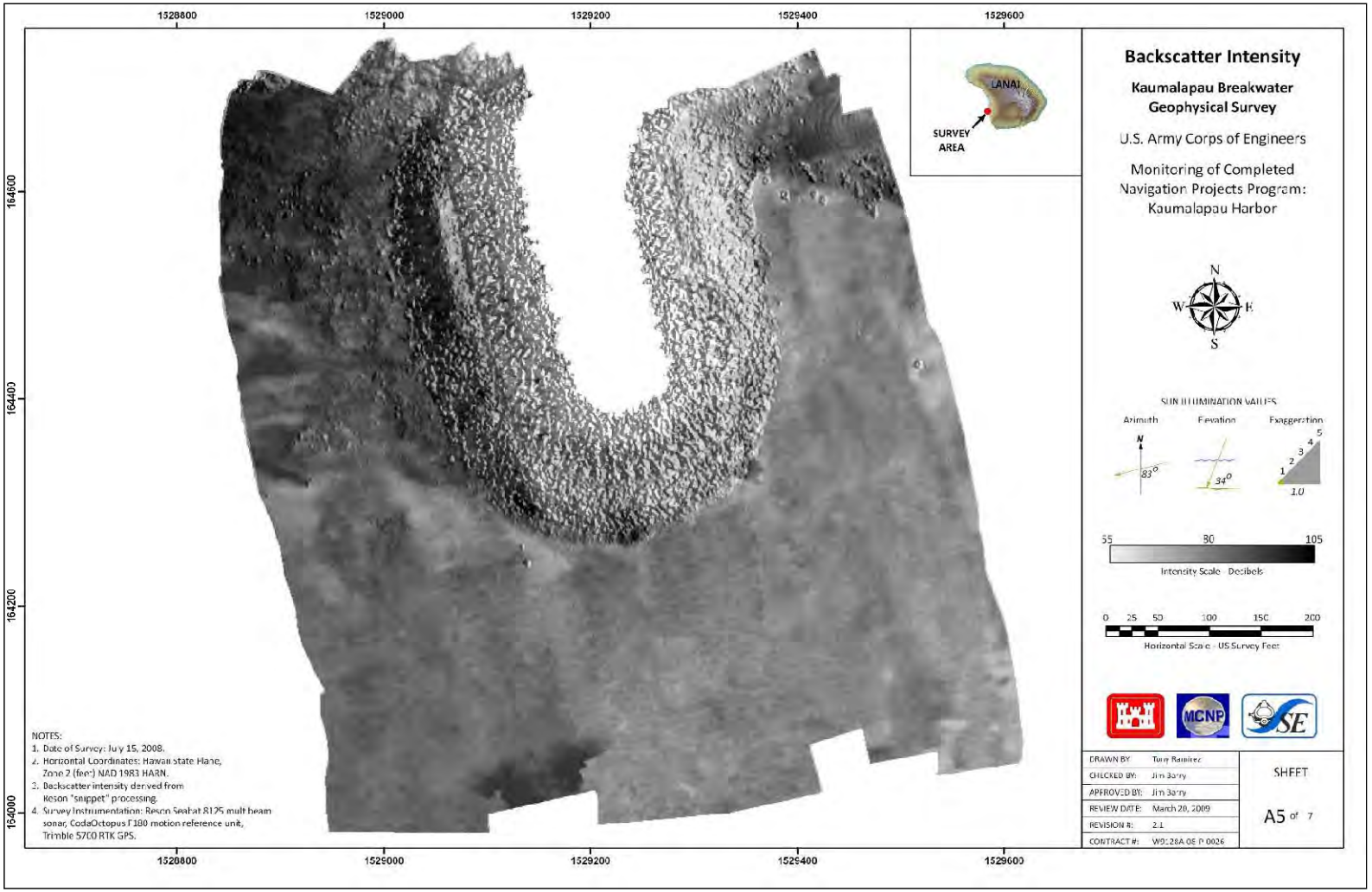

Figure 9.5. Backscatter intensity "snippet" data of the Kaumalapau Harbor breakwater, and near vicinity, 15 July 2009 (Sea Engineering, Inc. 2009).

Figure 9.6. Backscatter intensity "side scan" data of the Kaumalapau Harbor breakwater, and near vicinity, 15 July 2009 (Sea Engineering, Inc. 2009).

survey area. This was done in part by contouring the backscatter values for a visual separation of response variations, while also using known sediment types collected from within the identified intensity value ranges for sediment classification. This classification method makes the assumption that similar intensities reflect similar bottom types. While this is generally true, other factors besides grain size can affect the sediment response. In addition to identifying the Core-Loc and rock outcrops, sediment types in the survey area range from silty fine sands, to fine, to coarse sand with fine gravel. The side scan imagery (Figure 9.6) was used to validate the backscatter interpretation. Visual representation of the interpreted backscatter data are shown in Figure 9.7.

9.4.3 Point cloud data

Due to the complexity of the breakwater structure, this area is not well imaged by the surface interpretation used to create a gridded surface. A representation using all of the data points, known as a "point cloud", is used to best image the breakwater. Each point has horizontal and vertical coordinates (x, y, z), and can be presented in a 3-D framework. Several point cloud views of the breakwater structure are presented in Figures 9.8 (index) through 9.15.

Visual analysis of the point cloud images enables the identification of several features of the underwater portion of the structure. Figure 9.9 (Tile A) shows a defined demarcation at the top center of the figure where the ocean side root of the structure ties in to the existing rock outcrop, indicated by an abrupt change in the color scale of the point cloud near the water surface from red to yellow to green. It is also relatively easy to distinguish the difference between the angular Core-Loc units and the armor stones (or other more naturally shaped features such as the rocky seafloor). Figure 9.10 (Tile B) is an almost complete view of the ocean side of the structure from the root to the dogleg. This figure clearly shows the side slope of the structure composed of Core-Loc, and the stone toe buttress (in dark blue). Along the right side of the figure, several of the first row of Core-Locs (placed in the cannon orientation) are easily visible, as well as the interlocking row of Core-Locs placed directly above them also in a specific (but different) orientation. The remainder of the Core-Locs, resting higher on the side slope, clearly are in a more random orientation, as designed.

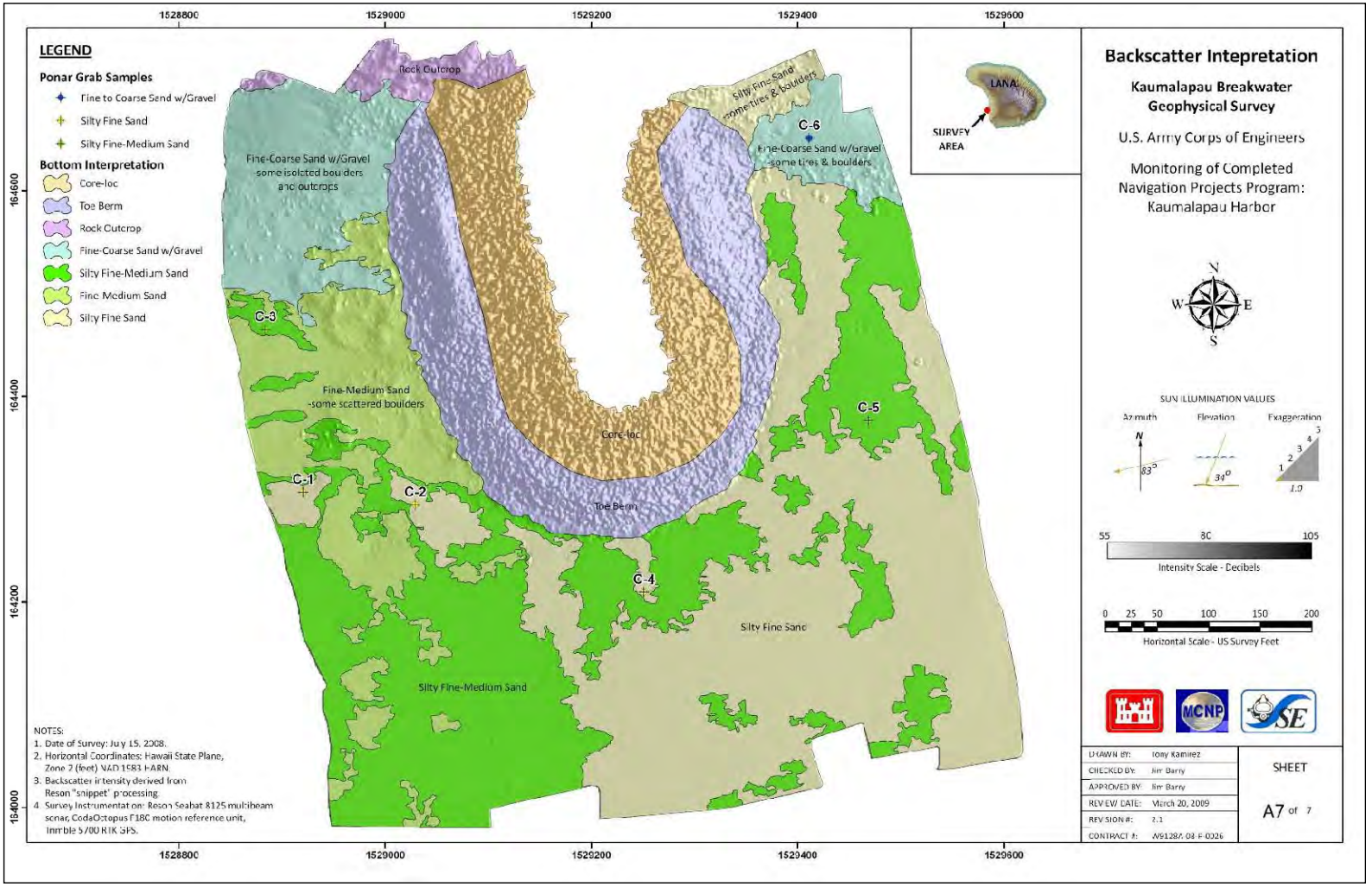

Figure 9.7. Backscatter interpretation of the sea floor sediments, in conjunction with selected bottom samples, of the near vicinity of the Kaumalapau Harbor breakwater, 15 July 2009 (Sea Engineering, Inc. 2009).

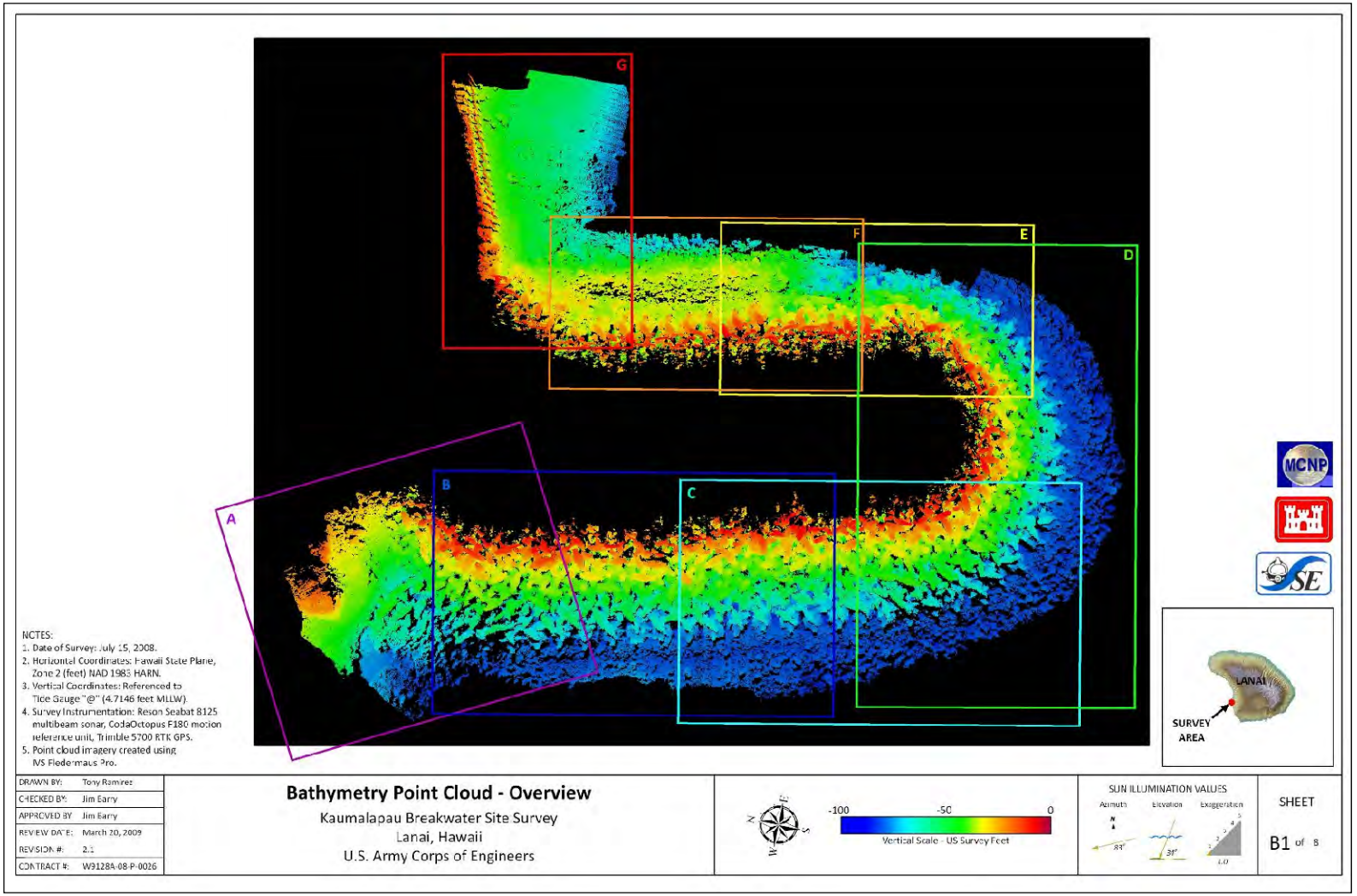

Figure 9.8. Bathymetry point cloud overview, and Section key, Kaumalapau Harbor breakwater (Sea Engineering, Inc. 2009).

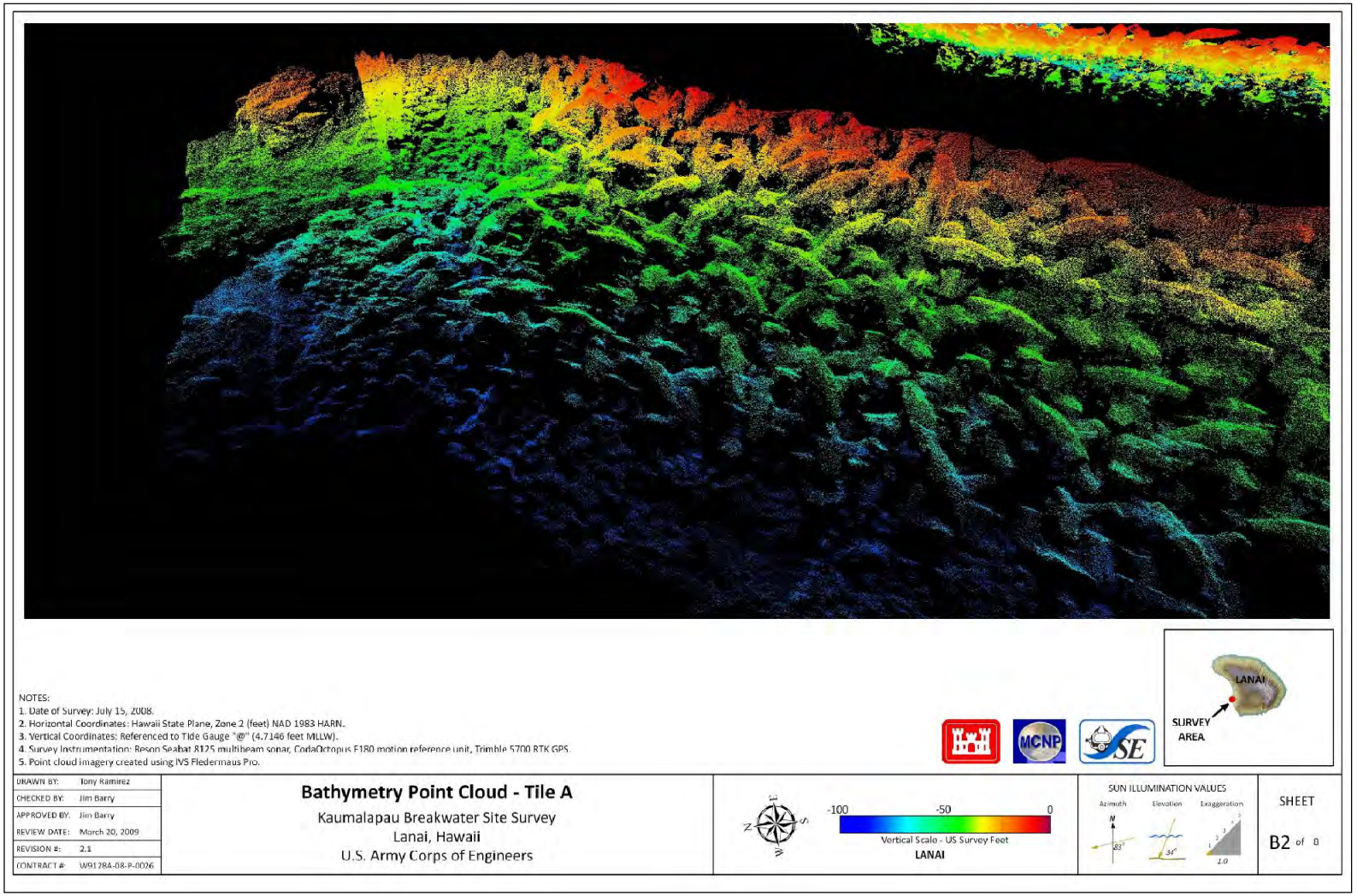

Figure 9.9. Bathymetry point cloud, Section A, Kaumalapau Harbor breakwater (Sea Engineering, Inc. 2009).

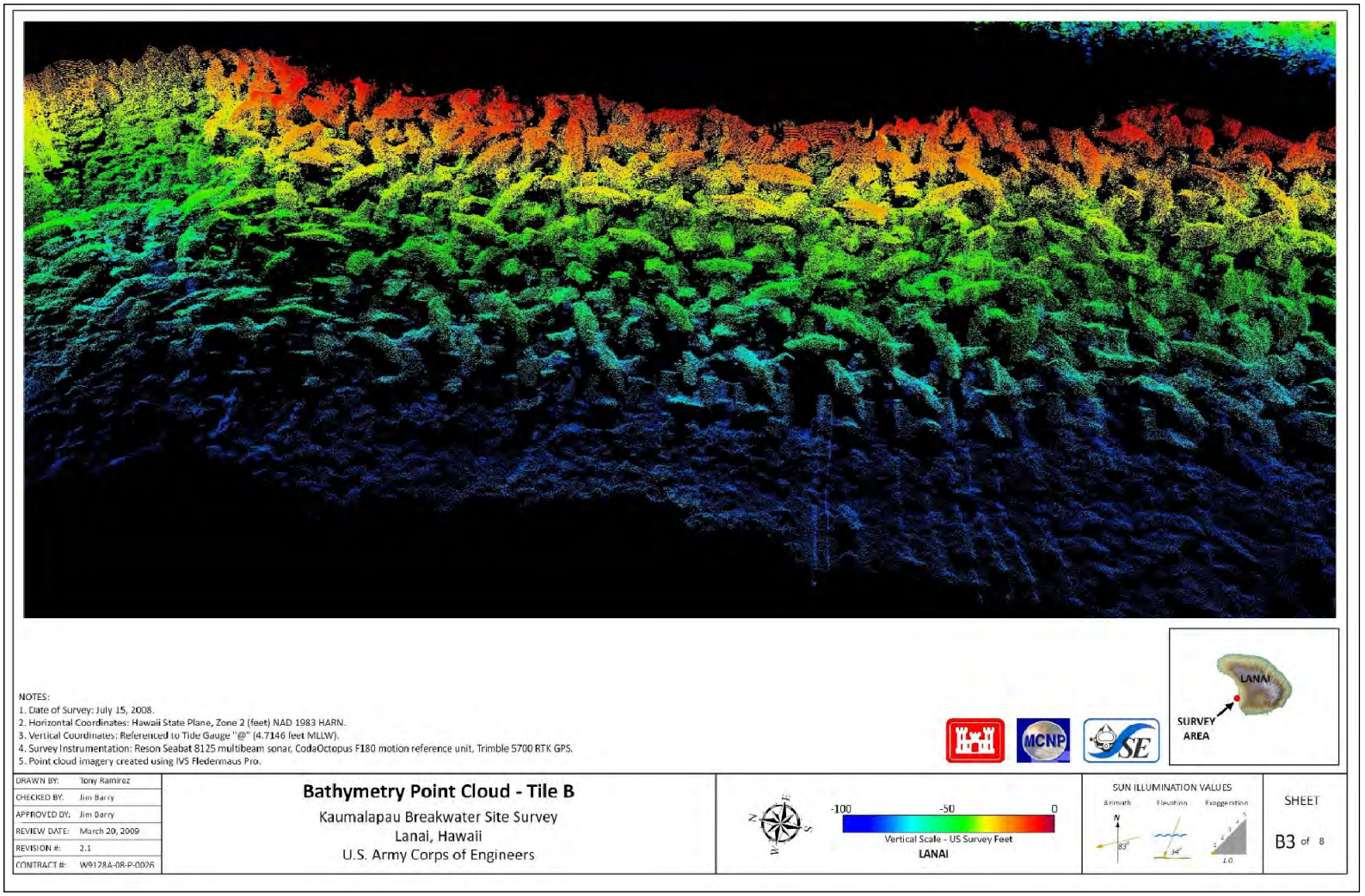

Figure 9.10. Bathymetry point cloud, Section B, Kaumalapau Harbor breakwater (Sea Engineering, Inc. 2009).

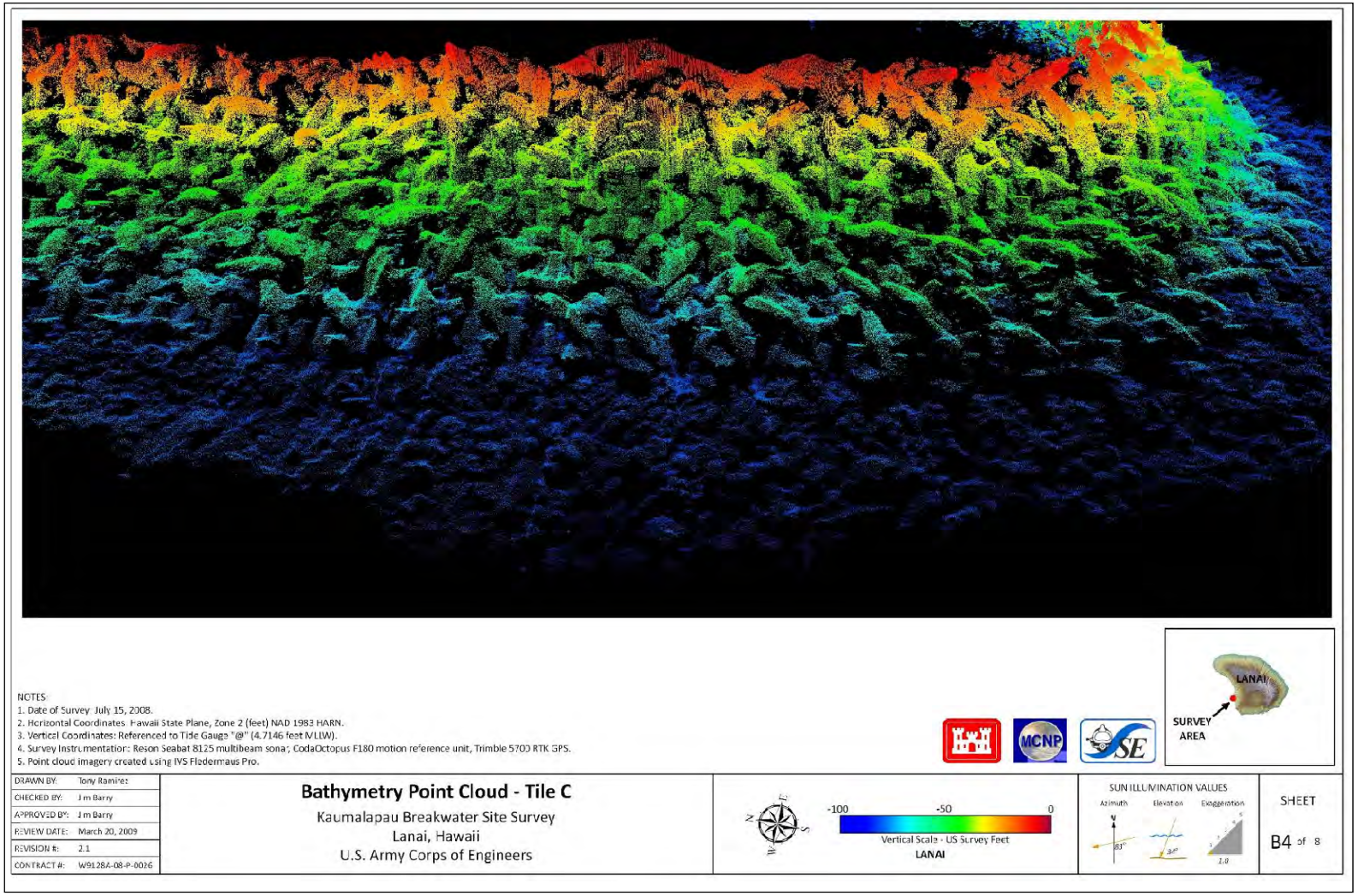

Figure 9.11. Bathymetry point cloud, Section C, Kaumalapau Harbor breakwater (Sea Engineering, Inc. 2009).

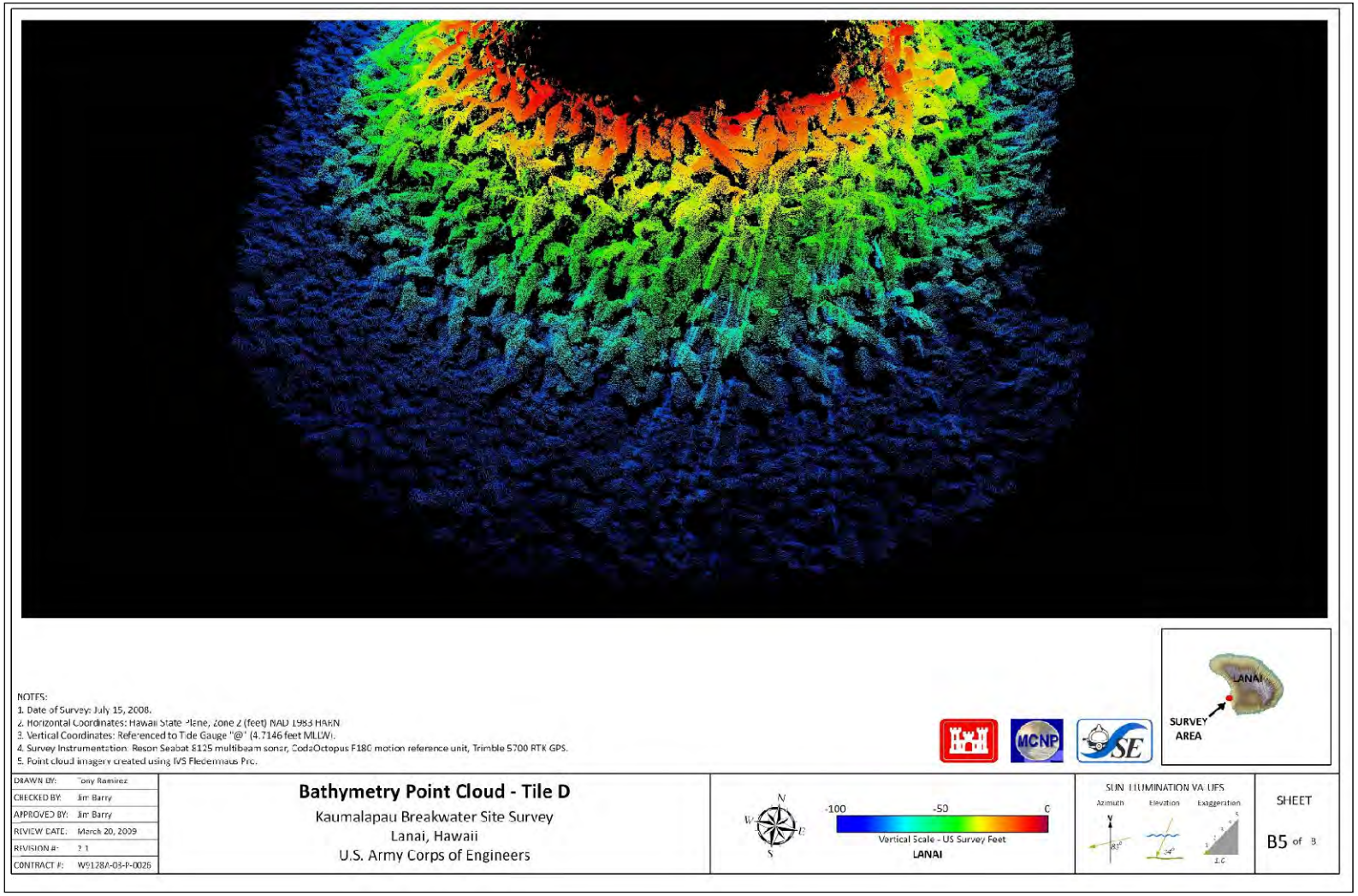

Figure 9.12. Bathymetry point cloud, Section D, Kaumalapau Harbor breakwater (Sea Engineering, Inc. 2009).

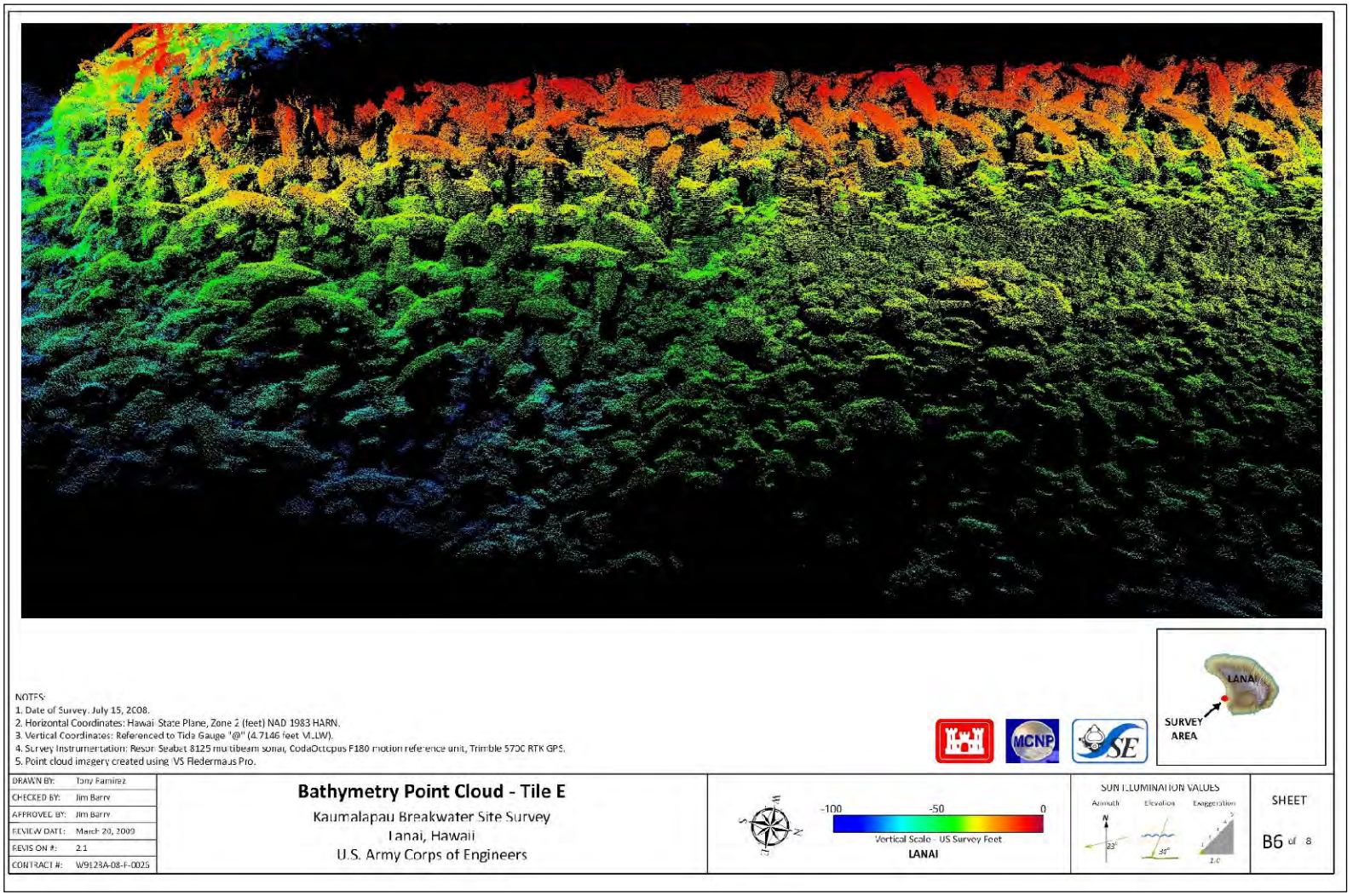

Figure 9.13. Bathymetry point cloud, Section E, Kaumalapau Harbor breakwater (after Sea Engineering, Inc. 2009).

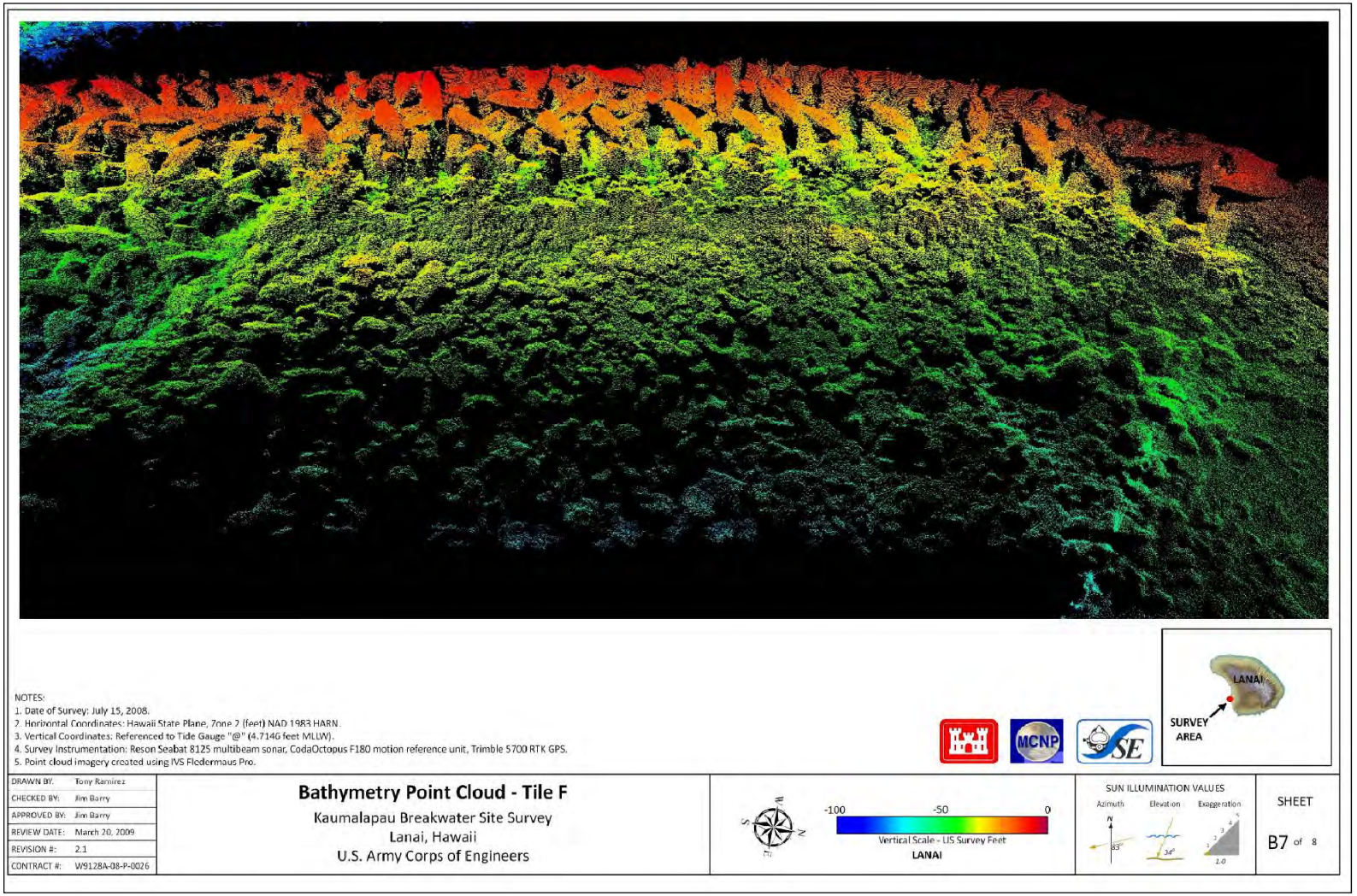

Figure 9.14. Bathymetry point cloud, Section F, Kaumalapau Harbor breakwater (Sea Engineering, Inc. 2009).

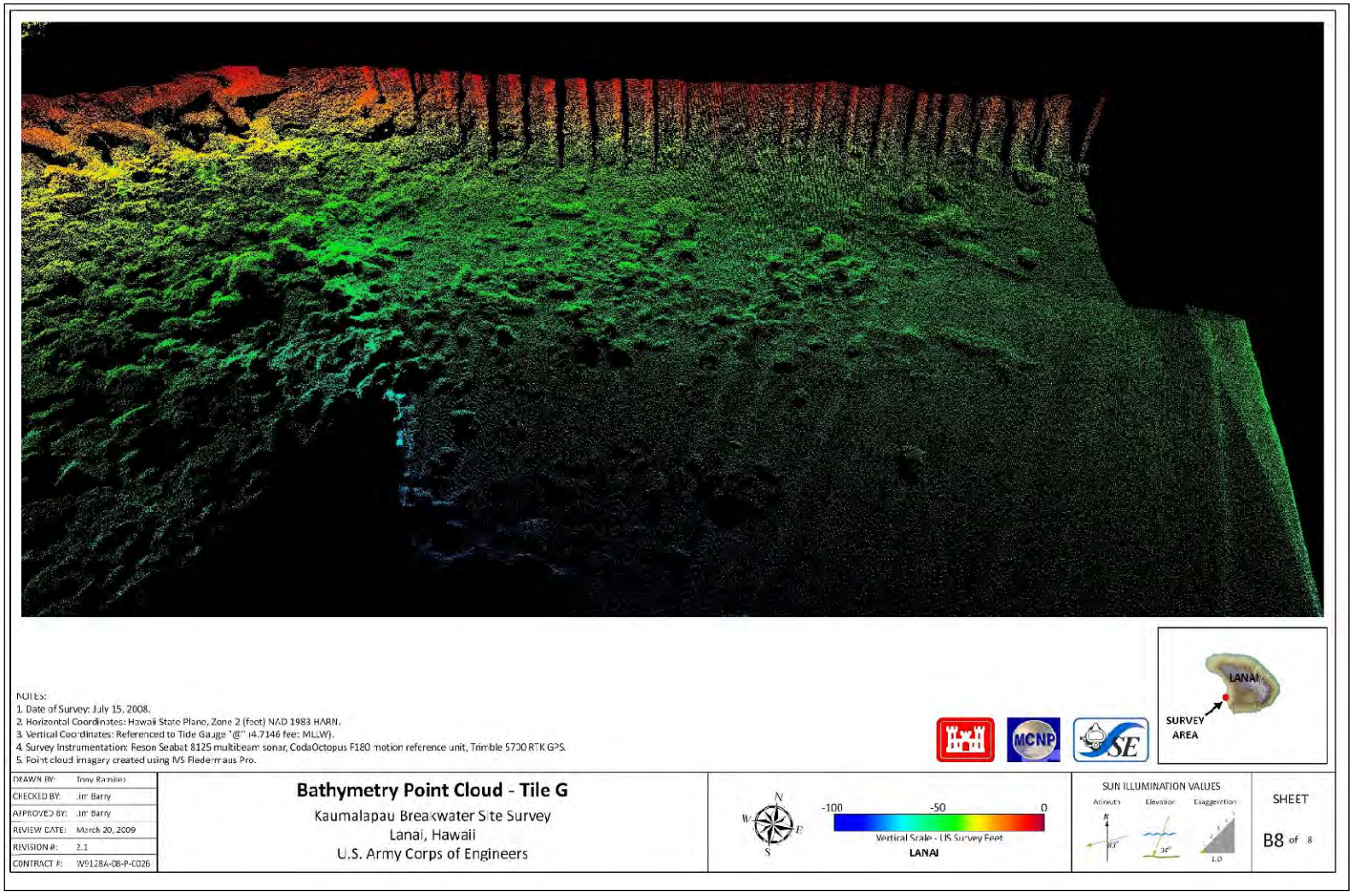

Figure 9.15. Bathymetry point cloud, Section G, Kaumalapau Harbor breakwater (Sea Engineering, Inc. 2009).

Figures 9.11 (Tile C) and 9.12 (Tile D) show similar representations of the point cloud data from the ocean side dogleg to the ocean side head, and the entire structure head, respectively. Both figures indicate that the structure toe appears to follow a consistent contour along the rock foundation, with no visible deviations or non-interlocked Core-Loc units. Figure 9.13 (Tile E) shows the harbor side head of the structure, as well as the transition to the harbor side toe berm (right half of figure). Examination of the point cloud of the toe berm indicates that there is likely a large gradation in stone size in this area, however, this is consistent with construction specifications allowing for the use of existing stone at the project site to be recovered and reshaped for use in the toe berm (refer to Chapter 2 of this document).

Also visible in Figures 9.13 and 9.14 (Tiles E and F) is what appears to be a steepened slope within the harbor side toe berm (approximately half way down the right side of the image in Figure 9.13 and half way down the majority of the image in Figure 9.14). Reference back to the contour plot of the multibeam survey (Figure 9.3) suggests that this may be due to the change from the relatively flat slope of the wide toe berm at approximately 15 ft below MLLW, to a more steep side slope between the 20-ft and 40-ft contour. It is also possible that the angle of the image may be causing an exaggerated view of this side slope, however, this location should be monitored for changes and/or stability in any future underwater surveys or inspections. Finally, Figure 9.15 (Tile G) shows the location where the harbor side root ties into the existing barge pier, as well as the underwater portion of the sheet pile bulkhead of the barge pier.

9.5 Project survey benchmark update

In addition to multibeam survey data collection, the USACE Honolulu District requested as part of the contract that the survey network at the project be re-established with an updated survey to ensure the horizontal and vertical accuracy of the network. This additional survey work was requested to ensure that the project (and multibeam survey data) was brought into compliance with the Comprehensive Evaluation of Project Datums (CEPD) program established by Engineering Circular (EC) 1110-2-6065 in July 2007 (updated by EC 1110-2-6070 in July 2009) (U.S. Army Corps of Engineers 2009). The result of this survey work was the establishment of five official survey benchmarks at the project, all of which were referenced to the accepted coordinate system of the High Accuracy Reference Network (HARN) North American Datum of 1983 (NAD83) using the 1980 Geodetic Reference System (GRS80) spheroid, in Hawaii

State Plane Zone 2, Transverse Mercator projection, and US Survey Feet. Elevations were determined at each benchmark and referenced to the Mean Lower Low Water (MLLW) as determined by the University of Hawaii (UH), School of Ocean and Earth Science and Technology (SOEST), Sea Level Center.

9.6 Summary of multibeam data collection

The result of the multibeam data collection performed on the Kaumalapau Harbor breakwater in July 2008 is a dense and highly accurate representation of the characteristics of the underwater portion of the breakwater approximately one year after construction was completed. These characteristics include not only the bathymetric contours that would be captured by a traditional single beam survey, but also a detailed view of the orientation of concrete armor units (especially the first two rows composing the breakwater toe), the transitions from armor units to stone, the structure tie-ins to land, and an estimation of the geologic classifications of sediments surrounding the structure. Though a follow up underwater survey was not possible as part of this monitoring study, a detailed “baseline” survey has been conducted and will enable comprehensive comparisons to future conditions if and when additional surveys are completed.

10 Breakwater Inspection Program

Visual inspection of the completed breakwater was an important method of augmenting and validating the data collected and presented in previous chapters of this report. As noted in the monitoring plan, field inspections of the above-water structure were conducted to locate and document any structure damage, identify displaced units, assess any effects of structure settlement on the concrete cap, and evaluate the overall structural condition of the breakwater. Spot measurements were made as part of these inspections to substantiate the T-LiDAR measurements used to determine breakwater settlement and armor unit movement. In addition, an ROV was used to conduct an underwater inspection of the breakwater. Due to the importance of the breakwater toe armor units in the overall stability of the armor layer, the underwater inspection focused heavily on the toe of the structure, in an effort to identify whether any armor units had become dislodged, settled dramatically, or broken in this location. The inspections on behalf of the MCNP program were conducted on the dates shown in Table 10.1.

Table 10.1. Breakwater inspection dates and descriptions.

November 6, 2007	Above-water visual inspection and underwater ROV inspection
April 18, 2008	Above-water visual inspection
August 28, 2009	Above-water visual inspection
September 9, 2010	Above-water visual inspection

The results and observations from these inspections are presented in the following. In addition, photos of underwater portions of the structure collected in August 2009 by a private individual and provided to USACE Honolulu District are included as additional data. These photos provide some additional information on the status of the underwater portion of the breakwater and are useful since an additional ROV inspection was not possible as part of the MCNP program in 2009.

10.1 Above-water inspections

The four above-water inspections of the breakwater, which included assessment of the concrete cap, ocean side and harbor side tiebacks, and

the armor units visible from the crest, were conducted on the dates noted in Table 10.1 by USACE Honolulu District and ERDC coastal engineers associated with the MCNP program. All of the inspection findings indicated that the structure has remained in very good condition in the first three years following construction. There have been no indications of broken, cracked, or severely damaged armor units, and the concrete cap has remained fully intact with no visible cracking or other damage. The armor units have experienced some weathering and minor damage, as would be expected. Some items that have been noted in the inspection reports for continued monitoring include the following:

1. voids in the armor layer with exposed underlayer stones,
2. limited contact of armor units with adjacent armor units and/or underlayer,
3. underlayer stone appears smaller than required,
4. underside of the concrete cap is exposed or cap is thin,
5. areas grouted after armor unit placement,
6. settlement of armor units creating gap between armor unit and concrete cap,
7. harbor side tieback where partial armor units join structure to existing wall.

Photos from various inspections documenting each of these items are presented below. When applicable, multiple photos indicating visible changes from year to year are provided, and if visible, noted armor unit numbers are provided. In addition, several field measurements of armor unit movement conducted during inspections have been compared with measured displacement from T-LiDAR surveys as a ground truthing method. The stationing established for the breakwater is shown in Figure 10.1.

10.1.1 Voids in the armor layer with exposed underlayer stones

Voids between armor units were observed in several locations, including Station -1+00 along the root of the structure on the ocean side (shown in Figure 10.2) and on the harbor side trunk at Station 1+58 (shown in Figure 10.3). In many cases, these voids exposed underlayer stones, which is undesirable because the stones may be exposed to greater wave attack and possibly become mobilized during very large wave events. If the void between armor units is larger than the armor stone diameter, the mobilized armor stone could potentially be pulled out of the structure through the void.

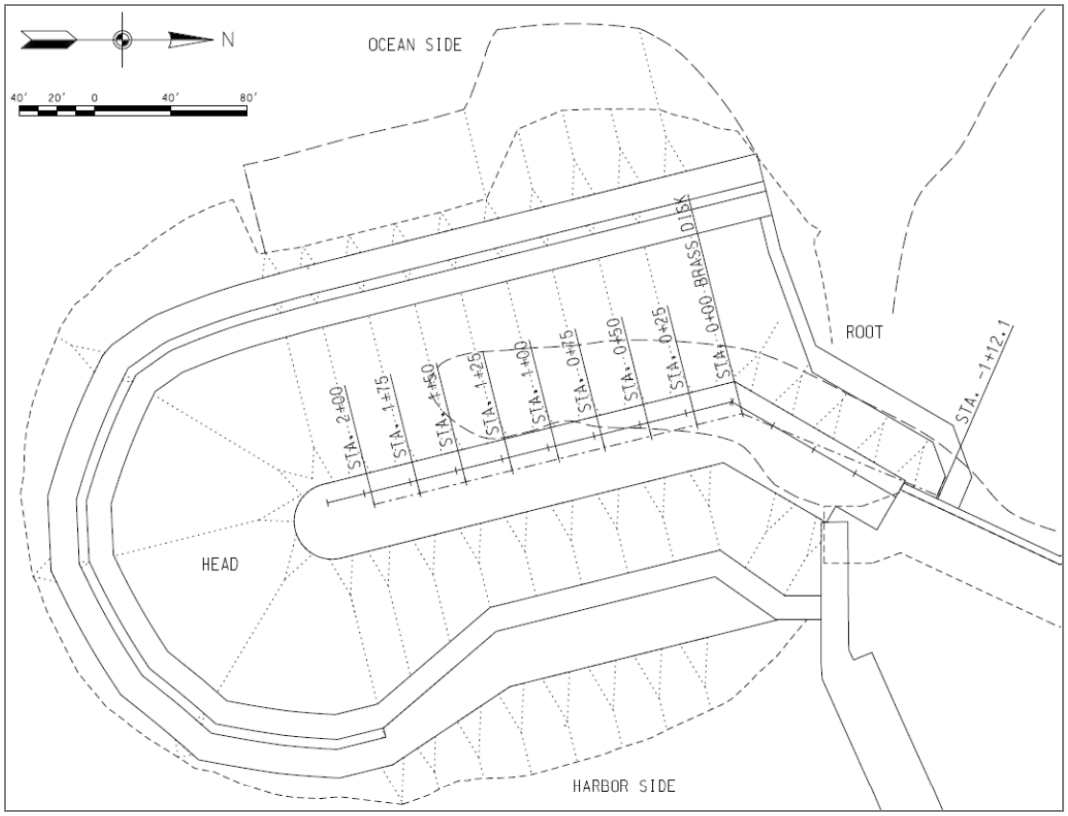

Figure 10.1. Stationing used for reference during inspections.

Figure 10.2. Void in armor layer on ocean side root at Station -1+00 with armor stone and water surface visible through void. (2007 photo)

Figure 10.3. Void in armor layer on harbor side trunk at Station 1+59 with armor stone exposed. (2007 photo)

10.1.2 Limited contact of armor units with adjacent armor units and/or underlayer

As noted in Chapter 3 of this report, the breakwater design specified that, "*Moving up the slope, successively higher units should be "keyed" into and between two units below (i.e., fit the higher CORE-LOC™ into the "pocket" between two adjacent lower units). Keying into the lower units should result in contact between at least one, and usually both, of the lower units* and *every CORE-LOC™ unit must rest on and contact the underlayer stone (Sea Engineering, Inc. and Group 70 International 2008).*" During the inspections, areas where there appeared to be less than adequate contact between armor units and/or limited contact between armor units and underlayer stone were noted. This limited unit-to-unit and unit-to-underlayer contact must be monitored because it can potentially allow long-term settling in the units that may affect armor layer stability. This may also enable rocking or other short-term dynamic motion during large wave events that could result in armor unit damage. In some observed cases, this condition has resulted in a void in the armor layer with exposed underlayer, as discussed in the previous section. Examples of these observations are shown in Figures 10.4 through 10.7.

10.1.3 Underlayer appears smaller than required

In certain locations where the underlayer is visible as described above, the underlayer stone appears to be smaller in size than the 2.5- to 4.5-ton requirement for underlayer specified in the design. Stone of the required size would have a diameter of between approximately 3.2 and 3.9 ft. This

size requirement is important because, as noted in the discussion of voids in the armor layer, the smaller the stone, the more likely it is to be mobilized by storm waves impacting the structure, and the easier it would be for this stone to fit through voids in the armor layer. This process would not only remove the stone from the structure and weaken the armor layer, it may have secondary effects of causing settling in the armor layer due to the uneven underlayer foundation, as well as making the mobilized stones projectiles that could damage the armor units or concrete cap. Examples of areas noted with undersized underlayer stones are shown in Figures 10.8 through 10.10. Size of stones are estimated based on known scale of armor unit "A" dimension of 2.27 ft, shown in Figures 10.8 and 10.9.

Figure 10.4. Approximately 2-in. gap between armor unit #605 and adjacent unit at Station 0+50 on ocean side trunk (2007 photo). Unit #605 has moved 1.6 in. (4 cm) from 2007-2010 (T-LiDAR).

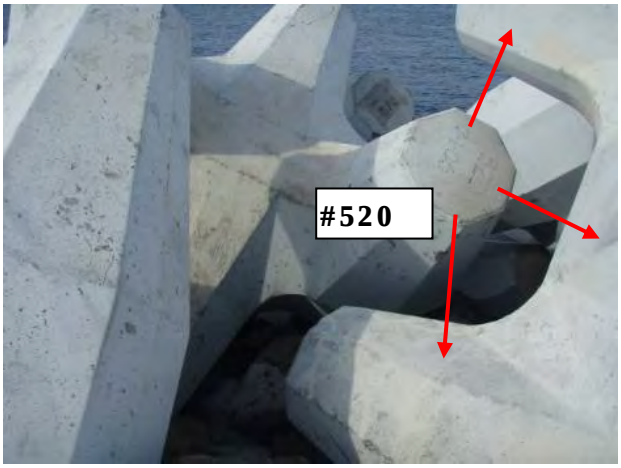

Figure 10.5. Poor contact between unit #520 and adjacent armor units at Station 1+36 on ocean side trunk (2007 photo). Unit #520 has moved 5.9 in. (15 cm) toward head from 2007-2010 (T-LiDAR).

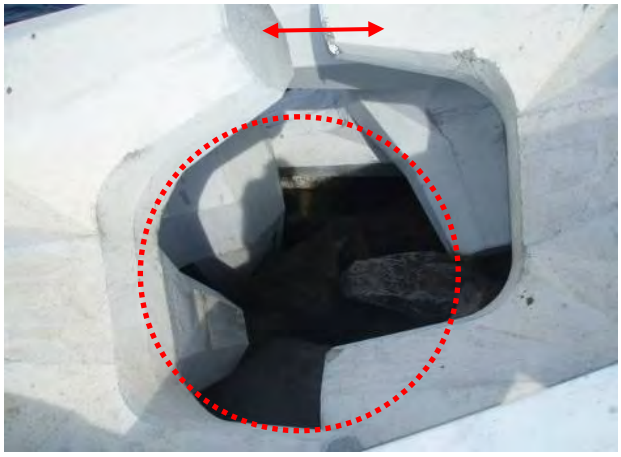

Figure 10.6. Limited contact between armor units placed end-to-end on ocean side trunk near crest at Station 1+82. Void with underlayer exposed. (2007 photo)

Figure 10.7. Limited contact between armor unit leg and underlayer stone on harbor side trunk at Station 1+26. Void in armor layer with underlayer exposed. (2010 photo)

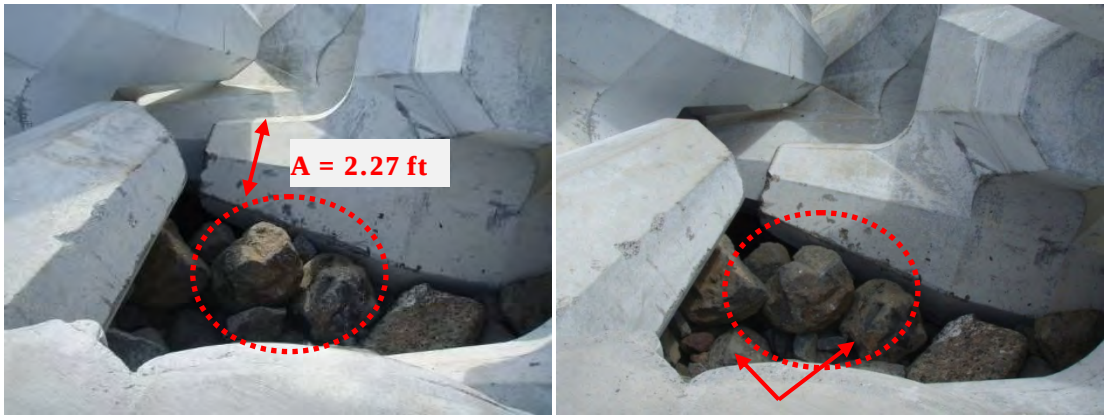

Figure 10.8. 2007 photo of undersized stone between ~0.8- and 2.5-ft diam, near crest on harbor side of breakwater head (left). 2009 photo of same location with noticeable changes including broken stones and additional small stones indicated by arrows (right).

Figure 10.9. Undersize stone between ~0.5- to 2-ft diam, in void between armor layers and concrete cap on harbor side of breakwater head (2010 photo).

Figure 10.10. Undersize underlayer stone on harbor side trunk at Station 1+51, estimated to be ~0.8- to 2.5-ft diam. (2007 photo)

10.1.4 Underside of the concrete cap is exposed or the cap is thin

Inspections also noted areas along the breakwater where the side of concrete cap was exposed (i.e., not protected by armor units). Some areas were also noted where the edge of the concrete cap was thin in comparison to the rest of the cap. These areas could be of potential concern due to their greater exposure to wave impact and potential for damage. Photos of these areas are shown in Figure 10.10 through 10.11.

Figure 10.11. Exposed underside of concrete cap at Station -0+28 along ocean side trunk.

Figure 10.12. Concrete cap is thin and overhangs armor unit along ocean side trunk at Station -0+36. Apparent movement of armor unit between 2007 (left) and 2009 (right).

10.1.5 Areas grouted after armor unit placement

Following placement of the armor layer during construction, areas identified as having insufficient contact between adjacent armor units were filled with grout by the construction contractor, with the concurrence of the USACE. The armor units could not be adjusted to improve contact after the entire armor layer was in place, and this method was intended to prevent movement of armor units if and when they were impacted by wave forces. This area was noted in the inspection reports to monitor the weathering and durability of the grouted areas over time, and to note any grout damage due to movement of the armor units. Photos of a grouted area on the harbor side trunk, near the crest at Station 1+80 are shown in Figures 10.13 through 10.15, from inspections in 2007, 2009, and 2010.

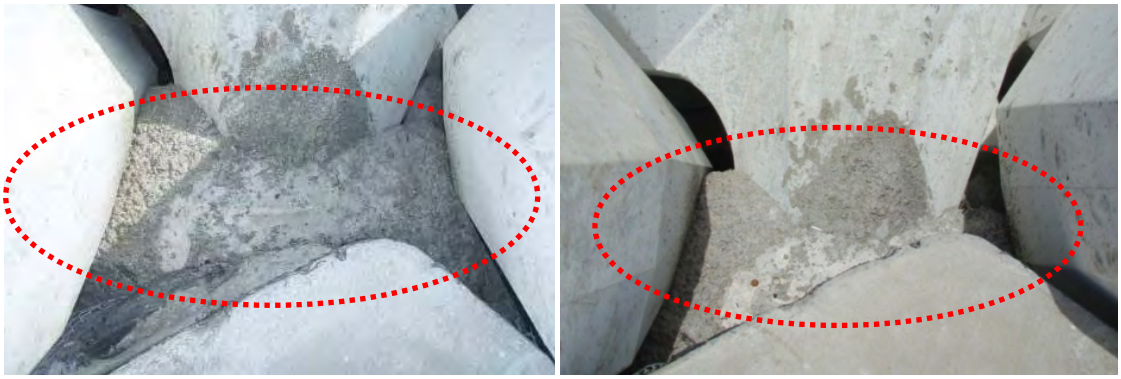

Figure 10.13. Grouted area along harbor side trunk at Station 1+80 (2007, left). Same area appears to have had some weathering and loss of grout (2009, right).

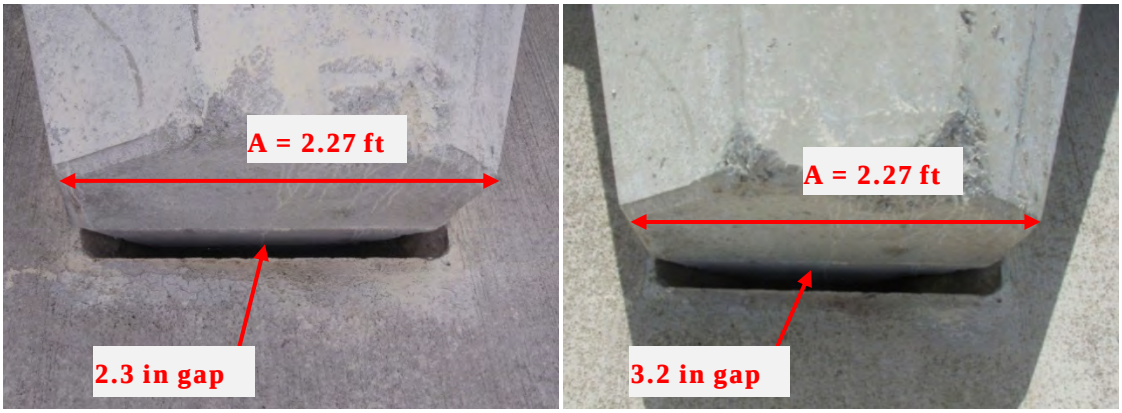

Figure 10.14. Gap created between armor unit and concrete cap on ocean side trunk at Station 0+55. Measured gap was 2.3 in. in 2008 (left) and 3.2 in. in 2009 (right).

Figure 10.15. Exposed edge of concrete cap with apparent pulling away of armor unit between 2007 (left) and 2009 (right) on ocean side trunk at Station -0+14.

10.1.6 Settlement of armor units creating gap between armor unit and cap

The inspections also noted several areas along the structure on both the harbor side and ocean side where armor units have gradually pulled away

from the concrete cap. Since the cap was poured following the placement of the armor layer (using a wire mesh overlaid with geotextile fabric to contain the concrete around the edges of the cap as it flowed into place), it was initially in contact with the armor units at the crest of the structure. Since completion of construction, the gravitational settlement of the armor units at the crest has caused them to pull away from the edge of the concrete cap. The gaps created by this occurrence are relatively small, usually on the order of 6 in. or less. At this scale, the separation of the armor units from the cap is not likely to affect the function or stability of either; however it is important to monitor these areas to keep track of the scale of movement over time. If the gap between the armor units and the cap becomes very large, the cap could become more exposed to damage from wave action. Photos of gaps observed are shown in Figures 10.14 and 10.15.

10.1.7 Harbor side tieback where partial armor units join structure to existing wall

As previously noted, six armor units that were broken (either the nose or a leg detached) during construction were set aside and later used to aid in construction of the tieback along the harbor side root of the structure. It was determined that, because this area was expected to have the least amount of wave impact, use of the partial armor units in this location would not adversely affect the stability of the armor layer. In addition, placing the partial units in this area solved a logistical issue – the fully-intact armor units would not fit securely against the existing wall and face of the barge pier, and the partial units were arranged to do so. This area was monitored closely during inspection to determine whether the partial units had settled, and whether any settlement had affected the adjacent armor units or the integrity of the harbor side tieback. The results of inspection (shown in Figures 10.16 through 10.19), as well as the results of T-LiDAR surveys presented in Chapter 8, indicate that there has been movement of the units in this location, on the order of 4.3 to 11.8 in. (11 to 30 cm) between 2007 and 2010.

10.2 Underwater inspections by ROV and underwater photos

As part of the November 2007 post-construction inspection of the breakwater, the USACE Honolulu District deployed the ROV that had been used during construction to inspect the progress of underwater stone and armor unit placement. The ROV was launched using a 30-ft rigid hulled inflatable boat; both the vessel and ROV are shown in Figure 10.20. Stationing

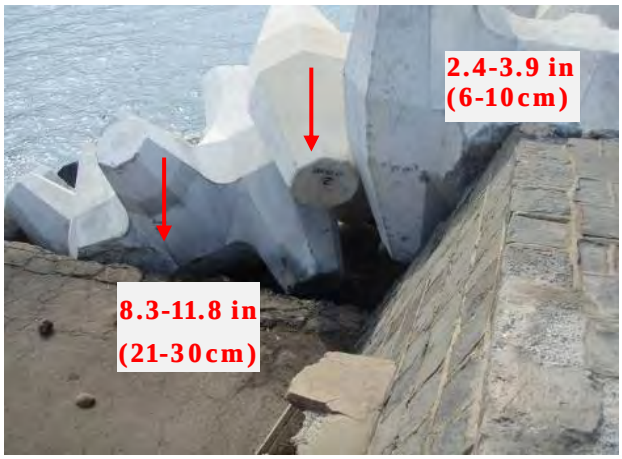

Figure 10.16. 2007 photo of harbor side tieback at Station -0+75. T-LiDAR measured settlement between 2007-2008 indicated for two armor units.

Figure 10.17. Photo from 2008 inspection showing side angle of harbor side tieback.

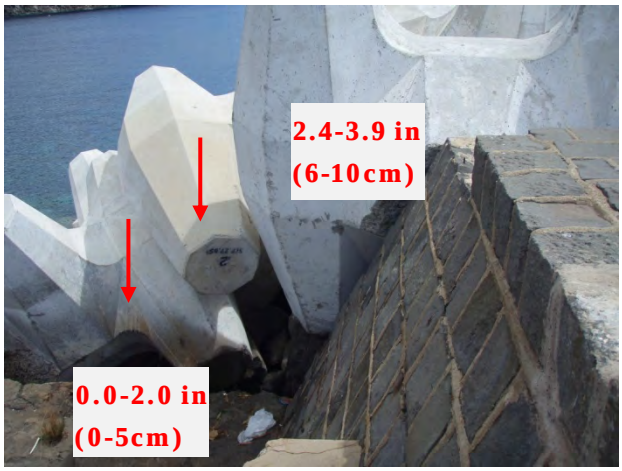

Figure 10.18. 2009 photo of harbor side tieback at Station -0+75. T-LiDAR measured settlement between 2008 -2010 indicated for two armor units.

Figure 10.19. 2010 photo of harbor side tieback at Station -0+75. T-LiDAR measured settlement between 2007-2010 indicated for two armor units.

Figure 10.20. Boat used for ROV deployment at Kaumalapau Harbor, with ROV shown in foreground.

corresponds to that used for the above water inspections shown in Figure 10.1, and was marked using underwater chains and neon flagging tape. The intent of the underwater inspection was to assess the baseline condition of the underwater armor units, with particular focus on the breakwater toe units. The ROV inspection aided in documenting the post-construction orientation and interlocking of the toe units, the armor stone toe trench and stone buttress at the ocean side toe, the ocean side tieback into an existing rock platform, and the stone berm at the harbor side toe.

A drawing of the approximate path of the ROV, showing the areas of coverage relative to the breakwater, is shown in Figure 10.21. A continuous digital video of this inspection was recorded, and still images from the video at various locations along the breakwater are presented in Figures 10.22 through 10.35. The green horizontal line and clear object in some of the images is a level bubble that was attached to the ROV and used to estimate the longitudinal rotation or "roll" of the vehicle, with respect to the horizontal plane. At the time of this 2007 inspection, there were no broken armor units, all toe units in the first (lowest elevation) row appeared to be in the correct "cannon" orientation and well embedded in the toe trench, and the "straddled" rows immediately above appeared uniform and well interlocked with units both above and below. The ocean side tieback to the rock platform including the armor units and tremie-placed concrete appeared stable and in good condition. The inspection did identify areas of the ocean side toe trench and harbor side toe berm where large variations in stone size and berm slope existed. Some variation in spacing between toe armor units was also noted. Interlocking and density of armor units along the side slope of the structure appeared satisfactory; however, comprehensive visual coverage of the entire side slope was not possible with the ROV.

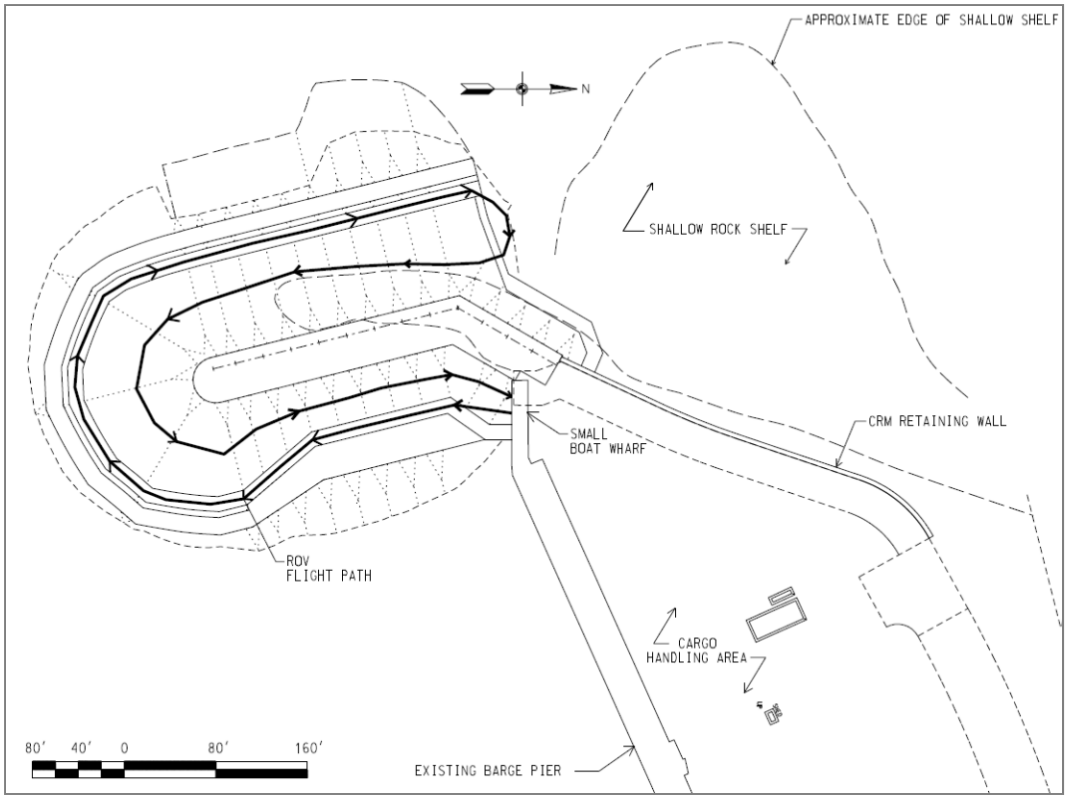

Figure 10.21. Approximate path of ROV during November 6, 2007 underwater inspection.

Figure 10.22. Harbor side root and tieback at approximate Station 0+00. Armor units in background and stone toe berm in foreground.

Figure 10.23. Harbor side trunk at approximate Station 0+50. Toe armor units in "cannon" orientation at 12- to 14-ft depth and varied size of toe berm armor stone.

Figure 10.24. Harbor side trunk at approximate Station 1+00. Multiple toe armor units in "cannon" position but in slightly varying orientation and variable size stone toe berm.

Figure 10.25. Harbor side trunk at approximately Station 1+50. Second row of tow armor units and stone toe berm with variable rock sizes are visible. Toe units are well seated into toe berm.

Figure 10.26. Harbor side head at approximately Station 2+20. Toe units in "cannon" orientation are visible at approximately 31-ft depth.

Figure 10.27. Breakwater head. Two well-entrenched toe units visible in "cannon" orientation.

Figure 10.28. Ocean side of breakwater head. Side slope of breakwater shown with armor units well interlocked.

Figure 10.29. Ocean side head at approximately Station 2+20. Toe units in "cannon" orientation and ocean side toe trench/stone buttress with varied sized of stone are visible.

Figure 10.30. Ocean side trunk at approximately Station 2+00. Toe armor units and second row of armor units visible. Slope of toe trench/stone buttress appears somewhat steep.

Figure 10.31. Ocean side trunk at approximately Station 1+50. Armor units appear well interlocked along breakwater side slope.

Figure 10.32. Ocean side trunk at approximately Station 1+00. Interlocking of armor units appears somewhat loose and toe trench appears to have widely varying stone sizes.

Figure 10.33. Ocean side trunk at approximately Station 0+50. Embedded toe unit in "cannon" orientation is visible with "straddled" unit directly above well interlocked.

Figure 10.34. Ocean side trunk at approximately Station 0+00. Several toe units and interlocked units in the row above are visible at approximately 25-ft depth.

Figure 10.35. Ocean side root. Tieback of armor layer into reef platform appears flush. Scattered armor stones from toe trench or stone buttress visible near tieback.

The following Figures 10.36 through 10.39 are photos of the underwater portion of the structure from August 2009, obtained by a private individual. The photos, in addition to the photographer's observations, indicated that there were no visible broken armor units, and that the armor layer still appeared to be well interlocked at that time. No location information is available for these photos.

Figure 10.36. Photo of underwater structure side slope. (Photo by Orville T. Magoon, August 2009).

Figure 10.37. Photo of side slope armor units. No damage visible and well interlocked. (Photo by Orville T. Magoon, August 2009).

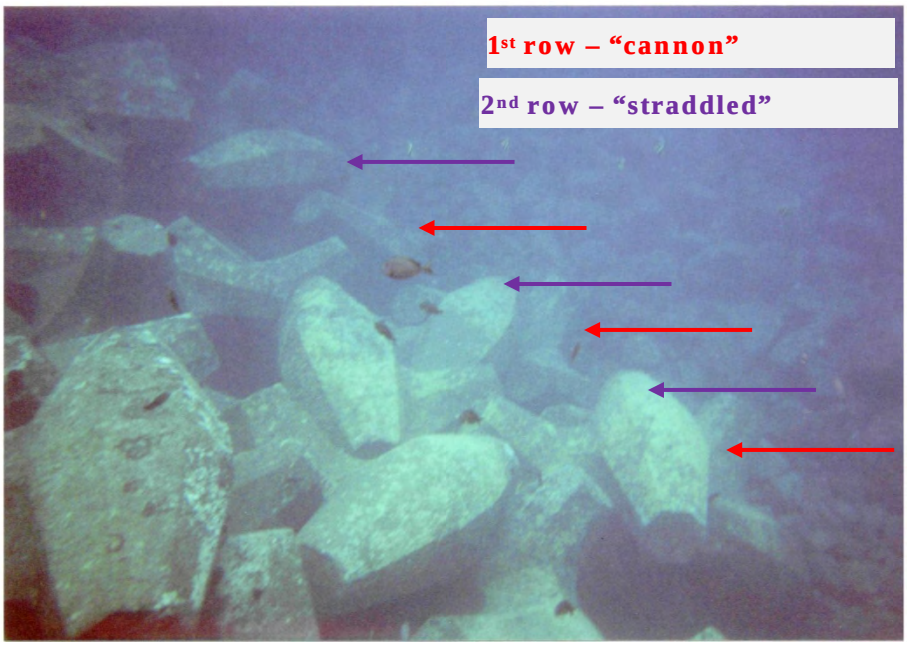

Figure 10.38. Photo of breakwater toe and toe trench. First row of "cannon" oriented units appears uniform and second row of "straddled" units well seated on first row. (Photo by Orville T. Magoon, August 2009).

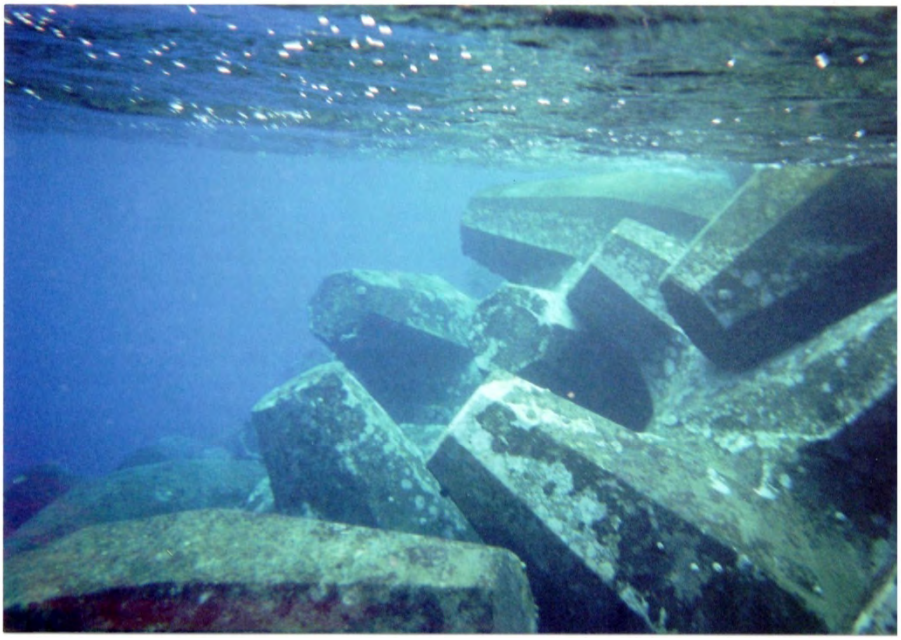

Figure 10.39. Photo of armor units near water surface showing no visible damage and consistent interlocking. (Photo by Orville T. Magoon, August 2009).

10.3 Summary of breakwater inspections

In summary, the inspections completed both above and below water documented the condition of the armor layer, ocean side toe trench, ocean side stone buttress, harbor side toe berm, concrete cap and structure

tiebacks. The visual inspection methods used are an important part of verifying the more dense and precise datasets collected with instrument data, and often provide additional insight into how elements of a structure relate to one another. In this study, the inspections were a means of establishing that no major or unexpected damage of the breakwater has occurred during the years immediately following construction, and also to note areas and items that should continue to be monitored in the future.

11 Summary and Conclusions

11.1 Summary

11.1.1 Problem

Kaumalapau Harbor is Lanai's only commercial harbor and provides the only deep-water access point to the island. Previous maintenance of the breakwater appears to have been done using rock, concrete rubble, cut-off pile butts, concrete filled pineapple wagons, etc. Repairs were made using dolos concrete armor units; however, the armor unit size using existing forms available in Hawaii was apparently too small for the design conditions as the units were quickly broken and turned into concrete rubble. In 1992, Hurricane Iniki badly damaged the breakwater, and only a portion of the structure remained above water level. Seventy five years of existence, storm events, and repairs, resulted in a large, broad rubble mound, with a side slope of about 1 vertical on 1.5 horizontal. By the 1990s the deteriorated condition of the breakwater permitted significant wave energy to reach the pier, resulting in berthed vessel motion that rendered cargo handling and fuel offloading difficult, and at times hazardous or impossible.

With exposure to storms arriving from the south through northwest, Kaumalapau Harbor was closed to vessel traffic several times during each winter storm season. These storms had steadily damaged the breakwater structure with a loss of about half of its original 400-ft length. Waves had removed armor stone over the outer 200 ft of the structure to the point where the structure crest elevation was below the MLLW elevation.

As a direct consequence of the breakwater deterioration, more wave energy was entering the harbor, thus making loading and unloading operations problematic during some conditions. Local barge operators were using multi-ton ballast weights on the barges fore and aft to counter the harbor surge during offloading operations. The situation worsened with continued deterioration of the breakwater; and during the winter of 1995, the fuel shipper refused to moor in the harbor because of dangerous conditions at the fuel pier. This caused serious concern about fuel availability on Lanai. The fuel shipper at that time decided to stop fuel delivery at the end of 1996 due to unsafe conditions in the harbor.

Cumulative damage to the Kaumalapau Harbor breakwater over the years resulted in nearly total failure of the breakwater armor layer both above and below the waterline. Project authorization and construction appropriation were provided by Congress, and non-Federal matching funds were received for repair of the structure. Due to the unavailability of stone on the Island of Lanai large enough to be stable under expected wave conditions at the site, it was necessary to manufacture concrete armor units to use in the rehabilitation of the breakwater. Project design incorporated use of the largest Core-Loc concrete armor units (35 ton) ever placed on a U.S. Army Corps of Engineers structure.

11.1.2 MCNP monitoring plan

The MCNP monitoring program for Kaumalapau Harbor breakwater was designed around the following hypotheses:

1. Settlement of the breakwater is expected as waves shift the armor units into a more compact matrix, but this settlement should not affect either structural integrity or project functionality.
2. A distinct correlation exists between concrete strength, Core-Loc movement, and armor unit breakage.
3. Armor layer stability and long-term breakwater integrity depends critically on placement and stability of the toe armor units.
4. The concrete breakwater cap will remain intact and functioning correctly despite expected breakwater settlement.
5. The breakwater will reduce wave heights at the loading dock to acceptable levels for routine loading and offloading operations.

Four aspects of the Kaumalapau Harbor breakwater rehabilitation project were proposed for monitoring. The objectives of monitoring these aspects were to obtain sufficient data to address the above specific hypotheses related to project performance.

Core-Loc armor unit material strength and breakage due to movement

Little knowledge exists on Core-Loc material strength distribution over the unit, material strength increases with aging, and the relationship between Core-Loc strength, movement, and breakage. There are numerous examples in the literature of various concrete armor shapes breaking as a result of movement and/or inadequate material strength (e.g., Davidson and Magoon 1989). Examining individual armor unit strength, detailed

structural response and movement to correlate cracking or breakage of units is useful for developing improved concrete mixture designs and detailed guidance on armor unit construction.

Breakwater structure and armor layer settlement

Structure and armor layer settlement as a function of time and spatial location has never been quantified for a Core-Loc structure. Monitoring data would give insight into the relationship between packing density and settlement, and those data would also be crucial for the task of assessing armor unit breakage. It was realized up front that the number of armor units monitored, their locations, as well as timing and frequency of monitoring would be important parameters to consider in relation to ultimate monitoring costs.

Concrete breakwater cap

The concrete breakwater cap is cast in place before initial settlement of the rubble mound, and it is important to judge how the cap and breakwater integrity is affected by armor layer settlement. The main purpose of the breakwater cap is to hold the structure crest together during severe wave overtopping events. Differential settlement of the rubble mound may fracture or dislodge portions of the cap that could then be carried away by strong storm waves.

Armor layer toe stability

Toe placement is expected to be critical to the success of the Kaumalapau breakwater rehabilitation, and the Honolulu District will be monitoring and documenting the underwater placement of the toe units. By augmenting the district's monitoring, sufficient data will be gathered to judge the success of the toe design and placement scheme. This information will be important for future application of Core-Loc armor units, and it will allow assessment of the relationship between breakwater toe stability and armor layer settlement.

11.1.3 Monitoring activities

In support of the monitoring aspects identified in the MCNP Plan, several MCNP monitoring activities at Kaumalapau Harbor were accomplished

between fiscal years 2006 and 2010. These activities and their results are summarized as follows.

Core-Loc concrete strength measurements

Non-destructive and destructive testing of one 35-ton Core-Loc concrete armor unit purchased from the normal production run of armor units being cast for the Kaumalapau harbor breakwater was performed during September 2006. The objective of the testing was to gather non-destructive material property data on the armor unit, and to determine the tensile load needed to break one of the legs of the unit from the rest of the body. These data were meant to further knowledge of the structural and materials properties of Core-Loc armor units in general, and specifically those units being used for the Kaumalapau Harbor breakwater repair. It was also hoped that the testing would provide further information on the relationship between the compressive and tensile flexural strength of the concrete (as determined by standardized testing practices and dictated in the contract specifications) and the tensile flexural load required to break a leg off the armor unit.

Conclusions from breakage tests of this specific Core-Loc armor unit were based on:

1. visual observations of the as-received and post-test conditions of the provided Core-Loc concrete armor unit,
2. analysis of the load and strain data collected during the failure test of the armor unit,
3. measured field data and calculations derived from that collected data, and
4. data from laboratory testing of cores for pulse-velocity, and compressive and split-tensile load data.

From observations made during receiving and set-up of the Core-Loc armor unit provided for non-destructive and destructive testing, it was concluded that the armor unit appeared normal in all aspects pertaining to dimensions of the unit and appearance, including surface cracking and blemishes. The 94,000 lbf actual failure load during the breakage test was significantly lower than the expected load calculated based on the required concrete tensile stress and generalized geometry of the armor unit. The cause of the low failure load cannot be explained fully by the primary and derived stress and strain data collected during the investigation, which implied that the

tensile stresses at and near critical failure locations in this particular specific Core-Loc armor unit were at or slightly above the minimum flexural tensile stress required by Core-Loc concrete contract acceptance criteria. The pulse velocity readings collected from core samples were within the acceptable ranges according to uncorrelated estimation guidelines. Visual observation of cut cross sections from the collected cores also confirmed consistency from the top to bottom in terms of aggregate distribution.

In the visual analysis of the failure surface of the broken Core-Loc armor unit, it was observed that a high percentage of aggregate particles had de-bonded from the cement paste and pulled out of one or the other face. This observation led to the possibility that the lower than expected tensile stress in the concrete could be partially due to low strength created by aggregate particles not participating in the strength development of the composite. The cause of this condition may be related to the development of a micro-thin layer of poor quality concrete forming at the paste/aggregate interface either from an accumulation of dirt and silt material on the aggregate or the accumulation of excess water on the surface of the aggregate that accompanies high water-to-cement pastes. These conditions cause weak bond strength, frequent pullout of aggregate particles, and ultimately lower strength concrete because the strength of the aggregate cannot contribute to the strength of the composite. These conclusions apply only to this particular specific armor unit, and to the data were not adequate to ascertain the concrete quality of any other Core-Loc units used in the Kaumalapau Harbor breakwater rehabilitation or elsewhere.

In-Situ wave measurements

At Kaumalapau Harbor, wave data was collected pre-construction to aid in design, as well as post-construction to aid in assessment of wave impacts on the completed structure and wave conditions at the barge pier. A Datawell Waverider buoy, located approximately 1 mile west of the harbor in 650-ft depth was deployed in May 2007 as part of this monitoring program, and presently remains active. This source of offshore data has proven to be an extremely valuable resource for both this monitoring program, as well as to users of Kaumalapau Harbor. Two bottom-mounted, non-directional pressure sensor wave gages in and near the harbor were deployed between October 2007 through early November 2008. Finally, a portable, directional wave buoy was deployed at various

locations around the harbor entrance and barge pier on December 5, 2008 to collect additional detailed and site-specific wave data.

Analysis of these wave data have resulted in the following conclusions. First, the amount of wave energy that reaches the areas just offshore of Kaumalapau Harbor (and would therefore be affecting both navigation into the harbor as well as breakwater stability) is highly dependent on refraction of waves over intermediate depths and island shadowing, and therefore depends greatly on both the wave directions and wave periods associated with a particular sea or swell event. Secondly, the waves that propagate from the harbor entrance toward the barge pier (areas where mooring operations would be affected) experience a significant amount of diffraction, and therefore proportional wave height at these locations is strongly correlated with wave period. From this, it can be concluded that high-intensity local events such as Kona storms or hurricanes would have the greatest effect on breakwater stability, while distant events generating long-period waves approaching the islands from south or west-northwest would be most likely to impact mooring operations at the barge pier. Although the existing data record does not include a hurricane event similar to that which was used for breakwater stability design, the full range of more typical events has been documented.

Wave hindcasts and transformation

The presence of long-term NDBC buoys in the islands, in addition to the medium- and short-term wave data sets collected as part of this monitoring program, has enabled an evaluation of the accuracy of the 24 years of available WIS hindcast data, the implementation of three validated wave transformation models (WW3 forecast model, SWAN, and REF/DIF), and development of a wave lookup table that correlates offshore buoy data to nearshore wave conditions at Kaumalapau Harbor. The lookup table output has been compared to physical model results conducted during the design phase of the breakwater project as well as compared and calibrated to short-term wave gage and buoy data in the areas of interest in and around the harbor. Finally, an easy-to-use computer program has been created which includes a predictive algorithm for relating real-time buoy data to wave heights at various harbor locations, based on these lookup table results. This program has enabled the calculation of several multi-year time series of estimated incident wave height at the breakwater as well as estimated wave conditions at locations along the barge pier within the harbor.

The analysis of calculated wave height time series indicates that the wave response along the barge pier varies in magnitude with location, the type of offshore conditions (swell direction, wave period) as well as the magnitude of particular wave events in terms of wave height. The modeled results at the locations along the barge pier, now protected by the repaired breakwater, indicate that safe mooring and offloading should be possible during all but the most extreme events such as hurricanes, large Kona storms and extreme W-NW or south swells. The time series of calculated wave heights at the location incident to the breakwater indicates that only the most extreme events (hurricanes passing south of the island chain or approaching the islands directly) are likely to generate incident waves approaching the design height of 35 ft and thereby threaten armor stability.

Breakwater settlement and armor unit movement measurements

Ground-based Tripod-LiDAR technology was used to collect settlement and movement data at the repaired breakwater at Kaumalapau Harbor. T-LiDAR data were collected and post-processed by the USGS as part of the monitoring program shortly before the breakwater construction was completed in June 2007, one year later in July 2008, and again in August 2010. Comparison of these ultra-dense georeferenced positional data (in point cloud form) has enabled the detection of armor unit movement (measured as maximum displacement at any point on an individual unit) as small as 5 cm, and in excess of 1 m for the various time increments over which data was collected. The comprehensive coverage area and high positional accuracy of these surveys resulted in the ability to visualize and compare movement of almost every armor unit visible above the waterline as well as the concrete cap, allowing for an overall analysis of the above water stability of the structure in the three years following construction. Armor unit movement was analyzed through both visual inspection of point cloud overlays and the use of color-coded change detection “maps”.

The analysis of the point cloud overlays and change detection maps has revealed several interesting characteristics of the movement that has occurred during this time. Firstly, the visible movement of individual armor units has been both rotational and translational, but has been primarily toward the structure (rather than being pulled away or “off” the breakwater) and/or lower in elevation. Secondly, the movement has typically been observed to occur in groups of several adjacent armor units, illustrating the interdependence of each armor unit on those surrounding it and in direct

contact with it, whether above, below, or alongside. In addition, the change measurements indicate that the largest movements of individual armor units, on the order of 20 cm to over 1 m (0.7 to 3.3 ft), occur at one of two locations: the ocean side head or ocean side dogleg of the structure. This phenomenon may be explained by the change in structure orientation and thereby armor layer shape resulting in lower packing density in these areas, potentially less optimal interlocking and contact of adjacent armor units due to this lower packing density, and/or increased wave impact and wave surge forces along the ocean side of the breakwater due to its greater exposure to incoming waves. The lack of significant armor unit displacement seen on the harbor side may be a result of the fact that the structure has not been overtopped by any major wave events.

Next, and likely one of the most significant results from this data collection, is the variation in both the quantity and magnitude of armor unit movement evident when comparing the change detection map from the first year following construction to the map for the two following years. Side-by-side evaluation of colorized change detection maps for these two time periods clearly shows that the majority of notable armor unit movement occurred within the first year post-construction, with comparatively much less discernable change in armor unit positions occurring between the second and third T-LiDAR surveys in 2008 and 2010. This may be due in part to a less energetic incident wave climate during 2008 - 2010, however; it is difficult to make a direct correlation between the magnitude of armor unit displacement and wave climate with only two relatively short-term periods of armor unit change analysis. It is likely that the majority of armor layer settling and nesting occurred within approximately the first year after placement due to a combination of gradual gravitational settling and persistent dynamic wave forces over this time.

There has been minimal displacement of armor units at the ocean side root of the structure, which was an area of concern during the design phase of the project due to a large submerged rock platform that exists adjacent to this part of the structure. The harbor side of the structure at the root, adjacent to the barge pier, became an area of concern during construction when a modification was made by using a partial armor unit to abut the existing bulkhead wall, due to the fact that a complete armor unit would not fit into this area. The displacement of armor units measured in this area between the 2007 and 2008 surveys was in the range of 21 to 30 cm (8.3 to 11.8 in.), however; the displacement measured between the 2008 and 2010

surveys shows that the area has not experienced additional significant movement. Finally, the analysis of the T-LiDAR survey data (and verification by visual inspection) has shown that there has been no breakage of any above water armor unit as of late 2010, and that there has not been a detectable settling of the concrete cap since its construction.

Toe stability monitoring and breakwater inspections

A marine geophysical survey was conducted in July 2008 to image the post-construction underwater portion of the Kaumalapau Harbor breakwater rehabilitation. The survey consisted of high resolution and high precision multi-beam instrumentation for accurate mapping of the breakwater structure. The primary objective was to provide a baseline for measurement and monitoring of any future changes to the structure due to settling or other movement of the Core-Loc concrete armor units. Multi-beam backscatter intensity was also analyzed and used in conjunction with several grab samples for identifying bottom sediment types in the project area. The areas surveyed include the Core-Loc armor units, the structural connections to the existing rock on the ocean side and to the pier on the harbor side, and the seafloor immediately surrounding the breakwater.

Point cloud images generated from the multi-beam survey indicate that the structure toe follows a consistent contour along the rock foundation, with no visible deviations or non-interlocked Core-Loc units. Examination of the point cloud of the toe berm indicates that there is likely a large gradation in stone size in this area, which is in agreement with observations from the underwater inspection using an ROV. Also visible in the survey data is what appears to be a steepened slope within the harbor side toe berm; this area is recommended for future monitoring of changes and/or stability in future surveys or inspections.

The result of the multibeam data collection is a dense and highly accurate representation of the characteristics of the underwater portion of the breakwater approximately one year after construction was completed. These characteristics include not only the bathymetric contours that would be captured by a traditional single beam survey, but also a detailed view of the orientation of concrete armor units (especially the first two rows composing the breakwater toe), the transitions from stone to armor units on the slope, the structure tie-ins to land, and an estimation of the geologic classifications of sediments surrounding the structure.

Field inspections of the above-water structure were conducted approximately annually to locate and document any structure damage, identify displaced Core-Loc units, assess any effects of structure settlement on the concrete cap, and evaluate the overall structural condition of the breakwater. Spot measurements were made as part of these inspections to substantiate the T-LiDAR measurements used to determine breakwater settlement and armor unit movement. In addition, an ROV was used to conduct an underwater inspection of the breakwater. Due to the importance of the breakwater toe armor units in the overall stability of the armor layer, the underwater inspection focused heavily on the toe of the structure, in an effort to identify whether any armor units had become dislodged, settled dramatically, or broken in this location. Additional photos of underwater portions of the structure that were collected in August 2009 and provided to USACE Honolulu District are included as supplemental data.

The four above-water inspections of the breakwater, which included assessment of the concrete cap, ocean side and harbor side tiebacks, and the armor units visible from the crest, were conducted by Honolulu District and ERDC coastal engineers associated with the MCNP program. All of the inspection findings indicated that the structure has remained in very good condition in the first three years following construction. There have been no indications of broken, cracked, or severely damaged armor units, and the concrete cap has remained fully intact with no visible cracking or other damage. The armor units have experienced some weathering and minor damage, as would be expected. Some items that have been noted in the inspection reports for continued monitoring include the following:

1. voids in the armor layer with exposed underlayer stones,
2. limited contact of armor units with adjacent armor units and/or underlayer,
3. underlayer stone appears smaller than required,
4. underside of the concrete cap is exposed or cap is thin,
5. areas grouted after armor unit placement,
6. settlement of armor units creating gap between armor unit and concrete cap, and
7. harbor side tieback where partial armor units join structure to existing wall.

The intent of the underwater inspection was to assess the baseline condition of the underwater armor units, with particular focus on the

breakwater toe units. The ROV inspection aided in documenting the post-construction orientation and interlocking of the toe units, the armor stone toe trench and stone buttress at the ocean side toe, the ocean side tieback into an existing rock platform, and the stone berm at the harbor side toe. At the time of the 2007 underwater inspection, there were no broken armor units, all toe units in the first (lowest elevation) row appeared to be in the correct "cannon" orientation and well embedded in the toe trench, and the "straddled" rows immediately above appeared uniform and well interlocked with units both above and below. The ocean side tieback to the rock platform including the armor units and tremie-placed concrete appeared stable and in good condition. The inspection did identify areas of the ocean side toe trench and harbor side toe berm where large variations in stone size and berm slope existed. Some variation in spacing between toe armor units was also noted. Interlocking and density of armor units along the side slope of the structure appeared satisfactory; however, comprehensive visual coverage of the entire side slope was not possible with the ROV. The photos and observations of the underwater portion of the structure provided to the Honolulu District in August 2009 indicated that there were no visible broken armor units, and that the armor layer still appeared well interlocked at that time.

11.2 Conclusions

An extensive amount of varied data has been collected between 2006 and 2010 in support of the monitoring of the repaired Kaumalapau breakwater. Conclusions drawn from the results of these investigations are presented in terms of the original project elements designated for monitoring, and the associated lessons that may be learned and applied to future comparable navigation projects.

11.2.1 Core-Loc armor unit material strength and breakage due to movement

Concrete strength measurements conducted on a single Core-Loc armor unit that was fabricated for a specific project and under unique conditions do not enable wide-ranging application of results to other projects. However, the measurements collected as part of this program do add to the base of knowledge for the relatively recently developed Core-Loc and concrete armor units in general in terms of concrete mix design, concrete strength, and the associated strength of the overall armor unit. The data obtained in this case indicated a potential limitation in armor unit

durability, based on the lower than expected load needed to break one leg from the unit in a controlled test. However, the only instances of armor unit breakage during the course of this project to this point have occurred during movement of the Core-Locs during construction operations. None of the in-situ armor units have experienced any observable damage, including breaking.

It is possible that the potential weakness identified may be due to deficient construction methods during armor unit fabrication. However, this explanation is contradicted by the results of multiple standardized tests of concrete strength during the construction process and following the load testing of the sample armor unit, which verified that the concrete used met the contract required strength. A likely reason for this discrepancy is that the relationship between specified concrete strength according to standardized testing methods and concrete strength of a geometrically complex armor unit is not well understood. Further data collection in this area on multiple samples and in a more controlled environment would help to improve design criteria.

Due to the fact that no substantial damage to Core-Locs has been observed on the post-construction breakwater, it is not possible to make a direct correlation between armor unit breakage, measured concrete strength, and the displacement of the armor units that has been observed. These results do, however, demonstrate that the scale of initial armor layer settlement and movement has not been significant enough to cause excessive stress and consequent damage to the individual armor units above the water line.

Lessons learned:

- Standard methods of specifying concrete strength are not necessarily applicable to coastal structures composed of concrete armor units – more research and development is needed.
- Construction methods are an integral part of concrete armor unit stability, and variability of methods may contribute to armor layer vulnerability.
- Small-scale post-construction armor unit movement will not necessarily lead to armor unit breakage.

11.2.2 Breakwater structure and armor layer settlement

The ground-based T-LiDAR method used to monitor the settlement and movement of the above-water armor units has proven to be successful in monitoring changes as a function of time and location on the breakwater. The data collected has shown that the armor layer has experienced movement as expected, but it appears that the majority of change has occurred in approximately the first year following construction. This initial "nesting" of armor units may possibly add to the armor layer stability by consolidating the units and increasing interlocking and unit-to-unit contact.

It is also apparent based on the locations of greatest displacement at the ocean side head and dogleg, that there is a likely relationship between the constructed packing density of armor units that is achieved and the amount of movement that is experienced. In addition, the results of this analysis show that greater movement of armor units can be expected in areas exposed to wave impact. Though it was not possible to establish a relationship between the wave climate experienced and the armor unit movement observed over the course of this monitoring program, this is an area of study that warrants additional long-term investigation.

The lack of armor unit damage is an indication that the overall stability of the armor layer in the three years since construction has been satisfactory and although expected settling has occurred, the constructed packing density and interlocking of the armor units has been sufficient to limit or preclude the amount of wave-induced dynamic movement that could result in unit-to-unit impacts and possible armor unit breakage.

Lessons learned:

- T-LiDAR is an accurate and comprehensive method for monitoring changes in complex coastal structures such as those with concrete armor units.
- Maintaining packing density around bends in structure and structure head as much as possible, especially where wave exposure is greatest, may limit the amount of armor unit movement and/or damage following construction.
- Minor settlement and movement of armor units following construction does not affect the integrity of the structure, and functionality should remain intact as long as structural design elements (i.e., crest height and width) are maintained.

11.2.3 Concrete breakwater cap

The results of the wave measurements and wave transformation modeling conducted as part of this study indicate that there has not been a post-construction wave event approaching the size that was used for design of the breakwater. Therefore, it is unlikely that the structure has experienced significant wave overtopping or direct wave impact that would affect the concrete cap. In addition, no detectable settling of the cap has been measured through the precise methods employed to monitor change of the breakwater elements, and no damage due to differential settlement of the underlayer or any other source has been observed in the visual inspections that have been conducted periodically.

Small-scale movement of armor units at the structure crest away from the concrete cap has been documented. However, there is no indication that movement of the armor layer has caused settlement or other discernible change to the concrete cap. The integrity of the cap and its functionality in holding the structure crest together during wave events has not been affected in the years following construction; however, there is some uncertainty in how the cap may perform during an overtopping event, since it was not tested for stability during design of this project.

Lessons learned:

- Small-scale post-construction armor unit movement will not necessarily lead to concrete cap settlement or damage.
- Stability of concrete cap can likely only be field-verified if a wave event causing overtopping of the structure is experienced.

11.2.4 Armor layer toe stability

The toe of the breakwater includes the interrelated elements of the first several rows or armor units, the toe trench and stone buttress on the ocean side, and the toe berm on the harbor side of the structure. Evaluation of the stability of these components has been completed through the use of images developed from multibeam survey and remote underwater inspection. Both of these methods have indicated that the armor units at the toe were uniform in placement, well-interlocked, and stable at the times of inspection. No damage or breakage of toe armor units has been observed in available data, and the units appear to be well seated in the ocean side toe trench. This signifies that the “cannon” placement of the

first row of Core-Locs, followed by a "straddled" placement of the second row of Core-Locs has been a stable orientation of the toe at this project.

The multibeam data and ROV images show that the stone buttress and toe berm appear to be intact, but both have significant variability in the size of stone present and potentially steep slopes in some areas. This may be partially due to construction allowances in specified armor stone size and slope for these areas; however, the reduced size and/or steepened slopes may enable the stones to be more easily subjected to movement during a design-level wave event, and should be monitored when practical in the future.

Underwater movement of armor units was not analyzed as part of this study, either through repeat multibeam surveys or other methods. Therefore, determination of a relationship between toe stability and armor layer movement can only be assumed based on the apparent soundness of the both structure toe and above-water armor units thus far. If toe unit movement or toe trench/toe berm changes are detected in the future, a follow-up survey of both the underwater and above water armor layer would be warranted to further assess this correlation.

Lessons learned:

- "Cannon" and "straddled" orientation of first and second row Core-Loc toe units appears to be a successful placement scheme in this case.
- Combination of traditional high-density survey methods (multibeam survey) augmented by visual observation techniques (such as ROV inspection) provided a thorough evaluation of underwater structure conditions.

11.3 Recommendations for future monitoring

The following are recommendations for future monitoring activities at Kaumalapau Harbor, based on the value of the varied data collected as part of the MCNP program and the lessons learned from these investigations:

1. Conduct strength measurements on submerged concrete cylinders and/or non-destructive tests on in-situ armor units to determine increase in concrete strength with age.

2. Continue shared financial support of the CDIP buoy located offshore of the harbor, and advocate that it remain in its current location until a significant wave event occurs, or as long as is practical.
3. Conduct pre- and post-construction numerical modeling of the harbor using a Boussinesq-type wave model to accurately assess the relative reduction in wave energy at the barge pier for various operational conditions.
4. Perform post-storm data collection following significant wave events ($H \geq 20$ ft at CDIP buoy) including wave data analysis (using KPWAVE as well as extremal analysis), visual above-water inspection and ROV below-water inspection, as well as T-LiDAR survey and/or multibeam survey (if warranted by visual inspections).
5. Repeat T-LiDAR and multibeam survey (or vessel-mounted combined LiDAR/multibeam survey) at 10 years post-construction (mid-2017) and complete comparative analysis with post-construction surveys. Determine subsequent interval for detailed remote-sensing surveys based on these results.
6. If future surveys are conducted, revisit analysis to correlate changes in structure condition to historical wave climate over time.
7. Continue periodic inspections by Honolulu District above-water annually using photos/GPS/measurement and perform below-water inspections biennially using ROV.
8. Request assistance from ERDC/CHL armor unit expert(s) for inspection and/or analysis if and when periodic inspections indicate significant damage to structure or movement of armor units.
9. Support additional involvement of the project in the MCNP program, through Periodic Inspections work unit, or any other means available.

References

Bawden, G., J. Podoski, S. Bond, T. Smith, J. Foster, J. Howel, M. Shulters, and J. Brandt. (in publication). Assessing the post-construction stability of a Core-Loc™ breakwater, Kaumalapau Harbor, Hawaii, with ground-based tripod LiDAR. U.S. Geological Survey, Scientific Investigations Report 2011-xx. U.S. Geological Survey. Reston, VA.

Crane M., T. Clayton, E. Raabe, J. Stoker, L. Handley, G. Bawden, K. Morgan, and V. Queija. 2004. Report of the U.S. Geological Survey Lidar workshop sponsored by the Land Remote Sensing Program and held in St. Petersburg, FL, November 2002. Open File Report 2004-1456. U.S. Geological Survey. Reston, VA.

Davidson, D. D., and O. T. Magoon (editors). 1989. *Stresses in Concrete Armor Units*, American Society of Civil Engineers. New York, NY.

Hays, J., T. Smith, and S. Hughes. 2007. Lessons learned and initial monitoring results following completion of a Core-Loc™ breakwater at Kaumalapau Harbor, Lanai, Hawaii. *Proceeding of the Fifth International Conference on Coastal Structures 2007*. American Society of Civil Engineers; Coastal, Oceans, Ports, and Rivers Institute. Venice, Italy.

Hays, J., T. Smith, and S. Sullivan. 2006. Challenges, innovative techniques, and ongoing monitoring of Kaumalapau breakwater construction, Lanai, Hawaii. *Proceedings of the 30th International Conference on Coastal Engineering 2006*. American Society of Civil Engineers. San Diego, CA.

HQUSACE. 1997. Engineering and design: Monitoring completed navigation projects. Engineer Regulation 1110-2-8151. Headquarters, U.S. Army Corps of Engineers. Washington, DC.

InnovMetric Software. PolyWorks point cloud software suite. Quebec City, Quebec, Canada.

Kirby, J. T., and R. A. Dalrymple. 1994. Combined refraction/diffraction model REF/DIF, Version 2.5; Documentation and user's manual. Research Report No. CACR-94-22. Center for Applied Coastal Research, Department of Civil Engineering, University of Delaware. Newark, NJ.

Kreylos, O. 2008. Environment-independent VR development. *Proceedings of the Fourth International Symposium on Visual Computing*. Las Vegas, NV. Proceedings published in *Lecture Notes in Computer Science Series* by Springer-Verlag, Berlin, Germany. pp. 901-912.

Kreylos, O., G. W. Bawden, and L. H. Kellogg. 2008. Immersive visualization and analysis of LiDAR data. *Proceedings of the Fourth International Symposium on Visual Computing*. Las Vegas, NV. Proceedings published in *Lecture Notes in Computer Science Series* by Springer-Verlag, Berlin, Germany. pp. 846-855.

M&E Pacific, Inc., Sea Engineering, Inc., SSFM International, Inc., W. F. Baird and Associates, Ltd. 2002. Basis of design for Kaumalapau Harbor breakwater repair, Island of Lanai, Hawaii. Report prepared for U.S. Army Engineer District, Honolulu. Honolulu, HI.

Melby, J. A. 2002. Kaumalapau, Hawaii, Core-Loc™ breakwater strength investigation. Unpublished manuscript. U.S. Army Engineer Research and Development Center. Vicksburg, MS.

Mlakar, P. F. 2005. Breakage of Lajes CORE-LOCs®. Unpublished manuscript. U.S. Army Engineer Research and Development Center. Vicksburg, MS.

O'Neil, E., and R. Haskins. 2008. Testing and analysis of a concrete Core-Loc™ armor unit, Kaumalapau breakwater rehabilitation, Lanai, Hawaii. Concrete Consulting. Vicksburg, MS. Report prepared for U.S. Army Engineer District, Honolulu. Honolulu, HI.

Podoski, J., G. Bawden, S. Bond, T. Smith, and J. Foster. 2009. Post-construction monitoring of Core-Loc™ breakwater using tripod-based LiDAR. *Proceedings of Coasts, Marine Structures, and Breakwaters 2009*. Institution of Civil Engineers. Edinburgh, Scotland, United Kingdom.

Podoski, J., T. Smith, and L. Hales. (in publication). Final monitoring results for Kaumalapau Harbor breakwater, Lanai, Hawaii. *Proceeding of the Conference on Coastal Engineering Practice 2011*. American Society of Civil Engineers; Coastal, Oceans, Ports, and Rivers Institute. San Diego, CA.

Scripps Institution of Oceanography. 2007. Coastal data information program. Scripps Institution of Oceanography. LaJolla, CA. *http://cdip.ucsd.edu/?xsearch=146&xsearch_type=Station_ID*

Sea Engineering, Inc. and Group 70 International. 2008. Kaumalapau breakwater repair: design and construction summary, with emphasis on Core-Loc™ armor units. Sea Engineering, Inc., Waimanalo, HI; and Group 70 International, Honolulu, HI. Report prepared for U.S. Army Engineer District, Honolulu. Honolulu HI.

Sea Engineering, Inc. 2009. Kaumalapau Harbor: Multibeam sonar survey investigations. Sea Engineering, Inc., Waimanalo, HI; and Sea Engineering, Inc., Santa Cruz, CA. Report prepared for U.S. Army Engineer District, Honolulu. Honolulu HI.

Sea Engineering Inc. 2009. KPWAVE: Program Modification and User Manual: A Report on Algorithm Modification, FORTRAN Code Implementation, Enhancements, and Usage. Sea Engineering, Inc., Waimanalo, HI. Report prepared for U.S. Army Engineer District, Honolulu. Honolulu, HI.

Sea Engineering Inc. and Group 70 International. 2009. Wave transmission modeling: Kaumalapau Harbor, Island of Lanai, Hawaii. Sea Engineering Inc., Waimanalo, HI; and Group 70 International, Honolulu, HI. Report prepared for U.S. Army Engineer District, Honolulu. Honolulu, HI.

Smith, E. R. 1998. Wave response of Kaumalapau Harbor, Lanai, Hawaii. Technical Report CHL-98-11, U.S. Army Engineer Waterways Experiment Station, Vicksburg, MS.

Smith, E. R. 2001. Kaumalapau Harbor, Lanai Hawaii, two-dimensional breakwater stability study. Technical Report CHL -01-3, U.S. Army Engineer Research and Development Center, Vicksburg, MS.

Sullivan, S. and D. Werren. 2003. Kaumalapau Harbor; engineering challenges of an exposed deepwater breakwater. Unpublished presentation at *Coastal Structures 2003 Conference*. American Society of Civil Engineers; Coastal, Oceans, Ports, and Rivers Institute. Portland, OR.

Turk, G. F., and J. A. Melby. 1997. Core-Loc™ concrete armor units: Technical guidelines. Miscellaneous Paper CHL-97-6, U.S. Army Engineer Waterways Experiment Station, Vicksburg, MS.

U.S. Army Corps of Engineers. 2009. Comprehensive evaluation of project datums. Engineer Circular EC 1110-2-6070. U.S. Army Corps of Engineers. Washington, DC.

U.S. Army Corps of Engineers. 1994. U.S. Army Engineer Research and Development Center, Field Data Collection and Analysis Branch (formerly Prototype Measurement and Analysis Branch). Vicksburg, MS. *http://sandbar.wes.army.mil/public_html/pmab2web/htdocs/hawaii/hawaii.html*

U.S. Army Corps of Engineers. Wave information studies. U.S. Army Engineer Research and Development Center, Coastal and Hydraulics Laboratory. Vicksburg, MS. http://frf.usace.army.mil/wis2010/wis.shtml

U.S. Army Engineer District, Honolulu. 2003. Decision document for Kaumalapau Harbor breakwater repair, Island of Lanai, Hawaii. U.S. Army Engineer District, Honolulu. Honolulu, HI.

U.S. Army Engineer Division, Pacific Ocean. 1996. Kaumalapau Harbor special design report, Island of Lanai, Hawaii. U.S. Army Engineer Division, Pacific Ocean. Honolulu, HI.

Appendix A: Concrete Strength Calculations[1]

Structural load calculations for failure load to break a Core-Loc™ Leg

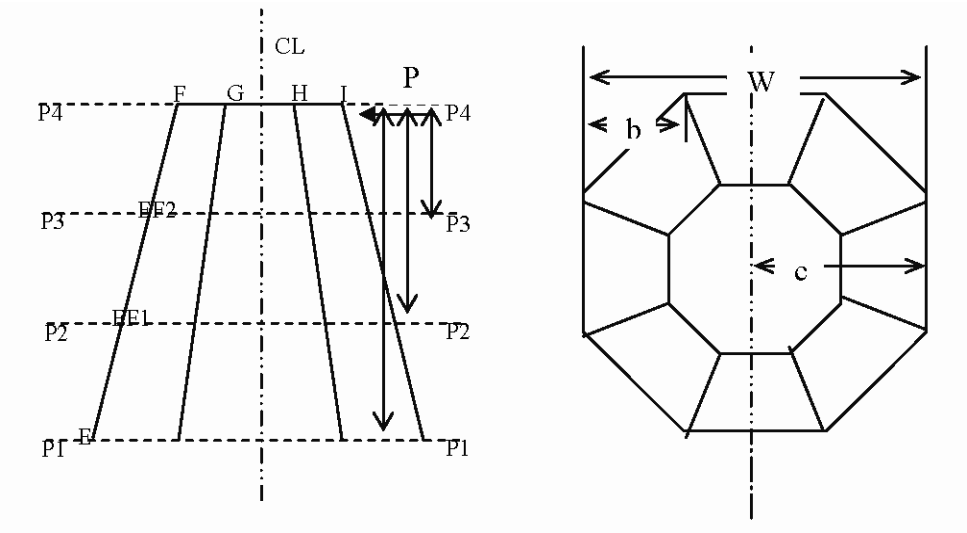

$\sigma = Mc/I$ or $M = \sigma I/c$ and $M = Pd$

thus, $Pd = \sigma I/c$ and $P = \sigma I/cd$

Failure sections were examined at P1-P1, P2-P2, and P3-P3. Load P was applied at P4-P4.

Table A.1. Dimensions associated with octagonal failure sections.

Section	W, in.	b, in.	c, in.
P1-P1	39.704	11.668	19.85
P2-P2	35.567	10.443	17.78
P3-P3	31.431	9.219	15.72

Table A.2. Moment of inertia, I, of octagonal failure sections.

$I=W^4/12-4[b^4/36+0.5b^2(W/2-b/3)^2]$, in^4	
P1-P1	135,649.09
P2-P2	87,415.61
P3-P3	53,359.19

[1] From O'Neil and Haskins (2008).

Table A.3. Calculated load based on P = σI/cd.

Load, P, lbf	σ, psi	I, in⁴	c, in.	d, in.
223600.3	925	135,649.09	19.85	28.27
241261.3	925	87,415.61	17.78	18.85
333309.4	925	53,359.19	15.72	9.42

The analysis shows that the smallest breaking load is 223600 lbf acting on the cross section P1-P1. Note if σ is smaller, then the breaking load will decrease.

Calculated outer fiber stress using failure load

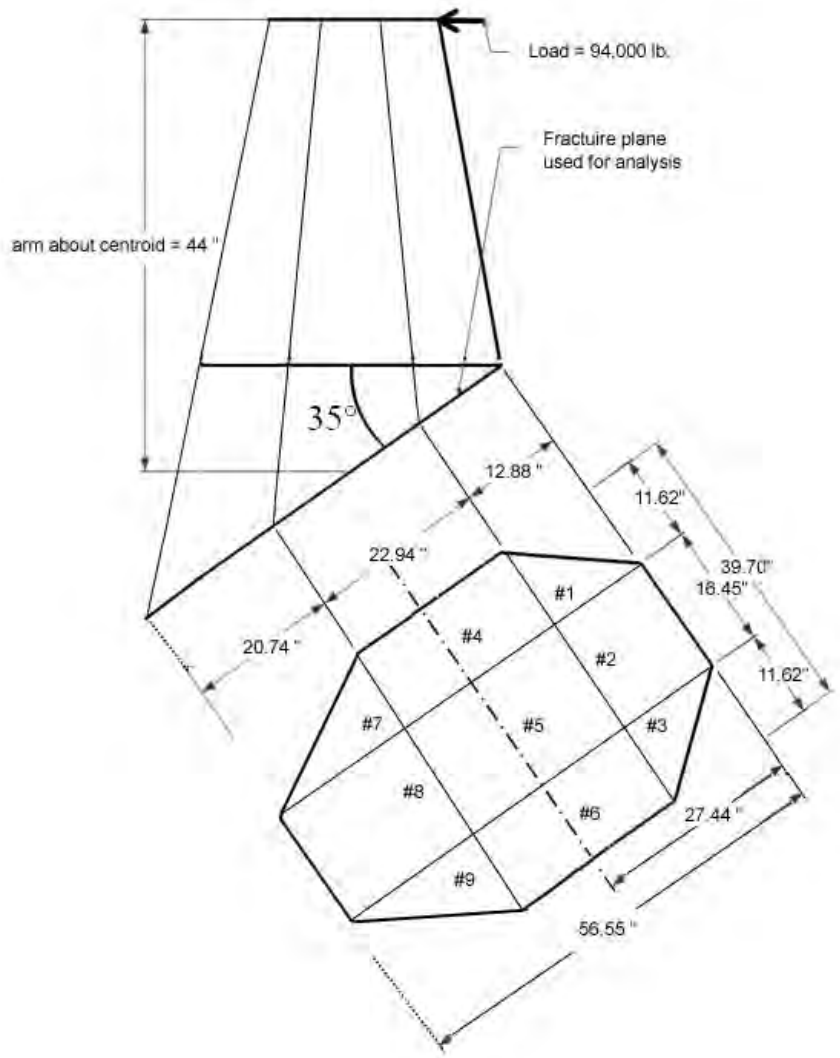

The fracture surface produces an elongated octagon like the picture above. The center of the area is 27.44 in. from the upper end of the fracture surface. The Moment of Inertia of elongated octagon can be determined by dividing the shape into nine rectangles and triangles and applying the parallel axis theorem to each of the sub-shapes. This is shown in the table below. The parallel axis theorem is;

$$I_{total} = \sum_{i=1}^{i=9} I_i + A_i y^2$$

I_{total} = the total moment about the centroid of the elongated octagon
I_i = the moment of the i^{th} sub area around itself, A_i = area of the i^{th} sub-region

Y = the distance between the moment axis of the sub-region and the centroid of the area

Calculated outer fiber stress using failure load

Table A.4. Determination of Moment of Inertia for elongated octagon.

Sub-area	Base b, in	Height h, in	I_i, in^4	Area A_i, in^2	Y_i^2, in^2	$I_i+A_iy_i^2$, in^4
1	11.62	12.88	689.7	74.8	355.4	27288.9
2	16.45	12.88	2929.1	211.9	441.0	96366.4
3	11.62	12.88	689.7	74.8	355.4	27288.9
4	11.62	22.94	11689.7	266.6	9.5	14234.9
5	16.45	22.94	16548.7	377.4	9.5	20151.8
6	11.62	22.94	11689.7	266.6	9.5	14234.9
7	11.62	20.73	2879.6	120.5	233.6	31025.9
8	16.45	20.73	12229.6	341.2	351.2	132045.3
9	11.62	20.73	2879.6	120.5	233.6	31025.9
Moment of Inertia of Elongated Octagon						393661.7

Stresses at the extremes of the fracture plane:

Using the above analysis of the moment of inertia of the section, maximum tensile and compressive stresses under the failure load of 94,000 lb can now be estimated. Since the centroid of the elongated octagon is not at the center of the long dimension of the shape there will be two dimensions to the extreme fibers of the cross-section; c_c, the distance to the maximum compressive stress is 29.11 in and c_t, the distance to the maximum tensile stress is 27.44 in. From the diagram above the moment arm of the applied force is 44 in. and σ_c and σ_t are:

$$\sigma_c = \frac{Mc_c}{I} = \frac{(94{,}000)(44)(29.11)}{393{,}662} = 305.8\,psi$$

$$\sigma_t = \frac{Mc_t}{I} = \frac{(94{,}000)(44)(27.44)}{393{,}662} = 288.3\,psi$$

Locations of the Strain Gauge Rosettes

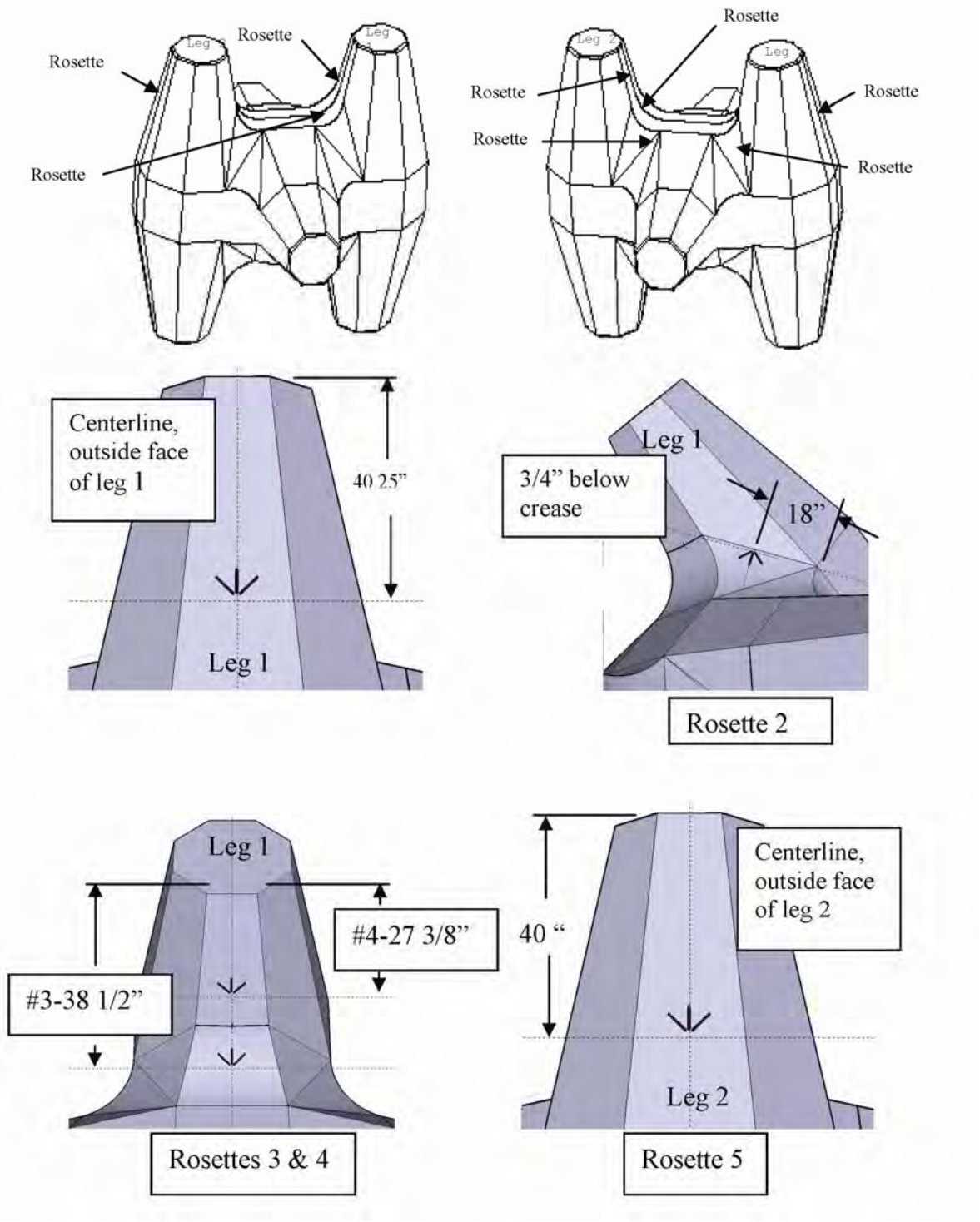

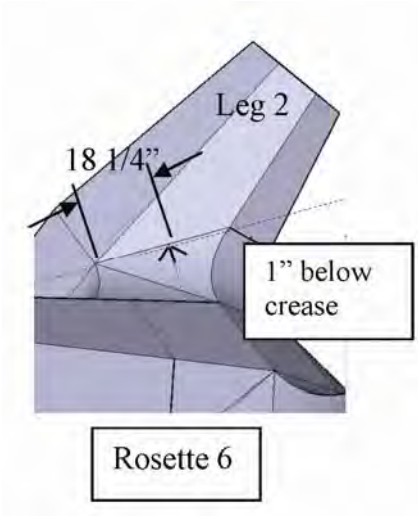

Rosette 6

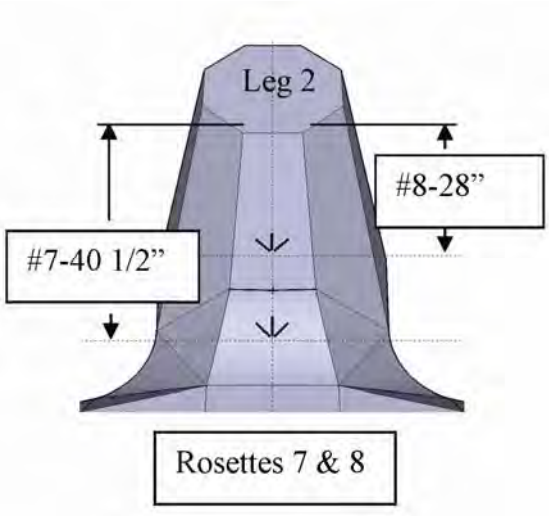

Rosettes 7 & 8

Pulse-Velocity Data Sheet
Core-Locs Armor Unit tested at
Barbers Point Precasting Facility, Capolei, HI
Sept 11 - 20, 2006

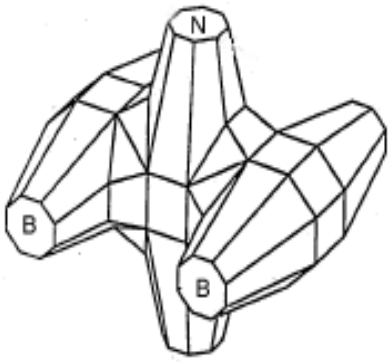

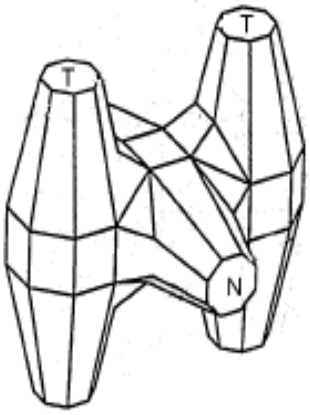

READING LOCATION	LOCATION LENGTH, in.	TIME OF ARRIVAL, ms.	VELOCITY, fps.	DATA OR COMMENTS

Broken_leg reading #	Time (uSec)	Solid_leg reading #	Time (uSec)	(from note pos x (inches)	y (inches)	note:
1	167.4	13	171	4.25	2.50	up from bottom
2	187.3	14	189.4	5.25	10.50	
3	224.7	15	225.6	16.00	26.50	
4	256	16	255.8	9.00	38.50	
5	291.3	17	296.7	10.13	12.00	down from bottom crease
6	325.3	18	325	11.13	1.00	above
7	327.1	19	323.2	11.00	13.50	above
8	325.3	20	321.4	11.13	1.00	below top crease
9	292.3	21	299.2	10.13	12.00	above top crease
10	241.7	22	239.6	16.00	26.50	down from top
11	193.7	23	189.3	5.25	10.50	
12	162	24	180.7	4.25	2.50	**material missing**

%; difference top vs. bottom	<-- averaged left and right
1.3	
1.7	
6.7	
14.4	<- elevation difference
9.5	
0.0	

% difference left vs. right	
2.1	
1.1	
0.4	
0.1	
1.8	
0.1	
1.2	
1.2	
2.3	
0.9	
2.3	
	<- last point removed due to material loss

% differences are low and indicate good consistancy between left and right sides and from top to bottom of unit

based on lab tested core samples the average material velocity is 14350 feet/second

Note: percent differences top vs. bottom goes from the vertical extremes (1.3 percent to the center 0 percent)

PLOTS OF STRAIN VERSUS TIME FOR THE GAUGES OF THE EIGHT ROSETTES

ROSETTE 1

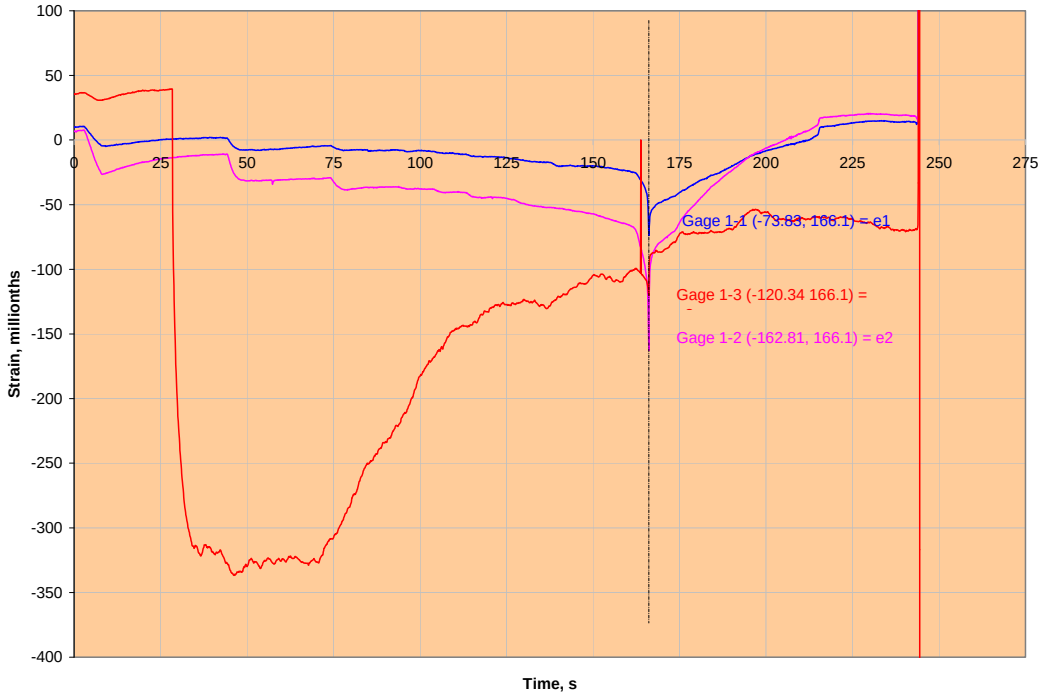

ROSETTE 2

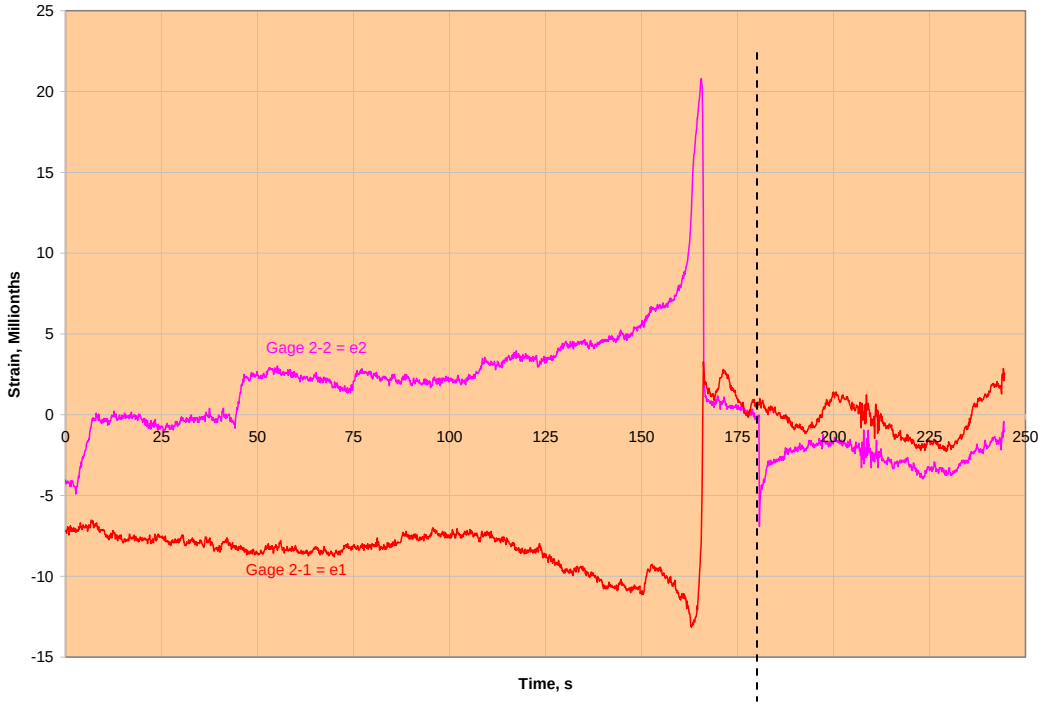

ROSETTE 3

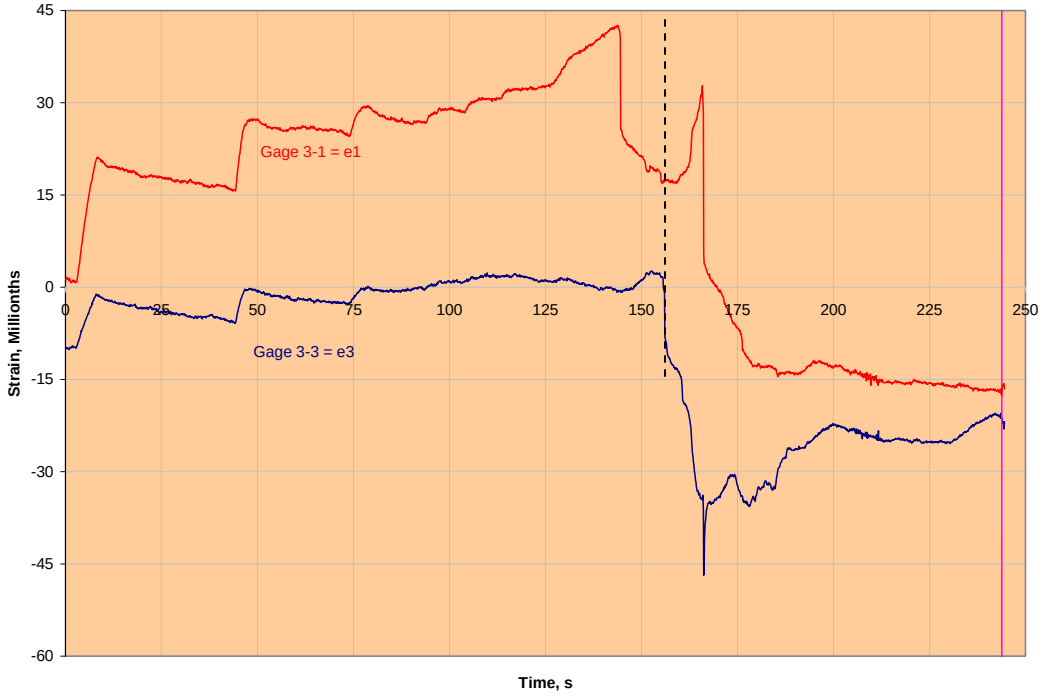

ROSETTE 4

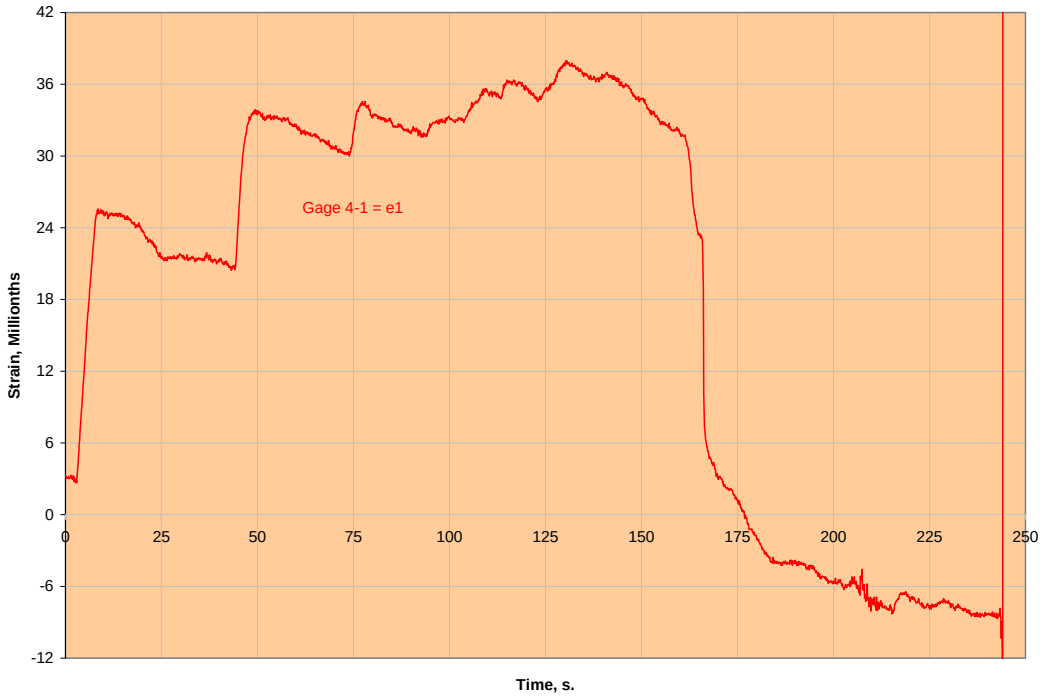

ROSETTE 5

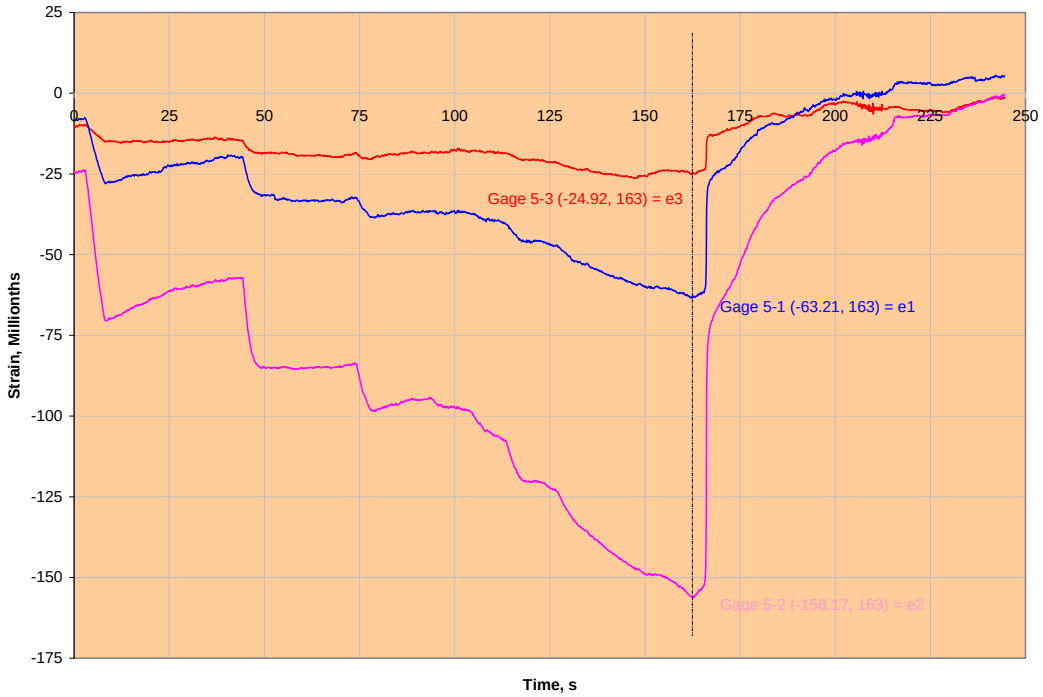

ROSETTE 6

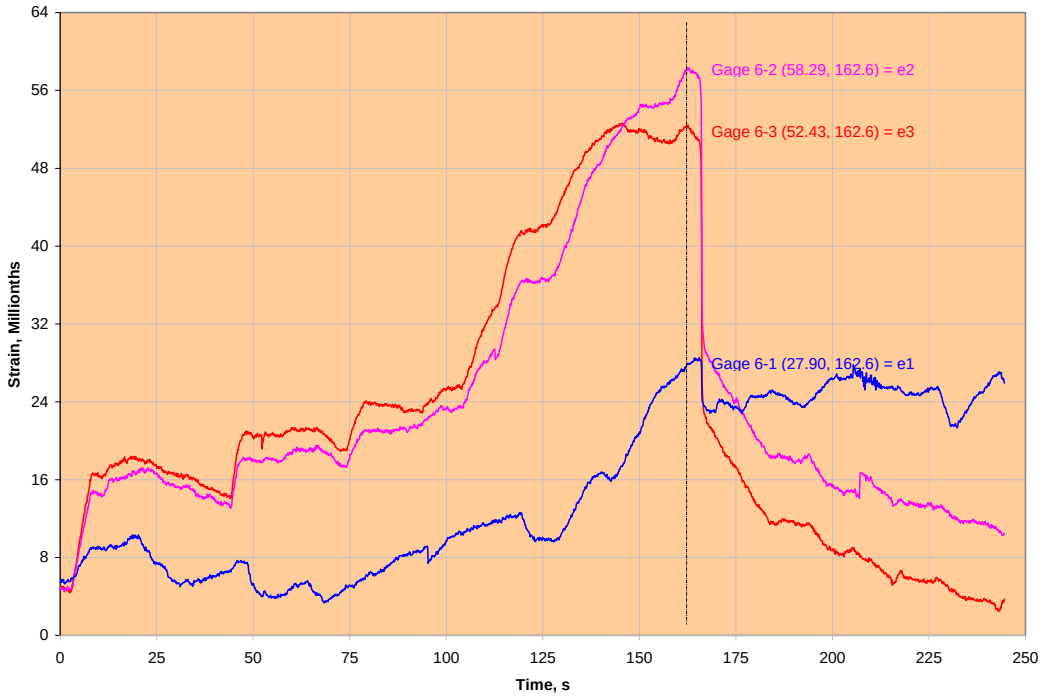

ROSETTE 7

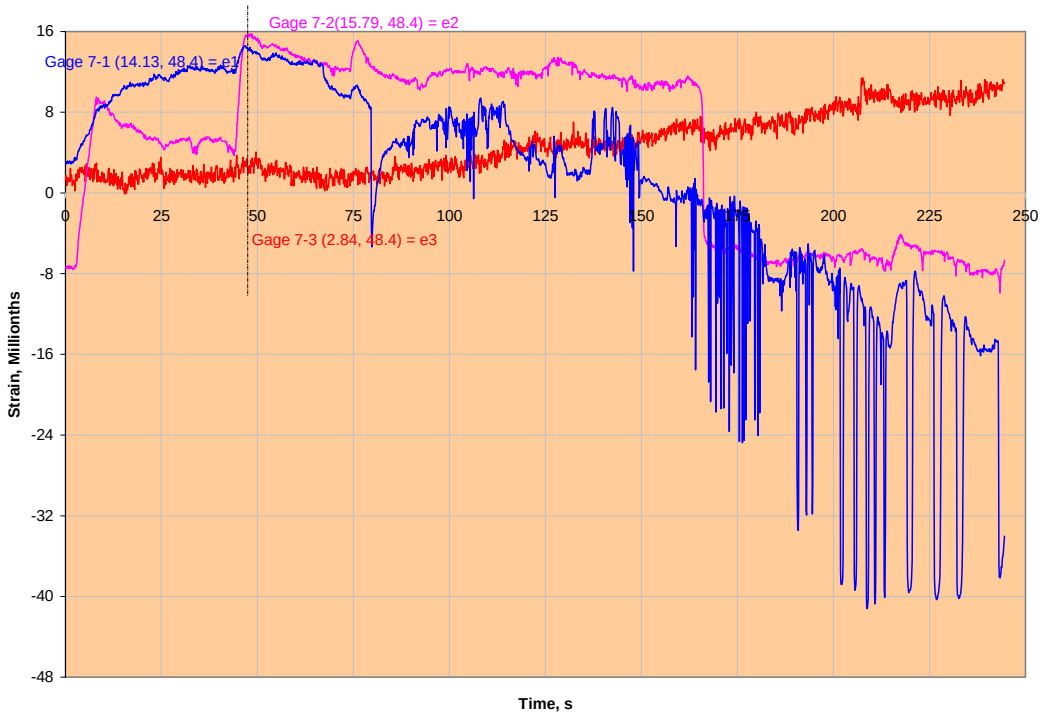

ROSETTE 8

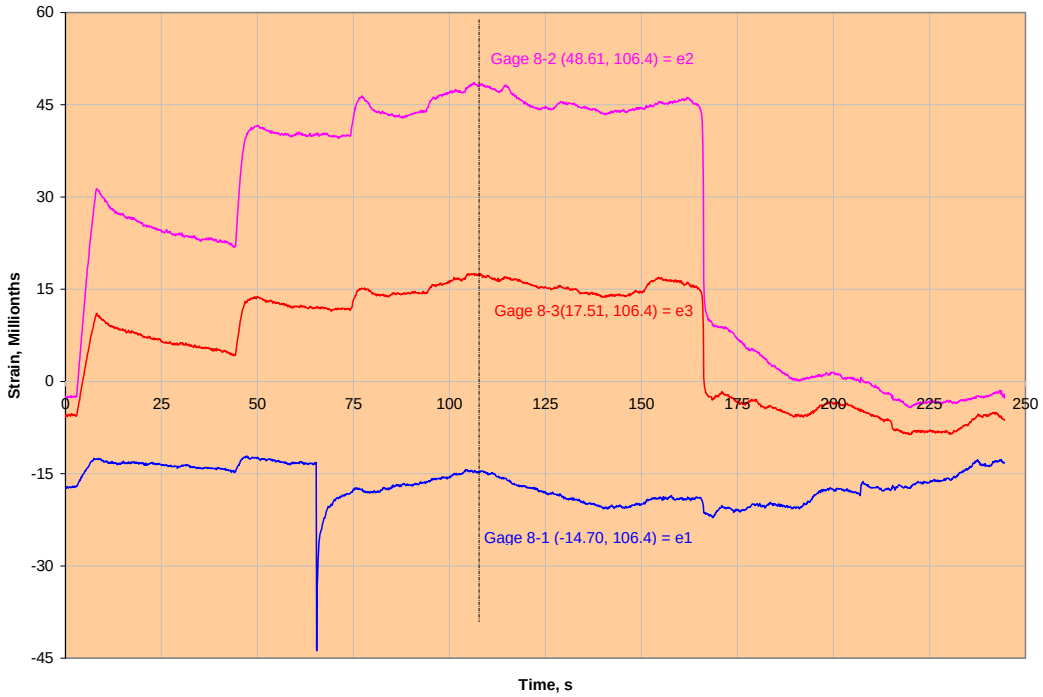

ORIENTATION OF THE MAJOR AND MINOR PRINCIPAL STRAINS GRAPHICAL DEPICTION OF THE STRAINS USING MOHR'S CIRCLE SAMPLE SET OF MOHR'S CIRCLE EQUATIONS

SAMPLE CALCULATIONS: (Using the strains in rosette 1. as an example)

Gauges are labeled ε_1 through ε_3 moving counter-clock-wise from right-most gauge (see rosette next page)

ε_1 = - 73.83 $\mu\varepsilon$

ε_2 = - 162.81 $\mu\varepsilon$

ε_3 = - 120.34 $\mu\varepsilon$

ε_p = The calculated major principal strain

ε_q = The calculated minor principal strain

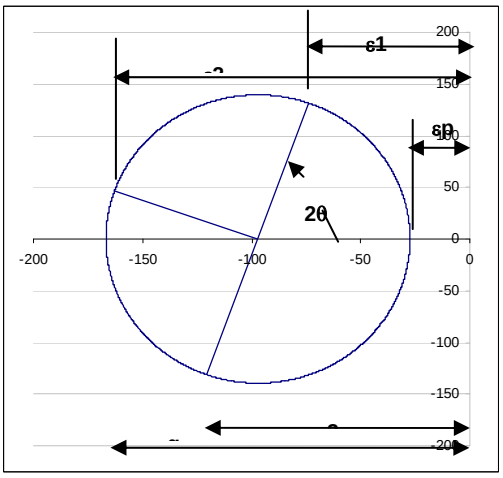

ε_p and ε_q are calculated by the equation:

$$\varepsilon_{p,q} = \frac{\varepsilon_1 + \varepsilon_3}{2} \pm \frac{1}{\sqrt{2}}\sqrt{(\varepsilon_1 - \varepsilon_2)^2 + (\varepsilon_2 - \varepsilon_3)^2}$$

where the first right-hand-side term is the x-coordinate of the center of the Mohr's Circle and the second term is the radius of the circle. ε_p = 1st term + 2nd term and ε_q = 1st term - 2nd term defining the two points that lie on the circle at the x-axis. Thus

$$\varepsilon_p = \frac{-73.83 + (-162.81)}{2} + \frac{1}{\sqrt{2}}\sqrt{(-73.83 - (-162.81))^2 + (-162.81 - (-120.34))^2} = -27.37\mu\varepsilon$$

$$\varepsilon_q = \frac{-73.83 + (-162.81)}{2} - \frac{1}{\sqrt{2}}\sqrt{(-73.83 - (-162.81))^2 + (-162.81 - (-120.34))^2} = -166.80\mu\varepsilon$$

ε_p and ε_q define the major and minor principal strains (they are 90° apart) but an angle with reference to the gauge ε_1 is necessary to fix the two axes on which they are located. 2ϕ on Mohr's circle represents ϕ on the strain surface. The equations for 2ϕ and thus ϕ are:

$$2\varphi = \tan^{-1}\left[\frac{2\varepsilon_2 - \varepsilon_1 - \varepsilon_3}{\varepsilon_1 - \varepsilon_3}\right] \text{ and}$$

$$\varphi = \frac{1}{2}\tan^{-1}\left[\frac{2\varepsilon_2 - \varepsilon_1 - \varepsilon_3}{\varepsilon_1 - \varepsilon_3}\right] = \frac{1}{2}\tan^{-1}\left[\frac{2(-162.81) - (-73.83) - (-120.34)}{-73.83 - (-120.34)}\right] = -35.26°$$

Rule of thumb is that if ϕ is positive the angle from the reference grid (gauge #1) to the principal axis is CCW (if negative the angle is CW). In this example ϕ is negative so the major principal axis would be 35.26° to the right of gauge #1 (see rosette next page). Because of the convention being used, tan 2ϕ = tan $2(\phi + 90)$, and there is confusion over which principal axis should be referenced. This is remedied by the following rules:

10. if $\varepsilon_1 > \varepsilon_3$ then $\phi_{p,q} = \phi_p$
11. if $\varepsilon_1 < \varepsilon_3$ then $\phi_{p,q} = \phi_q$
12. if $\varepsilon_1 = \varepsilon_3$ and $\varepsilon_2 < \varepsilon_1$ then $\phi_{p,q} = \phi_p$ = -45°
13. if $\varepsilon_1 = \varepsilon_3$ and $\varepsilon_2 > \varepsilon_1$ then $\phi_{p,q} = \phi_q$ = +45°
14. if $\varepsilon_1 = \varepsilon_2 = \varepsilon_3$ then $\phi_{p,q}$ is indeterminate

Calculations of principal stresses from principal strain

If it is assumed that the concrete is homogeneous in composition and isotropic in mechanical properties, then the biaxial form of Hooke's law can be used to calculate the principal stresses. Hooke's law is expressed as follows:

$$\sigma_P = \frac{E}{1 - \upsilon^2}(\varepsilon_P + \upsilon\varepsilon_Q)$$

and

$$\sigma_Q = \frac{E}{1 - \upsilon^2}(\varepsilon_Q + \upsilon\varepsilon_P)$$

and substituting values of ε_P and ε_Q gives

$$\sigma_P = \frac{3{,}628{,}768}{1-0.33^2}(-166.8 + 0.33(-27.37)) = -716\,psi$$

and

$$\sigma_Q = \frac{3{,}628{,}768}{1-0.33^2}(-27.37 + 0.33(-166.8)) = -335.6\,psi$$

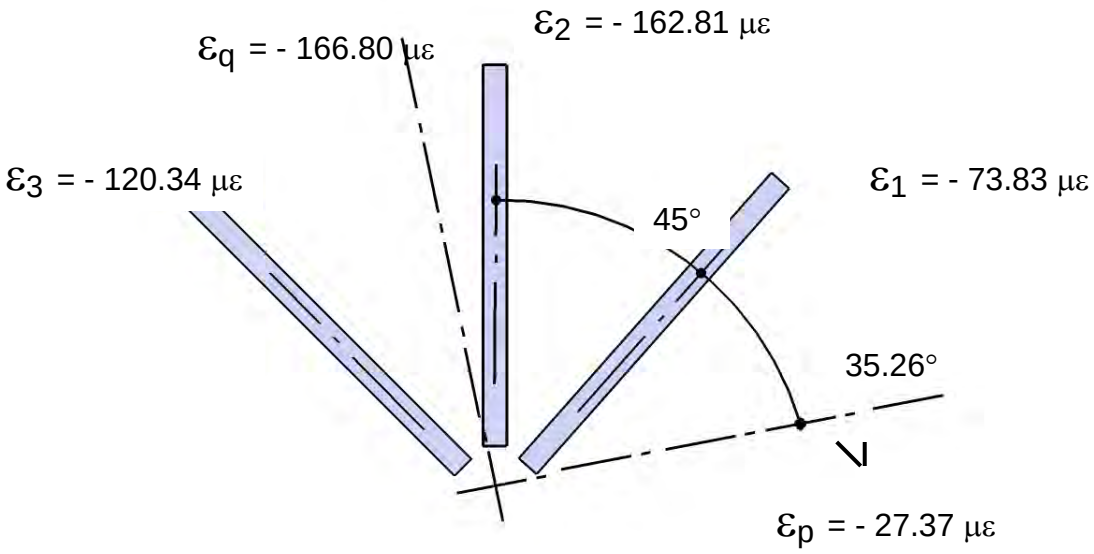

Rosette # 1

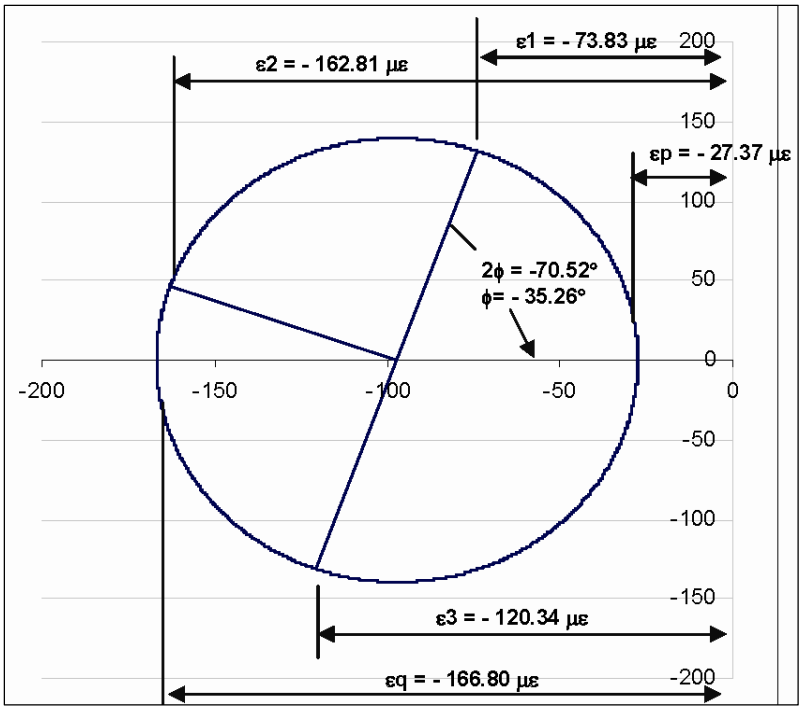

Mohr's Circle for Rosette # 1

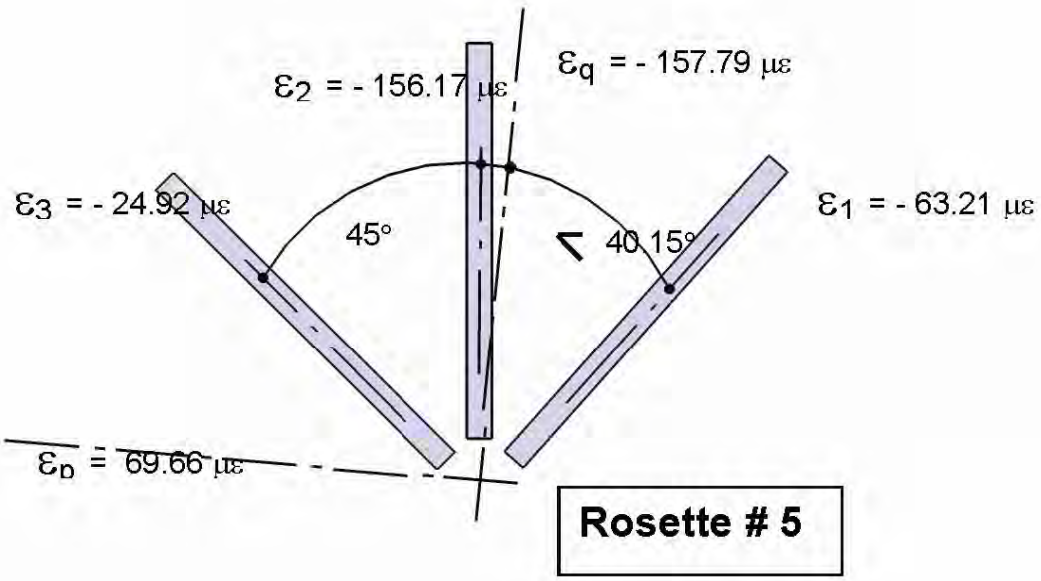

Rosette # 5

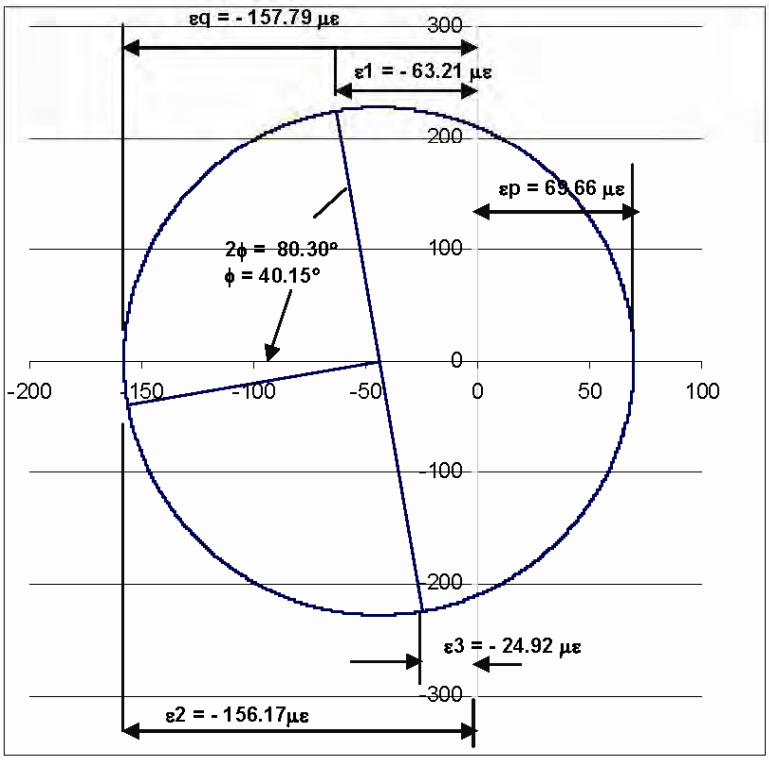

Mohr's Circle for Rosette # 5

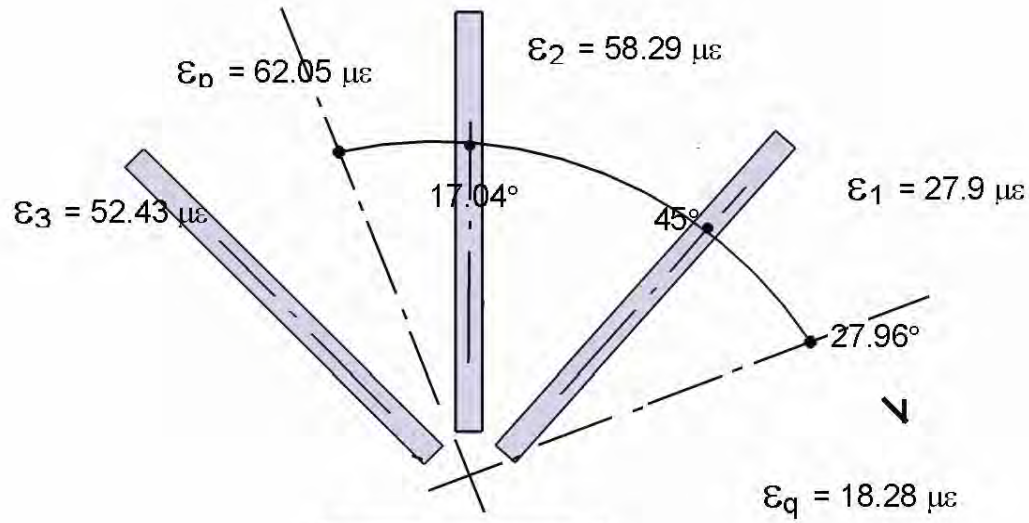

Rosette # 6

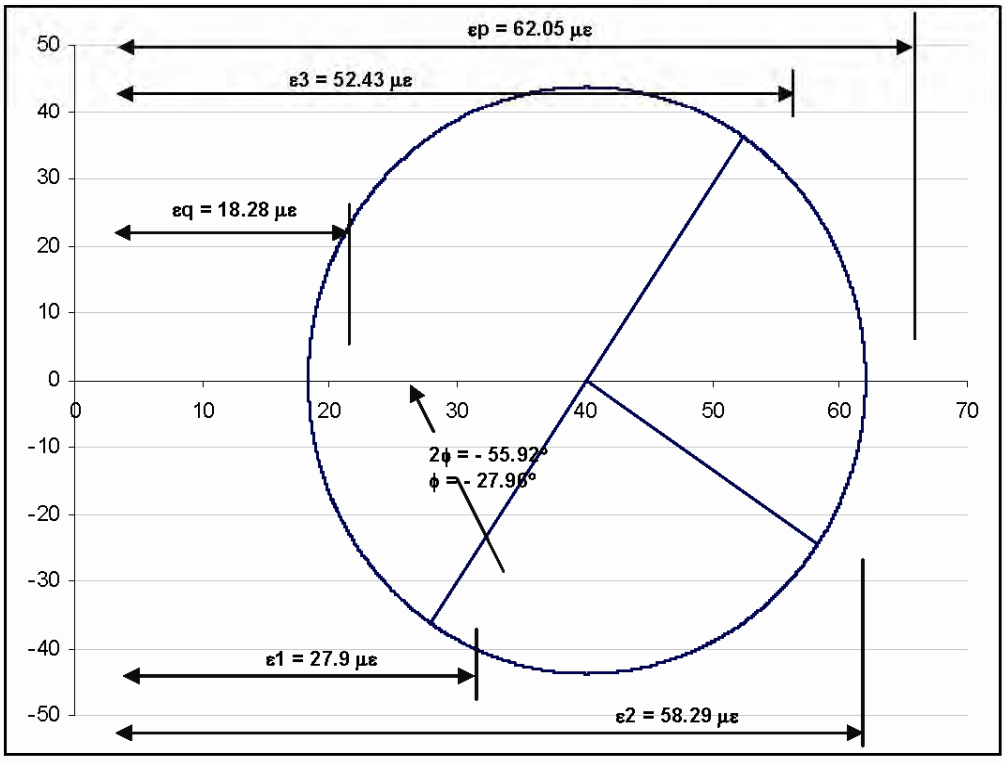

Mohr's Circle for Rosette # 6

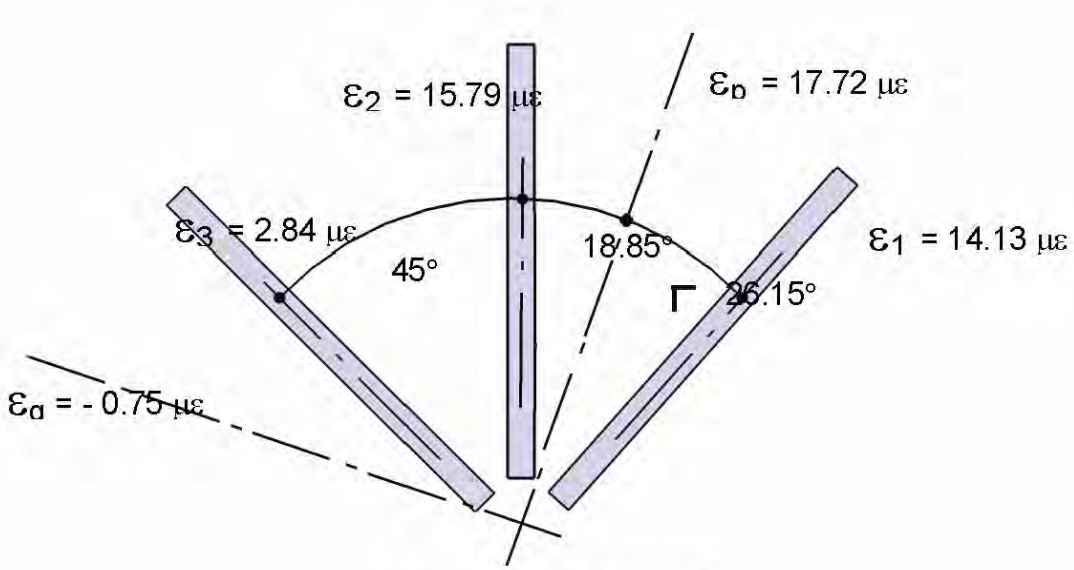

Rosette # 7

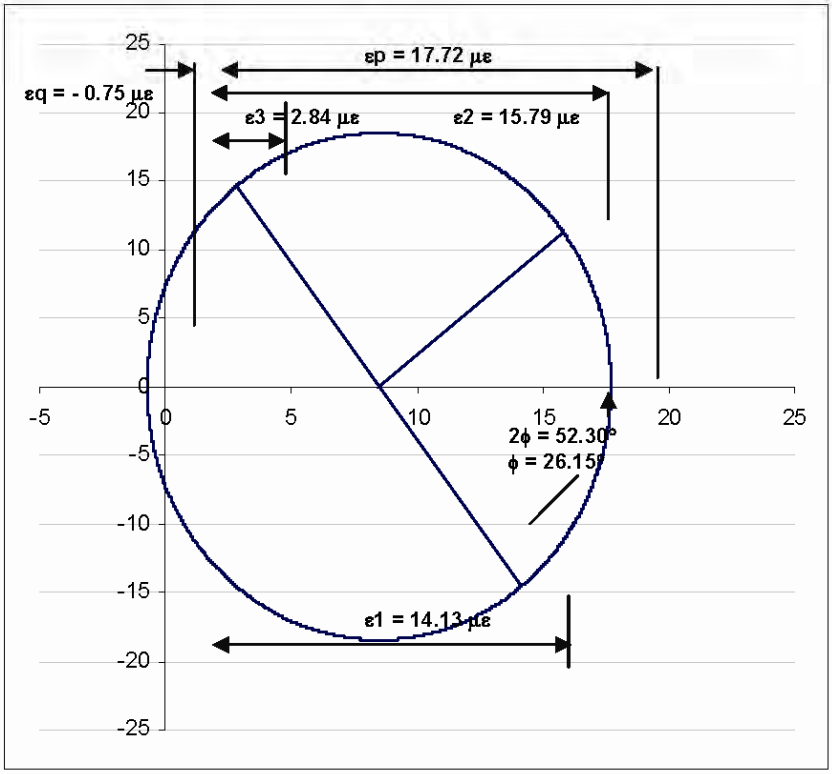

Mohr's Circle for Rosette # 7

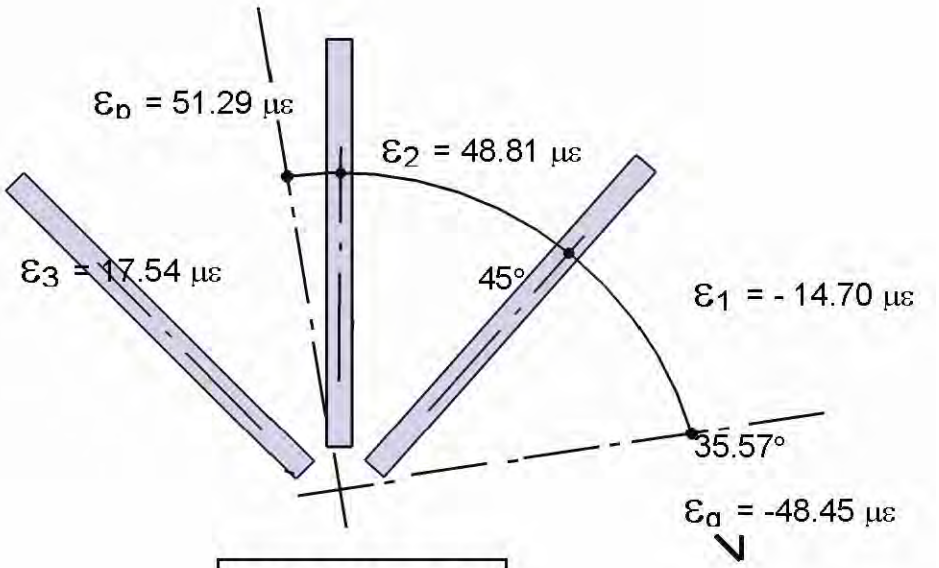

Rosette # 8

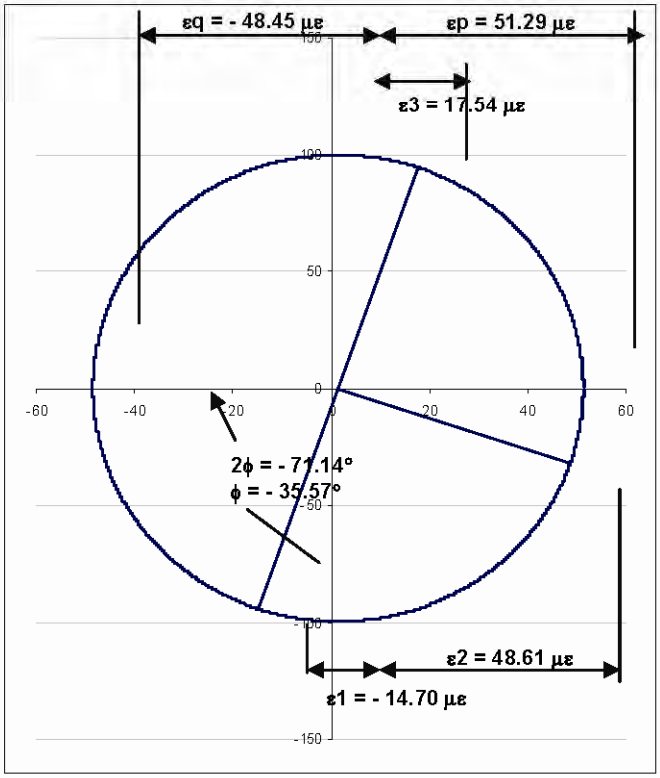

Mohr's Circle for Rosette # 8

Compressive and Tensile Testing Data from Cores and Core Location Legend

Specimen Origin Legend

Core #1 Top Leg (unbroken side)
Core #2 Top Center haunch
Core #3 Top Leg (broken side)
Core #4 Bottom Leg (unbroken side)
Core #5 Bottom Center haunch

U.S. Army Corps of Engineers579 1:07:08 PM 7/3/2008

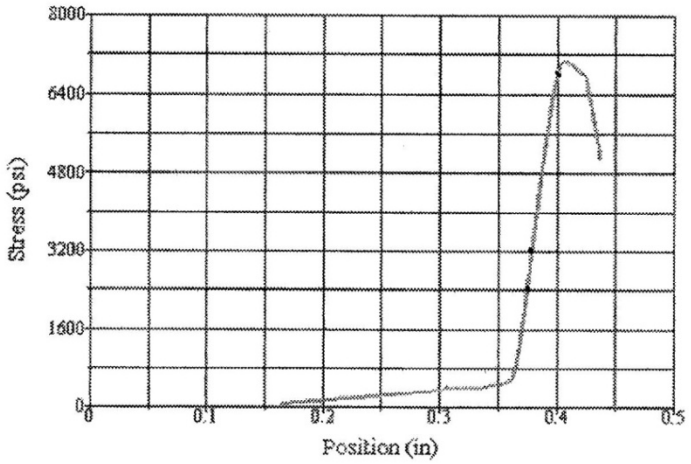

Test Summary	
Counter:	579
Elapsed Time:	00:03:21
Sample I.D.:	HASKINS HAWAII CORE #3
Type and Size:	4X8 CORE
Project:	HAWAII
PI:	HASKINS
Age, Days:	?
Type of Failure:	A
Curing History:	
Operator:	wilson
Length:	7.58
Procedure Name:	DAN Compressive Strength
Start Date:	7/3/2008
Start Time:	1:03:40 PM
End Date:	7/3/2008
End Time:	1:07:01 PM
Workstation:	U.S. Army Corps of Engineers
Tested By:	WILSON

Test Results	
Diameter:	3.6800 in
Area:	10.6362 in²
Peak Stress:	7057 psi
Peak Load:	75059 lbf

U.S. Army Corps of Engineers581 1:16:59 PM 7/3/2008

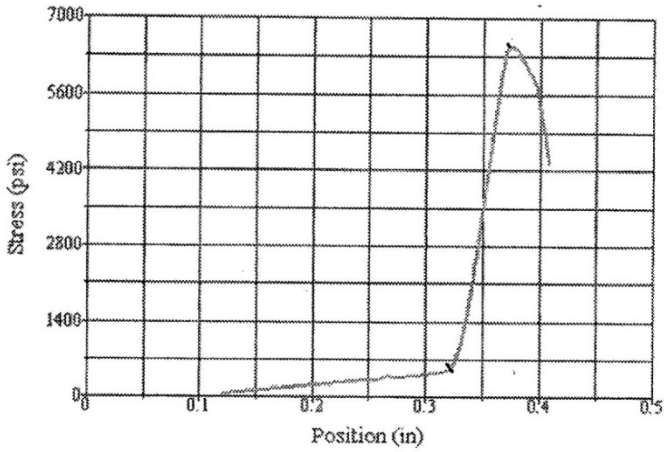

Test Summary

Counter:	581
Elapsed Time:	00:03:04
Sample I.D.:	HASKINS HAWAII CORE #5
Type and Size:	4X8 CORE
Project:	HAWAII
PI:	HASKINS
Age, Days:	?
Type of Failure:	A
Curing History:	
Operator:	wilson
Length:	7.58
Procedure Name:	DAN Compressive Strength
Start Date:	7/3/2008
Start Time:	1:13:46 PM
End Date:	7/3/2008
End Time:	1:16:50 PM
Workstation:	U.S. Army Corps of Engineers
Tested By:	WILSON

Test Results

Diameter:	3.6800 in
Area:	10.6362 in²
Peak Stress:	6488 psi
Peak Load:	69003 lbf

U.S. Army Corps of Engineers580 1:12:28 PM 7/3/2008

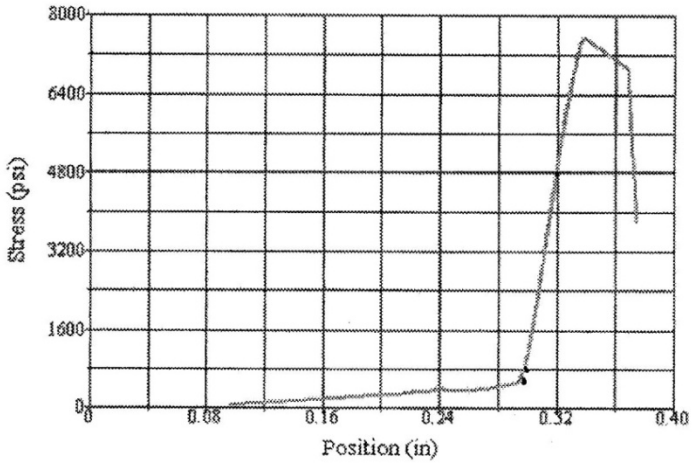

Test Summary		Test Results	
Counter:	580	Diameter:	3.6800 in
Elapsed Time:	00:03:35	Area:	10.6362 in²
Sample I.D.:	HASKINS HAWAII CORE #4	Peak Stress:	7537 psi
Type and Size:	4X8 CORE	Peak Load:	80164 lbf
Project:	HAWAII		
PI:	HASKINS		
Age, Days:	?		
Type of Failure:	A		
Curing History:			
Operator:	wilson		
Length:	7.58		
Procedure Name:	DAN Compressive Strength		
Start Date:	7/3/2008		
Start Time:	1:08:47 PM		
End Date:	7/3/2008		
End Time:	1:12:22 PM		
Workstation:	U.S. Army Corps of Engineers		
Tested By:	WILSON		

U.S. Army Corps of Engineers597 3:04:50 PM 7/7/2008

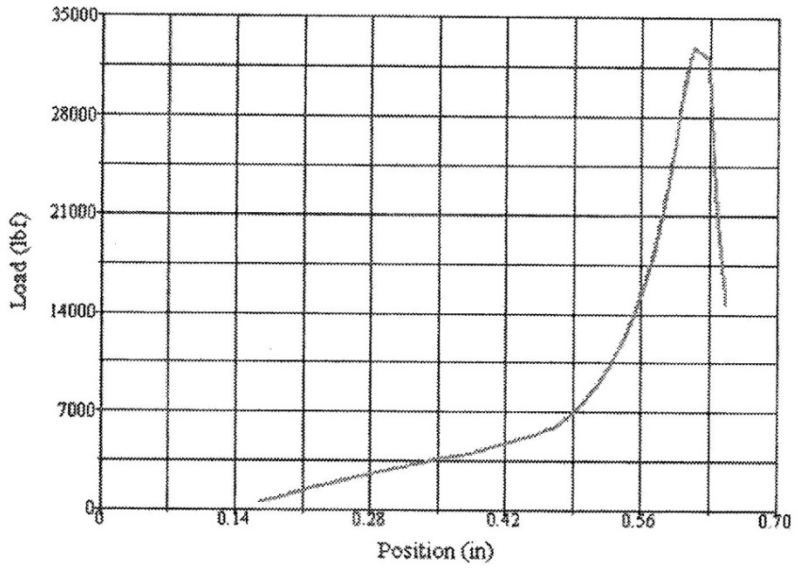

Test Summary

Counter:	597
Elapsed Time:	00:01:56
Specimen Identification:	HAWAII CORE #1
Sample Lot:	HAWAII
Sample I.D.:	1
Type and Size:	4X8 CORE
Project:	HAWAII
PI:	HASKINS
Age, Days:	OLD
Curing History:	AMBIENT
Operator:	WILSON
Length:	7.85
Procedure Name:	DAN TENSILE SPLIT
Start Date:	7/7/2008
Start Time:	3:02:46 PM
End Date:	7/7/2008
End Time:	3:04:42 PM

Test Results

Specimen Gage Length:	7.8500 in
Diameter:	3.7300 in
Area:	10.9272 in²
Splitting Tensile Strength:	717 psi
Peak Load:	32964 lbf

U.S. Army Corps of

U.S. Army Corps of Engineers598 3:16:14 PM 7/7/2008

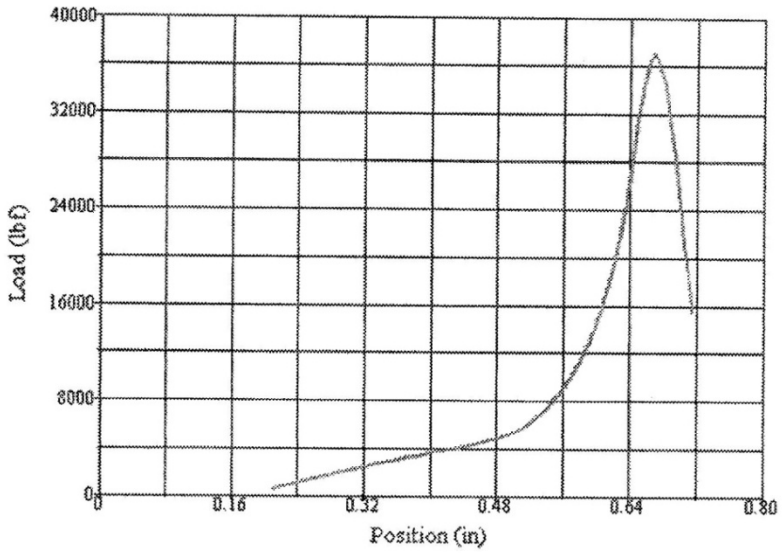

Test Summary

Counter:	598
Elapsed Time:	00:02:09
Specimen Identification:	HAWAII CORE #2
Sample Lot:	HAWAII
Sample I.D.:	1
Type and Size:	4X8 CORE
Project:	HAWAII
PI:	HASKINS
Age, Days:	OLD
Curing History:	AMBIENT
Operator:	WILSON
Length:	7.85
Procedure Name:	DAN TENSILE SPLIT
Start Date:	7/7/2008
Start Time:	3:13:54 PM
End Date:	7/7/2008
End Time:	3:16:03 PM
Workstation:	U.S. Army Corps of Engineers

Test Results

Specimen Gage Length:	7.8300 in
Diameter:	3.7300 in
Area:	10.9272 in²
Splitting Tensile Strength:	806 psi
Peak Load:	36965 lbf

U.S. Army Corps of Engineers599 3:22:22 PM 7/7/2008

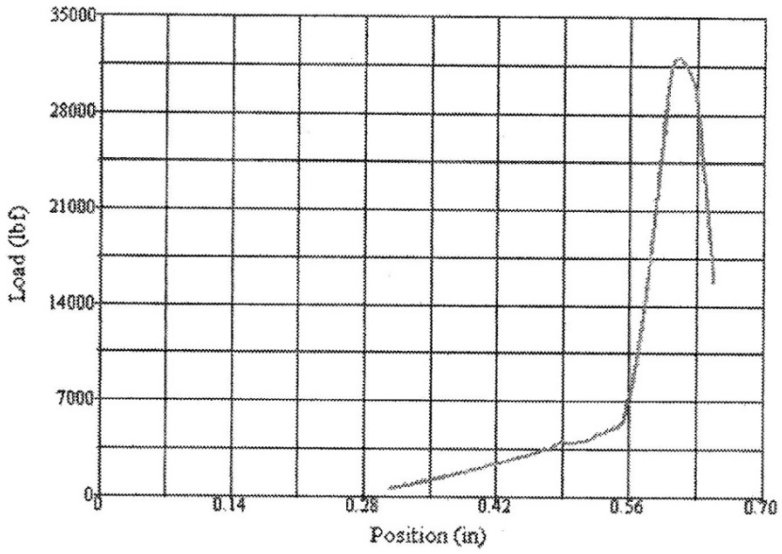

Test Summary

Counter:	599
Elapsed Time:	00:01:54
Specimen Identification:	HAWAII CORE #3
Sample Lot:	HAWAII
Sample I.D.:	1
Type and Size:	4X8 CORE
Project:	HAWAII
PI:	HASKINS
Age, Days:	OLD
Curing History:	AMBIENT
Operator:	WILSON
Length:	7.85
Procedure Name:	DAN TENSILE SPLIT
Start Date:	7/7/2008
Start Time:	3:19:14 PM
End Date:	7/7/2008
End Time:	3:21:08 PM
Workstation:	U.S. Army Corps of Engineers

Test Results

Specimen Gage Length:	7.8200 in
Diameter:	3.7300 in
Area:	10.9272 in²
Splitting Tensile Strength:	702 psi
Peak Load:	32159 lbf

U.S. Army Corps of Engineers601 3:31:31 PM 7/7/2008

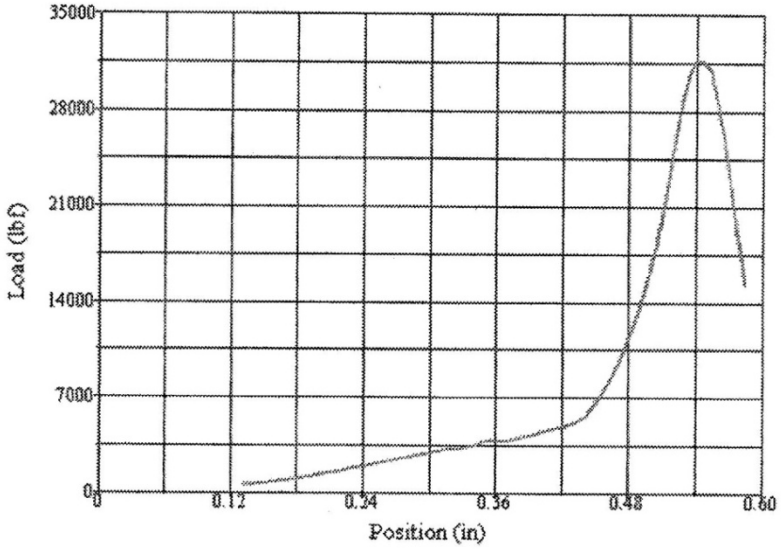

Test Summary

Counter:	601
Elapsed Time:	00:01:51
Specimen Identification:	HAWAII CORE #4
Sample Lot:	HAWAII
Sample I.D.:	1
Type and Size:	4X8 CORE
Project:	HAWAII
PI:	HASKINS
Age, Days:	OLD
Curing History:	AMBIENT
Operator:	WILSON
Length:	7.85
Procedure Name:	DAN TENSILE SPLIT
Start Date:	7/7/2008
Start Time:	3:29:31 PM
End Date:	7/7/2008
End Time:	3:31:22 PM
Workstation:	U.S. Army Corps of Engineers

Test Results

Specimen Gage Length:	7.8200 in
Diameter:	3.7300 in
Area:	10.9272 in²
Splitting Tensile Strength:	691 psi
Peak Load:	31647 lbf

U.S. Army Corps of Engineers600

3:26:49 PM 7/7/2008

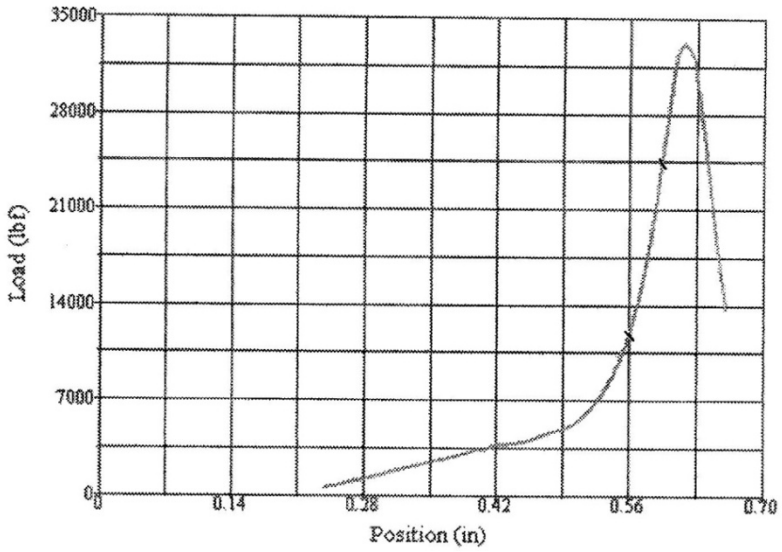

Test Summary

Counter:	600
Elapsed Time:	00:01:57
Specimen Identification:	HAWAII CORE #4
Sample Lot:	HAWAII
Sample I.D.:	1
Type and Size:	4X8 CORE
Project:	HAWAII
PI:	HASKINS
Age, Days:	OLD
Curing History:	AMBIENT
Operator:	WILSON
Length:	7.85
Procedure Name:	DAN TENSILE SPLIT
Start Date:	7/7/2008
Start Time:	3:24:44 PM
End Date:	7/7/2008
End Time:	3:26:41 PM
Workstation:	U.S. Army Corps of Engineers

Test Results

Specimen Gage Length:	7.8400 in
Diameter:	3.7300 in
Area:	10.9272 in²
Splitting Tensile Strength:	721 psi
Peak Load:	33128 lbf

U.S. Army Corps of Engineers577 12:57:14 PM 7/3/2008

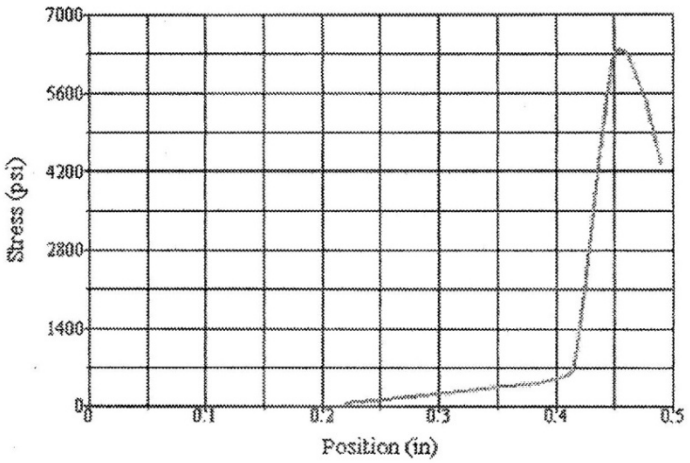

Test Summary		Test Results	
Counter:	577	Diameter:	3.6800 in
Elapsed Time:	00:03:01	Area:	10.6362 in²
Sample I.D.:	HASKINS HAWAII CORE #1	Peak Stress:	6373 psi
Type and Size:	4X8 CORE	Peak Load:	67784 lbf
Project:	HAWAII		
PI:	HASKINS		
Age, Days:	?		
Type of Failure:	A		
Curing History:			
Operator:	wilson		
Length:	7.58		
Procedure Name:	DAN Compressive Strength		
Start Date:	7/3/2008		
Start Time:	12:51:57 PM		
End Date:	7/3/2008		
End Time:	12:54:58 PM		
Workstation:	U.S. Army Corps of Engineers		
Tested By:	WILSON		

U.S. Army Corps of Engineers578 1:02:02 PM 7/3/2008

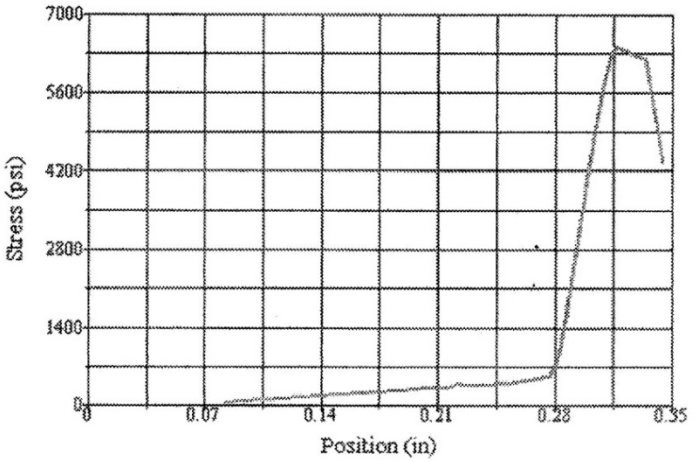

Test Summary	
Counter:	578
Elapsed Time:	00:03:03
Sample I.D.:	HASKINS HAWAII CORE #2
Type and Size:	4X8 CORE
Project:	HAWAII
PI:	HASKINS
Age, Days:	?
Type of Failure:	A
Curing History:	
Operator:	wilson
Length:	7.58
Procedure Name:	DAN Compressive Strength
Start Date:	7/3/2008
Start Time:	12:58:50 PM
End Date:	7/3/2008
End Time:	1:01:53 PM
Workstation:	U.S. Army Corps of Engineers
Tested By:	WILSON

Test Results	
Diameter:	3.6800 in
Area:	10.6362 in²
Peak Stress:	6416 psi
Peak Load:	68241 lbf

Appendix B: Wave Spectra, Lookup Tables, and Predictive Surface Plots[1]

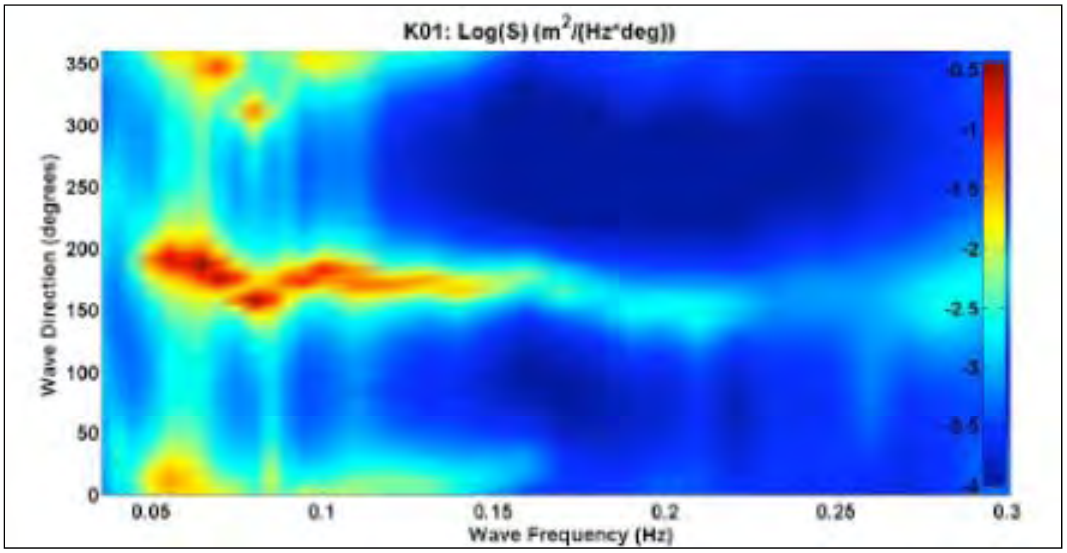

Figure B.1. Wave spectrum at K01 (H_s = 1.0 ft, T_p = 15.3 sec, D_p = 190 deg).

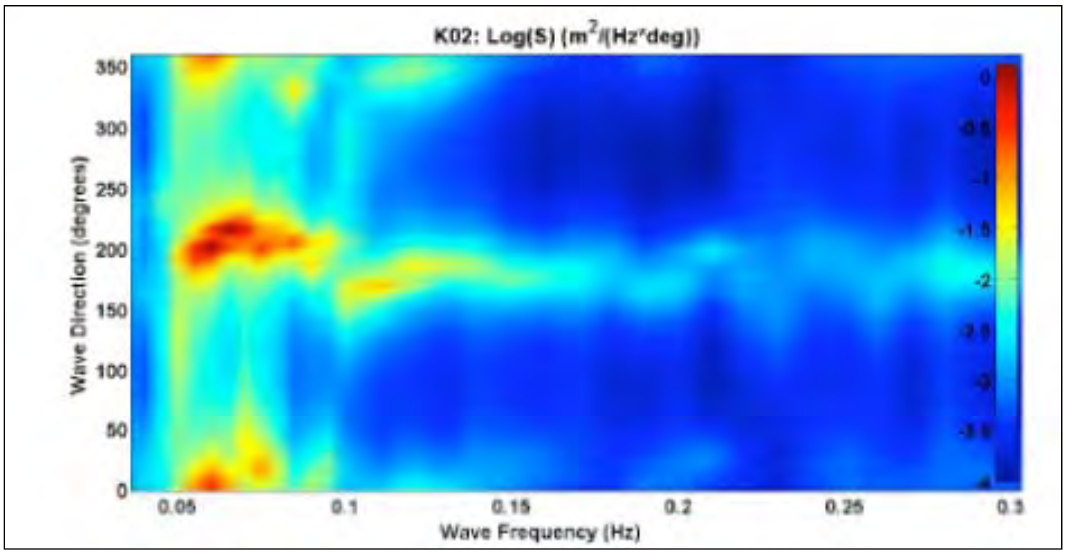

Figure B.2. Wave spectrum at K02 (H_s= 1.4 ft, T_p = 17.1 sec, D_p = 200 deg).

[1] From Sea Engineering, Inc. and Group 70 International, 2009.

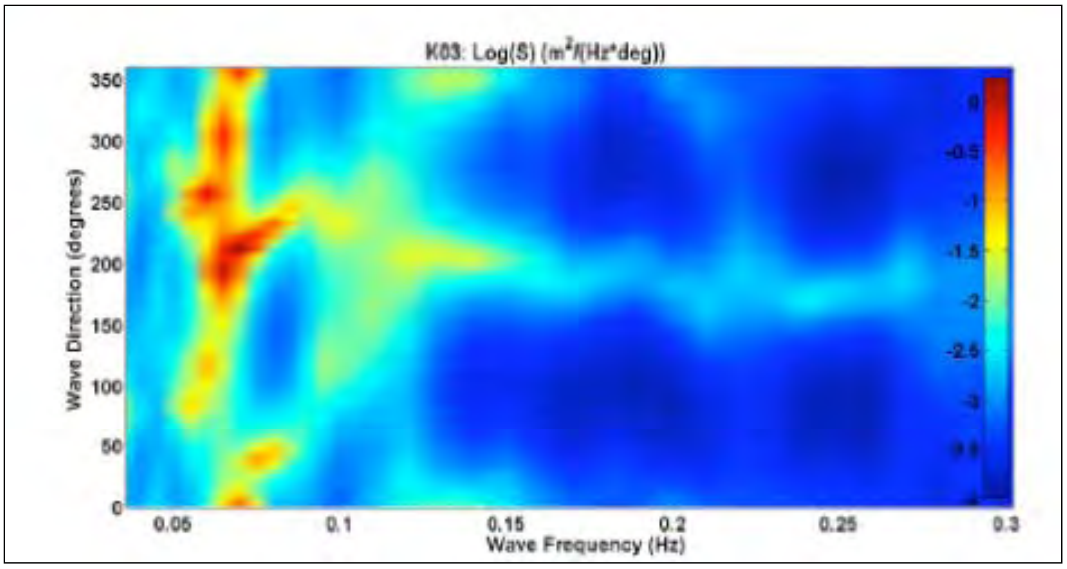

Figure B.3. Wave spectrum at K03 (H_s= 1.6 ft, T_p = 15.4 sec, D_p = 235 deg).

Table B.1. Revised scene 2 lookup table

case	VBL01 = NDBC 51203			Adjusted Predicted Wave Height (ft)							Adjusted Transmission Coefficients							Change in predicted Wave Height (ft)						
	dp	hs (ft)	tp (s)	W2	W3	W4	W5	K01	K02	K03	W2	W3	W4	W5	K01	K02	K03	W2	W3	W4	W5	K01	K02	K03
1	180	2.4	10.5	2.6	2.0	1.3	1.2	0.6	0.9	1.3	1.074	0.828	0.539	0.504	0.260	0.378	0.537	0.0	0.0	0.0	0.0	-0.2	0.0	0.0
2	180	3.1	10.5	3.3	2.5	1.7	1.5	0.8	1.2	1.6	1.074	0.828	0.539	0.504	0.260	0.378	0.537	0.2	0.1	0.1	0.0	0.1	-0.2	-0.1
3	190	2.7	10.5	2.6	1.4	1.5	1.5	0.6	0.7	1.2	0.949	0.516	0.542	0.560	0.225	0.271	0.440	-0.2	0.5	0.0	0.0	0.1	0.0	-0.1
6	190	3.0	10.5	2.9	1.6	1.6	1.7	0.7	0.8	1.3	0.949	0.516	0.542	0.560	0.225	0.271	0.440	-0.1	-0.5	-0.4	-1.0	-0.4	-0.6	-0.5
5	190	3.4	12.1	2.5	3.3	1.7	2.0	1.1	1.0	1.2	0.750	0.960	0.507	0.582	0.315	0.306	0.354	0.2	-0.5	0.0	0.0	-0.7	-0.1	0.1
4	190	3.5	10.5	3.3	1.8	1.9	2.0	0.8	1.0	1.5	0.949	0.516	0.542	0.560	0.225	0.271	0.440	-0.1	0.8	0.1	0.1	0.1	0.0	0.0
9	190	3.9	10.5	3.7	2.0	2.1	2.2	0.9	1.1	1.7	0.949	0.516	0.542	0.560	0.225	0.271	0.440	-0.1	-0.7	-0.5	-1.3	-0.6	-0.4	-0.4
43	200	1.2	16.0	0.9	0.9	0.5	1.0	0.5	0.5	0.5	0.788	0.801	0.463	0.828	0.406	0.439	0.453	-0.1	-0.1	0.0	0.0	-0.3	0.0	-0.1
42	200	1.2	13.9	0.9	0.9	0.6	0.9	0.5	0.5	0.4	0.755	0.738	0.521	0.717	0.414	0.423	0.320	0.1	0.2	-0.2	0.0	-0.4	-0.1	0.1
45	200	2.0	16.0	1.5	1.6	0.9	1.6	0.8	0.9	0.9	0.788	0.801	0.463	0.828	0.406	0.439	0.453	-0.2	-0.1	-0.1	-0.1	-0.5	-0.4	-0.3
44	200	2.0	13.9	1.5	1.5	1.1	1.5	0.8	0.9	0.6	0.755	0.738	0.521	0.717	0.414	0.423	0.320	0.2	0.2	0.1	-0.1	-0.7	-0.4	0.1
8	200	2.8	13.9	2.1	2.1	1.5	2.0	1.2	1.2	0.9	0.755	0.738	0.521	0.717	0.414	0.423	0.320	0.3	0.3	0.1	0.0	-1.0	-0.5	0.2
7	200	2.9	12.1	2.5	2.3	1.7	2.0	1.0	1.3	1.0	0.859	0.781	0.568	0.684	0.333	0.441	0.352	-0.1	-0.4	0.5	0.3	-0.3	0.3	0.1
16	200	3.2	12.1	2.7	2.5	1.8	2.2	1.1	1.4	1.1	0.859	0.781	0.568	0.684	0.333	0.441	0.352	0.0	0.4	0.2	-0.1	-0.3	0.2	-0.2
15	200	3.2	10.5	3.3	2.7	2.0	2.4	0.9	1.6	1.6	1.019	0.827	0.630	0.729	0.269	0.488	0.484	-0.1	0.1	-0.3	-0.2	-0.4	-0.2	-0.2
12	200	3.5	16.0	2.8	2.8	1.6	2.9	1.4	1.5	1.6	0.788	0.801	0.463	0.828	0.406	0.439	0.453	-0.4	-0.3	0.0	-0.1	-0.9	-0.7	-0.5
11	200	3.6	13.9	2.8	2.7	1.9	2.6	1.5	1.5	1.2	0.755	0.738	0.521	0.717	0.414	0.423	0.320	0.6	0.5	0.3	-0.1	-1.3	-0.7	0.2
10	200	3.8	12.1	3.2	2.9	2.1	2.6	1.3	1.7	1.3	0.859	0.781	0.568	0.684	0.333	0.441	0.352	0.0	-0.6	0.6	0.4	-0.3	0.5	-0.1
20	200	4.0	12.1	3.5	3.2	2.3	2.8	1.3	1.8	1.4	0.859	0.781	0.568	0.684	0.333	0.441	0.352	0.1	0.4	-0.1	0.2	-0.6	0.4	-0.4
19	200	4.2	10.5	4.2	3.4	2.6	3.0	1.1	2.0	2.0	1.019	0.827	0.630	0.729	0.269	0.488	0.484	-0.1	-0.2	-0.2	-0.4	-0.6	-0.1	-0.1
14	200	4.5	13.9	3.4	3.3	2.3	3.2	1.9	1.9	1.4	0.755	0.738	0.521	0.717	0.414	0.423	0.320	0.8	0.5	0.4	0.0	-1.6	-0.9	-0.1
13	200	4.6	12.1	4.0	3.6	2.6	3.2	1.5	2.0	1.6	0.859	0.781	0.568	0.684	0.333	0.441	0.352	0.1	-0.7	0.5	0.4	-0.5	0.5	-0.1
23	200	5.0	12.1	4.3	3.9	2.8	3.4	1.7	2.2	1.7	0.859	0.781	0.568	0.684	0.333	0.441	0.352	0.1	0.5	1.0	-0.1	-0.6	0.6	-0.4
26	200	5.8	12.1	5.0	4.6	3.3	4.0	1.9	2.6	2.1	0.859	0.781	0.568	0.684	0.333	0.441	0.352	-0.1	0.6	0.2	0.2	-0.8	1.1	-0.3
47	210	1.3	16.0	0.9	1.0	0.6	0.9	0.4	0.8	0.5	0.716	0.798	0.455	0.716	0.344	0.636	0.404	0.0	-0.1	0.0	0.0	-0.3	-0.1	-0.1
46	210	1.3	13.9	1.1	0.8	0.6	1.1	0.5	0.6	0.4	0.823	0.627	0.481	0.820	0.392	0.468	0.266	0.0	0.1	0.0	0.0	-0.5	0.1	0.2
49	210	2.1	16.0	1.5	1.7	1.0	1.5	0.7	1.4	0.9	0.716	0.798	0.455	0.716	0.344	0.636	0.404	-0.3	-0.2	-0.2	-0.1	-0.6	0.0	-0.3
48	210	2.2	13.9	1.8	1.4	1.1	1.8	0.9	1.0	0.6	0.823	0.627	0.481	0.820	0.392	0.468	0.266	0.0	0.1	0.2	0.1	-0.8	-0.1	0.2
18	210	3.0	16.0	2.1	2.4	1.4	2.1	1.0	1.9	1.2	0.716	0.798	0.455	0.716	0.344	0.636	0.404	-0.4	-0.2	-0.1	-0.1	-0.7	-0.2	-0.6
17	210	3.1	13.9	2.5	1.9	1.5	2.5	1.2	1.4	0.8	0.823	0.627	0.481	0.820	0.392	0.468	0.266	0.2	0.1	0.3	0.2	-1.2	-0.1	0.0
29	210	3.4	10.5	3.5	2.5	2.1	3.4	1.0	1.6	1.5	1.022	0.732	0.630	0.991	0.294	0.469	0.448	0.0	-0.1	-0.1	0.0	-0.2	-0.1	-0.2
22	210	3.8	16.0	2.7	3.1	1.7	2.7	1.3	2.4	1.5	0.716	0.798	0.455	0.716	0.344	0.636	0.404	-0.6	-0.3	-0.2	-0.1	-0.8	-0.3	-0.8
21	210	3.9	13.9	3.2	2.5	1.9	3.2	1.5	1.8	1.0	0.823	0.627	0.481	0.820	0.392	0.468	0.266	0.2	0.1	0.6	0.0	-1.5	-0.2	0.0
33	210	4.3	10.5	4.4	3.2	2.7	4.3	1.3	2.0	1.9	1.022	0.732	0.630	0.991	0.294	0.469	0.448	-0.1	-0.1	0.1	0.0	-0.1	0.1	0.0
25	210	4.7	16.0	3.4	3.7	2.1	3.4	1.6	3.0	1.9	0.716	0.798	0.455	0.716	0.344	0.536	0.404	-0.5	-0.6	0.0	-0.1	-0.8	0.3	-0.9
24	210	4.8	13.9	4.0	3.0	2.3	4.0	1.9	2.3	1.3	0.823	0.627	0.481	0.820	0.392	0.468	0.266	0.4	0.1	0.7	-0.1	-1.8	-0.1	-0.2
28	210	5.5	16.0	4.0	4.4	2.5	4.0	1.9	3.5	2.2	0.716	0.798	0.455	0.716	0.344	0.636	0.404	-0.7	-0.4	0.2	-0.1	-0.7	0.7	-1.2
27	210	5.7	13.9	4.7	3.6	2.7	4.7	2.2	2.7	1.5	0.823	0.627	0.481	0.820	0.392	0.468	0.266	0.5	0.1	0.5	0.2	-2.1	0.0	-0.5
32	220	3.2	16.0	2.4	2.8	1.6	2.0	1.1	2.5	1.9	0.770	0.890	0.519	0.621	0.335	0.791	0.611	-0.1	0.0	-0.1	0.0	-0.5	0.0	0.0
31	220	3.2	13.9	2.7	2.5	1.8	2.3	1.1	2.2	1.7	0.820	0.780	0.540	0.699	0.348	0.672	0.539	0.2	-0.2	0.2	0.2	-0.6	-0.1	-0.2
30	220	3.3	12.1	3.0	2.4	1.8	2.7	1.2	1.8	1.4	0.893	0.711	0.545	0.829	0.374	0.544	0.437	-0.1	0.3	-0.2	-0.1	-0.4	0.1	0.0
36	220	4.1	16.0	3.1	3.6	2.1	2.5	1.4	3.2	2.5	0.770	0.890	0.519	0.621	0.335	0.791	0.611	-0.2	0.0	0.1	-0.2	-0.6	0.4	0.2
35	220	4.2	13.9	3.4	3.2	2.2	2.9	1.4	2.8	2.2	0.820	0.780	0.540	0.699	0.348	0.672	0.539	0.1	-0.3	0.3	0.1	-0.6	0.2	-0.2
34	220	4.2	12.1	3.8	3.0	2.3	3.5	1.6	2.3	1.9	0.893	0.711	0.545	0.829	0.374	0.544	0.437	-0.2	0.4	-0.4	0.0	-0.4	0.6	0.2
38	220	5.1	13.9	4.2	4.0	2.8	3.6	1.8	3.4	2.7	0.820	0.780	0.540	0.699	0.348	0.672	0.539	0.1	-0.3	0.6	0.2	-0.5	0.9	-0.3
37	220	5.2	12.1	4.6	3.7	2.8	4.3	1.9	2.8	2.3	0.893	0.711	0.545	0.829	0.374	0.544	0.437	-0.1	0.5	-0.6	-0.1	-0.7	0.7	0.3
39	230	3.5	10.5	3.8	2.7	2.6	3.2	1.6	1.9	1.6	1.103	0.768	0.746	0.910	0.457	0.560	0.466	0.0	0.1	0.1	0.2	0.1	-0.1	-0.1
40	230	4.4	12.1	4.6	3.4	3.2	4.3	2.1	2.3	1.8	1.048	0.778	0.730	0.987	0.487	0.532	0.417	-0.1	0.0	-0.5	-0.2	-0.4	0.1	0.1
41	240	4.4	12.1	4.9	4.4	4.0	4.7	2.4	2.7	1.9	1.114	0.994	0.918	1.066	0.554	0.616	0.430	0.0	0.0	-0.1	0.0	-0.3	0.0	0.0
50	230	38.5	16.0	30.3	34.8	9.9	40.4	9.2	20.4	14.7	0.787	0.903	0.256	1.050	0.239	0.530	0.381	0.7	-0.4	2.0	16.8	-3.8	8.7	-0.3
51	227	39.8	12.1	38.8	31.0	18.0	36.1	14.6	21.9	18.4	0.976	0.780	0.453	0.908	0.368	0.549	0.463	-0.3	0.5	0.0	2.1	1.9	12.1	7.6
52	227	34.9	12.1	34.1	27.2	15.8	31.7	12.8	19.2	16.2	0.976	0.780	0.453	0.908	0.368	0.549	0.463	-0.4	0.4	-0.2	1.0	1.4	10.4	5.4
53	227	29.9	12.1	29.2	23.3	13.5	27.1	11.0	16.4	13.8	0.976	0.780	0.453	0.908	0.368	0.549	0.463	-0.3	0.7	-2.0	0.0	0.6	8.3	3.8
54	218	13.0	10.5	12.2	10.0	7.1	13.0	4.1	5.7	3.9	0.937	0.767	0.548	1.003	0.314	0.437	0.302	0.1	-0.3	0.2	-0.2	-0.1	0.1	0.1
55	218	9.6	10.5	9.0	7.4	5.3	9.6	3.0	4.2	2.9	0.937	0.767	0.548	1.003	0.314	0.437	0.302	-0.4	-0.3	-0.1	-0.1	-0.2	0.0	-0.1
56	226	17.0	9.2	17.4	14.2	5.7	14.7	4.0	9.1	8.3	1.024	0.836	0.334	0.862	0.237	0.537	0.487	0.1	-0.4	0.5	0.0	0.0	0.0	0.0

Table B.2. Revised scene 3 lookup table

	VBL01 = NDBC 51203			Adjusted Predicted Wave Height (ft)							Adjusted Transmission Coefficients							Change in predicted Wave Height (ft)						
case	dp	hs (ft)	tp (s)	W2	W3	W4	W5	K01	K02	K03	W2	W3	W4	W5	K01	K02	K03	W2	W3	W4	W5	K01	K02	K03
1	260	3.3	10.5	2.6	2.9	1.3	3.0	0.9	1.5	1.2	0.798	0.869	0.394	0.902	0.264	0.463	0.368	-0.1	0.0	-0.1	0.1	0.0	-0.1	-0.1
3	260	4.2	12.1	3.1	3.5	1.3	4.0	1.1	1.8	1.2	0.744	0.832	0.319	0.962	0.255	0.427	0.282	0.1	0.1	0.1	-0.1	0.0	0.1	0.1
2	260	4.2	10.5	3.4	3.7	1.7	3.8	1.1	2.0	1.6	0.798	0.869	0.394	0.902	0.264	0.463	0.368	-0.1	0.0	0.2	0.1	-0.1	0.0	0.0
4	260	5.1	12.1	3.8	4.3	1.6	4.9	1.3	2.2	1.4	0.744	0.832	0.319	0.962	0.255	0.427	0.282	-0.2	0.1	0.2	0.0	-0.1	0.2	0.1
5	270	3.1	10.5	2.2	2.7	0.8	3.0	0.6	1.3	1.3	0.695	0.875	0.249	0.973	0.197	0.404	0.404	0.1	-0.1	0.0	0.0	0.0	0.1	-0.2
7	270	3.9	12.1	2.9	3.2	0.8	4.0	1.1	1.6	0.9	0.730	0.813	0.216	1.026	0.271	0.420	0.221	0.0	0.1	0.0	-0.1	0.0	-0.1	0.3
6	270	4.0	10.5	2.8	3.5	1.0	3.9	0.8	1.6	1.6	0.695	0.875	0.249	0.973	0.197	0.404	0.404	0.0	0.1	-0.4	0.2	0.0	0.1	-0.3
9	270	4.8	12.1	3.5	3.9	1.0	4.9	1.3	2.0	1.1	0.730	0.813	0.216	1.026	0.271	0.420	0.221	-0.3	0.2	0.1	0.2	0.0	-0.1	0.4
8	270	4.9	10.5	3.4	4.3	1.2	4.7	1.0	2.0	2.0	0.695	0.875	0.249	0.973	0.197	0.404	0.404	-0.1	0.2	-0.3	0.1	-0.2	0.2	-0.2
10	270	5.7	12.1	4.1	4.6	1.2	5.8	1.5	2.4	1.3	0.730	0.813	0.216	1.026	0.271	0.420	0.221	-0.7	0.1	0.1	0.1	0.1	0.1	0.5
11	280	2.8	10.5	1.9	2.3	0.6	2.6	0.8	1.0	1.2	0.690	0.812	0.212	0.927	0.270	0.370	0.425	0.0	-0.1	-0.2	0.1	0.0	0.1	-0.3
13	280	3.6	12.1	2.8	2.9	0.9	3.5	1.0	1.4	1.5	0.781	0.810	0.260	0.984	0.284	0.385	0.409	0.0	0.3	0.5	-0.2	0.0	-0.3	0.8
12	280	3.6	10.5	2.5	2.9	0.8	3.4	1.0	1.3	1.5	0.690	0.812	0.212	0.927	0.270	0.370	0.425	-0.2	-0.1	-0.1	0.1	0.1	0.2	-0.4
16	280	4.3	13.9	3.8	3.7	1.7	4.4	1.7	1.5	2.2	0.882	0.856	0.394	1.016	0.400	0.351	0.502	-0.1	-0.2	-0.4	0.1	-0.4	0.2	-0.5
15	280	4.4	12.1	3.4	3.5	1.1	4.3	1.2	1.7	1.8	0.781	0.810	0.260	0.984	0.284	0.385	0.409	-0.1	0.3	0.8	-0.3	-0.1	-0.4	1.0
14	280	4.4	10.5	3.1	3.6	0.9	4.1	1.2	1.6	1.9	0.690	0.812	0.212	0.927	0.270	0.370	0.425	-0.2	-0.1	-0.4	0.2	0.3	0.3	-0.5
19	280	5.1	13.9	4.5	4.4	2.0	5.2	2.0	1.8	2.6	0.882	0.856	0.394	1.016	0.400	0.351	0.502	-0.1	-0.2	-0.6	-0.6	-0.4	0.0	-0.3
18	280	5.2	12.1	4.0	4.2	1.3	5.1	1.5	2.0	2.1	0.781	0.810	0.260	0.984	0.284	0.385	0.409	-0.4	0.4	0.6	-0.2	0.0	-0.3	1.3
17	280	5.2	10.5	3.6	4.2	1.1	4.8	1.4	1.9	2.2	0.690	0.812	0.212	0.927	0.270	0.370	0.425	-0.3	0.0	-0.4	0.3	0.2	0.4	-0.5
21	280	5.9	13.9	5.2	5.0	2.3	6.0	2.4	2.1	3.0	0.882	0.856	0.394	1.016	0.400	0.351	0.502	-0.5	-0.6	-0.7	-0.5	-0.7	0.2	-0.2
20	280	6.0	12.1	4.7	4.8	1.5	5.9	1.7	2.3	2.4	0.781	0.810	0.260	0.984	0.284	0.385	0.409	-0.2	0.3	0.8	-0.1	0.1	-0.5	1.5
23	280	6.7	13.9	5.9	5.7	2.6	6.8	2.7	2.3	3.3	0.882	0.856	0.394	1.016	0.400	0.351	0.502	-0.5	-0.7	-0.7	-1.0	0.6	0.3	-0.1
22	280	6.7	12.1	5.3	5.5	1.8	6.6	1.9	2.6	2.8	0.781	0.810	0.260	0.984	0.284	0.385	0.409	-0.2	0.3	0.9	-0.4	0.2	-0.4	1.9
25	280	7.5	13.9	6.6	6.4	2.9	7.6	3.0	2.6	3.7	0.882	0.856	0.394	1.016	0.400	0.351	0.502	-1.0	-1.0	-0.6	0.6	-0.5	0.2	-0.3
24	280	7.5	12.1	5.9	6.1	2.0	7.4	2.1	2.9	3.1	0.781	0.810	0.260	0.984	0.284	0.385	0.409	-0.8	0.2	0.9	-0.5	0.3	-0.3	2.4
26	280	8.2	13.9	7.2	7.0	3.2	8.3	3.3	2.9	4.1	0.882	0.856	0.394	1.016	0.400	0.351	0.502	-1.3	-1.0	-0.5	-0.3	-0.3	-0.1	-0.3
47	290	2.1	10.5	1.8	1.6	0.3	1.6	0.5	0.6	0.9	0.883	0.781	0.129	0.763	0.242	0.302	0.444	0.0	0.0	0.1	0.0	0.0	0.1	-0.1
27	290	2.5	10.5	2.2	1.9	0.3	1.9	0.6	0.7	1.1	0.883	0.781	0.129	0.763	0.242	0.302	0.444	0.2	0.0	-0.1	-0.3	0.0	0.1	-0.2
49	290	2.6	12.1	2.3	1.8	0.8	2.3	0.8	0.9	1.2	0.895	0.704	0.292	0.869	0.318	0.340	0.465	-0.1	0.3	0.1	0.2	0.0	-0.3	0.2
48	290	2.6	10.5	2.3	2.1	0.3	2.0	0.6	0.8	1.2	0.883	0.781	0.129	0.763	0.242	0.302	0.444	0.3	0.1	0.0	0.1	-0.1	0.2	0.0
30	290	3.1	13.9	2.7	2.4	1.4	3.1	1.4	1.0	1.7	0.886	0.778	0.464	1.010	0.451	0.336	0.549	0.0	-0.2	-0.2	-0.2	0.0	0.2	-0.1
29	290	3.1	12.1	2.8	2.2	0.9	2.7	1.0	1.1	1.5	0.895	0.704	0.292	0.869	0.318	0.340	0.465	0.1	0.2	0.2	-0.3	0.0	-0.4	0.5
52	290	3.2	13.9	2.8	2.5	1.5	3.2	1.4	1.1	1.7	0.886	0.778	0.464	1.010	0.451	0.336	0.549	0.3	-0.1	-0.3	-0.3	0.1	0.4	-0.2
28	290	3.2	10.5	2.8	2.5	0.4	2.4	0.8	1.0	1.4	0.883	0.781	0.129	0.763	0.242	0.302	0.444	0.4	0.1	-0.1	-0.3	-0.1	0.3	-0.2
51	290	3.2	12.1	2.9	2.3	0.9	2.8	1.0	1.1	1.5	0.895	0.704	0.292	0.869	0.318	0.340	0.465	0.0	0.5	0.0	0.2	0.0	-0.3	0.3
50	290	3.2	10.5	2.9	2.5	0.4	2.5	0.8	1.0	1.4	0.883	0.781	0.129	0.763	0.242	0.302	0.444	0.0	0.0	0.0	0.0	-0.1	0.3	-0.2
55	290	3.7	13.9	3.3	2.9	1.7	3.8	1.7	1.2	2.0	0.886	0.778	0.464	1.010	0.451	0.336	0.549	0.3	-0.1	-0.3	-0.4	0.1	0.4	-0.1
54	290	3.8	12.1	3.4	2.7	1.1	3.3	1.2	1.3	1.8	0.895	0.704	0.292	0.869	0.318	0.340	0.465	0.0	0.5	0.1	0.3	0.1	-0.3	0.4
33	290	3.8	13.9	3.3	2.9	1.8	3.8	1.7	1.3	2.1	0.886	0.778	0.464	1.010	0.451	0.336	0.549	-0.2	-0.4	-0.2	-0.2	0.0	0.3	-0.3
53	290	3.8	10.5	3.4	3.0	0.5	2.9	0.9	1.2	1.7	0.883	0.781	0.129	0.763	0.242	0.302	0.444	0.1	0.1	0.0	0.0	0.1	0.3	-0.3
32	290	3.8	12.1	3.4	2.7	1.1	3.3	1.2	1.3	1.8	0.895	0.704	0.292	0.869	0.318	0.340	0.465	0.3	0.2	0.4	-0.3	-0.1	-0.5	0.7
31	290	3.9	10.5	3.4	3.0	0.5	3.0	0.9	1.2	1.7	0.883	0.781	0.129	0.763	0.242	0.302	0.444	0.3	0.0	-0.2	-0.4	0.1	0.4	-0.4
57	290	4.3	13.9	3.8	3.3	2.0	4.3	1.9	1.4	2.4	0.886	0.778	0.464	1.010	0.451	0.336	0.549	0.3	-0.3	-0.4	-0.5	0.1	0.4	-0.1
37	290	4.4	16.0	3.7	3.9	2.5	4.9	2.0	1.3	2.9	0.855	0.896	0.570	1.127	0.458	0.305	0.668	0.0	0.0	0.1	0.0	0.0	-0.1	0.0
56	290	4.4	12.1	3.9	3.1	1.3	3.8	1.4	1.5	2.0	0.895	0.704	0.292	0.869	0.318	0.340	0.465	0.0	0.6	0.2	0.2	0.1	-0.4	0.6
36	290	4.4	13.9	3.9	3.5	2.1	4.5	2.0	1.5	2.4	0.886	0.778	0.464	1.010	0.451	0.336	0.549	-0.1	-0.3	-0.3	-0.5	-0.2	0.2	-0.4
35	290	4.5	12.1	4.0	3.2	1.3	3.9	1.4	1.5	2.1	0.895	0.704	0.292	0.869	0.318	0.340	0.465	0.2	0.2	0.4	-0.5	-0.1	-0.7	0.9
34	290	4.6	10.5	4.0	3.6	0.6	3.5	1.1	1.4	2.0	0.883	0.781	0.129	0.763	0.242	0.302	0.444	0.3	0.1	-0.2	-0.4	0.2	0.4	-0.4
59	290	4.9	13.9	4.3	3.8	2.3	4.9	2.2	1.6	2.7	0.886	0.778	0.464	1.010	0.451	0.336	0.549	0.3	-0.4	-0.5	-0.9	0.3	0.5	0.1
58	290	4.9	12.1	4.4	3.5	1.4	4.3	1.6	1.7	2.3	0.895	0.704	0.292	0.869	0.318	0.340	0.465	0.2	0.7	0.2	0.2	0.1	-0.5	0.7
40	290	5.0	16.0	4.3	4.5	2.9	5.7	2.1	1.5	3.4	0.855	0.896	0.570	1.127	0.458	0.305	0.668	-0.6	-0.1	0.1	0.1	0.0	-0.1	0.3
39	290	5.1	13.9	4.6	4.0	2.4	5.2	2.1	1.7	2.8	0.886	0.778	0.464	1.010	0.451	0.336	0.549	-0.3	-0.7	-0.4	-0.9	0.0	0.2	-0.1
38	290	5.2	12.1	4.7	3.7	1.5	4.5	1.7	1.8	2.4	0.895	0.704	0.292	0.869	0.318	0.340	0.465	0.2	0.3	0.5	-0.6	0.0	-0.6	1.2
42	290	5.8	13.9	5.2	4.5	2.7	5.9	2.6	2.0	3.2	0.886	0.778	0.464	1.010	0.451	0.336	0.549	-0.3	-0.8	-0.5	-0.4	0.0	0.4	0.2
41	290	5.9	12.1	5.3	4.2	1.7	5.1	1.9	2.0	2.7	0.895	0.704	0.292	0.869	0.318	0.340	0.465	0.6	0.1	0.7	-0.6	0.0	-0.8	1.4
45	290	6.4	16.0	5.5	5.7	3.6	7.2	2.9	1.9	4.3	0.855	0.896	0.570	1.127	0.458	0.305	0.668	-1.1	-0.5	0.3	-0.4	-0.1	-0.2	0.9
44	290	6.5	13.9	5.8	5.1	3.0	6.6	2.9	2.2	3.6	0.886	0.778	0.464	1.010	0.451	0.336	0.549	-0.6	-1.1	-0.5	-1.0	-0.1	0.4	0.4
43	290	6.6	12.1	5.9	4.6	1.9	5.7	2.1	2.2	3.1	0.895	0.704	0.292	0.869	0.318	0.340	0.465	0.2	0.0	0.8	-0.7	0.2	-1.0	1.8
46	290	7.2	13.9	6.4	5.6	3.3	7.3	3.2	2.4	3.9	0.886	0.778	0.464	1.010	0.451	0.336	0.549	-0.8	-1.2	-0.3	-0.3	-0.1	-0.6	0.2
60	300	2.1	10.5	1.9	1.4	0.3	1.7	0.5	0.5	1.0	0.929	0.676	0.145	0.801	0.244	0.229	0.461	-0.1	-0.1	0.1	0.0	0.0	0.1	0.0
62	300	2.5	12.1	2.2	1.4	0.7	2.0	0.7	0.8	1.1	0.857	0.566	0.282	0.781	0.279	0.325	0.421	0.1	0.1	-0.1	0.1	0.0	-0.1	0.1
61	300	2.5	10.5	2.4	1.7	0.4	2.0	0.6	0.6	1.2	0.929	0.676	0.145	0.801	0.244	0.229	0.461	0.1	-0.1	0.1	0.0	-0.1	0.1	0.1
64	300	3.0	12.1	2.5	1.7	0.8	2.3	0.8	1.0	1.2	0.857	0.566	0.282	0.781	0.279	0.325	0.421	0.3	0.2	-0.1	0.0	0.0	-0.1	0.1
63	300	3.0	10.5	2.8	2.0	0.4	2.4	0.7	0.7	1.4	0.929	0.676	0.145	0.801	0.244	0.229	0.461	0.1	-0.2	0.1	0.1	0.0	0.0	0.1

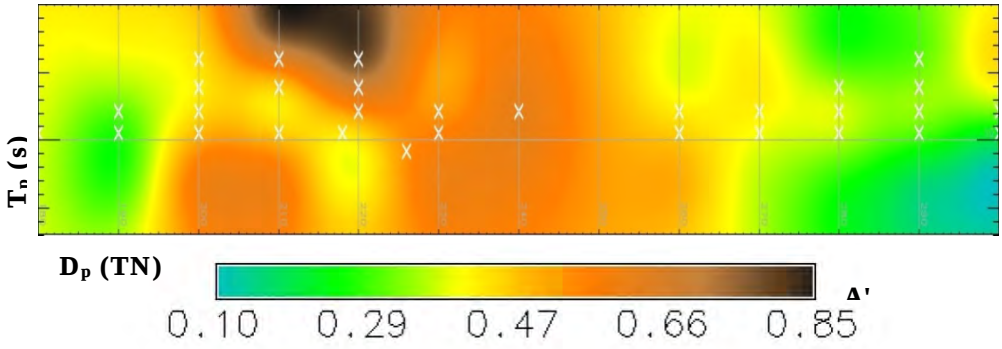

Figure B.4. K02 surface from lookup table.

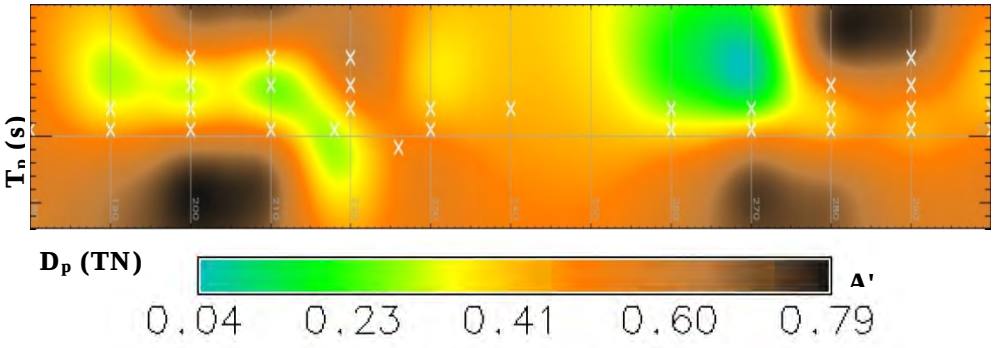

Figure B.5. K03 surface from lookup table.

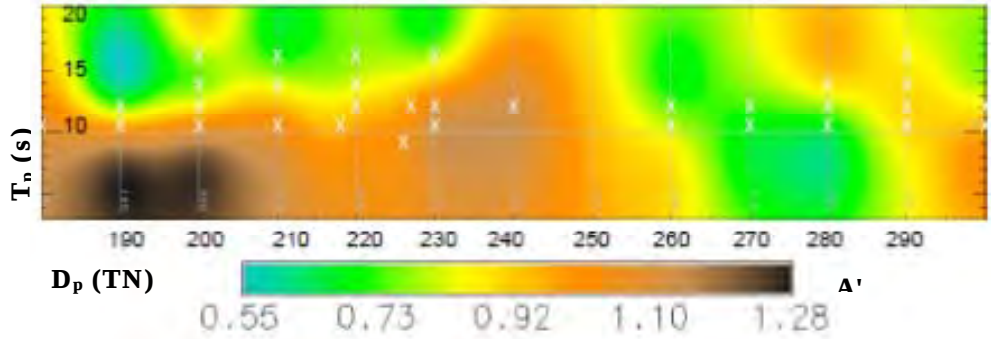

Figure B.6. W2 surface from lookup table.

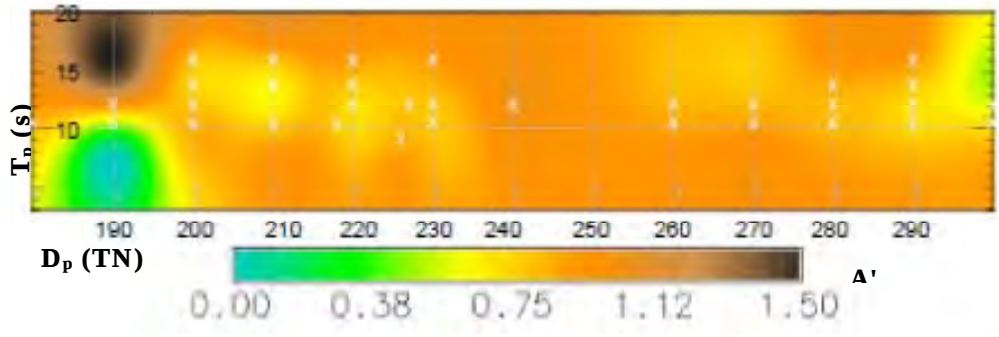

Figure B.7. W3 surface from lookup table.

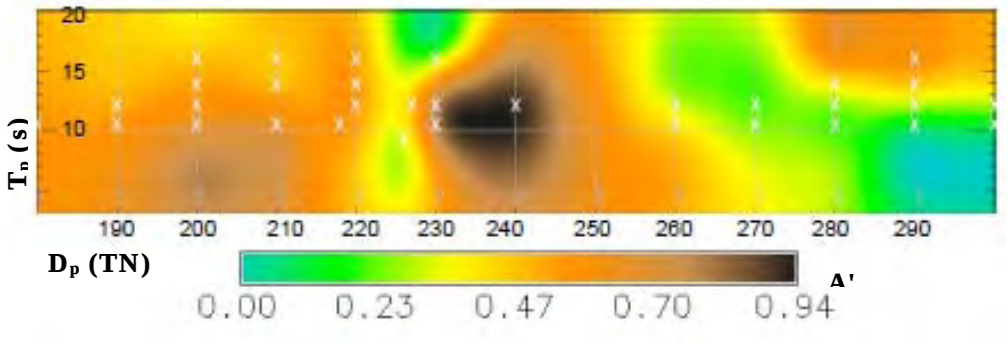

Figure B.8. W4 surface from lookup table.

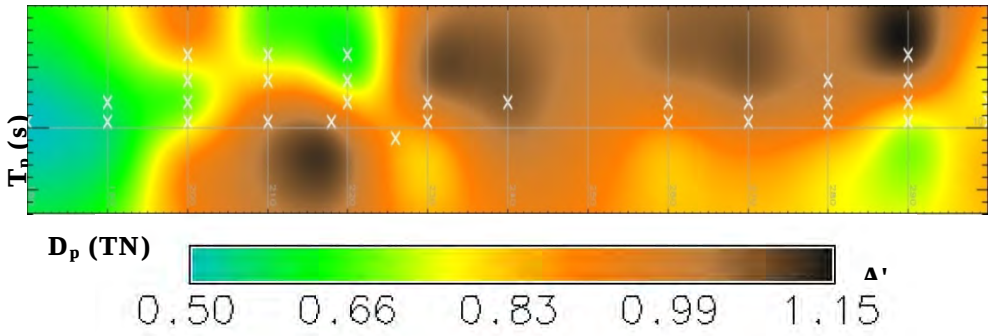

Figure B.9. W5 surface from lookup table.

REPORT DOCUMENTATION PAGE

Form Approved
OMB No. 0704-0188

1. REPORT DATE *(DD-MM-YYYY)*	2. REPORT TYPE	3. DATES COVERED *(From - To)*
May 2012	Final report	

4. TITLE AND SUBTITLE

Kaumalapau Harbor, Hawaii, Breakwater Repair

5a. CONTRACT NUMBER

5b. GRANT NUMBER

5c. PROGRAM ELEMENT NUMBER

6. AUTHOR(S)

Jessica H. Podoski and Thomas D. Smith

5d. PROJECT NUMBER

5e. TASK NUMBER

5f. WORK UNIT NUMBER

7. PERFORMING ORGANIZATION NAME(S) AND ADDRESS(ES)

U.S. Army Corps of Engineers, Honolulu District
Bldg. T223, CEPOH-EC-T
Fort Shafter, Hawaii 96858-5440

8. PERFORMING ORGANIZATION REPORT NUMBER

ERDC/CHL TR-12-7

9. SPONSORING / MONITORING AGENCY NAME(S) AND ADDRESS(ES)

U.S. Army Corps of Engineers
441 G. Street, NW
Washington, DC 20314-1000

10. SPONSOR/MONITOR'S ACRONYM(S)

11. SPONSOR/MONITOR'S REPORT NUMBER(S)

12. DISTRIBUTION / AVAILABILITY STATEMENT

Approved for public release; distribution is unlimited.

13. SUPPLEMENTARY NOTES

14. ABSTRACT

Cumulative damage to the Kaumalapau Harbor breakwater over the years resulted in nearly total failure of the breakwater armor layer both above and below the waterline. Breakwater repair incorporated use of the largest CORE-LOC® concrete armor units (35 ton) ever placed on a U.S. Army Corps of Engineers structure. Actual construction took about 18 months, and was completed in June 2007.

Four different pertinent aspects of this rehabilitation were monitored. Lessons learned from monitoring these four aspects include:

1. **CORE-LOC® armor unit material strength and breakage due to movement:** (a) Standard methods of specifying concrete strength are not necessarily applicable to coastal structures composed of concrete armor units – more research and development is needed; (b) Construction methods are an integral part of concrete armor unit stability, and variability of methods may contribute to armor layer vulnerability; (c) Small-scale post-construction armor unit movement will not necessarily lead to armor unit breakage.
2. **Breakwater structure and armor layer settlement:** (a) T-LiDAR is an accurate and comprehensive method for monitoring changes in complex coastal structures such as those with concrete armor units; (b) Maintaining packing density around bends in structure and structure head as much as possible may limit the amount of unit movement and/or damage following construction; (c) Minor settlement and movement of armor units following construction does not affect the integrity of the structure.
3. **Concrete breakwater cap:** (a) Small-scale post-construction armor unit movement will not necessarily lead to concrete cap settlement or damage; (b) Stability of concrete cap can likely only be field-verified if a wave event causing overtopping of the structure is experienced.
4. **Armor layer toe stability:** (a) "Cannon" and "straddled" orientation of the first and second rows of CORE-LOC® toe units appears to be a successful placement scheme in this case; (b) Combination of traditional high-density survey methods augmented by visual observation techniques provided a thorough evaluation of underwater structure conditions.

15. SUBJECT TERMS

Breakwater
Concrete armor units
Concrete strength
CORE-LOC®
MCNP
Multibeam survey
T-LiDAR
Wave modeling

16. SECURITY CLASSIFICATION OF:			17. LIMITATION OF ABSTRACT	18. NUMBER OF PAGES	19a. NAME OF RESPONSIBLE PERSON
a. REPORT	b. ABSTRACT	c. THIS PAGE			19b. TELEPHONE NUMBER *(include area code)*
UNCLASSIFIED	UNCLASSIFIED	UNCLASSIFIED		247	